Catalytic and Non-Catalytic Co-Pyrolysis of Torrefied Bamboo Biomass and Plastic: Synergism, Kinetics and Reaction Mechanism

A Thesis
Submitted in Partial Fulfilment of the Requirement for the Degree of

DOCTOR OF PHILOSOPHY

By

MAHBOOB ALAM

Department of Chemical Engineering
Indian Institute of Technology Guwahati
Guwahati-781039, Assam, India
July, 2021

Dedicated to My Parents and My Mentor

Indian Institute of Technology Guwahati

Department of Chemical Engineering

Declaration

I hereby declare that the work contained in this thesis entitled **"Catalytic and Non-Catalytic Co-Pyrolysis of Torrefied Bamboo Biomass and Plastic: Synergism, Kinetics and Reaction Mechanism"** is original and has been done by me under the guidance of **Dr. Nageswara Rao Peela**. The work has not been submitted to any other institute for any degree or diploma. I have followed the guidelines provided by the institute in preparing the thesis. I have confirmed to the norms and guidelines given in the Ethical Code of Conduct of the institute. Whenever I have used materials (data, theoretical analysis, figures and text) from other sources, I have given due credit to them by citing them in the text of the thesis and giving their details in the references. Further, I have taken permission from the copyright owners of the sources, whenever necessary.

Student name: Mahboob Alam

(Roll no. 156107018)

Indian Institute of Technology Guwahati

Department of Chemical Engineering

Certificate

It is certified that the work described in this thesis entitled **"Catalytic and Non-Catalytic Co-Pyrolysis of Torrefied Bamboo Biomass and Plastic: Synergism, Kinetics and Reaction Mechanism"** by Mr. Mahboob Alam for the award of degree of Doctor of Philosophy is an authentic record of the results obtained from the research work carried out under my supervision at the Department of Chemical Engineering, Indian Institute of Technology Guwahati, Guwahati, India, and this work has not been submitted elsewhere for a degree.

Dr. Nageswara Rao Peela
(Supervisor)
Associate Professor
Department of Chemical Engineering
IIT Guwahati, Guwahati – 781039

ACKNOWLEDGEMENT

This doctoral thesis would not have been completed without the help and extended hands of several people. I take this opportunity to express my sincere thankfulness to all of them.

First of all, I am extremely grateful to my supervisor **Dr. Nageswara Rao Peela** for providing me a precious opportunity to work in his group. His continuous support, scientific guidance, deep insights, patience and motivation encouraged me to take up the tasks that otherwise were hard and demanding. I earnestly thank him for having trust in me and giving me total freedom in choosing the direction of my research. I feel fortunate to having him as my mentor who always motivated me with his hard work, dedication and optimism.

Besides my supervisor, I am highly indebted to my doctoral committee members, **Prof. G. Pugazhenthi, Prof. Animes Kumar Golder and Dr. Aksai Kumar A. S.** for assessing my research work regularly. Their insightful advices, suggestions and crucial comments helped me to widen my research from various perspectives and improve my thesis. I would also like to thank my comprehensive committee members **Prof. V.V. Goud, Prof. Mahuya De, and Prof. Animes Kumar Golder.**

I also thank **Prof. Anugrah Singh,** Head, Department of Chemical Engineering, for his administrative support. Furthermore, I would like to thank other faculty members, research scholars, non-teaching staff of the Department of Chemical Engineering, IIT Guwahati for their kind cooperation in all aspects. I also thank technical staff of Central Instruments Facilities **(CIF)** and Centre for Nanotechnology and analytical lab of **Department of Chemical Engineering** of Indian Institute of Technology Guwahati for their support during the analysis.

I deeply acknowledge my lab mates, *Devipriya Gogoi, Rambabu Ponnala, Bharath Velaga, Anirban Chowdhury, Laxmi Prasad Pala, Ameer Suhail, Hanumanth Reddy, Rammohan, Sarmistha Baruah, Masresha Adasho Achomo, Naga Phani Sai Kumar, Reddi Ramu and my graduated lab mates Pooja Saxena, Sourdip Choudhary, Pardeep Soni and Madhav Solanke*.

I extend my sincere thanks to my friends Kuldeep, Barnali, Bitang, Rupam, Gufran, Rizwan, Mehsar, Shama, Rasool, Abdul Qadir, Sandeep, Islam, Vaseek Khan, Waseem, Nadim,

Nizamuddin, Qadeer Khan, Wasi, Sharif, Adil, Asif, Furqan, Saban, Kamil, Ankit, Maqsood, Malick, Shajar, Tufail, Kalimuddin, Mohsin, Nergis Khan, Shavez, Saghir, Tipu, Maimur, Kafeel, Adnan, Khalid Wani and other friends for their constant unfailing support, their encouragement and all the help they extended whenever required.

My sincere thanks to Dr. Sameer, Dr. Shaad, Dr. Adil, Dr. Pallab, and Dr. CV Rao for their brotherly caring nature, sharing all kinds of moments and helping to improve my thinking approach.

My Ph.D. endeavor could not have been completed without the endless love, support, tolerance and blessings from my family. I am fortunate and blessed enough to have such a caring and supportive parents. It is because of their prayers, sacrifice and struggle, I am able to live my dream to complete my higher education from a prestigious institute. I would like to thank my wife Soophiya for her lovely support and patience in all these years and for encouraging me to face the difficulty. You are the source of my inspiration and happiness. Without you all this would never have been possible.

I wish to thank many other people whose names are not mentioned here but this does not mean that I have forgotten their help.

Finally, I thank almighty Allah for giving me a great life, strength to chase my dreams, and being with me in all my failure and success!

Mahboob Alam

ABSTRACT

The depletion of fossil fuels and environmental deterioration leads researchers to search for alternative, renewable, sustainable, and eco-friendly energy resources. The lignocellulosic biomass (LCB) is one of the most promising renewable resources for the production of biofuels, due to its mass availability, eco-friendliness, and CO_2 neutrality. A total of 220 and 0.686 billion tons/year of LCB is being produced worldwide and in India, respectively. The LCB consists majorly of hemicellulose, cellulose, lignin and minor amounts of extractives and ash. The solid biomass cannot directly be used as fuel in industrial applications, because of several drawbacks including hygroscopic nature, high moisture content, high oxygen content, low heating value, lower grindability, low bulk density, fewer compositional homogeneity and lower resistance to biological degradation. Recently, the thermochemical conversion processes such as catalytic and non-catalytic (co-)pyrolysis has increased attention to convert biomass into biofuel. The biofuel obtained from the pyrolysis of raw biomass is inferior and the process itself is inefficient due to heteropolymeric nature of the hemicellulose present in the biomass. Therefore, it was hypothesized that the selective removal of hemicellulose by wet-torrefaction would help in improving the biofuel quality as well as overall economics of the process due to extra useful product (xylose) formation in the process. Addition of plastic also improves the biofuel characteristics and mitigates the plastic pollution. Further, addition of catalyst improves the biofuel quality by forming desired products such as aromatics (BTEX).

The overall aim of this thesis is to develop wet-torrefaction process to selectively remove the hemicellulose in the form of xylose and to form the hydrochar with better pyrolysis characteristics. Further, to explore the potential of various zeolite catalysts (MesoHY and HZSM-5) for the catalytic co-pyrolysis (CCP) of wet-torrefied bamboo

biomass and plastic (linear low-density polyethylene, LLDPE). The catalytic co-pyrolysis and pyrolysis and non-catalytic co-pyrolysis and pyrolysis of wet-torrefied (or raw) bamboo biomass and LLDPE were carried out using thermogravimetric analysis (TGA) in the temperature range of 30 to 900°C at heating rates 5, 10, 20 and 40°C min^{-1}, under argon atmosphere. The kinetic parameters were determined using three models based on the isoconversional method: Kissinger-Akahira-Sunose **(**KAS), Flynn–Wall–Ozawa (FWO), and Friedman (FM) models. The reaction mechanisms for the above mentioned reactions were predicted using the Criado's master plot.

Initially, the co-pyrolysis of bamboo sawdust (BSD) and LLDPE was studied. A blend containing 25 wt.% BSD and 75 wt.% LLDPE (BP1:3) showed the highest synergism as compared to other blends studied. The activation energy drop (36% with respect to biomass) was the highest with this blend. The mean values of apparent activation energy ($\bar{E}_\alpha$) for the decomposition of blends (BP3:1 (75 wt.% BSD and 25 wt.% LLDPE), BP1:1 (50 wt.% BSD and 50 wt.% LLDPE) and BP1:3) are determined to be 357, 371 and 143 kJ mol^{-1} from KAS, 368, 400 and 165 kJ mol^{-1} from OFW and 468, 356 and 255 kJ mol^{-1} from FM, respectively. The reaction follows a multistep mechanism. The decomposition of the blend BP1:3 follows a nucleation growth (A2) model in the lower conversion range and diffusion (D2) model in the higher conversion range.

As a next study, the bamboo saw dust (BSD) was wet-torrefied to selectively remove hemicellulose in the form of pentoses (xylose + arabinose) and to produce hydrochar (with high energy density of 24 MJ/kg, which is similar to that of lignite). The best torrefaction activity, with xylose yield 85% and complete removal of hemicellulose, was obtained with formic acid:BSD 1:1 and NaCl:BSD 3:1 w/w, at temperature 140°C and time 30 min. Further, the pyrolysis and co-pyrolysis behavior of hydrochar, LLDPE, and their blends

were studied. The blend with one part hydrochar and three parts LLDPE (TBP1:3) showed the highest positive synergism during co-pyrolysis at 40°C min^{-1} heating rate. The average apparent activation energies of co-pyrolysis of blends (TBP3:1, TBP1:1, and TBP1:3) were found to be 232, 261, 247 kJ mol^{-1}, respectively. The Criado's master plot showed the reaction mechanism of co-pyrolysis to be multistep. For example, the blend TBP1:3 followed the trend of two-dimensional Avrami-Erofeyev model (A2) at lower conversions, diffusion-reaction model (D2) at high conversions and end with a first-order reaction.

The torrefied BSD (TBSD) was catalytically co-pyrolyzed with LLDPE over HZSM-5. The apparent activation energies (E_α) of catalytic pyrolysis (CP) of TBSD, and LLDPE were 187 and 147 kJ mol^{-1}, respectively, from Kissinger–Akahira–Sunose (KAS) model. Those of catalytic co-pyrolysis (CCP) of blends TBP3:1, TBP1:1 and TBP1:3 were 163, 135 and 133 kJ mol^{-1}, respectively. The CCP of TBP1:3 and TBP1:1 showed synergism between TBSD and LLDPE in terms of $\bar{E}_\alpha$ and TBP1:3 showed the highest synergism with the least $\bar{E}_\alpha$. The CCP mechanism of blends with higher fraction of TBSD was more complex, as depicted from the Criado's master plot.

Finally, the catalytic co-pyrolysis (CCP) of wet-torrefied bamboo sawdust (TB) and linear low-density polyethylene (LLDPE) over MesoHY zeolite was carried out. Four degradation stages were found in the CCP of TB and LLDPE blends, the first stage being moisture removal. The peak decomposition temperature of catalytic pyrolysis (CP) of LLDPE over FAU was reduced by 251°C as compared to that over HZSM-5 and the enhancement can be attributed to the topology of HY. The $\bar{E}_\alpha$ of the blends TBP3:1, TBP1:1, and TBP1:3 were 176, 133, and 122 kJ mol^{-1}, respectively. The E_α of the blends was much lower as compared to that of TBSD, indicating a clear synergism. A multistep mechanism was observed in both CP of individual samples and CCP of blends, as analysed by Criado's

master plot. For example, the CCP of TBP1:3 followed geometric (volume) contraction (R3) and first-order reaction models at low and high conversions, respectively.

Keywords: Wet-torrefaction of bamboo sawdust; Linear low-density polyethylene (LLDPE); Catalytic co-pyrolysis; Biofuel; Criado's master plot; Reaction mechanism

TABLE OF CONTENTS

LIST OF FIGURE CAPTIONS

LIST OF TABLE CAPTIONS

ABBREVIATIONS

5-HMF	5-hydroxymethylfurfural
AA	Acetic Acid
BAS	Brønsted acidic sites
BET	Brunauer, Emmett and Teller
BJH	Barrett, Joyner and Halenda
BSD	Bamboo Saw Dust
DTG	Derivative thermogravimetric curve (first)
FA	Formic acid
FF	Furfural
FM	Friedman Model
FRAG	Fragmentation reaction
FTIR	Fourier transform infrared spectroscopy
HHV	High heating value (MJ kg-1)
HPLC	High–performance liquid chromatography
KAS	Kissinger–Akahira–Sunose Model
LAS	Lewis acidic sites
LLDPE	Linear Low-Density Polyethylene
MP	Master Plot
NC	Non- Catalyst
FWO	Flynn–Wall–Ozawa Model
RAR	Rearrangement reaction
RID	Refractive Index Detector
TBSD	Torrefied Bamboo Saw Dust
TGA	Thermogravimetric analysis
XRD	X–Ray diffraction

NOMENCLATURES

t : Time (min) in wet torrefaction reaction

DR_{MAX} : Maximum degradation rate (wt % $.min^{-1}$) in a particular stage

T_{MAX} : Temperature at which the maximum of the DTG peak occurs in a particular stage

$d\alpha/dt$:Rate of pyrolysis reaction

α : Extent of conversion or Fractional conversion rate

A : Pre-exponential factor (min^{-1})

f (α) : Reaction model

β : Linear heating rate of thermogravimetric analysis (°C min^{-1})

g (α) : Integral form of the reaction model

T_α : Temperature at which the extent of conversion (α) reached

E_α : Activation energy (kJ mol^{-1}) at fixed conversion value (α)

$\bar{E}_\alpha$: Average activation energy (kJ mol^{-1}) of solid sample

R : Universal gas constant (8.314 J mol^{-1} K^{-1})

T : Temperature (K)

ΔW : Extent of synergism (wt. %) during copyrolysis of TBSD and LLDPE

Z (α) : f (α) x g (α)

Mr. MAHBOOB ALAM

Email: **mahboob.alam@iitg.ac.in; mahboob.iitm@gmail.com**

Education:

Ph.D. pursuing

Department of Chemical Engineering
Indian Institute of Technology, Guwahati
Guwahati 781039, Assam, India
2015–2021

M. Tech in Chemical Engineering

Department of Chemical Engineering
Indian Institute of Technology, Madras
Chennai 600036, Tamil Nadu, India
2012–2014
Marks obtained: 7.5/10.00

M. Sc in Industrial Chemistry

Department of Chemistry
Aligarh Muslim University, Aligarh 202002
Uttar Pradesh, India
2007–2009
Marks obtained: 77%, 1st Class with distinction

B. Sc in Industrial Chemistry

Department of Chemistry
Aligarh Muslim University, Aligarh 202002
Uttar Pradesh, India
2003–2006
Marks obtained: 69%

Higher Secondary in UPB

Govt. Inter College
Lakhimpur Kheri, 262701 Uttar Pradesh, India
2000–2002
Marks obtained: 64%

Publications

Journal papers

- **M. Alam**, A. Bhavanam, A. Jana, J. Kumar S. Viroja, N.R. Peela, Co-pyrolysis of bamboo sawdust and plastic: Synergistic effects and kinetics, Renew. Energy. 149 (2020) 1133–1145. https://doi.org/10.1016/J.RENENE.2019.10.103.
- **M. Alam**, D. Rammohan, A. Bhavanam, N.R. Peela, Wet torrefaction of bamboo saw dust and its co-pyrolysis with plastic, Fuel. 285 (2021). https://doi.org/10.1016/j.fuel.2020.119188
- **M. Alam**, D. Rammohan, N.R. Peela, Catalytic co-pyrolysis of wet-torrefied bamboo sawdust and plastic over the zeolite H-ZSM-5: Synergistic effects and kinetics, Renew. Energy. 178 (2021) 608–619. https://doi.org/10.1016/j.renene.2021.06.109
- **M. Alam,** N.R. Peela, Catalytic co-pyrolysis of wet-torrefied bamboo sawdust and plastic over the zeolite HY: Synergism and kinetics, J. Energy Inst. 100 (2021) 76–88. https://doi.org/10.1016/j.joei.2021.11.004.
- **M. Alam**, N.R. Peela, Catalytic co-pyrolysis of bamboo sawdust and plastic over HZSM-5: Synergistic effects and kinetics (under preparation)
- **M. Alam**, N.R. Peela, Catalytic co-pyrolysis of bamboo sawdust and plastic over MesoHY: Synergistic effects and kinetics (under preparation)

Book Chapter

- **M. Alam**, S.K. Yedla, S.T. Bhutia, V.V. Goud, **N.R. Peela*** (2017) "Advancement in development of biodiesel production in last two decades: An Indian overview on raw materials, synthesis, by-products and application" in Sustainable Biofuels Development in India, A.K. Chandel, R.K. Sukumaran (eds.), Springer International Publishing, Pages 167-188. **DOI: 10.1007/978-3-319-50219-9_7**

National/International Conferences and Workshop

- **M. Alam,** "Wet Torrefaction of Bamboo Saw Dust and Its Co-Pyrolysis with Plastic" 3rd International Conference on Material science and Research (Madridge), November 28-29, 2019; Kuala Lumpur, Malaysia
- Attended an online short-term course on "Valorization of Lignocellulosic Biomass towards Sustainable Fuels, Chemicals and Materials" conducted by NIT Jalandhar - Sept. 2020
- **M. Alam,** N. R. Peela "An overview of bio-oil up-gradation by ketonization and esterification reactions" in Reflux-2016-Annual Chemical Engineering Symposium, Department of Chemical Engineering, 25-27 March, IIT Guwahati, Assam, India.

Job Experience:

- Worked as Chemical Engineer in Al –Jazeera Factory for paints (Tinting System Company) in Kingdom of Saudi Arabia from 2009 to 2010.

Chapter 1

Background of the Work and Research Objectives

1. Introduction

The energy crisis and solid waste management are the two vital issues faced by mankind.[1,2] The fossil resources are depleting rapidly and alternative renewable and sustainable resources are required, on an urgent basis, to meet the energy demands of the society. The depletion of fossil fuels and environmental deterioration lead researchers to search for alternative, renewable, sustainable, and eco-friendly energy resources, as in Fig. 1.1. [3,4] Among all the renewable resources, lignocellulosic biomass (LCB) has been identified as the most promising feedstock for the production of biofuels, due to its mass availability, eco-friendliness, and CO_2 neutrality.[5–9] [10] The LCB includes agricultural residues, energy crops, and forest residue. A total of 220 and 0.686 billion tons/year of LCB is being produced worldwide [11] and in India, [12] respectively. The greenhouse gases can significantly be reduced by utilizing biomass in the production of transportation fuels. [13–15]

The bamboo comes under the family of *poaceae* or *gramineae* and Bambusa genera, monocot plants, and rarely flowering and irregular cycle known as grass. It is the fastest-growing plant on earth, grows on even poor soil conditions and/or degraded lands. The high productivity and self-regeneration ability, make it one of the best-known Bioresource. [16] The plant cell wall of Bambusa *tulda* consists majorly of biopolymers, namely cellulose, hemicellulose, and lignin and non-structural components (extractives and ash) in minor amounts. [17]

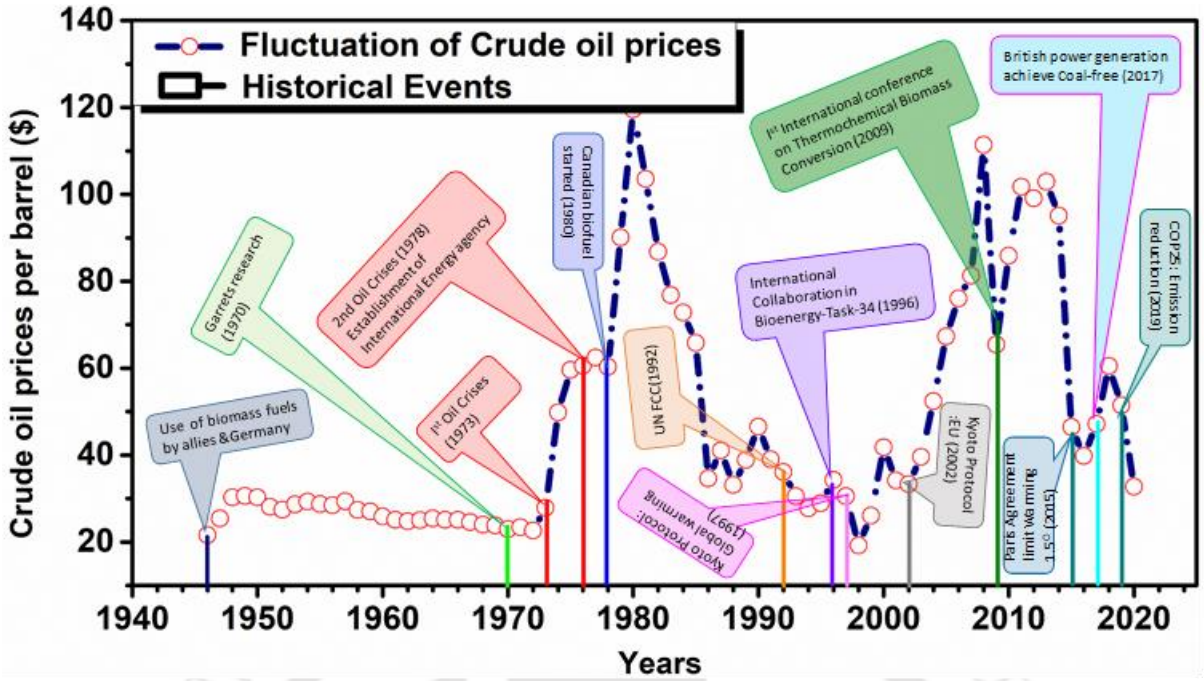

Figure 1.1: Various historical events such as Oil crises, war, economy and global warming responsible for biofuel research initiatives.

The hexose monomers are the building blocks of cellulose and join each other by glycosidic bonds in a regular array to form microfibrils that act as a skeleton in the cell wall. These microfibrils also connect with hemicellulose and lignin through inter and intramolecular hydrogen bonding. [11] The cellulose is crystalline. Based on the crystallographic configuration, two types of crystalline cellulose (I_α and I_β) occur in lignocellulosic biomass having triclinic, with one chain, and monoclinic, with two chains, structures (Fig. 1.2a). [18]

The hemicellulose is a heteropolysaccharide, an amorphous and lower degree of polymerization compared to cellulose. Its backbones consist of pentose units (xylose and arabinose), and these units are also attached with oligosaccharide chains having hexose monomers such as galactose, mannose, glucose, and fructose.[17] Acetyl units are attached with C2 or C3 in xylose ring and glucuronic acid also attached with xylose ring in xylan backbone (Fig. 1.2b). It acts as a linking material, connected through lignin and cellulose by hydrogen and covalent bonds. The lignin is a tridimensional polymer (Fig. 1.2c), amorphous,

and composition varies from species to species. The hardwood, softwood, and grasses contain 20–25, 25–35, and 10–15% lignin, respectively.[17] The linkage or bond between lignin and carbohydrate are categorized into five categories including phenyl glycosides (C_6H_5–O–C1), benzyl ether (α–O–4 or β–O–4), alkyl benzyl ether, γ–ester or ester linkages with glucuronic acid and acetal bonds (Fig. 1.2d).[19] The strength and rigidity of the cell wall depend upon the extent of the lignin matrix which consists of three basic units p–hydroxyphenyl (H), guaiacyl (G), and syryngyl (S). These units are differentiated based on the number of methoxy groups they contain. The H, G, and S units possess zero, one, and two methoxy groups, respectively [20]. These monomers are joined to each other by different linkages such as ether (α–O–4, β–O–4 and γ–O–4), carbon-carbon linkage in aromatic and alkylated carbon (β–5, β–1, 5–5), resinol type (β–β, α –O–γ′, γ–O–α′) and phenyl-coumarane (β–5, α–O4) .[21]

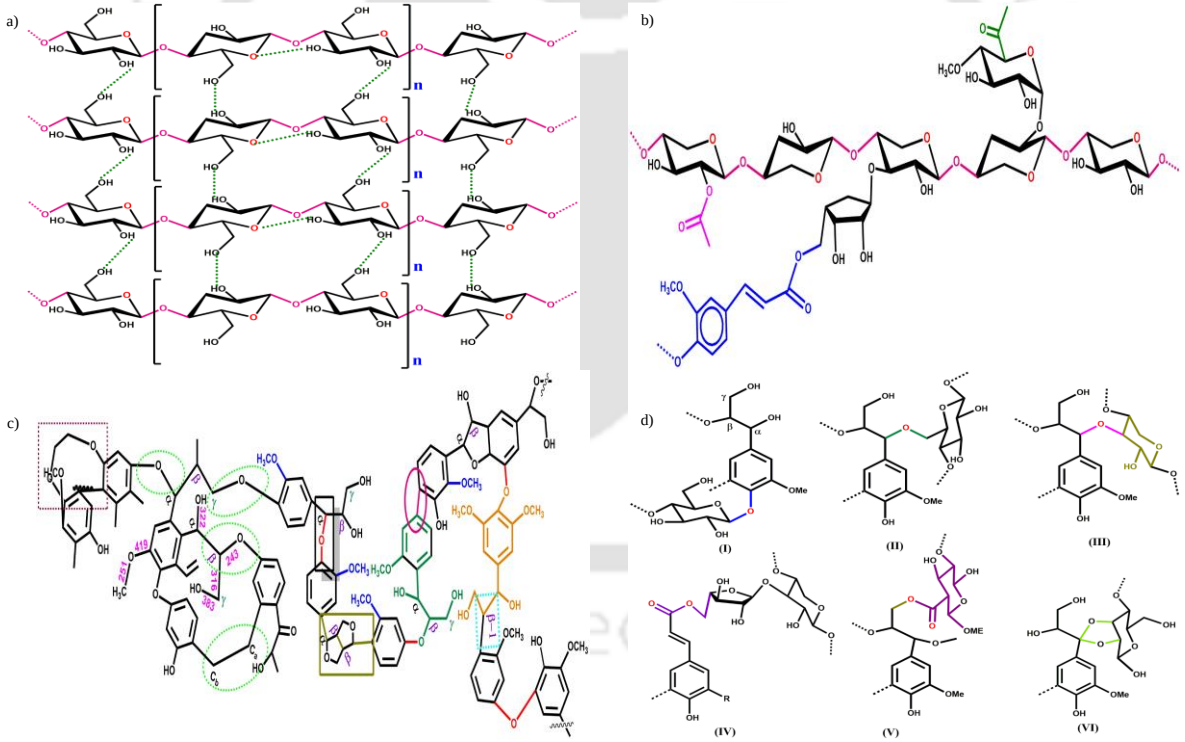

Figure 1.2: Schematic illustration of cellulose (a), hemicellulose (b) and lignin (c) in the cell wall of bambusa *tulda* and lignin carbohydrate complex having different bonds [glycosidic (I), benzyl ether (II), γ–ester (III), acetal (IV), etc.] (d).

The liquid fuel produced from pyrolysis of biomass is known as bio-oil. Six major fractions are present in bio-oil, namely water (15-30 wt%), light oxygenates including acids, esters, ketone and aldehyde and alcohols (8-26 wt%), monophenols (2-7 wt%), water-insoluble oligomers originated from lignin (15-25 wt%), and water-soluble molecules (10-30 wt%).[22] It consists of highly oxygenated compounds including acids, esters, ketones, aldehydes, alcohols, aromatic species with some traces of polymeric carbohydrates and lignin fragments.[23,24] It has high oxygen content, acidity, viscosity (flash pyrolysis 51 cp, slow pyrolysis 300 cp at 40ºC) [25]**,** and low heating value.[26] The presence of water and high oxygen content (50 wt % on dry basis) contribute to the low heating value of the bio-oil.[27] The corrosive nature of bio-oil is mainly due to acids and its instability is due to aldehydes and phenols.[25] The presence of these compounds makes bio-oil not suitable to be used directly as a transportation fuel and hence needs an up-gradation. Therefore, researchers have tried to obtain mono-aromatic components (benzene, toluene, and para-xylene), using zeolite catalyst in pyrolysis.[28] The bio-oil has been proposed to be used directly as fuel in a variety of applications, including diesel engines, boilers, turbines, and furnaces [14]. The by-products (biochar or pyrochar) from the bio-oil production process are also used as fertilizers, lime, pesticides, antioxidants, carbon electrodes, etc.[29–31]

Plastic has attracted huge attention globally because of its remarkable properties such as high thermal stability, durability, and polymeric structure.[32,33] However, it is non-biodegradable and takes centuries for complete degradation by abiotic and biotic methods.[32,34] The plastic has two backbone structures, namely C-C bonds and heteroatoms (mainly oxygen). Polyethylene (Low-density polyethylene (LDPE), Linear low-density polyethylene (LLDPE), and High-density polyethylene (HDPE)), Polyvinyl chloride, Polypropylene, and Polystyrene comes under the former category. While, Polyethylene terephthalate, Polyurethane, etc., are identified as heteroatoms containing plastic [32,35]. The total market share of PET and PU is

lower (18%) as compared to that of C-C bond plastic (77%). The PEs are resistant to hydrolysis and biodegradation because of high strength of C-C bond in the backbone of plastic but are susceptible to thermal oxidation. The production of plastic globally is increasing day-by-day and the total plastic production from 1950 to 2018 was estimated as 8.3 billion metric tonnes. However, 76% of total plastic is considered as waste out of which 14% is recycled, 14% is incinerated, and 72% is landfilled. Therefore, the plastic waste accumulated in the earth's atmosphere, pollutes our natural ecosystem and adversely affects human health (Fig. 1.3).[32] The production and consumption of plastic in the Asian continent has significantly been increased from 114 to 131 Million tonnes oil equivalant (Mtoe) during 2013-2015. The production quantity of major plastic resins was 82 Mtoe in Asian countries while China plays as a major role (44.79 Mtoe), followed by India and Republic of Korea with 14.17 Mtoe and 13.68 Mtoe, respectively [33]. The consumption of plastic in India (12 kg/capita/year) is still low as compared to that from the USA and China.[36]

The LLDPE, with building blocks ethylene and α-olefins (e.g., butene-1 and hexene-1), is produced using Ziegler–Natta catalyst. It possesses a short chain length identical to HDPE but the occurrence of lower frequency as compared to HDPE. It also has lower lamellar thickness than that of LDPE and HDPE. It also has a lower temperature range (T_m: 125–128°C) and density (0.919 g cm^{-3}) compared to LDPE (ρ: 0.920 gcm^{-3} and T_m: 85−130°C) and HDPE (ρ: 0.953 gcm^{-3} and T_m: 130−140°C). It is generally used in packaging materials.[36,37] Due to its durability and buoyancy nature, it is found in all oceans. It fragments into various sizes (micro, and mm) by weathering and photo-degradation processes and is considered hazardous waste. Therefore, these fragments are transferred into aquatic animals (e.g., fish) by different modes. Moreover, these fragments also reduce the growth of plankton and cause global warming. [38] These micro-plastics, if absorbed by humans, may create severe problems such as inflammation, apoptosis, oxidative stress, tissue damage, fibrosis, and

carcinogenesis.[32,35] Therefore, the utilization of the waste-LLDPE is highly warranted. The thermochemical conversion or chemical recycling process of plastic waste to produce value added-products or fuel could be considered an effective eco-friendly and sustainable alternative to overcome plastic waste pollution.[34,39]

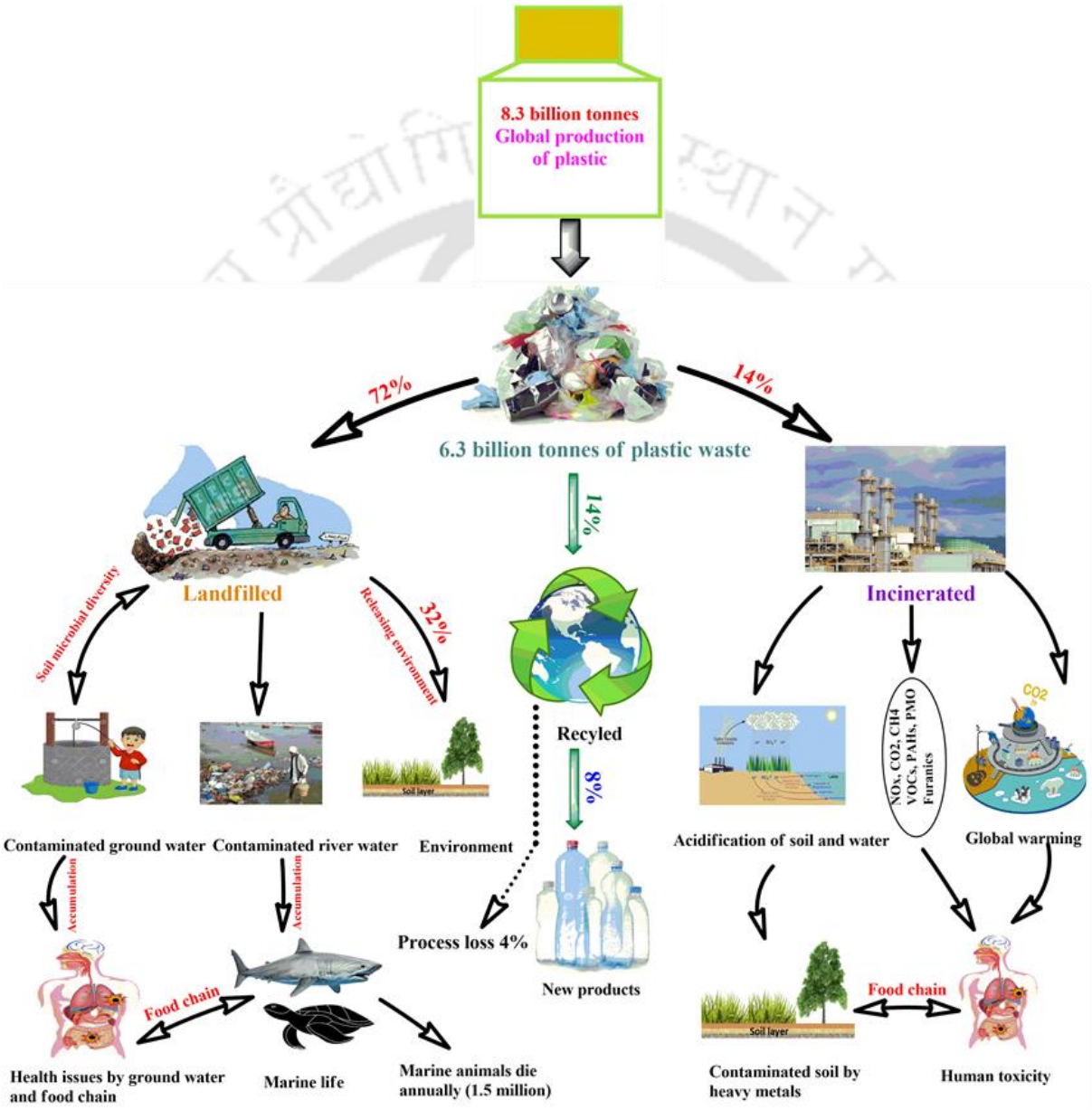

Figure 1.3. Plastic waste fate and their harmful impact on the environment as well as human health.

The raw biomass has various shortcomings such as high moisture content, low bulk density, low energy density, and unfavourable pyrolysis characteristics. The quality of biofuels obtained directly from the lignocellulosic biomass is inferior. Therefore, certain pre-treatment methods such as torrefaction are used to improve the quality of biomass and thereby the quality of biofuel. The torrefaction of raw biomass removes hemicellulose and overcomes the above-mentioned issues.[4] Two torrefaction methods, namely wet and dry torrefaction which produce hydrochar and biochar, respectively[40], have been reported in the literature. Both the methods have their pros and cons. The dry torrefaction suffers from the challenges such as increased ash content, the requirement of pre-drying step, and the risk of self-ignition. Further, the dry torrefaction (DT) is energy-intensive as it requires high temperature and the enhancement of the high heating value (HHV) of biochar is lower. On the other hand, the wet torrefaction is highly promising, as the hydrochar obtained from this process possesses excellent properties.[40,41] Moreover, the wet torrefaction (WT) is less energy-intensive and gives higher enhancement of HHV, by increasing the H/C ratio (due to dominant decarboxylation reactions).[4] The wet torrefied biomass (WTB) is superior to dry torrefied biomass in terms of grindability, hydrophobicity, and ease of pelletization.[4] The WT removes more ash by demineralizing the sample. It preserves active –OH groups that rearrange themselves and increase the crystallinity of macromolecules (cellulose).[42] It is sustainable and eco-friendly due to less emission of pollutants and dust particles as compared to DT.[43] The furanic and phenolic resins formed during WT adhere to the solid surface of hydrochar which, in turn, acts as binders in pelletization avoiding the need for external binders.[44] In the wet torrefaction, the biomass in aqueous suspension is treated at autogenous pressure and temperatures in the range of 150–260°C for 30–60 min.[45] It was hypothesized that using a suitable catalyst (such as NaCl and formic acid) in the wet-torrefaction process, the

hemicellulose can selectively be removed in the form of a useful platform chemical, which improves the overall economics of the process.

The lower effective hydrogen to carbon ratio (H/C_{eff}) of biomass is responsible for the formation of carbonaceous materials (such as char).[46] The co-feeding of waste plastic, along with (torrefied) biomass, in a process called co-pyrolysis, provides hydrogen and leads to the enhanced formation of aromatic content.[45,47] However, the non-catalytic co-pyrolysis produces the unwanted side-products[48] or the products of the individual pyrolysis of lignocellulosic biomass and plastic[49] and requires higher temperatures. While the catalytic pyrolysis of lignocellulosic biomass may lead to the loss of C and H in the form of CO_2 and CO in decarboxylation and decarbonylation reactions and dehydration while eliminating the oxygen in the bio-oil.[17] In catalytic pyrolysis of biomass, the breakdown of biomass occurs on the surface of the zeolite. The degraded volatiles move into the pore of zeolite where different reactions take place for the formation of aromatic fractions. The zeolite contains both Brønsted and Lewis type acid sites. Therefore, catalytic co-pyrolysis (CCP) is the best technology to obtain high-quality biofuels, even though the reaction is complex.[28,50] In this regard, zeolites are seen to be valuable catalysts due to strong acidity, shape selectivity, and aromaticity for degradation of biomass.[47]

The catalytic co-pyrolysis enhances the aromatic content and reduces the coke formation.[51] The Diels-Alder reaction is dominant in the co-pyrolysis process. While, the Diels-Alder, hydrocarbon pool and hydrogen transfer mechanisms are dominant in the catalytic co-pyrolysis process.[52] The plastic, a hydrogen rich (high H/C_{eff} ratio) feedstock, provides a hydrogen atmosphere to the hydrocarbon pool inside the zeolite pores.[50,53] The interaction of cellulose/hemicellulose-derived furan derivatives with the olefins from plastic produces aromatic content (monomer or dimer compounds) by Diels-Alder reaction followed by dehydration.[51]

The use of wet-torrefied biomass in the catalytic co-pyrolysis with plastic (or hydrogen-rich compounds) [54]) could enhance the pyrolysis characteristics and quality of pyrolysis oil.[10,50,55] A clear increase in aromatics yield and decrease of char formation was observed with such a combination. Therefore, it was hypothesized that the CCP of torrefied biomass and LLDPE could result in better quality biofuels. Although the catalytic co-pyrolysis of torrefied biomass and plastic (hydrogen-rich source) is highly potential, the reported studies in this research area are scarce.

In the CCP, the acidity and topology of zeolites play an important role in the decomposition of biomass and plastic during catalytic copyrolysis process. For obtaining high quality biofuel, ZSM-5 is seen to be a valuable catalyst due to its strong acidity and shape selectivity for the degradation of biomass. It enhances the aromaticity and reduce coke formation due to strong acidity and shape selectivity.[47] The derivatives of oxygenates from lignin can effectively be eliminated using MesoHY as catalyst in the catalytic fast pyrolysis of lignin. For example, the 2,6-dimethoxyphenol and 1,2,3-trimethoxybenzene remained in the final products when ZSM-5 or MOR was used while completely disappeared when HY was used.[56] The product distribution during (hydro-)cracking of waste plastics is affected by acidity of FAU zeolite. The gasoline range hydrocarbons (C_5–C_{12}) are obtained at low silica-to-alumina ratio (SAR) and jet and diesel ranges hydrocarbons (C_8–C_{22}) are obtained at higher SAR.[57] The FAU zeolite has possessed higher ability to break C−C and C−O bonds and regenerability from coke. The deoxygenation for lignin macromolecule occurs at a faster rate over HY than that over HZSM-5, due to larger size pores (7.4 Å) and internal pore space (11.2 Å) of FAU. [13] The diffusional resistances are the major limitation in the CCP of biomass and plastic due to larger molecular sizes of the reactants. The mesoporous zeolites (pore size: 2–50 nm) resolve this issue.[58–60] The mesoporous HY zeolite (MesoHY) reduces most acidic and carbonyl compounds (which are responsible for the corrosiveness and instability) and boosts the amount

of desirable hydrocarbons (monoaromatic hydrocarbons (MAH), especially the BTEX) by Diels-Alder reactions.[59] Therefore, both MesoHY (FAU) and HZSM-5 (MFI) zeolites with silica alumina ratio of 80 are explored as potential catalysts in this study for the catalytic co-pyrolysis of (torrefied) biomass and plastic (LLDPE).

1.2 Literature Review

1.2.1 Theory

The pyrolysis of biomass is a complex process involving many reactions.[36,37] The rate of reaction depends upon three variables: temperature, the extent of fractional conversion, and pressure of the system[61], given as the following expression

$$\frac{d\alpha}{dt} = k(T)f(\alpha)h(p) \ldots \ldots \ldots \ldots \ldots \ldots \ldots \ldots \ldots \ldots \ldots \ldots \ldots \ldots \ldots \ldots \ldots \ldots \ldots \ldots .1.1$$

Neglecting the pressure dependence, since the operation is at negligible pressure drop, equation 1.1 can be modified as

$$\frac{d\alpha}{dt} = k(T)f(\alpha) \ldots \ldots \ldots \ldots \ldots \ldots \ldots \ldots \ldots \ldots \ldots \ldots \ldots \ldots \ldots \ldots \ldots \ldots \ldots \ldots \ldots \ldots ..1.2$$

Where k(T) is the Arrhenius constant (a function of temperature) and f(α) is the reaction model (a function of conversion). The temperature dependence of the rate constant follows the Arrhenius equation which is given below

$$k(T) = A\ exp\left(\frac{-E_\alpha}{RT}\right) \ldots \ldots \ldots \ldots \ldots \ldots \ldots \ldots \ldots \ldots \ldots \ldots \ldots \ldots \ldots \ldots \ldots \ldots \ldots \ldots \ldots .1.3$$

Substituting the value of k(T) in equation 1.1, the following equation is obtained:

$$\frac{d\alpha}{dt} = A\ exp\left(\frac{-E_\alpha}{RT}\right) f(\alpha) \ldots \ldots \ldots \ldots \ldots \ldots \ldots \ldots \ldots \ldots \ldots \ldots \ldots \ldots \ldots \ldots \ldots \ldots ..1.4$$

The equation 1.4 is applied as a tool for differential kinetics methods. It applies to any type of temperature program i.e. isothermal or non-isothermal process [62]. For constant heating rate (β = dT/dt), the equation 1.4 can be simplified as

$$\beta \frac{d\alpha}{dT} = A\, exp\left(\frac{-E_\alpha}{RT}\right) f(\alpha) \ldots\ldots\ldots\ldots\ldots\ldots\ldots\ldots\ldots\ldots\ldots\ldots\ldots\ldots\ldots\ldots\ldots\ldots 1.5$$

Integration of equation 1.4 or 1.5 results in the following equations

$$g(\alpha) = \int_0^\alpha \frac{d\alpha}{f(\alpha)} = A \int_0^t exp\left(\frac{E_\alpha}{RT}\right) dt \ldots\ldots\ldots\ldots\ldots\ldots\ldots\ldots\ldots\ldots\ldots\ldots\ldots\ldots 1.6$$

Or

$$g(\alpha) = \frac{A}{\beta} \int_0^T exp\left(\frac{E_\alpha}{RT}\right) dT \ldots\ldots\ldots\ldots\ldots\ldots\ldots\ldots\ldots\ldots\ldots\ldots\ldots\ldots\ldots\ldots\ldots 1.7$$

where, g(α) is the integral form of the reaction model. equation 1.7 does not have any exact analytical solution. Various approximations produced a significant number of approximate integral methods.[36]

1.2.1.1 Isoconversional methods

All isoconversional methods originate from isoconversional principle state that indicates that the rate of reaction at the constant extent of conversion is only the function of temperature.[61] This can be proven by the following equation

$$\frac{d\alpha}{dt} = k(T) f(\alpha) \ldots\ldots\ldots\ldots\ldots\ldots\ldots\ldots\ldots\ldots\ldots\ldots\ldots\ldots\ldots\ldots\ldots\ldots\ldots\ldots 1.8$$

By taking logarithmic derivatives of equation 1.8 at the constant extent of conversion (α). Thus,

$$\left[\frac{\partial\, ln\left(\frac{d(\alpha)}{dt}\right)}{\partial (T)^{-1}}\right]_\alpha = \left[\frac{\partial\, ln\, k(T)}{\partial (T)^{-1}}\right]_\alpha + \left[\frac{\partial\, ln\, f(\alpha)}{\partial (T)^{-1}}\right]_\alpha \ldots\ldots\ldots\ldots\ldots\ldots\ldots\ldots\ldots 1.9$$

At the constant extent of conversion (α), f (α) is also constant because of a given value of α, the above equation 1.9 can be expressed as

$$\left[\frac{\partial\, ln\left(\frac{d(\alpha)}{dt}\right)}{\partial(T)^{-1}}\right]_{\alpha} = \frac{-E_{\alpha}}{R} \ldots\ldots\ldots\ldots\ldots\ldots\ldots\ldots\ldots\ldots\ldots\ldots\ldots\ldots\ldots\ldots\ldots\ldots\ldots 1.10$$

From equation 1.10, it is concluded that Eα can be evaluated by taking the temperature dependence of isoconversional rate. Therefore, Isoconversional methods are also known as "model free" methods [61]. The model-free methods can be separated into two groups such as integral and differential isoconversional models. Kissinger-Akahira-Sunose (KAS) and Flynn-Wall-Ozawa (FWO) models are identified as integral and Friedman (FM) model comes under the category of differential isoconversional model.

Kissinger-Akahira-Sunose model (KAS) model

The KAS model is used to determine the kinetic parameters (E_α and A) of (co-)pyrolysis reaction, by using a mathematical approximation for the exponential term. The equation for the KAS model is given as [63–65]:

$$\ln\left[\frac{\beta}{T_{\alpha_i}^2}\right] = \ln\left[\frac{A_\alpha\, R}{E_\alpha\, g(\alpha)}\right] - \left[\frac{E_\alpha}{R\, T_{\alpha_i}}\right] \ldots\ldots\ldots\ldots\ldots\ldots\ldots\ldots\ldots\ldots\ldots\ldots\ldots\ldots\ldots\ldots\ldots\ldots 1.11$$

Where T_{α_i} and the subscript i represent the temperature at which the extent of conversion (α) is reached and the individual heating rate. The apparent activation energy (E_α) can be estimated from the slope [E_α/R] of the line when the graph was drawn between $\ln\left[\frac{\beta}{T_{\alpha_i}^2}\right]$ vs $\frac{1}{T_{\alpha_i}}$ for different fractional conversion levels (α).

Flynn-Wall-Ozawa model

Doyle's approximation is used in the FWO model to obtain an equation which is expressed as [63,65,66]:

$$\ln[\beta] = \ln\left[\frac{AE_\alpha}{Rg(\alpha)}\right] - 2.315 - 0.457\left[\frac{E_\alpha}{R\,T_{\alpha_i}}\right] \ldots\ldots\ldots\ldots\ldots\ldots\ldots\ldots\ldots\ldots\ldots\ldots\ldots\ldots 1.12$$

After plotting the graph $\ln[\beta]$ vs $\left[\frac{1}{T_{\alpha_i}}\right]$, E_α can be obtained from the slope of line $0.457\left[\frac{E_\alpha}{R}\right]$ at a particular value of conversion (α).

Friedman model

The equation for the Friedman model is as follows [65,67]:

$$ln\left[\frac{d\alpha}{dt}\right]_{\alpha_i} = \ln\left[\beta\frac{d\alpha}{dT}\right] = \ln[Af(\alpha)] - \left[\frac{E_\alpha}{R\,T_{\alpha_i}}\right] \ldots\ldots\ldots\ldots\ldots\ldots\ldots\ldots\ldots\ldots\ldots\ldots\ldots\ldots 1.13$$

E_α was determined by FM model from the slop of the line $\left[\frac{E_\alpha}{R}\right]$ by plotting the graph $\ln\left[\beta\frac{d\alpha}{dT}\right]$ vs $\left[\frac{1}{T_{\alpha_i}}\right]$.

1.2.1.2 Reaction mechanism from Criado's master plot method

In 1965, Ozawa used the concept of generalized time (θ) to understand the master plot method describing a solid-state reaction. This permits the use of master plot to analyze the reaction mechanism of solid-state reaction in an isothermal and non-isothermal process.[68] To construct the experimental master plot, the knowledge of activation energy and conversion rate (α) as a function of temperature is needed.[37] The experimental data is converted to an experimental master plot and compare with the theoretical master plot which is drawn by assuming various reaction mechanisms. This comparison helps us to select appropriate reaction mechanisms.[68] Based on the generalized concept of reaction time (θ), the Master plot can be categorized into three forms including differential, integral, and both.

The rate of solid-state reaction can be presented as the following equation

$$\frac{d\alpha}{dt} = A \exp\left(\frac{-E_{\alpha}}{RT}\right) f(\alpha) \ldots\ldots 1.14$$

where, α is the reacted fraction at time t; *f (α)* is a function that depends upon the reaction mechanism, E_{α} activation energy, A and T are the frequency factor and absolute temperature respectively.

By introducing generalized time (θ), the kinetic reaction rate at infinite temperature can be achieved as follows

$$\theta = \int_{0}^{t} exp\left(\frac{-E_{\alpha}}{RT}\right) dt \ldots\ldots 1.15$$

While θ is the reaction time taken to attain a particular value of conversion fraction (α) at infinite temperature. Differentiation of equation 1.15, we get

$$\frac{d\theta}{dt} = exp\left(\frac{-E_{\alpha}}{RT}\right) \ldots\ldots 1.16$$

Combining equation 1.15 and 1.16, the following equation obtained as

$$\frac{d\alpha}{d\theta} = A\, f(\alpha) \ldots\ldots 1.17$$

or

$$\frac{d\alpha}{d\theta} = \frac{d\alpha}{dt}\, exp\left(\frac{E_{\alpha}}{RT}\right) \ldots\ldots 1.18$$

Where dα/dθ is the generalized reaction rate, obtained by extrapolating the reaction rate in real-time, dα/dt to infinite temperature. Integration of equation 1.17 as follows

$$g(\alpha) = \int_{0}^{\alpha} \frac{d\alpha}{f(\alpha)} = A \int_{0}^{\theta} d\theta = A\,\theta \ldots\ldots 1.19$$

By taking reference α: 0.5, three forms of master plot such as the differential, integral, and both as presented by following equations 1.20, 1.21, and 1.23 respectively.

$$\frac{\left(\frac{d\alpha}{d\theta}\right)}{\left(\frac{d\alpha}{d\theta}\right)_{\alpha:0.5}} = \frac{f(\alpha)}{f(0.5)} \quad \ldots\ldots\ldots\ldots\ldots\ldots\ldots\ldots\ldots\ldots\ldots\ldots\ldots\ldots\ldots\ldots 1.20$$

$$\frac{g(\alpha)}{g(0.5)} = \frac{\theta}{\theta_{0.5}} \quad \ldots\ldots\ldots\ldots\ldots\ldots\ldots\ldots\ldots\ldots\ldots\ldots\ldots\ldots\ldots\ldots\ldots 1.21$$

$$\frac{\theta\left(\frac{d\alpha}{d\theta}\right)}{\theta_{0.5}\left(\frac{d\alpha}{d\theta}\right)_{\alpha:0.5}} = \frac{f(\alpha)\, g(\alpha)}{f(0.5)g(0.5)} \quad \ldots\ldots\ldots\ldots\ldots\ldots\ldots\ldots\ldots\ldots\ldots\ldots\ldots\ldots\ldots\ldots 1.22$$

$$\frac{Z(\alpha)}{Z(0.5)} = \frac{f(\alpha)\, g(\alpha)}{f(0.5)\, g(0.5)} = \left[\frac{T_\alpha}{T_{0.5}}\right]^2 \frac{(d\alpha/dt)_\alpha}{(d\alpha/dt)_{0.5}} \quad \ldots\ldots\ldots\ldots\ldots\ldots\ldots\ldots\ldots\ldots 1.23$$

The pyrolysis of fossil fuel or biomass is a complex process, the evaluation of such processes needs a significant number of reaction models. All of these models can be grouped into three major types such as accelerating, deaccelerating, and sigmoidal or autocatalytic. Each of these types has a characteristic "reaction profile or kinetic curve, shown in Table 1.1.[61] In an accelerating model, the weight loss rate increases with conversion throughout the process and reaches its maximum at the end of the process. The power-law model comes under this category and can be depicted as

$$f(\alpha) = n(\alpha)^{\frac{n-1}{n}} \quad \ldots\ldots\ldots\ldots\ldots\ldots\ldots\ldots\ldots\ldots\ldots\ldots\ldots\ldots\ldots\ldots\ldots\ldots\ldots\ldots 1.24$$

where, n is constant. In the deaccelerating model, the weight loss rate decreases continuously in the entire process. The order of reaction and diffusion model belongs to this type and the mathematical formula can be represented as

$$f(\alpha) = (1-\alpha)^n \quad \ldots\ldots\ldots\ldots\ldots\ldots\ldots\ldots\ldots\ldots\ldots\ldots\ldots\ldots\ldots\ldots\ldots\ldots\ldots\ldots 1.25$$

where, n is the order of the reaction. In sigmoidal model, the rate of reaction reaches its maximum point at some intermediate conversion level. The Avrami Erofeyev is applied to the model. It can be expressed as

$$f(\alpha) = n(1-\alpha)[-\ln(1-\alpha)]^{\frac{n-1}{n}} \quad \ldots\ldots\ldots\ldots\ldots\ldots\ldots\ldots\ldots\ldots\ldots\ldots\ldots\ldots\ldots\ldots\ldots\ldots\ldots\ldots\ldots\ldots 1.26$$

Avrami-Erofeyev (A) and power law (P) models come under the category of nucleation mechanism, which is related to the phase transformation that depends upon temperature, time, and heterogeneity of the material (edge dislocation, defects, surfaces, impurities).[69,70] The reaction between reactants from two different crystal lattices is often controlled by diffusion and its mechanism follows the diffusion (D) mechanism.[69] A complete list of soli-reaction models is given in Table 1.1.

Table 1.1. Various solid-state reaction mechanisms and corresponding expressions for f(α), g(α), and z(α).

Model	**Model code**	**differential form** $f(\alpha) = \frac{1}{k}\frac{d\alpha}{dt}$	**Integral form** $g(\alpha) = (kt)$	$z(\alpha) = f(\alpha) * g(\alpha)$
Nucleation model				
Power law	P2/3	$2/3(\alpha)^{-1/2}$	$(\alpha)^{3/2}$	$2/3(\alpha)^{-1/2} * (\alpha)^{3/2}$
Power law	P2 (n=1/2)	$2(\alpha)^{1/2}$	$(\alpha)^{1/2}$	$2(\alpha)^{1/2} * (\alpha)^{1/2}$
Power law	P3 (n=1/3)	$3(\alpha)^{2/3}$	$(\alpha)^{1/3}$	$3(\alpha)^{2/3} * (\alpha)^{1/3}$
Power law	P4 (n=1/4)	$4(\alpha)^{3/4}$	$(\alpha)^{1/4}$	$4(\alpha)^{3/7} * (\alpha)^{1/4}$
Avrami–Erofeyev	A2	$2(1-\alpha)[(-\ln(1-\alpha)]^{1/2}$	$[(-\ln(1-\alpha)]^{1/2}$	$2(1-\alpha)[(-\ln(1-\alpha)]^{1/2} * [(-\ln(1-\alpha)]^{1/2}$
Avrami–Erofeyev	A3	$3(1-\alpha)[(-\ln(1-\alpha)]^{2/3}$	$[(-\ln(1-\alpha)]^{1/3}$	$3(1-\alpha)[(-\ln(1-\alpha)]^{2/3} * [(-\ln(1-\alpha)]^{1/3}$
Avrami–Erofeyev	A4	$4(1-\alpha)[(-\ln(1-\alpha)]^{3/4}$	$[(-\ln(1-\alpha)]^{1/4}$	$4(1-\alpha)[(-\ln(1-\alpha)]^{3/4} * [(-\ln(1-\alpha)]^{1/4}$
Geometrical contraction model				
Contracting area	R2	$2(1-\alpha)^{1/2}$	$1-(1-\alpha)^{1/2}$	$2(1-\alpha)^{1/2} * 1-(1-\alpha)^{1/2}$
Contracting volume	R3	$3(1-\alpha)^{2/3}$	$1-(1-\alpha)^{1/3}$	$3(1-\alpha)^{2/3} * 1-(1-\alpha)^{1/3}$

Diffusion model				
1–D diffusion	D1	$\frac{1}{(2\alpha)}$	$(\alpha)^2$	$\frac{1}{(2\alpha)} * (\alpha)^2$
2–D diffusion	D2	$-\left[\frac{1}{\ln(1-\alpha)}\right]$	$[(1-\alpha)\ln(1-\alpha)]+\alpha$	$-\left[\frac{1}{\ln(1-\alpha)}\right] * [(1-\alpha)\ln(1-\alpha)]+\alpha$
3–D diffusion	D3	$\left[\frac{3(1-\alpha)^{1/2}}{2(1-(1-\alpha)^{1/3}}\right]$	$1-(2/3)\alpha-(1-\alpha)^{2/3}$	$\left[\frac{3(1-\alpha)^{1/2}}{2(1-(1-\alpha)^{1/3}}\right] * 1-(2/3)\alpha-(1-\alpha)^{2/3}$
Reaction order model				
Zero order	F0	1	α	$1^*\alpha$
First order	F1	$(1-\alpha)$	$-ln(1-\alpha)$	$(1-\alpha) * -ln(1-\alpha)$
Second order	F2	$(1-\alpha)^2$	$\left[\frac{1}{(1-\alpha)}-1\right]$	$(1-\alpha)^2 * \left[\frac{1}{(1-\alpha)}-1\right]$
Third order	F3	$(1-\alpha)^3$	$\frac{1}{2}\left[\frac{1}{(1-\alpha)^2}-1\right]$	$(1-\alpha)^3 * \frac{1}{2}\left[\frac{1}{(1-\alpha)^2}-1\right]$

1.2.2 Torrefaction of biomass

Chen et al. (2014) [71] torrefied the rice husk biomass at temperatures 200, 230, 260 and 290°C for 30 min and characterized the torrefied biomass using TG-FTIR, GCMS, and fast pyrolysis. They reported the removal of hemicellulose from the biomass and increased HHV (11−16 MJ kg^{-1}) upon torrefaction. In addition, the activation energy of pyrolysis of torrefied biomass decreases, in the range of 72−45 kJ mol^{-1}, with torrefaction temperature. Bach et al. (2015) [72] studied the effect of wet torrefaction (at T: 175, 200, 250°C; t: 5, 15, 30 min; and 70 bar) on the thermal behaviour and kinetics pyrolysis of woody biomasses namely, Norway spruce, and Birchwood. The torrefaction process improves the homogeneity of materials and also the HHV (from 20.2 to 23.0 MJ kg^{-1}). A lesser amount of volatiles release and the reduction of the activation energy are observed during the pyrolysis of torrefied biomass in comparison to those with raw biomass. Wang et al. (2016) [73] reported an increase of H/C_{eff} and HHV (12.7 to 19.3 MJ kg^{-1}) of hemicellulose model compound upon dry-torrefaction (T: 200–300°C and 30 min) by removal of small oxygenates. Zhang et al. (2016) [74] examined the effect of torrefaction of biomass (at T: 250–280°C and 20 min) on its pyrolysis. The authors found that

the activation energy increases with increasing torrefaction temperature. They also concluded that the pretreatment of biomass decreases the acids, ketones, aldehydes, and furan compounds while the content of sugars significantly increased, as shown by Py-GC-MS analysis of biomass. Wang et al. (2017) [75] performed the torrefaction (T: 200–300°C and 30 min) in a tubular reactor using cellulose as feedstock. They observed that the O/C ratio decreases because of the removal of small oxygenates by dehydration and decarboxylation reaction and found the improvement of heating value ranges from 15.2 to 16.4 MJ kg^{-1}. Zhang et al. (2018) [76] studied the torrefaction process (T: 200–300°C and 15–60 min) in a tubular furnace by using spent coffee grounds, Chinese medicine residue, and algae as feedstocks. They reported that the HHV increases due to the improvement of the H/C ratio and evolution of small oxygenates upon torrefaction. The rates of reactions to remove elements O, H, and C are as follows: deoxygenation (DO) > dehydrogenation (DH) > decarbonisation (DC). They also concluded that the biomass torrefaction with lower severity has higher energy efficiency. Bach et al. (2019) [77] used the TG analyzer to examine the thermal and kinetic behavior of industrial solid waste (ISW) and oilcloth waste as feedstock in the pyrolysis and non-isothermal torrefaction process. They used three torrefaction temperature ranges 235-265, 220-280, and 205-295°C for three different heating rates (0.5, 1, and 1.5°C min^{-1}) for 60 min and reported activation energy of 337−668 kJ mol^{-1} for ISW and 272-496 kJ mol^{-1} for oilcloth waste. Dacres et al. (2019) [78] investigated the influence of gas-pressurized (GP at 50 bar in an autoclave) and atmospheric (AP in fixed bed reactor) torrefaction using two feedstocks, rice straw and pine sawdust at 250°C for 15 min. The GP torrefied biomasses have lower activation energies in their pyrolysis as compared to those of raw and normal torrefied biomasses. Dai et al. (2019) [79] studied the torrefaction of corn cob at 240°C for 30 min in a tubular furnace in anoxic condition and catalytic fast pyrolysis of torrefied corn cob. They revealed that 8% Ni-ZSM-5 produced a maximum amount of aromatics (54.4%) than that over 11%Ni-ZSM-5. Singh et al.

(2020) [80] studied the torrefaction of Acacia nilotica (T: 220−280°C for 40 min) and examined the suitability of torrefied biomass for bioenergy generation. They found the activation energy of pyrolysis of torrefied biomass to be in the range of 122−42 kJ mol^{-1} (Entries 47–50, Table 1.2). Gan et al. (2021) [81] have studied the wet torrefaction of two microalgae species (Chlorella vulgaris ESP-31and FSP-E) at 160°C for 10 min in a microwave reactor in presence of 0.1M sulfuric acid solution. The authors reported that the activation energy of pyrolysis for raw and pretreated microalgae samples (with higher carbohydrate amounts) are found to be 221, 183 and 65 kJ mol^{-1} while the other species containing higher amounts of lipid exhibited reverse order (Entries 51–56, Table 1.2). A detailed list of torrefaction studies of lignocellulosic biomass reported in the literature are summarized in Table 1.2

Table 1.2. Reaction conditions and kinetics of catalytic and non-catalytic pyrolysis of torrefied and raw lignocellulosic biomass.

S No	FS-1	HHV (MJ kg^{-1})	Torrefaction (W/D)		TR (°C) (RR)	Catalyst	AE (E_α) or Range of AE (kJ mol^{-1})		Ref.
			T (°C) or TR and W/D	t (min)			E_α or RAE	Model Code Or methods	
1	Rice husk (RH)	11.0	–	–	30–700 (10–30; 3)	–	–	CR	[71]
2	Dried rice husk (DRH)	12.8	110	360	do	–	71.6	CR	
3	RH	13.6	200 (DT)	30	do	–	73.2	CR	
4	RH	14.3	230 (DT)	30	do	–	74.3	CR	
5	RH	15.6	260 (DT)	30	do	–	69.9	CR	
6	RH	16.2	290 (DT)	30	do	–	45.0	CR	
7	Raw spruce (RS)	20.42	–	–	30–700 (10)	–	108.0	–	[72]
8	Raw birch (RB)	19.94	–	–		–	111.8	–	
9	RS	20.8	175 (WT) F/W: 1/5	30	do	–	102.4	–	
10	RB	20.21	do	–	–	–	97.1	–	
11	RS	21.08	200 (WT) F/W: 1/5	10	do	–	93.3	–	

12	RB	20.01	do				96.1	–	
13	RS	21.33	200 (WT) F/W: 1/5	30	do	–	92.2	–	
14	RB	20.78	do				90.5	–	
15	RS	21.51	200 (WT) F/W: 1/5	60	do	–	91.2	–	
16	RB	20.51	do				90.0	–	
17	RS	22.97	225 (WT) F/W: 1/5	60	do	–	89.0	–	
18	RB	22.93	do	–	–		89.1	–	
19	Cellulose (CL)	14.95	–	–	25–800 (5–20; 4)	–	113.9 113.2	FWO Am − DAEM	
20	CL	15.18	200 (DT)	30	do	–	117.7 117.8	FWO Am − DAEM	
21	CL	15.26	225 (DT)	30	do	–	117.6 117.6	FWO Am − DAEM	[75]
22	CL	15.26	250 (DT)	30	do	–	116.9 117.0	FWO Am − DAEM	
23	CL	15.48	275 (DT)	30	do	–	116.2 116.0	FWO Am − DAEM	
24	CL	16.36	300 (DT)	30	do	–	125.2 119.5	FWO Am − DAEM	
25	Xylan (XYL) part of HCL	12.55	–	–	25–800 (20)	–	149.8	DG–DAEM	[73]

26	XYL	12.77	200 (DT)	30	do	–	150.9	DG–DAEM	
27	XYL	13.35	225 (DT)	30	do	–	172.3	DG–DAEM	
28	XYL	16.39	250 (DT)	30	do	–	172.5	DG–DAEM	
29	XYL	19.46	275 (DT)	30	do	–	167.0	DG–DAEM	
30	XYL	19.34	300 (DT)	30	do	–	166.6	DG–DAEM	
31	Rice husk (RH)	16.58	–	–	25–700 (10–40; 3)	–	146.3 148.4	ST FWO	
32	Water washing Rice husk (WRH)	–	60 F/W: 1g/70ml	360	do	–	136.1 138.8	ST FWO	[74]
33	WRH	–	250 (DT)	30	do	–	140.6 143.3	ST FWO	
34	WRH	–	280 (DT)	30	do	–	146.6 149.1	ST FWO	
35	Industrial solid waste (ISW)	19.97	235−265 (DT) at 0.5 RR	60	30–800 (20)	–	667.5	–	
36	Oil cloth waste (OCW)	20.61	do	do	do	–	495.8	–	
37	Industrial solid waste (ISW)	19.97	220–280 (DT) at 1.0 RR	60	do	–	336.7	–	[77]
38	Oil cloth waste (OCW)	20.61	do	do	do	–	272.3	–	
39	Industrial solid waste (ISW)	19.97	205–295 (DT) at 1.5 RR	60	do	–	361.5	–	

40	Oil cloth waste (OCW)	20.61	do	do	do	–	274.6	–	
41	Rice straw (RS)	–	–	–	25–900 (5–20; 3	–	213.3; 210.9 221.1	DAEM; FWO FM	[78]
42	Pine Saw dust (SD)	–	–	–	do	–	220.2; 218.9 230.9	DAEM; FWO FM	
43	RS	–	250 (DT)	30	do	–	195.4; 195.5 217.2	DAEM; FWO FM	
44	SD	–	do	do	do	–	279.2; 275.2 296.6	DAEM; FWO FM	
45	RS	–	250; 25Pa (DT)	30	do	–	202.3; 201.4 218.3	DAEM; FWO FM	
46	SD	–	do	do	do	–	181.4; 182.4 238.7	DAEM; FWO FM	
47	Acacia nilotica (AN)	18.66	–	–	25–800 (5–15; 3)	–	211.5; 221.6 216.8; 211.9	KAS; FWO FM; ST	[80]
48	AN	20.33	220 (DT)	40	do	–	241.6; 252.3 261.8; 241.8	KAS; FWO FM; ST	
49	AN	22.51	250 (DT)	40	do	–	185.1; 198.9 188.4; 185.5	KAS; FWO FM; ST	

50	AN	25.94	280 (DT)	40	do	–	121.8; 132.9 122.1; 122.3	KAS; FWO FM; ST	
51	Chlorella vulgaris (ESP-31)	20.8	–	–	30–800 (20)	–	117.0	–	[81]
52	Chlorella vulgaris (FSP-E)	20.9	–	–	do	–	85.6	–	
53	ESP-31	25.2	160 (WT) F/W: 1/5	10	do	–	116.1	–	
54	FSP-E	22.5	do	–	do	–	91.1	–	
55	ESP-31	31.7	do	–	do	H_2SO_4	121.1	–	
56	FSP-E	23.1	do	–	do	H_2SO_4	99.4	–	
57	Corn cob (CC)	–	240 (DT) F/C: 1/5	10	30–800 (10)	ZSM-5	70.1	RO	[79]
58	CC	–	do	do	do	MZSM-5 (M: meso.)	74.1	RO	
59	CC	–	do	do	do	NiMZSM-5; 2 wt. % Ni MS: $[Ni\ H_2O)_6]$ $(NO3)_2$	70.2	RO	
60	CC	–	do	do	do	NiMZSM-5; 5 wt. % Ni MS: $[Ni\ (H_2O)_6]$ $(NO3)_2$	68.1	RO	

61	CC	–	do	do	do	NiMZSM-5 8 wt. % Ni MS: [Ni $(H_2O)_6$] $(NO3)_2$	68.5	RO	
62	CC	–	–	–	do	NiMZSM-5; 11 wt. % Ni MS: [Ni $(H_2O)_6$] $(NO3)_2$	70.3	RO	
63	Water hyacinth (WH)	–	–	–	30–750 (10–40; 4)	–	65.3	FWO	[82]
64	WH	–	–	–	do	CaO (10%)	69.2	FWO	
65	WH	–	126 W	3	do	do	60.0	FWO	
66	WH	–	126 W	5	do	do	89.8	FWO	
67	WH	–	126 W	10	do	do	64.8	FWO	
68	WH	–	329 W	3	do	do	64.9	FWO	
69	WH	–	329 W	5	do	do	56.7	FWO	
70	WH	–	329 W	10	do	do	65.1	FWO	
71	WH	–	567 W	3	do	do	76.7	FWO	
72	WH	–	567 W	5	do	do	52.9	FWO	
73	WH	–	567 W	10	do	do	67.0	FWO	

74	Wood saw dust (SD)	–	–	–	30 – 600 (35–45; 3)	–	164.0; 166.0 162.4	KAS; FWO FM	[83]
75	SD	–	–	–	do	Sodium zirconate C/F:1/1	112.5; 117.3 116.7	KAS; FWO FM	
76	SD	–	–	–	do	Lithium silicate C/F:1/1	112.6; 116.7 113.7	KAS; FWO FM	
77	Municipal solid waste (MSW)	–	–	–	30–900 (10–30; 3)	–	179.6; 180.3	KAS; FWO	[84]
78	MSW	–	–	–	do	Iron ore (Hematite)	154.6; 151.8	KAS; FWO	
79	MSW	–	–	–	do	Iron oxide Fe_2O_3	154.0; 150.2	KAS; FWO	
80	Pine needle (PN)	–	–	–	30 – 800 (10–40; 4)	–	111 – 55.6 108 – 44.8	KAS FWO	[85]
81	PN	–	–	–	–	γ–Al_2O_3 C/F:1/1	38.1 – 90.0 42.3 – 97.6	KAS FWO	
82	PN	–	–	–	–	Ni/γ–Al_2O_3 C/F:1/1	18.5 – 86.3 23.3 – 93.9	KAS FWO	

Note: HHV: High Heating Value; F/W: Feed water ratio; C/F: Catalyst to Feed ratio; D/W: Dry or Wet torrefaction; T: Temperature (°C); t: Torrefaction time in minutes; TR: Temperature range (°C); RR: Ramp rate (°C min^{-1}); AE: Activation energy in kJ mol^{-1}; (E_α); RAE: Range of Activation energy; KAS: Kissinger-Akahira-Sunose model; FWO: Flynn-Wall Ozawa- model; FM: Friedman; CR: Coats- Redfern model; Am: Avrami −Erofeyev model; DG: Double Gaussian; DAEM: Distributed Activation Energy Model; RO: Reaction order model (F1 or F2 or F3); W: Unit of power;

1.2.3 Co-pyrolysis of lignocellulosic biomass and plastics

Chin et al. (2014) [86] studied the co-pyrolysis behaviour of rubber seed sell (RSS) and high-density polyethylene (HDPE). They reported that the blended sample exhibited positive synergism (ΔW nagetive) in a temperature range of 710−850 K. They also reported the activation energies for RSS, HDPE, and their mixture (RSS/HDPE) as 54, 264, and 49−70 kJ mol^{-1}, respectively. Bu et al. (2014) [87] studied the thermal behavior, kinetics and synergism of co-pyrolysis of cellulose (CE), hemicellulose (HCE), and lignin (LIG) with bituminous coal (BC) using a TG analyzer in the temperature of 30−950°C. They reported the activation energies of individual components CE, HCL, LIG, and BC as 135, 118, 185, and 271 kJ mol^{-1}, respectively, by the FWO model. The authors also estimated the activation energies of BC and CE mixture as 129, 113, and 123 kJ mol^{-1}. Similarly, the activation energy for other blended samples (BC and HCE) was calculated as 209, 105, and 247 kJ mol^{-1} (Entries 7–12, Table 1.3). Oyedun et al (2014) [88] studied the co-pyrolysis of plastic (PS and HDPE) and biomass (bamboo, empty fruit bunch, and sawdust) and reported the activation energies for the blended samples with blend ratio (BB:HDPE) of 4:1, 3:2, 2:3, and 1:4 w/w as 66−69 kJ mol^{-1} (Entries 16–26, Table 1.3). Gunasee et al. (2016) [89] studied the synergism and kinetics of co-pyrolysis of pine wood branches (BR) and cardboard (CB) with polypropylene (PP). The authors reported that the maximum values of ΔW for the mixture of lignocellulosic biomass with plastic are -3.5 and -4 wt% at 400 and 480°C, respectively. They also reported the activation energy of (co-)pyrolysis of individual and mixed samples as 160, 65 and 250 kJ mol^{-1} for lignocellulosic biomass (BR & CB) with PP by FM model (Entries 27–30, Table 1.3). Burra et al. (2018) [90] examined the kinetics of co-pyrolysis of pine wood (PW) with synthetic polymer (PP). They reported the activation energy of PP and PW as in the range of 100−294 and 122−260 kJ mol^{-1} by DAEM model. In addition, they reported the activation energies for mixed samples PW:PP (1:1 w/w) as in the range of 115−295 kJ mol^{-1}. Garba et al. (2018) [91]

studied the co-pyrolysis of Iroko wood fuel (WF) with polyethylene (LDPE and HDPE). The authors evaluated the activation energy of individual samples (WF, LDPE and HDPE) as 25, 148, and 250 kJ mol^{-1} and that for blends (WF/LDPE and WF/HDPE) as 37 and 96 kJ mol^{-1}, respectively. Chen et al. (2019) [92] studied the co-pyrolysis of tobacco stalk (TS) with polymers scrap tire (TS), PP, and polyvinyl chloride (PVC) and estimated the kinetics. They found the activation energy of individual feedstocks as 32, 46, 250, and 119 kJ mol^{-1} for ST, TS, PP, and PVC, respectively and those of blends TS:ST, TS:PP, and TS:PVC (with 1:1 w/w ratio) were 28, 80, and 48 kJ mol^{-1}, respectively (Entries 65–71, Table 1.3). Kai et al. (2019) [93] studied the co-pyrolysis of corn stalk (CS) and HDPE by using TG-FTIR-MS, analyzed the evolved gases from feedstock materials and explored the synergism. The strongest positive synergy was found with CS content 80 wt% in the blend of CS and HDPE. The gases including CH_4, C_2H_6, C_3H_8, C_4H_{10}, H_2, and CO/C_2H_4 were formed in the temperature range of 400-800°C. The activation energies of blends CS:HDPE (4:1 w/w), CS:HDPE (3:2), CS:HDPE (2:3) and CS:HDPE (1:4) were estimated to be 171, 208, 212, and 220 kJ mol^{-1}, respectively, by FWO model. Sun et al. [94] studied the kinetics, synergism and the product distribution of the co-pyrolysis of blends of wood fiber and polylactic acid (WF/PLA) by TG-FTIR-MS and Py-GCMS. The activation energy of the co-pyrolysis of blends was lower as compared to that of pyrolysis of individual feedstocks by at least 28% (Entries 92–96, Table 1.3). Wang et al. (2019) [95] examined the co-pyrolysis behavior of xylan (XYL) and PVC with different weight ratios of XYL:PVC blends (4:1, 3:2, 2:3, and 1:4 w/w). They studied the bio-oil composition by using a horizontal quartz tube reactor at different temperatures of 400, 500, and 600°C for the constant residence time of 10 min. They observed a lower amount of oxygenates during co-pyrolysis of blends than that of pyrolysis of xylan biomass only. The activation energy of the co-pyrolysis of the blend (1:4 w/w) was lower as compared to that of pyrolysis of individual feedstocks by 55% (Entries 97–103, Table 1.3). Varma et al. (2020) [96] studied the

thermochemical properties of pine needles (PN), Styrofoam (SF), and their blend with the ratio of 1:1. The average activation energy of the co-pyrolysis of blend was reduced by a factor of at least 2 compared to that of pyrolysis of individual feedstock. Chen et al. (2021) [97] explored the co-pyrolysis of microalgae Dunaliella salina (DS) and typical plastics (PP, PS, PET, and PVC) by employing TG-FTIR in a temperature range of 35−800°C. The authors noticed the evolution of carbon dioxide, carbonyl, alkyl, and aromatics during the co-pyrolysis of the blends. The average activation energy of the co-pyrolysis of blend was lowered by 6 folds compared to that of pyrolysis of individual feedstocks as estimated by the Arrhenius equation (Entries 107–115, Table 1.3).

Table 1.3. Reaction conditions and kinetics of non-catalytic co-pyrolysis of torrefied and raw lignocellulosic biomass (and its derivatives) with plastic

S No	FS-1* (wt.%)	FS-2# (wt.%)	HHV (MJ kg^{-1})	Torrefaction (W/D)		TR (°C) (RR)	AE (E_α) or Range of AE (k J mol^{-1})		Synergistic effect		Ref.
				T (°C) and W/D	t (min)		E_α or RAE	Model Code Or methods	ΔW (wt. %)	TR (°C) or T_{max}	
1	Rubber Seed Shell (RSS)	–	–	–	–	50–900 (10–50; 4)	54.4	F1	–	–	[98]
2	–	HDPE	–	–	–	do	264.1	F1	–	–	
3	RSS (20%)	HDPE (80%)	–	–	–	do	55.0	F1 at 10 RR	(-) 6.3	377−502	
4	RSS (20%)	HDPE (80%)	–	–	–	do	57.2	F1 at 20 RR	(+) 12.3	247−377	
5	RSS (20%)	HDPE (80%)	–	–	–	do	58.1	F1 at 30 RR	(+) 11.8	247−377	
6	RSS (20%)	HDPE (80%)	–	–	–	do	69.6	F1 at 50 RR	(+) 13.5	247−377	
7	Cellulose (CE)	–	–	–	–	25–950 (10–40; 3)	134.6	OFW	–	–	[87]
8	Hemicellulose (HCE)	–	–	–	–	do	117.7	OFW	–	–	
9	Lignin (LIG)	–	–	–	–	do	184.5	OFW	–	–	
10	–	Bituminous coal (BC)	–	–	–	do	271.4	OFW	–	–	

10	BC (25%)	CE (75%)	–	–	–	do	123.0	OFW	(-) 4.5 (+) 2.8	400 380	
11	BC (50%)	CE (50%)	–	–	–	do	113.1	OFW	(-) 10.79 (+) 6.2	400 400	
12	BC (75%)	CE (25%)	–	–	–	do	129.1	OFW	(-) 4.2	400	
13	Rubber Seed Shell (RSS)	–	–	–	–	50–900 (10–50; 4)	47.0–63.2	F1	–	–	[86]
14	–	HDPE	–	–	–	do	242.1–278.2	F1	–	–	
15	RSS (20%)	HDPE (80%)	–	–	–	–	49.2–83.1	F1	–	–	
16	Bamboo biomass (BB)		–	–	–	30–800 (10)	66.0	CR	–	–	[88]
17	–	PS	–	–	–	do	213.5	CR	–	–	
18	BB (80%)	PS (20%)	–	–	–	do	69.9	CR	–	–	
19	BB (60%)	PS (40%)	–	–	–	do	64.8	CR	–	–	
20	BB (40%)	PS (60%)	–	–	–	do	62.4	CR	–	–	
21	BB (20%)	PS (80%)	–	–	–	do	69.8	CR	–	–	
22	–	HDPE	–	–	–	do	253.6	CR			
23	BB (80%)	HDPE (20%)	–	–	–	do	68.6	CR	–	–	
24	BB (60%)	HDPE (40%)	–	–	–	do	66.4	CR	–	–	

25	BB (40%)	HDPE (60%)	–	–	–	do	65.4	CR	–	–	
26	BB (20%)	HDPE (80%)	–	–	–	do	65.1	CR	–	–	
27	Pine wood branch (BR)	–	–	–	–	25–1000 (20)	160	FM	–	–	[89]
28	Cardboard (CB)	–	–	–	–	do	65	FM	–	–	
29	–	PP	–	–	–	do	250	FM	–	–	
30	BR (100%) + CB (100%)	PP (100)	–	–	–	do	300–60	FM	(-) 3.5 (-) 4%	400 480	
31	Lignin (LIG)	–	–	–	–	25–900 (20)	33.56	CR	–	–	[99]
32	–	LDPE	–	–	–	do	296.0	CR	–	–	
33	–	PC	–	–	–	do	294.8	CR	–	–	
34	–	PS	–	–	–	do	309.6	CR	–	–	
35	LIG (50%)	LDPE (50%)	–	–	–	do	180.1	CR	–	–	
36	LIG (50%)	PC (50%)	–	–	–	do	73.1	CR	–	–	
37	LIG (50%)	PS (50%)	–	–	–	do	179.9	CR	–	–	
38	Pinewood (PW)	–	–	–	–	110–1000 (10–30; 3)	112–260	DAEM	–	–	[90]
39	–	PP	–	–	–	do	100–294	DAEM	–	–	

40	–	PETE	–	–	–	do	101–348	DAEM	–	–	
41	–	BPC	–	–	–	do	100–150	DAEM	–	–	
42	PW (50%)	PP (50%)	–	–	–	do	115–295	DAEM	–	–	
43	PW (50%)	BPC (50%)	–	–	–	do	105–295	DAEM	–	–	
44	PW (50%)	PETE (50%)	–	–	–	do	104–282	DAEM	–	–	
45	Iroko wood (WF)	–	–	–	–	30–900 (10)	24.6	AE	–	–	[91]
46	–	LDPE	–	–	–	do	147.5	AE	–	–	
47	WF (80%)	LDPE (20%)	–	–	–	do	29.1	AE	(-) 10.3 (+) 8.2	450 510	
48	WF (20%)	LDPE (80%)	–	–	–	do	137.1	AE	–	–	
49	–	HDPE	–	–	–	do	250.4	AE	–	–	
50	WF (80%)	HDPE (20%)	–	–	–	do	29.9	AE	(+) 8.2	510	
51	WF (20%)	HDPE (80%)	–	–	–	do	188.7	AE	–	–	
52	Pine wood (PW)	–	–	–	–	30–600 (10)	88.1	CR	–	–	[100]
53	–	PE	–	–	–	do	220.6	CR	–	–	
54	PW (75%)	PE (25%)	–	–	–	do	84.7	CR	–	–	

55	PW (50%)	PE (50%)	–	–	–	do	80.6	CR	–	–	
56	PW (25%)	PE (75%)	–	–	–	do	78.3	CR	–	–	
57	Chestnut shell (CNS)	–	–	–	–	25–1000 (5–40; 4)	175.2	DAEM	–	–	[101]
58		PS	–	–	–	do	208.9	DAEM	–	–	
59	CNS (50%)	PS (50%)	–	–	–	do	191.6	DAEM	–	–	
60	Yunnan pine (YP)	–	–	–	–	25–600 (5–60; 5)	185.9	OFW	–	–	[102]
61	Cellulose (CL)	–	–	–	–	do	168.3	OFW	–	–	
62	–	LDPE	–	–	–	do	249.9	OFW	–	–	
63	YP (50%)	LDPE (50%)	–	–	–	do	224.3	OFW	–	–	
64	CL (50%)	LDPE (50%)	–	–	–	do	201.6	OFW	–	–	
65	Tobacco Stalk (TS)	–	–	–	–	25–800 (10)	31.7	F1	–	–	[92]
66	Scrape Tire (ST)	–	–	–	–	do	46.1	F1	–	–	
67	–	PP	–	–	–	do	249.7	F1	–	–	
68	–	PVC	–	–	–	do	118.7	F1	–	–	
69	TS (50%)	ST (50%)	–	–	–	do	28.1	F1	–	–	

70	TS (50%)	PP (50%)	–	–	–	do	80.1	F1	–	–	
71	TS (50%)	PVC (50%)	–	–	–	do	48.2	F1	–	–	
72	Corn Stalk (CS)	–	–	–	–	25–900 (40)	48.5	D3	–	–	[103]
73	–	PE	–	–	–	do	313.8	D1	–	–	
74	–	Anthracite Coal (AC)	–	–	–	do	75.9	D3	–	–	
75	CS (20%)	PE (20%) + AC (60%)	–	–	–	do	88.4	D1	–	–	
76	CS (60%)	PE (20%) + AC (20%)	–	–	–	do	73.4	D1	–	–	
77	CS (10%)	PE (40%) + AC (50%)	–	–	–	Do	83.9	D1 and D3	–	–	
78	CS (50%)	PE (40%) + AC (10%)	–	–	–	do	49.0	D1 and D3	–	–	
79	CS (10%)	PE (60%) + AC (30%)	–	–	–	do	99.0	D1 and D3	–	–	
80	CS (30%)	PE (60%) + AC (10%)	–	–	–	do	70.8	D1 and D3	–	–	
81	Corn Stalk (CS)	–	–	–	–	35–850 (5–30; 4)	177.3 176.4	OFW KAS	–	–	[104]
82	–	HDPE	–	–	–	do	229.0 228.2	OFW KAS	–	–	
83	CS (80%)	HDPE (20%)	–	–	–	do	170.7 168.6	OFW KAS	(-) 2.97	280–390	

84	CS (60%)	HDPE (40%)	–	–	–	do	208.1 207.3	OFW KAS	(-) 1.87 (+) 4.2	280–390 480–510	
85	CS (40%)	HDPE (60%)	–	–	–	do	211.5 210.3	OFW KAS	(-) 0.40 (+) 7.5	280–390 480–510	
86	CS (20%)	HDPE (80%)	–	–	–	do	220.3 219.2		(-) 0.76 (+) 4.5	280–390 280–390	
87	Rice husk (RH)	–	–	–	–	25 – 800 (20)	82.8 7.2 54.8	JDE AEE CR	–	–	[105]
88	–	Sewage sludge (SS)	–	–	–	do	68.1	JDE	–	–	
89	RH (70%)	SS (30%)	–	–	–	do	65.8 4.0 27.2	JDE AEE CR	–	–	
90	RH (50%)	SS (50%)	–	–	–	do	59.7 3.0 18.7	JDE AEE CR	–	–	
91	RH (30%)	SS (70%)	–	–	–	do	57.2 2.0 26.3	JDE AEE CR	–	–	
92	Poplar Wood Fiber (PWF)	–	–	–	–	30–700 (10–40; 4)	139.0–214.0 137.2–214.2 137.0–214.0	OFW ST DAEM	–	–	[94]
93	–	PLA	–	–	–	do	179.0–209.0 178.3–209.0 178.0–209.0	OFW ST DAEM	–	–	
94	PWF (40%)	PLA (60%)	–	–	–	do	121.0–200.9 117.1–201.0	OFW ST	–	–	

							117.0– 206.7	DAEM			
95	PWF (30%)	PLA (70%)	–	–	–	do	129.0–171.6 126.0–170.3 125.4–170.0	OFW ST DAEM	–	–	
96	PWF (20%)	PLA (80%)	–	–	–	do	140.0–154.0 138.0–151.0 137.5–151.6	OFW ST DAEM	–	–	
97	Xylan (Xyl)	–	–	–	–	30–700 (20)	70.5	CR	–	–	[95]
98	–	PVC	–	–	–	do	168.2	CR	–	–	
99	Xyl (80%)	PVC (20%)	–	–	–	do	122.5	CR	–	–	
101	Xyl (60%)	PVC (40%)	–	–	–	do	110.3	CR	–	–	
102	Xyl (40%)	PVC (60%)	–	–	–	do	94.9	CR	–	–	
103	Xyl (20%)	PVC (80%)	–	–	–	do	76.3	CR	–	–	
104	Pine Needles (PN)	–	–	–	–	35–850 (5–20; 3)	79.1 71.0 228.2	OFW KAS FM	–	–	[106]
105	–	Styrofoam (SF)	–	–	–	do	210.8 209.0 202.9	OFW KAS FM	–	–	
106	PN (50%)	SF (50%)	–	–	–	do	109.7 96.4 202.9	OFW KAS FM	–	–	

107	Dunaliella salina (DS)	–	–	–	–	35–800 (20)	50.2	F1	–	–	[97]
108	–	PP	–	–	–	do	289.4	F1	–	–	
109	–	PS	–			do	249.9	F1	–		
110	–	PET	–	–	–	do	280	F1	–	–	
111	–	PVC	–	–	–	do	115.4	F1	–	–	
112	DS (50%)	PP (50%)	–	–	–	do	85.2	F1	–	–	
113	DS (50%)	PS (50%)	–	–	–	do	84.7	F1	–	–	
114	DS (50%)	PET (50%)	–	–	–	do	44.5	F1	–	–	
115	DS (50%)	PVC (50%)	–	–	–	do	52.2	F1	–	–	
116	Vine pruning (VP)	–	16.9	–	–	30–900 (20)	53.0	CR	–		[107]
117	VP	–	–	300 (DT)	30	do	51.7	CR	–	–	
118	Olive pruning (OP)	–	17.83			do	47.3	CR	–	–	
119	OP	–	–	300 (DT)	30	do	58.9	CR	–	–	
120	Corn stalk (CS)	–	18.1			do	108.1	CR	–	–	
121	CS	–	–	300 (DT)	30	do	75.5	CR	–	–	

122	Boiler litter BL)	–	14.4			do	32.8	CR	–	–	
123	BL	–	–	300 (DT)	30	do	39.1	CR	–	–	
124	Laying hens litter (LL)	–	12.1			do	42.2	CR	–	–	
125	LL	–	–	300 (DT)	30	do	53.6	CR	–	–	
126	–	Lignite (LN)	25.1	–	–	do	38.3	CR	–	–	
127	LL (25%) + BL (25%)	LN (50%)	–	–	–	do	49.1	CR	–	–	
128	OP, CS & VP each 25%	LN (25%)	–	–	–	do	48.2	CR	–	–	
129	OP, CS, VP, LL & BL; each 17%	LN (15%)	–	–	–	do	45.4	CR	–	–	
130	Camphor (CAM)	–	18.8	–	–	30–800 (10–40; 4)	96.9–100.4	CR	–	–	[108]
131	CAM (85%)	Caster (CAS:15%)	–	–	–	do	94.1–97.9	CR	–	–	
132	CAM (70%)	CAS (30%)	–			do	88.1–92.6	CR	–	–	
133	CAM	–	18.9	240 (DT)	–	do	104.6–105.4	CR	–	–	
134	CAM	–	20.5	270 (DT)	–	do	98.3–107.6	CR	–	–	
135	CAM	–	22.4	300 (DT)	–	do	78.8–86.3	CR	–	–	

136	CAM (85%)	CAS (15%)	–	240 (DT)	–	do	97.3–106.9	CR	–	–	
137	CAM (70%)	CAS (30%)	–	240 (DT)	–	do	90.8–101.8	CR	–	–	
138	CAM (85%)	CAS (15%)	–	270 (DT)	–	do	95.4–101.0	CR	–	–	
139	CAM (70%)	CAS (30%)	–	270 (DT)	–	do	83.3–103.3	CR	–	–	
140	CAM (85%)	CAS (15%)	–	300 (DT)	–	do	75.8–77.9	CR	–	–	
141	CAM (70%)	CAS (30%)	–	300 (DT)	–	do	74.9–79.6	CR	–	–	
142	Microwave torrefied lignin (MTL)	–	–	–	–	25–550 (40)	41.4	CR	–	–	[109]
143	–	LDPE	–	–	–	do	91.8	CR	–	–	
144	MTL (70%)	LDPE (30%)	–	–	–	do	51.5	CR	–	–	
145	Sugarcane bagasse (RBG)	–	–	–	–	30–800 (20)	313.6	PBCR	–	–	[110]
146	RBG	–	–	–	–	do	37.5	PBCR	–	–	
147	–	HDPE	–	–	–	do	389.4	PBCR	–	–	
148	–	EVA	–	–	–	do	127.7	PBCR	–	–	
149	–	PS	–	–	–	do	267.7	PBCR	–	–	

150	–	TIRE (TE)	–	–	–	do	69.0	PBCR	–	–	
151	TBG (70%)	HDPE (30%)	–	–	–	do	192.1	PBCR	–	–	
152	TBG (70%)	EVA (30%)	–	–	–	do	148.3	PBCR	–	–	
153	TBG (70%)	PS (30%)	–	–	–	do	158.7	PBCR	–	–	
154	TBG (70%)	TE (30%)	–	–	–	do	110.9	PBCR	–	–	

Note: FS-1*: Feedstock-1 (wt.% or ratio); FS-2$^{\#}$: Feedstock-2 (wt.% or ratio); HHV: Higher heating values (MJ kg^{-1}); D/W: Dry or Wet torrefaction; T: Temperature (°C); t: Torrefaction time in minutes; TR: Temperature range (°C); RR: Ramp rate (°C min^{-1}); AE: Activation energy in kJ mol^{-1}; (E_α); RAE: Range of Activation energy; KAS: Kissinger-Akahira-Sunose model; FWO: Flynn-Wall Ozawa- model; FM: Friedman; CR: Coats- Redfern model; DAEM: Distributed Activation Energy Model; AH: Arrhenius equation; JDE: Jander diffusion eqn.; AEE: Avrami Erofeyev eqn.; CA: Chemical reaction model (F1 or F2 or F3); (+) Syn.: Positive Synergism; (-) Syn.: Inhibitive Synergism; PE: PBCR: Phase boundary controlled reaction; HDPE: High density polyethylene; PS: Polystyrene; PP: Polypropylene; LDPE: Low density polyethylene; PC: Polycarbonate; PETE: Polyethylene terephthalate; BPC: Black polycarbonate; PE: Polyethylene; PVC: Polyvinyl chloride; PLA: Polylactic acid; PET: Polyethylene terephthalate; EVA: Ethyl vinyl acetate

1.2.4 Catalytic co-pyrolysis (CCP) of torrefied biomass with plastic

Lee et al. (2016) [111] studied the effect of catalyst (HZSM-5 and H-β) on the co-pyrolysis of torrefied cellulose (TCL) and PP with different combinations of biomass and plastic (3:1, 1:1, and 1:3 w/w) by employing Py-GCMS/TCD/FID-system at 550°C. A higher amount of aromatics was obtained from catalytic pyrolysis of TCL than that of raw cellulose (CL) due to structural change of cellulose and formation of intermediates. Further, they reported the higher amount of BTEX yield (33.4%) during catalytic co-pyrolysis of torrefied cellulose with PP. Zhou et al. (2017) [112] examined the influence of potassium content on the thermochemical properties, synergism, and kinetics of the (co-)pyrolysis of individual (wood sawdust: WS and LDPE) and blended (mass ratio 1:1) samples. The potassium treated WS/LDPE mixture with 5 wt% potassium acetate exhibited the highest positive synergism (ΔW = -24.2%). The activation energy of WS treated with potassium content (1.25, 2.5, 3.75, and 5 wt%) was found as 103, 105, 113, and 114 kJ mol^{-1}, respectively. The K-treated blends exhibited higher activation energy in their co-pyrolysis as compared to that of pyrolysis of K-treated WS (Entries 1–11, Table 1.4). Xiang et al. (2018) [113] studied the thermal behavior, synergism, and kinetics of the co-pyrolysis of rice straw (RS) and LLDPE (4:1 w/w) over Ni modified ZSM-5 catalyst (25 wt%). The maximum synergism (ΔW) for RS/LLDPE, CE/LLDPE, and LIG/LLDPE was reported as -6.2, -18.2, and -9.8 wt%, respectively. The activation energies for blends were computed as 56, 164, and 34 kJ mol^{-1} by Arrhenius equation (Entries 12–19, Table 1.4). Wang et al. (2018) [114] investigated the synergism and kinetics of the catalytic co-pyrolysis (CCP) of cellulose (CE) and polyethylene (PE) mixture (1:1 w/w) over different transition metals, namely Mn, Fe, Co, and Ni. They reported that the initial thermal decomposition temperature of CE and PE in the mixture reduced by 91−136°C and 8-15°C, respectively. The maximum positive synergism (ΔW) for mixture of CE and PE over different transition metal catalysts during CCP (CE/PE-Ni, CE/PE-Co, CE/PE-Fe, and CE/PE-Mn) was

determined as -9.3% at 279°C, -11.7% at 238°C, -14.1% at 258°C and -12.9% at 244°C, respectively. The activation energies for pyrolysis of CE in presence of transition metal catalysts were 52, 45, 32, and 42 kJ mol^{-1} and those of CCP of blends were 57, 70, 49, and 62 kJ mol^{-1}, respectively (Entries 33–42, Table 1.4). Chi et al. (2018) [115] studied the catalytic pyrolysis and CCP of cellulose (CE) and polypropylene (PP) and their blends (CL:PP 3:1 w/w) over MCM-41 and Al-MCM-41 (feedstock:catalyst ratio 1:10 w/w), for a residence time of 18 s. They reported a higher yield of furan and aromatics (MAH) over both the catalysts due to the presence of higher number of active centres (Brønsted and Lewis acids). The activation energy for the blend over the two catalysts was determined as 114 and 138 kJ mol^{-1} by the Coats-Redfern model (Entries 20–25, Table 1.4). Kumar et al. (2019) [116] studied the CCP of ground nut shell with waste plastic, PP and PS (feed ratio 1:1 w/w) over FCC catalyst (10 wt%). The experiment was carried out at 510°C in a semi batch reactor. A maximum aromatic selectivity of 49% with PP and 82% with PS was reported in the CCP. Xu et al. (2020) [117] studied the thermal degradation behavior, synergism, and kinetics of CCP of enteromorpha proliferate (EP) and HDPE over HZSM-5, at 500 and 550°C for 30 min. They reported that the higher yield of bio-oil produced over HZSM-5 catalyst as compared to the non-catalytic process. The bio-oil obtained over HZSM-5 has a lower concentration of acids, oxygenates, and nitrogen-containing compounds and significantly higher light-hydrocarbons and aromatics. Further, the activation energy of CCP of blend (1:1 w/w) was determined as 109 kJ mol^{-1} by FM model (Entries 50–53, Table 1.4). Zhao et al. (2020) [118] examined the synergy in the CCP of cellulose (CE) and PE (1:1 w/w) over HZSM-5 (feed to catalyst ratio 4:1 w/w), at 650°C for 30 min. The maximum synergism (ΔW) was found as -0.15 wt% in CCP. Zhong et al. (2021) [119] studied the thermal behavior and kinetics of the CCP of WH and HDPE (3:1, 1:1, and 1:3 w/w) over HZSM-5 (feed to catalyst ratio 1:1 w/w). The maximum synergism (ΔW) for WH3:1 was reported as -22.3 for CCP and -6.2 wt% for co-pyrolysis. The activation

energy for WH and HDPE was determined as 121.2 and 263 kJ mol^{-1} in absence of the catalyst by FWO model. Furthermore, activation energy of CCP of blends followed the order of WH (1:3) > WH (1:1) > WH (3:1) > WH (3:1) (Entries 70–75, Table 1.4). Lin et al. (2021) [120] investigated the co-pyrolysis and CCP of raw and torrefied poplar wood (TPW) and HDPE over hierarchical HZSM-5 in a fixed bed reactor at 550°C for 20 min under inert atmosphere. The yield of bio-oil in CCP of raw PW/HDPE was 48.7% which was lower than that from non-catalytic co-pyrolysis due to further cracking of the vapors by zeolite active sites to generate small oxygenates such as CO, CO_2, and HCOOH. In addition, they also observed a higher amount of monoaromatics (BTEX) produced during CCP of TPW/HDPE as compared to that in non-catalytic process. The role of alkali and alkaline earth metal halides in lignocellulosic biomass degradation is summarized in Table 1.5.

Table 1.4. Reaction conditions and kinetics of catalytic co-pyrolysis of torrefied and raw lignocellulosic biomass (and its derivatives) with plastic.

S No	FS-1* (wt. %)	FS-2# (wt. %)	HHV (MJ kg^{-1})	Torrefaction (W/D)		Catalyst (wt %)	TR (°C) (RR)	AE (E_α) or Range of AE (k J mol^{-1})		Synergistic effect		Ref.
				T (°C) and W/D	t (min)			E_α or RAE	MC or methods	ΔW (wt. %)	TR (°C) or T_{max}	
1	Biomass wood saw dust (WS)	–	–	–	–	CH_3COOK (1.25)	30–700 (10)	103	F1	–	–	[112]
2	WS	–	–	–	–	CH_3COOK (2.5)	do	105	F1	–	–	
3	WS	–	–	–	–	CH_3COOK (3.75)	do	113	F1	–	–	
4	WS	–	–	–	–	CH_3COOK (5.0)	do	114	F1	–	–	
5	WS	–	–	–	–	AOC	do	98	F1	–	–	
6	–	LDPE	–	–	–	–	do	307	F1	–	–	
7	WS (50%)	LDPE (50%)	–	–	–	AOC	do	113–411	F1	(-) 17.5	480	
8	WS (50%)	LDPE (50%)	–	–	–	CH_3COOK (1.25)	do	117–294	F1	(-) 6.5 (+) 2.6	480 360	
9	WS (50%)	LDPE (50%)	–	–	–	CH_3COOK (2.5)	do	122–487	F1	(-) 22.8	480	
10	WS (50%)	LDPE (50%)	–	–	–	CH_3COOK (3.75)	do	129–410	F1	(-) 21.2 (+) 3.8	480 360	

11	WS (50%)	LDPE (50%)	–	–	–	CH_3COOK (5.0)	do	133–384	F1	(-) 24.2	480	
12	Rice straw (RS)	–	–	–	–	CoZSM-5 (25)	25–600 (30)	101.3	–	–	–	[113]
13	–	LLDPE	–	–	–	–	do	266.7	–	–	–	
14	RS (80%)	LLDPE (20%)	–	–	–	AOC	do	46.7	–	(-) 6.2 (+) 6.8	480 350	
15	RS (80%)	LLDPE (20%)	–	–	–	CoZSM-5 (25)	do	55.7	–	–	–	
16	CL (80%)	LLDPE (20%)	–	–	–	AOC	do	224.3	–	(-) 18.2 (-) 9.8	350 460	
17	CL (80%)	LLDPE (20%)	–	–	–	CoZSM-5 (25)	do	164.0	–	–	–	
18	LIG (80%)	LLDPE (20%)	–	–	–	AOC	do	34.0	–	(-) 9.8	450	
19	LIG (80%)	LLDPE (20%)	–	–	–	CoZSM-5 (25)	do	34.3	–	–	–	
20	Cellulose (CL)	–	–	–	–	AOC	50–900 (10–30; 3)	218–215; 264	FM CR	–	–	[115]
21	CL	–	–	–	–	MCM41; (C/F:10/1)		333–74.6; 149	FM CR	–	–	
22	–	PP	–	–	–	AOC	do	219–200; 281	FM CR	–	–	
23	–	PP	–	–	–	MCM41 (C/F:10/1)	do	58.8–102; 114	FM CR	–	–	
24	CL	–	–	–	–	Al-MCM41 (C/F:10/1)	do	228–284; 206	FM CR	–	–	

25	–	PP	–	–	–	Al-MCM41 (C/F:10/1)	do	81.3–72.4; 138	FM CR	–	–	
26	Corn Stover (CS)	–	–	–	–	AOC	30 – 800 (10)	73.5	F1	–	–	[96]
26		HDPE	–	–	–	AOC	do	253	F1	–	–	
27	Cellulose (CL)		–	–	–	AOC	do	152	F1	–	–	
28	CS (50%)	HDPE (50%)	–	–	–	AOC	do	177.3	F1	(-) 7.8	482	
29	CS (50%)	HDPE (50%)	–	–	–	HZSM-5 (C/F:1/4)	do	152.5	F1	–	–	
30	CS (50%)	HDPE (50%)	–	–	–	Ni-HZSM-5 (5); (C/F:1/4);	do	159.3	F1	–	–	
31	CS (50%)	HDPE (50%)	–	–	–	Ni-HZSM-5 (10); (C/F:1/4)	do	161.3	F1	–	–	
32	CS (50%)	HDPE (50%)	–	–	–	Ni-HZSM-5 (10); (C/F:1/4);	do	164.3	F1	–	–	
33	Cellulose (CL)	–	–	–	–	AOC	30 – 750 (10)	209	F1	–	–	[114]
34	–	PE	–	–	–	AOC	do	154	F1	–	–	

35	CL	–	–	–	–	$[Ni(H_2O)_6](NO3)_2$ C/F: 1/1	do	52	F1	–	–	
36	CL	–	–	–	–	$[Co(H_2O)_6](NO3)_2$ C/F: 1/1	do	45	F1	–	–	
37	CL	–	–	–	–	$[Fe(H_2O)_9](NO3)_3$ C/F: 1/1	do	32	F1	–	–	
38	CL	–	–	–	–	$[Mn(H_2O)_4](NO3)_2$ C/F: 1/1	do	42	F1	–	–	
39	CL (50%)	PE (50%)	–	–	–	$[Ni(H_2O)_6](NO3)_2$ C/F: 1/1	do	57.0	F1	(-) 9.3 (+) 12.1	279 456	
40	CL (50%)	PE (50%)	–	–	–	$[Co(H_2O)_6](NO3)_2$ C/F: 1/1	do	70.0	F1	(-) 11.7 (+) 6.2	238 468	
41	CL (50%)	PE (50%)	–	–	–	$[Fe(H_2O)_9](NO3)_3$ C/F: 1/1	do	49.0	F1	(-) 14.1 (+) 1.3	258 453	
42	CL (50%)	PE (50%)	–	–	–	$[Mn(H_2O)_4](NO3)_2$ C/F: 1/1	do	62.0	F1	(-) 13.9 (+) 8.4	244 447	
43	Pine saw dust (PSD)	–	–	–	–	AOC	25–600 (5–60; 5)	202	OFW	–	–	[121]

44	Cellulose (CL)	–	–	–	–	AOC	do	169	OFW	–	–	
45	–	LDPE	–	–	–		do	250	OFW	–	–	
46	PSD (50%)	LDPE (50%)	–	–	–	HZSM-5 (25) C/F: 2/1	do	173	OFW	(-) 23.5	451	
47	PSD (50%)	LDPE (50%)	–	–	–	AOC	do	224	OFW	–	–	
48	CL (50%)	LDPE (50%)	–	–	–	AOC	do	202	OFW	(-) 21.4	325	
49	CL (50%)	LDPE (50%)	–	–	–	HZSM-5 (25) C/F: 2/1	do	167	OFW	(-) 9.9	451	
50	Enteromorpha *prolifera* (EP)	–	–	–	–	AOC	30–800 (10–40; 4)	229.5 229.0 229.2 228.8 229.4	FM KAS FWO VYZ DAEM	–	–	
51	–	HDPE	–	–	–	–	do	146.4 146.3 146.3 146.1 146.3	FM KAS FWO VYZ DAEM	–	–	[117]
52	EP (50%)	HDPE (50%)	–	–	–	AOC	do	120.3 119.9 119.9 119.9 120.1	FM KAS FWO VYZ DAEM	–	–	

53	EP (50%)	HDPE (50%)	–	–	–	HZSM-5 C/F: 2/1	do	109.1 106.7 108.8 108.6 108.9	FM KAS FWO VYZ DAEM	–	–	
54	Cellulose (CL)	–	–	–	–	AOC	30–600 (30)	–	–	–	–	[118]
55	–	PE	–	–	–	–	do	–	–	–	–	
56	CL (50%)	PE (50%)	–	–	–	AOC	do	–	–	(-) 0.09	370	
57	CL (50%)	PE (50%)	–	–	–	HZSM-5 C/F: 4/1	do	–	–	(-) 0.15	460	
58	Lignin (LIG)	–	–	–	–	–	30–900 (10–40; 4)	26.4	F1	–	–	[122]
59	–	PE	–	–	–	–	do	190.5	F1	–	–	
60	LIG (50%)	PE (50%)	–	–	–	AOC	do	65.6	F1	(-) 6.3 (+) 8.3	445 486	
61	LIG (50%)	PE (50%)	–	–	–	$[Ni(H_2O)_6](NO3)_2$ C/F: 0.5/1	do	52.9	F1	(-) 6.3	520	
62	LIG (50%)	PE (50%)	–	–	–	$[Co(H_2O)_6](NO3)_2$ C/F: 0.5/1	do	31.1	F1	(-) 5.4 (+) 6.4	432 506	
63	LIG (50%)	PE (50%)	–	–	–	$[Fe(H_2O)_9](NO3)_3$	do	50.8	F1	(-) 5.9 (+) 6.9	445 484	

						C/F: 0.5/1						
64	LIG (50%)	PE (50%)	–	–	–	$[Mn(H_2O)_4](NO3)_2$ C/F: 0.5/1	do	57.9	F1	(-) 4.1 (+) 6.1	455 488	
65	LIG (80%)	PE (20%)	–	–	–	$[Ni(H_2O)_6](NO3)_2$ C/F: 0.5/1	do	47.7	F1	–	–	
66	LIG (67%)	PE (33%)	–	–	–	$[Ni(H_2O)_6](NO3)_2$ C/F: 0.5/1	do	54.1	F1	–	–	
67	LIG (50%)	PE (50%)	–	–	–	$[Ni(H_2O)_6](NO3)_2$ C/F: 0.5/1	do	52.9	F1	–	–	
68	LIG (33%)	PE (67%)	–	–	–	$[Ni(H_2O)_6](NO3)_2$ C/F: 0.5/1	do	65.4	F1	–	–	
69	LIG (20%)	PE (80%)	–	–	–	$[Ni(H_2O)_6](NO3)_2$ C/F: 0.5/1	do	66.6	F1	–	–	
70	Water hyacinth (WH)	–	–	–	–	AOC	30–800 (15–35; 3)	121.2 114.4	FWO KAS	–	–	[119]
71	–	HDPE	–	–	–	AOC	do	263.0 264.1	FWO KAS	–	–	
72	WH (75%)	HDPE (25%)	–	–	–	AOC	do	90.3 81.7	FWO KAS	(-) 6.2 (-) 6.8	342 494	
73	WH (50%)	HDPE (50%)	–	–	–	AOC	do	206.4 199.5	FWO KAS	(+) 16.2	515	

74	WH (25%)	HDPE (75%)	–	–	–	AOC	do	311.1 327.3	FWO KAS	–	–	
75	WH (75%)	HDPE (25%)	–	–	–	HZSM-5 C/F: 1/1	do	70.5 61.3	FWO KAS	(-) 22.3	483	
76	Cellulose (CL)	–	–	–	–	AOC	30–700 (5) T: 550°C	–	–	BTX	Low	[111]
77	CL	–	–	250 (DT)	60	HZSM-5 C/F: 1:1	T: 550°C	–	–	BTX	High	
78	–	PP	–	–	–		do	–	–	–	–	
79	CL	PP	–	–	–	HZSM-5 SAR:30, 50, 80 C/F: 3:1	do	–	–	BTEX	High	
80	CL	PP	–	–	–	HBEA SAR: 25 C/F: 3:1	do	–	–	BTEX	High	
81	Yellow poplar (YP)	–	–	250 (DT)	30	HZSM-5 SAR: 30 Al-MCM-41 C/F: 1:1; 10:1	30–700 (20) T: 550°C	–	–	BTX	High	[50]
82	–	HDPE	–	–	–	HZSM-5 SAR: 30 Al-MCM-41 C/F: 1:1; 10:1	do	–	–	–	–	
83	TYP (50%)	HDPE (50%)	–	–	–	HZSM-5 SAR: 30 Al-MCM-41	do	–	–	BTEX	High	

						C/F: 1:1; 10:1						
84	Cork oak (Oak)	–	–	–	–	HY (30) C/F: 1:1	30–700 (10) T: 550°C	–	–	OXY	Low	
85	Torrefied cork oak (TOak)	–	–	250	–	M-HY1 & M-HY2 SAR:30 C/F: 1:1	do	–	–	OXY	High	[55]
86	–	HDPE	–	–	–	M-HY1 & M-HY2 SAR:30 C/F: 1:1	do	–	–	MAH	High	
87	Raw Sugarcane bagasse (RSB)	–	–	–	–	ZSM-5 C/F: 2:22 T1: 180-320°C FR:(BOG1) T2: 320-450°C FR:(BOG2) T3: 450-700°C FR:(BOG3)	30–800 (10)	–	–	–	–	[123]
88	SB	–	–	180	30	do	do	–	–	MAH	Medium	
89	SB	–	–	200	30	do	do	–	–	MAH	Medium	
90	SB	–	–	240	30	do	do	–	–	MAH	Medium	
91	SB	–	–	270	30	do	do	–	–	MAH	Medium	

92	TSB (70%)	HDPE (30%)	–	–	–	do	do	–	–	MAH	Medium	
93	Poplar wood (PW)	–	–			T: 550	30–800 (10) T: 550°C	–	–	–	–	[120]
94	PW	–	–	220	30	HZSM-5 SAR: 35 0.2-HZSM-5 0.3-HZSM-5 0.4-HZSM-5 C/F: 1:1	do	–	–	BTX	Medium	
95	PW	–	–	240	30	do	do	–	–	BTX	Medium	
96	PW	–	–	260	30	do	do	–	–	BTX	Medium	
97	PW	–	–	280	30	do	do	–	–	BTX	Medium	
98	TPW (50%)	HDPE (50%)	–	–		do	do	–	–	BTEX	High	

Note: FS-1*: Feedstock-1 (wt %); FS-2#: Feedstock-2 (wt %); HHV: Higher heating values (MJ kg^{-1}); D/W: Dry or Wet torrefaction; T: Temperature (°C); t: Torrefaction time in minutes; TR: Temperature range (°C); RR: Ramp rate (°C min^{-1}); AE: Activation energy in kJ mol^{-1}; (E_α); RAE: Range of Activation energy; AOC: Absence of catalyst; KAS: Kissinger-Akahira-Sunose model; FWO: Flynn-Wall Ozawa- model; FM: Friedman; CR: Coats- Redfern model; DAEM: Distributed Activation Energy Model; T_{max}: Maximum peak temperature; Chemical reaction model (F1 or F2 or F3); (+) Syn.: Positive Synergism; (-) Syn.: passive or inhibitive Synergism; C/F; Catalyst to feed ratio; BOG: Bio-oil grades; BTEX: Benzene; Toluene, Ethyl benzene, Xylene; OXY: Oxygenates; MAH: Monoaromatics; HDPE: High density polyethylene; PP: Polypropylene; LDPE: Low density polyethylene; LLDPE: Linear low density polyethylene; PE: Polyethylene;

Table 1.5. Role of alkali and alkaline earth metal halides in the degradation of lignocellulosic biomass and its derivatives.

S NO	Feed Stock (FS)	Alkali or alkaline salts or carbonate	Process Parameters: T, t	TR (°C) (RR)	Major Findings	Ref.
1	Cellulose (CL)	$(CH_3COO)_2Ca$: 0.006, 0.02, 0.05, 0.15 & 0.3 mmol per CL $(CH_3COO)_2Mg$, CH_3COONa, CH_3COOK	–	–	➢ The yield of aromatic and olefin decreases with increasing conc. of AAEM salts and follow the order $K^+ +> Na^+ +> Ca^{2+} +> Mg^{2+}$ ➢ The formation of a higher amount of non-condensable gas and char occurs resulting in less condensable organic vapor suitable for catalytic deoxygenation ➢ AAEMs enhance the cleavage of several bonds in the pyranose ring leading to small oxygenates in competition with the cleavage of glycosidic linkages leading to the formation of LVG	[124]
2	Rice husk (RH)	NaCl: 1, 2, 3, 4 and 5 wt% of RH	T: 350°C; t: 60 min;	–	➢ Sodium chloride suppresses the generation of LVG and promotes cellulose degradation	[125]

					➢ It enhances the formation of ketones and organic acid by decarbonylation and decarboxylation reactions ➢ It improves the heating value of bio-oil (27.09 MJ kg^{-1})	
3	Cellobiose as a model compound	AAEMs (Na^+, K^+, Mg^{2+}, Ca^{2+})	DFT Calculation with Gaussian code, Set (M06-CX with 6−31 + G (2d, p)	–	➢ Mg2+ reduces the Eα barrier of glycosidic bond breaking which consist of glycosylation, trans glycosylation, ring contraction, and mannose pathways ➢ Mg2+ and Ca2+ inhibit dehydration reactions ➢ Absence of AAEMs, breaking of glycosidic bonds occurs by direct trans glycosylation and two-step dehydration pathway resulting LVG formation	[126]
4	Rubber wood (RW)	K_2CO_3: 0.004M, 0.008, 0.012, 0.022 & 0.036M	T:150, 200, 250 & 300°C (DT) t: 120 min	105–800°C (20)	➢ The potassium salt is responsible for the cleavage of hydrogen bonds and glycosidic linkages ➢ Solid residue increases from 13.4 to 38.1 wt.% due to poly-	[127]

					condensation reactions facilitated by impregnated alkali metals ➢ Alkali modifies the cellulose reactivity and lowers the decomposition temperature	
5	Microcrystalline Cellulose (MCL), Alpha Cellulose (ACL)	NaCl, HCl, and NaOH F/A: 1g/100ml F/ B: 1g/100ml F/ S: 1g/100ml	T: 300°C; t: 50 min; Super-heated steam	–	➢ Sodium metal reduce Levoglucosan quantity by inhibiting terminal hydroxyl group contained cellulose	[128]
6	Corn cob lignin (CCL)	AAEMS (Na, K, Mg and Ca) F/MS: 1g/20ml	T: 550°C @ 10; PY t: 50 min	30–800°C (10)	➢ AAEMs improve the bio oil composition ➢ Bio-oil consist of phenol, o-cresol, p-cresol, and catechol ➢ It involves demethylation, demethoxylation, or alkyl substitution reactions ➢ AAEMs loaded char having an excellent hierarchical porous structure	[129]

7	Beech wood xylan (DX)	Na^+ doped XYL (0.4, 0.5, and 1.1 wt% of Na^+)	T: 400 −7 00°C τ: 2 sec	30–700°C (5)	➢ Maximum weight loss rate and devolatilization temperature XYL was reduced by alkali metal (Na^+) ➢ The rate of formation of various acids including CH_3CH_2COOH, CH_3COOH, HCOOH was increased due to the presence of alkali metals by dehydration and rearrangement reaction ➢ Na^+ ion favours the ring-opening and rearrangement of xylose ring to furan derivatives ➢ Alkali metal enhance the yield of char by polycondensation reactions	[130]
8	Typical biomass	AAEM halides (NaCl, KCl, $MgCl_2$, $CaCl_2$) F/MH: 1/5	T: 550°C @ 10; PY t: 120 min	–	➢ AAEM halides improve carbon retention in biochar during pyrolysis ➢ percentage of C-retention in biochar as following the order	[131]
	Cow manure (CM)	AAEM halides	–	–		

		(NaCl, KCl, $MgCl_2$, $CaCl_2$) F/MH: 1/5			$MgCl_2$ (64.1 wt%) > $CaCl_2$ (60.7 wt%) NaCl (53.7 wt%) > KCl (52.5 wt%) > Biomass (49.8 wt%)	
9	Acid washing corn cob (ACS)	KCl: 0.05M, 0.1, 0.15 & 0.30M	–	–	➢ It promotes 2° reactions due to which the yield of gas and char increased by the expense of liquid fraction ➢ It promotes the scission of HDPE by improving alkene production ➢ The coupling effect of K and HZSM-5 favours the formation of monoaromatics (toluene and xylene) and suppress the formation of alkyl naphthalene (PAHs)	[132]
	ACS +HDPE (1:1)	–	T: 550°C @ 10; CPY; t: 20 min	100–800°C (10)		
	ACS +HDPE (1:1)	KCl: 0.05M	do	do		
	ACS +HDPE (1:1)	KCl: 0.10M	do	do		
	ACS +HDPE (1:1)	KCl: 0.15M	do	do		
	ACS +HDPE (1:1)	KCl: 0.30M	do	do		
	ACS +HDPE (1:1)	HZSM-5 (1)	do	–		
10	Bamboo powder (BP)	Molten alkali carbonate (MC): Li_2CO_3, Na_2CO_3, $CaCO_3$	T: 450°C; PY; t: 20 min	–	➢ Biochar obtained by MC pyrolysis possess a large BET surface area, porous structure, and higher aromatic hydrogen sites ➢ MC weakened inter and intramolecular hydrogen bonding found in cellulose and hemicellulose	[133]
	MBC	MC: 3:Li_2CO_3, : 3Na_2CO_3, : 4K_2CO_3	T: 450, 500, 550 & 600°C	–		

					➢ MC related biochar hydrolyze cellulose to produce a higher yield of total reducing sugars (52.8%) and glucose (43.5%)	
11	Rice straw (RS)		P: 800W; t: 8 min	–	➢ AAEM species reduce the decomposition temperature and rate of individual and mixed samples ➢ K_2CO_3 promote decomposition and condensation of lignin ➢ Alkaline earth metals bring down activation energy because of the uniform distribution of K_2CO_3 in mixed samples	[134]
	RS: AB	Alkaline base (AB): 0,1,5 &10 wt%)	do	–		
	RS: KC	Potassium carbonate (KC): 0,1,5 &10 wt%)	do	–		
Note: DT: Dry torrefaction; (HR): Number of heating rate is used e.g. (;3 or 4); PP: Process Parameters; F/S: Feed salt ratio; F/A: Feed acid ratio; AAEM: Alkali and Alkaline Earth Metal species; Tau (τ): Residence time; MH: Metal halides; P: Power in a micro reactor (W)						

1.3 Knowledge Gap and Objectives

Based on the literature review, it is clear that the lignocellulosic biomass (agriculture residue, forest materials, crop residue and various grasses family species) is a potential renewable energy source and has high potential for the replacing the fossil fuels. It also reduces CO_2 by closing the carbon cycle quickly through photosynthesis, increases energy security and supports sustainable development. A total of 220 and 0.686 billion tons/year of LCB is being produced worldwide and in India, respectively. The North-East India is one of the regions with richest biodiversity in the world. The highest amount of bamboo biomass (34%) is available in the North-East India among all the states in India. Moreover, bamboo is among the fastest growing plants, can tolerate adverse climatic conditions such as acidic soil. [135,136] The LCB consists majorly of hemicellulose, cellulose, lignin and minor amounts of extractives and ash.

The solid biomass cannot directly be used as fuel in industrial applications, because of several drawbacks including hygroscopic nature, high moisture content, high oxygen content, low heating value, lower grindability, low bulk density, fewer compositional homogeneity and lower resistance to biological degradation. Recently, the thermochemical conversion processes such as catalytic and non-catalytic (co-)pyrolysis has got increased attention to convert biomass into biofuel. The biofuel obtained from the pyrolysis of raw biomass is inferior and the process itself is inefficient due to heteropolymeric nature of the hemicellulose present in the biomass. Therefore, it was hypothesized that the selective removal of hemicellulose by wet-torrefaction would help in improving the biofuel quality as well as overall economics of the process due to extra useful product (xylose) formation in the process.

The addition of plastic also improves the biofuel characteristics and mitigates the plastic pollution. There are various reports on co-pyrolysis of lignocellulosic biomass (such as Pine wood, Bamboo biomass, Rice husk, Rubber seed shell and Yellow Poplar) and plastic (such as

HDPE, LDPE, PP, PS and PET).[93,95,97,106] However, the co-pyrolysis of raw (or torrefied) bamboo biomass with linear low density polyethylene (LLDPE) has not been reported for the production of fuels. The linear low-density polyethylene is highly suitable for co-pyrolysis with (torrefied) bamboo sawdust because of higher H/C_{eff} (2.16 mol/mol), lower melting temperature range (125−128°C) and as compared to LDPE, PP and HDPE.[36] It provides different volatiles at low temperature which further react with biomass for degradation of cellulose and lignin.[48]

Further, the addition of catalyst improves the biofuel quality by forming desired products such as aromatics (BTEX). Various studies performed on the catalytic co-pyrolysis of biomass and plastic indicate that the catalyst addition improves the biofuel quality in terms of aromaticity, yield, selectivity and minimization of coke.[59] To the best of my knowledge, the reports on the use of linear low density polyethylene (LLDPE) as a co-feed along with the (torrefied) bamboo sawdust feed in the co-pyrolysis process is scarce in the open literature. Moreover, no literature reports are present on the use of catalytic torrefaction of bamboo sawdust to remove hemicellulose selectively in the form of xylose.

Objectives of the thesis

Based on the literature review and research gaps as discussed above, the following objectives have been formulated:

❖ Pre-treatment of bamboo biomass by wet-torrefaction to selectively remove hemicellulose in the form of xylose and to form hydrochar.

❖ Kinetics, reaction mechanism and synergism study of co-pyrolysis of raw bamboo biomass and linear low density polyethylene (LLDPE).

❖ Kinetics, reaction mechanism and synergism study of co-pyrolysis of wet-torrefied bamboo biomass and LLDPE.

❖ Kinetics, reaction mechanism and synergism study of catalytic co-pyrolysis of wet-torrefied bamboo biomass and LLDPE over HZSM-5 zeolite.

❖ Kinetics, reaction mechanism and synergism study of catalytic co-pyrolysis of wet-torrefied bamboo biomass and LLDPE over MesoHY zeolite.

1.4 Organization of the Thesis and Major Findings

The contents of this thesis have been organized into seven chapters based on the results of experimental work carried out during the complete course of the research period.

CHAPTER 1: Background of the work and Research Objectives

This chapter includes the problem statement, literature survey, research gaps and objectives.

CHAPTER 2: Materials and Methods

This chapter summarizes the materials used, the bamboo biomass and plastic sample preparation. In addition, this chapter also describes the wet torrefaction procedure and product quantification by HPLC. The characterization of the solid sample obtained after wet-torrefaction using various characterization techniques including FTIR, XRD and FESEM. Furthermore, the procedure for the proximate and ultimate analyses of BSD, TBSD, and LLDPE is also included in this chapter. The thermal behavior determination procedure of the individual or mixed samples with or without catalyst using thermogravimetric analyzer, under the non-isothermal conditions at four different heating rates (5−40°C min^{-1}) from 30 to 800°C in presence of the inert atmosphere, is also included. The isoconversional models, such as KAS, FWO, and FM models, employed to determine the apparent activation energy for individual

and mixed samples are discussed. The procedure for the reaction mechanism determination using Criado's master plot method are detailed.

CHAPTER 3: Co-Pyrolysis of Bamboo Sawdust and Plastic: Synergistic Effects and Kinetics

In this chapter, the co-pyrolysis of bamboo sawdust (BSD) and linear low-density polyethylene (LLDPE) is reported by using a thermogravimetric analyzer at three different heating rates (5, 10 and 20°C min^{-1}) in the temperature range of 30–900°C under non-isothermal conditions. The bamboo sawdust and LLDPE were mixed at various mass ratios and termed as BP3:1 (75 wt.% BSD and 25 wt.% LLDPE), BP1:1 (50 wt.% BSD and 50 wt.% LLDPE), and BP1:3 (25 wt.% BSD and 75 wt.% LLDPE). The interaction between biomass and plastic was evaluated. The highest positive synergism was observed with the blend BP1:3. The mean values of apparent activation energy ($\bar{E}_\alpha$) for the decomposition of blends (BP3:1, BP1:1 and BP1:3) were determined to be 357, 371 and 143 $kJ \cdot mol^{-1}$ from KAS, 368, 400 and 165 $kJ \cdot mol^{-1}$ from OFW and 468, 356 and 255 $kJ \cdot mol^{-1}$ from FM, respectively. The decomposition of the blend BP1:3 followed a nucleation growth (A2) model in the lower conversion range and a diffusion (D2) model in the higher conversion range.

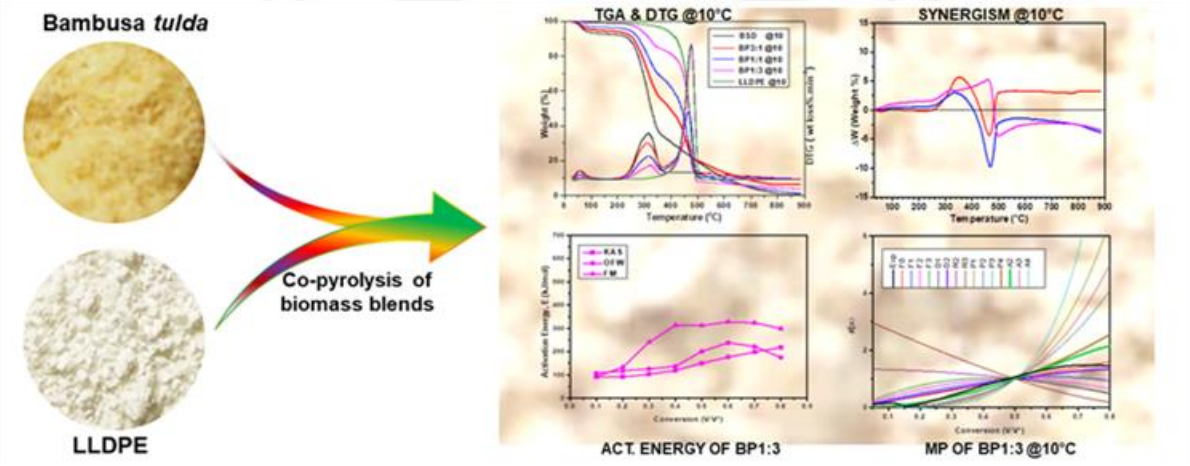

CHAPTER 4: Wet Torrefaction of Bamboo Sawdust (BSD) and Its Co-Pyrolysis with Plastic

In this chapter, the results of wet torrefaction (of BSD) and co-pyrolysis (of torrefied BSD and plastic) are reported. The wet torrefaction of BSD was carried out in presence of an organic acid and sodium chloride and observed that the hemicellulose part of the biomass was selectively removed in the form of xylose. The best torrefaction activity, with xylose yield 85% and complete removal of hemicellulose, was obtained with formic acid:BSD 1:1 and NaCl:BSD 3:1 w/w, at temperature 140°C and time 30 min. The blend with one part hydrochar and three parts LLDPE (TBP1:3) showed the highest positive synergism during co-pyrolysis at 40°C min^{-1} heating rate. The average apparent activation energies (as calculated using isoconversional method: KAS model) of co-pyrolysis of blended samples (TBP3:1, TBP1:1, and TBP1:3) were found to be 207, 264, 245 kJ mol^{-1}, respectively. The Criado's master plot showed the reaction mechanism of co-pyrolysis to be multistep. For example, the co-pyrolysis of the blend TBP1:3 followed the trend of two-dimensional Avrami-Erofeyev model (A2) at lower conversions, diffusion-reaction model (D2) at high conversions and end with a first-order reaction.

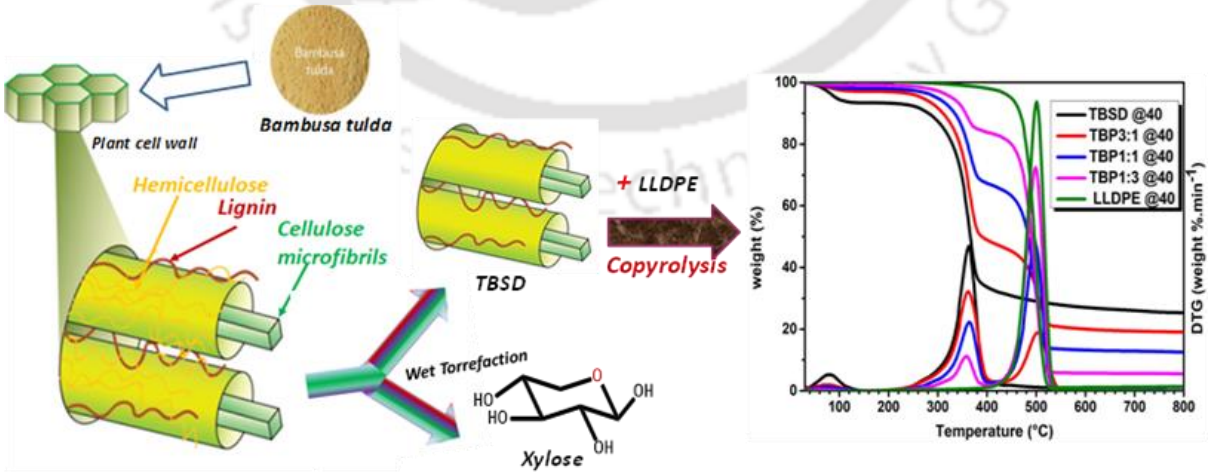

CHAPTER 5: Catalytic Co-pyrolysis of Wet-Torrefied Bamboo Sawdust and Plastic over the Zeolite H-ZSM-5: Synergistic Effects and Kinetics

Chapter 5 delineated the catalytic co-pyrolysis of TBSD and LLDPE over HZSM-5. The TBP1:3 showed positive synergism at 20°C min^{-1} and obtained the highest ΔW value about -1.47 wt%. The average apparent activation energies ($\bar{E}_\alpha$) of catalytic pyrolysis of TBSD, and LLDPE were 187 and 147 kJ mol^{-1}, respectively, from the KAS model. Those of catalytic co-pyrolysis (CCP) of blends TBP3:1, TBP1:1 and TBP1:3 were 163, 135 and 133 kJ mol^{-1}, respectively. The CCP of TBP1:3 and TBP1:1 showed synergism between TBSD and LLDPE in terms of E_α and TBP1:3 (TBSD: LLDPE 1:3 w/w) showed the highest synergism with the least $\bar{E}_\alpha$. The CCP mechanism of samples with a higher fraction of TBSD was more complex, as depicted from Criado's master plot. The probable reaction pathways of cellulose, lignin, LLDPE and their blends during catalytic pyrolysis and co-pyrolysis are also included in this chapter.

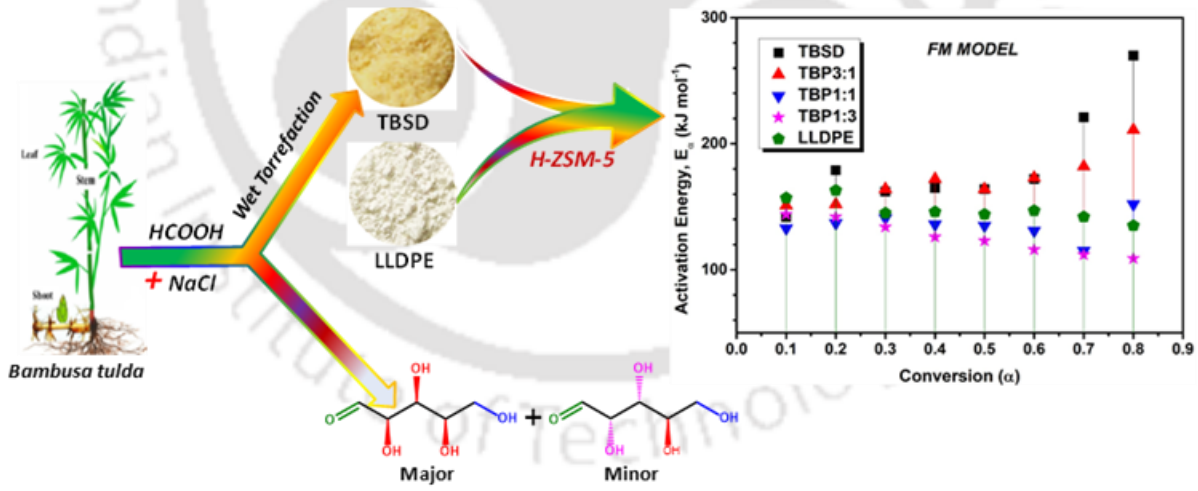

CHAPTER 6: Catalytic Co-Pyrolysis of Wet-Torrefied Bamboo Sawdust and Plastic over the Zeolite HY: Synergism and Kinetics

In this chapter, the catalytic (co-)pyrolysis of wet torrefied biomass sawdust (TBSD), linear low-density polyethylene (LLDPE), and their blends over zeolite MesoHY (MesoHY: 60 wt. %) is reported. In catalytic pyrolysis of TBSD, three thermal degradation stages were observed over HY catalyst including moisture removal. The moisture removal stage extends from 30 to 150°C. While, the catalytic co-pyrolysis of blends exhibited four degradation stages. The peak decomposition temperature of catalytic pyrolysis (CP) of LLDPE over MesoHY (FAU) was reduced by 251°C as compared to that over HZSM-5 and the enhancement can be attributed to the topology of MesoHY. The activation energies were calculated using isoconversional models. The $\bar{E}_\alpha$ of the blends TBP3:1, TBP1:1, and TBP1:3 were 171, 128, and 117 kJ mol^{-1}, respectively, from the KAS model. The $\bar{E}_\alpha$ of the blends was much lower as compared to that of TBSD, indicating a clear synergism. A multistep mechanism was observed in both CP of individual samples and CCP of blends, as analysed by Criado's master plot. For example, the CCP of TBP1:3 followed geometric (volume) contraction (R3) and first-order reaction models at low and high conversions, respectively.

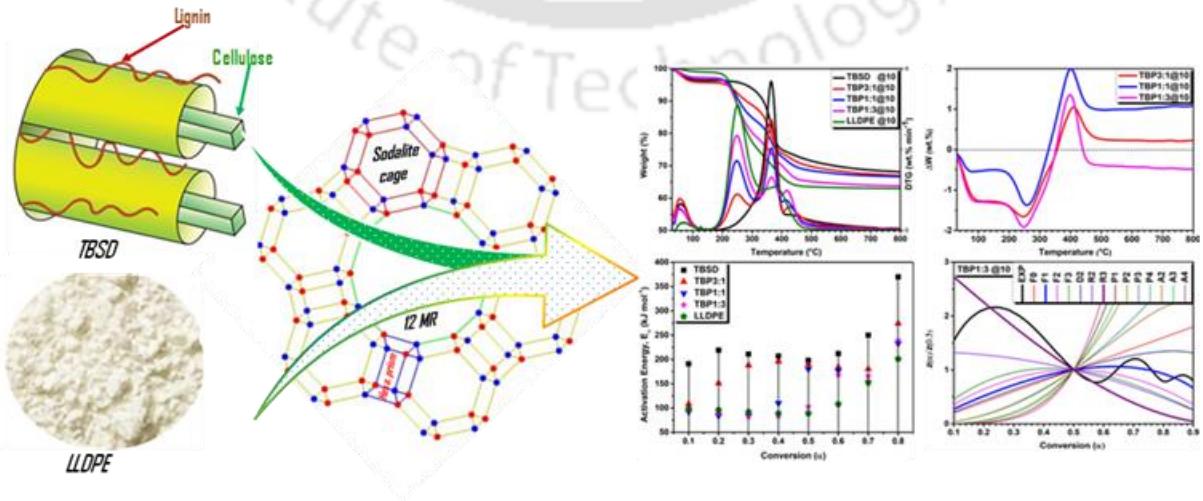

CHAPTER 7: Major Findings and Future Directions

The key findings of the research work carried out are summarized in this chapter. After that, the recommendations for the future work directions are appended with a brief outline of the limitations of the present work.

References

[1] R. Miandad, M.A. Barakat, M. Rehan, A.S. Aburiazaiza, I.M.I. Ismail, A.S. Nizami, Plastic waste to liquid oil through catalytic pyrolysis using natural and synthetic zeolite catalysts, Waste Manag. 69 (2017) 66–78. https://doi.org/10.1016/j.wasman.2017.08.032.

[2] S. Zhang, S. Zhu, H. Zhang, X. Liu, H. Zhang, Evaluation of pyrolysis behavior and products properties of rice husk after combined pretreatment of washing and torrefaction, Biomass and Bioenergy. 127 (2019) 105293. https://doi.org/10.1016/j.biombioe.2019.105293.

[3] S. Zhang, T. Chen, Y. Xiong, Q. Dong, Effects of wet torrefaction on the physicochemical properties and pyrolysis product properties of rice husk, Energy Convers. Manag. 141 (2017) 403–409. https://doi.org/10.1016/j.enconman.2016.10.002.

[4] C. Tang, C. Li, J. Yuan, K. Tran, Q. Bach, Wet torrefaction of biomass for high quality solid fuel production : A review, Renew. Sustain. Energy Rev. 91 (2018) 259–271. https://doi.org/10.1016/j.rser.2018.03.097.

[5] S. Raza, R. Tariq, Z. Hameed, I. Ali, M. Naqvi, W. Chen, S. Ceylan, H. Rashid, J. Ahmad, S.A. Taqvi, M. Shahbaz, Pyrolysis of high ash sewage sludge : Kinetics and thermodynamic analysis using Coats-Redfern method, Renew. Energy. 131 (2019)

854–860. https://doi.org/10.1016/j.renene.2018.07.094.

[6] B. Muneer, Influence of in-situ and ex-situ HZSM-5 catalyst on co-pyrolysis of corn stalk and polystyrene with a focus on liquid yield and quality, J. Clean. Prod. (2019).

[7] Z. Hameed, Z. Aman, S.R. Naqvi, R. Tariq, I. Ali, A.A. Makki, Kinetic and Thermodynamic Analyses of Sugar Cane Bagasse and Sewage Sludge Co-pyrolysis Process, Energy & Fuels. 32 (2018) 9551–9558. https://doi.org/10.1021/acs.energyfuels.8b01972.

[8] S. Wen, Y. Yan, J. Liu, M. Buyukada, F. Evrendilek, Pyrolysis performance , kinetic , thermodynamic , product and joint optimization analyses of incense sticks in N2 and CO2 atmospheres, Renew. Energy. 141 (2019) 814–827. https://doi.org/10.1016/j.renene.2019.04.040.

[9] M. Sajjad, M. Aamer, C. Liu, A. Tawab, F. Bai, C. Sakdaronnarong, J. Xu, S. Abdulaziz, M. Gull, Bioenergy potential of Wolffia arrhiza appraised through pyrolysis , kinetics , thermodynamics parameters and TG-FTIR-MS study of the evolved gases, Bioresour. Technol. 253 (2018) 297–303. https://doi.org/10.1016/j.biortech.2018.01.033.

[10] E.B. Hassan, I. Elsayed, A. Eseyin, Production high yields of aromatic hydrocarbons through catalytic fast pyrolysis of torrefied wood and polystyrene, Fuel. 174 (2016) 317–324. https://doi.org/10.1016/j.fuel.2016.02.031.

[11] F. Abnisa, W. Mohd, A. Wan, A review on co-pyrolysis of biomass : An optional technique to obtain a high-grade pyrolysis oil, Energy Convers. Manag. 87 (2014) 71–85. https://doi.org/10.1016/j.enconman.2014.07.007.

[12] M. Hiloidhari, D. Das, D.C. Baruah, Bioenergy potential from crop residue biomass in

India, Renew. Sustain. Energy Rev. 32 (2014) 504–512.

[13] B.S. Kim, Y.M. Kim, H.W. Lee, J. Jae, D.H. Kim, S.C. Jung, C. Watanabe, Y.K. Park, Catalytic Copyrolysis of Cellulose and Thermoplastics over HZSM-5 and HY, ACS Sustain. Chem. Eng. 4 (2016) 1354–1363. https://doi.org/10.1021/acssuschemeng.5b01381.

[14] E.K.L. Morais, S. Jiménez-Sánchez, H. Hernando, C. Ochoa-Hernández, P. Pizarro, A.S. Araujo, D.P. Serrano, Catalytic Copyrolysis of Lignocellulose and Polyethylene Blends over HBeta Zeolite, Ind. Eng. Chem. Res. 58 (2019) 6243–6254. https://doi.org/10.1021/acs.iecr.8b06158.

[15] M.Z. Siddiqui, Y.K. Park, Y. Kang, A. Watanabe, S. Kim, Y.M. Kim, Effective use of aluminum-plastic laminate as a feedstock for catalytic pyrolysis over micro and mesoporous catalysts, J. Clean. Prod. 229 (2019) 1093–1101. https://doi.org/10.1016/j.jclepro.2019.04.404.

[16] B. Engler, Benjamin; Siegmar Schoenherr; Zheke, Zhong; Gero, Suitability of Bamboo as an Energy Resource : Analysis of Bamboo Combustion Values Dependent on the Culm ' s Age, Int. J. For. Eng. 23 (2012) 114–121.

[17] L.Z. Wang S, Dai G, Yang H, Lignocellulosic biomass pyrolysis mechanism : A state-of-the-art review, Prog. Energy Combust. Sci. 62 (2017) 33–86. https://doi.org/10.1016/j.pecs.2017.05.004.

[18] J. Zhang, J. Luo, D. Tong, L. Zhu, L. Dong, C. Hu, The dependence of pyrolysis behavior on the crystal state of cellulose, Carbohydr. Polym. 79 (2010) 164–169. https://doi.org/10.1016/j.carbpol.2009.07.038.

[19] N. Giummarella, M. Lawoko, A.J. Ragauskas, A critical review on the analysis of

lignin carbohydrate bonds, Green Chem. 21 (2019) 1573–1595. https://doi.org/10.1039/c8gc03606c.

[20] M. Lawoko, Lignin Polysaccharide Networks in Softwood and Chemical Pulps : Characterisation , Structure and Reactivity, 2005.

[21] H. Kawamoto, Lignin pyrolysis reactions, J. Wood Sci. 63 (2017) 117–132. https://doi.org/10.1007/s10086-016-1606-z.

[22] A.P. Pinheiro Pires, J. Arauzo, I. Fonts, M.E. Domine, A. Fernández Arroyo, M.E. Garcia-Perez, J. Montoya, F. Chejne, P. Pfromm, M. Garcia-Perez, Challenges and opportunities for bio-oil refining: A review, Energy and Fuels. 33 (2019) 4683–4720. https://doi.org/10.1021/acs.energyfuels.9b00039.

[23] J.C. Serrano-Ruiz, J. a. Dumesic, Catalytic routes for the conversion of biomass into liquid hydrocarbon transportation fuels, Energy Environ. Sci. 4 (2011) 83–99. https://doi.org/10.1039/C0EE00436G.

[24] D. Mohan, C.U. Pittman, P.H. Steele, Pyrolysis of Wood / Biomass for Bio-oil : A Critical Review, Energy & Fuesl. 20 (2006) 848–889. https://doi.org/10.1021/ef0502397.

[25] A. V. Bridgwater, Catalysis in thermal biomass conversion, Appl. Catal. A, Gen. 116 (1994) 5–47. https://doi.org/10.1016/0926-860X(94)80278-5.

[26] W.L.Z.Y.C.L.G.Y.Y.Z.J.K. Chen, Catalytic transformation of acids, aldehydes and phenol in bio-oil to alcohols and ester, Fuel. 135 (2014) 55–62.

[27] A. Oasmaa, S. Czernik, Fuel oil quality of biomass pyrolysis oils-state of the art for the end users, Fuel Energy Abstr. 13 (1999) 914–921. https://doi.org/10.1016/S0140-6701(00)96592-5.

[28] M.M. Rahman, R. Liu, J. Cai, Catalytic fast pyrolysis of biomass over zeolites for high quality bio-oil – A review, Fuel Process. Technol. 180 (2018) 32–46. https://doi.org/10.1016/j.fuproc.2018.08.002.

[29] Y. Makarfi Isa, E.T. Ganda, Bio-oil as a potential source of petroleum range fuels, Renew. Sustain. Energy Rev. 81 (2018) 69–75. https://doi.org/10.1016/j.rser.2017.07.036.

[30] X. Yuan, X. Ding, L. Leng, H. Li, J. Shao, Y. Qian, H. Huang, X. Chen, G. Zeng, Applications of bio-oil-based emulsions in a DI diesel engine: The effects of bio-oil compositions on engine performance and emissions, Energy. 154 (2018) 110–118. https://doi.org/10.1016/j.energy.2018.04.118.

[31] S.H. Chang, Bio-oil derived from palm empty fruit bunches: Fast pyrolysis, liquefaction and future prospects, Biomass and Bioenergy. 119 (2018) 263–276. https://doi.org/10.1016/j.biombioe.2018.09.033.

[32] S.S. Ali, T. Elsamahy, E. Koutra, M. Kornaros, M. El-Sheekh, E.A. Abdelkarim, D. Zhu, J. Sun, Degradation of conventional plastic wastes in the environment: A review on current status of knowledge and future perspectives of disposal, Sci. Total Environ. 771 (2021) 144719. https://doi.org/10.1016/j.scitotenv.2020.144719.

[33] Y. Liang, Q. Tan, Q. Song, J. Li, An analysis of the plastic waste trade and management in Asia, Waste Manag. 119 (2021) 242–253. https://doi.org/10.1016/j.wasman.2020.09.049.

[34] O. Dogu, M. Pelucchi, R. Van de Vijver, P.H.M. Van Steenberge, D.R. D'hooge, A. Cuoci, M. Mehl, A. Frassoldati, T. Faravelli, K.M. Van Geem, The chemistry of chemical recycling of solid plastic waste via pyrolysis and gasification: State-of-the-art, challenges, and future directions, Prog. Energy Combust. Sci. 84 (2021) 100901.

https://doi.org/10.1016/j.pecs.2020.100901.

[35] M.B. Al Rayaan, Recent advancements of thermochemical conversion of plastic waste to biofuel-A review, Clean. Eng. Technol. 2 (2021) 100062. https://doi.org/10.1016/j.clet.2021.100062.

[36] M. Alam, A. Bhavanam, A. Jana, J. kumar S. Viroja, N.R. Peela, Co-pyrolysis of bamboo sawdust and plastic: Synergistic effects and kinetics, Renew. Energy. 149 (2020) 1133–1145. https://doi.org/10.1016/J.RENENE.2019.10.103.

[37] M. Alam, D. Rammohan, A. Bhavanam, N.R. Peela, Wet torrefaction of bamboo saw dust and its co-pyrolysis with plastic, Fuel. 285 (2021). https://doi.org/10.1016/j.fuel.2020.119188.

[38] M. Eriksen, L.C.M. Lebreton, H.S. Carson, M. Thiel, C.J. Moore, J.C. Borerro, F. Galgani, P.G. Ryan, J. Reisser, Plastic Pollution in the World's Oceans: More than 5 Trillion Plastic Pieces Weighing over 250,000 Tons Afloat at Sea, PLoS One. 9 (2014) 1–15. https://doi.org/10.1371/journal.pone.0111913.

[39] A.W. Gin, H. Hassan, M.A. Ahmad, B.H. Hameed, A.T. Mohd Din, Recent progress on catalytic co-pyrolysis of plastic waste and lignocellulosic biomass to liquid fuel: The influence of technical and reaction kinetic parameters, Arab. J. Chem. 14 (2021) 103035. https://doi.org/10.1016/j.arabjc.2021.103035.

[40] M. Akbari, A.O. Oyedun, A. Kumar, Techno-economic assessment of wet and dry torrefaction of biomass feedstock, Energy. 207 (2020) 118287. https://doi.org/10.1016/j.energy.2020.118287.

[41] Q.V. Bach, O. Skreiberg, Upgrading biomass fuels via wet torrefaction: A review and comparison with dry torrefaction, Renew. Sustain. Energy Rev. 54 (2016) 665–677.

https://doi.org/10.1016/j.rser.2015.10.014.

[42] X. Wang, J. Wu, Y. Chen, A. Pattiya, H. Yang, H. Chen, Comparative study of wet and dry torrefaction of corn stalk and the effect on biomass pyrolysis polygeneration, Biore Source Technol. 258 (2018) 88–97. https://doi.org/10.1016/j.biortech.2018.02.114.

[43] Q. Bach, Ø. Skreiberg, Upgrading biomass fuels via wet torrefaction : A review and comparison with dry torrefaction, Renew. Sustain. Energy Rev. 54 (2016) 665–677. https://doi.org/10.1016/j.rser.2015.10.014.

[44] S.K. Hoekman, A. Broch, A. Warren, L. Felix, J. Irvin, S.K. Hoekman, A. Broch, A. Warren, L. Felix, J. Irvin, Laboratory pelletization of hydrochar from woody biomass, Biofuels. 7269 (2015). https://doi.org/10.1080/17597269.2015.1012693.

[45] H.W. Ryu, D.H. Kim, J. Jae, S.S. Lam, E.D. Park, Y.K. Park, Recent advances in catalytic co-pyrolysis of biomass and plastic waste for the production of petroleum-like hydrocarbons, Bioresour. Technol. 310 (2020) 123473. https://doi.org/10.1016/j.biortech.2020.123473.

[46] B.B. Uzoejinwa, X. He, S. Wang, A. El-Fatah Abomohra, Y. Hu, Q. Wang, Co-pyrolysis of biomass and waste plastics as a thermochemical conversion technology for high-grade biofuel production: Recent progress and future directions elsewhere worldwide, Energy Convers. Manag. 163 (2018) 468–492. https://doi.org/10.1016/j.enconman.2018.02.004.

[47] M.H.M. Ahmed, N. Batalha, H.M.D. Mahmudul, G. Perkins, M. Konarova, A review on advanced catalytic co-pyrolysis of biomass and hydrogen-rich feedstock: Insights into synergistic effect, catalyst development and reaction mechanism, Bioresour. Technol. 310 (2020). https://doi.org/10.1016/j.biortech.2020.123457.

[48] Z. Wang, K.G. Burra, T. Lei, A.K. Gupta, Co-pyrolysis of waste plastic and solid biomass for synergistic production of biofuels and chemicals-A review, Prog. Energy Combust. Sci. 84 (2021) 100899. https://doi.org/10.1016/j.pecs.2020.100899.

[49] X. Li, H. Zhang, J. Li, L. Su, J. Zuo, S. Komarneni, Y. Wang, Improving the aromatic production in catalytic fast pyrolysis of cellulose by co-feeding low-density polyethylene, Appl. Catal. A Gen. 455 (2013) 114–121. https://doi.org/10.1016/j.apcata.2013.01.038.

[50] Y.M. Kim, J. Jae, B.S. Kim, Y. Hong, S.C. Jung, Y.K. Park, Catalytic co-pyrolysis of torrefied yellow poplar and high-density polyethylene using microporous HZSM-5 and mesoporous Al-MCM-41 catalysts, Energy Convers. Manag. 149 (2017) 966–973. https://doi.org/10.1016/j.enconman.2017.04.033.

[51] X. Zhang, H. Lei, S. Chen, J. Wu, Catalytic co-pyrolysis of lignocellulosic biomass with polymers: A critical review, Green Chem. 18 (2016) 4145–4169. https://doi.org/10.1039/c6gc00911e.

[52] Y. Xue, A. Kelkar, X. Bai, Catalytic co-pyrolysis of biomass and polyethylene in a tandem micropyrolyzer, Fuel. 166 (2016) 227–236. https://doi.org/10.1016/j.fuel.2015.10.125.

[53] Y. Hong, Y. Lee, P.S. Rezaei, B.S. Kim, J.K. Jeon, J. Jae, S.C. Jung, S.C. Kim, Y.K. Park, In-situ catalytic copyrolysis of cellulose and polypropylene over desilicated ZSM-5, Catal. Today. 293–294 (2017) 151–158. https://doi.org/10.1016/j.cattod.2016.11.045.

[54] Z. Yang, A. Kumar, A.W. Apblett, A.M. Moneeb, Co-Pyrolysis of torrefied biomass and methane over molybdenum modified bimetallic HZSM-5 catalyst for hydrocarbons production, Green Chem. 19 (2017) 757–768.

https://doi.org/10.1039/c6gc02497a.

[55] H.W. Lee, Y.M. Kim, B. Lee, S. Kim, J. Jae, S.C. Jung, T.W. Kim, Y.K. Park, Catalytic copyrolysis of torrefied cork oak and high density polyethylene over a mesoporous HY catalyst, Catal. Today. 307 (2018) 301–307. https://doi.org/10.1016/j.cattod.2017.01.036.

[56] Y. Yu, X. Li, L. Su, Y. Zhang, Y. Wang, H. Zhang, The role of shape selectivity in catalytic fast pyrolysis of lignin with zeolite catalysts, Appl. Catal. A Gen. 447–448 (2012) 115–123. https://doi.org/10.1016/j.apcata.2012.09.012.

[57] S. Liu, P.A. Kots, B.C. Vance, A. Danielson, D.G. Vlachos, Plastic waste to fuels by hydrocracking at mild conditions, Sci. Adv. 7 (2021) 1–10. https://doi.org/10.1126/sciadv.abf8283.

[58] X. Peng, K. Cheng, J. Kang, B. Gu, X. Yu, Q. Zhang, Y. Wang, Impact of Hydrogenolysis on the Selectivity of the Fischer-Tropsch Synthesis: Diesel Fuel Production over Mesoporous Zeolite-Y-Supported Cobalt Nanoparticles, Angew. Chemie - Int. Ed. 54 (2015) 4553–4556. https://doi.org/10.1002/anie.201411708.

[59] H. Hassan, J.K. Lim, B.H. Hameed, Catalytic co-pyrolysis of sugarcane bagasse and waste high-density polyethylene over faujasite-type zeolite, Bioresour. Technol. 284 (2019) 406–414. https://doi.org/10.1016/j.biortech.2019.03.137.

[60] H.W. Lee, Y.M. Kim, B. Lee, S. Kim, J. Jae, S.C. Jung, T.W. Kim, Y.K. Park, Catalytic copyrolysis of torrefied cork oak and high density polyethylene over a mesoporous HY catalyst, Catal. Today. 307 (2018) 301–307. https://doi.org/10.1016/j.cattod.2017.01.036.

[61] S. Vyazovkin, A.K. Burnham, J.M. Criado, L.A. Pérez-Maqueda, C. Popescu, N.

Sbirrazzuoli, ICTAC Kinetics Committee recommendations for performing kinetic computations on thermal analysis data, Thermochim. Acta. 520 (2011) 1–19. https://doi.org/10.1016/j.tca.2011.03.034.

[62] A.I. Osman, A. Abdelkader, C. Farrell, D. Rooney, K. Morgan, Reusing, recycling and up-cycling of biomass: A review of practical and kinetic modelling approaches, Fuel Process. Technol. 192 (2019) 179–202. https://doi.org/10.1016/j.fuproc.2019.04.026.

[63] M. Heydrai, M. Raman, R. Gupta, Kinetic Study and Thermal Decomposition Behavior of Lignite Coal, Int. J. Chem. Eng. 2015 (2015) 1–9. https://doi.org/http://dx.doi.org/10.1155/2015/481739.

[64] A. Chandrasekaran, S. Ramachandran, S. Subbiah, Determination of kinetic parameters in the pyrolysis operation and thermal behavior of Prosopis juliflora using thermogravimetric analysis, Bioresour. Technol. 233 (2017) 413–422. https://doi.org/10.1016/j.biortech.2017.02.119.

[65] A. Aboulkas, K.E.L. Harfi, Study of the kinetics and mechanism of thermal decomposition Moroccan Tarfaya oil shaleand its kerogen, Oil Shale. 25 (2008) 426–443. https://doi.org/10.3176/oil.2008.4.04.

[66] D. Chen, Shuang E, L. Liu, Analysis of pyrolysis characteristics and kinetics of sweet sorghum bagasse and cotton stalk, J. Therm. Anal. Calorim. 131 (2018) 1899–1909. https://doi.org/10.1007/s10973-017-6585-9.

[67] P.R. Havilah, P.K. Sharma, M. Gopinath, Combustion characteristics and kinetic parameter estimation of Lantana camara by thermogravimetric analysis, Biofuels. 7269 (2016) 1–8. https://doi.org/10.1080/17597269.2016.1259521.

[68] F.J. Gotor, José, M. Criado, J. Malek, N. Koga, Kinetic analysis of solid-state

reactions: The universality of master plots for analyzing isothermal and nonisothermal experiments, J. Phys. Chem. A. 104 (2000) 10777–10782. https://doi.org/10.1021/jp0022205.

[69] A. Khawam, D.R. Flanagan, Solid-State Kinetic Models : Basics and Mathematical Fundamentals Solid-State Kinetic Models : Basics and Mathematical Fundamentals, J. Phys. Chem. B. 110 (2006) 17315–17328. https://doi.org/10.1021/jp062746a.

[70] M. Avrami, Granulation, phase change, and microstructure kinetics of phase change. III, J. Chem. Phys. 9 (1941) 177–184. https://doi.org/10.1063/1.1750872.

[71] D. Chen, J. Zhou, Q. Zhang, Effects of torrefaction on the pyrolysis behavior and bio-oil properties of rice husk by using TG-FTIR and Py-GC/MS, Energy and Fuels. 28 (2014) 5857–5863. https://doi.org/10.1021/ef501189p.

[72] Q. Bach, K. Tran, Ø. Skreiberg, T.T. Trinh, Effects of wet torrefaction on pyrolysis of woody biomass fuels, Energy. 88 (2015) 443–456. https://doi.org/10.1016/j.energy.2015.05.062.

[73] S. Wang, G. Dai, B. Ru, Y. Zhao, X. Wang, J. Zhou, Z. Luo, K. Cen, Effects of torrefaction on hemicellulose structural characteristics and pyrolysis behaviors, Bioresour. Technol. 218 (2016) 1106–1114. https://doi.org/10.1016/j.biortech.2016.07.075.

[74] S. Zhang, Q. Dong, L. Zhang, Y. Xiong, Effects of water washing and torrefaction on the pyrolysis behavior and kinetics of rice husk through TGA and Py-GC/MS, Bioresour. Technol. 199 (2016) 352–361. https://doi.org/10.1016/j.biortech.2015.08.110.

[75] S. Wang, G. Dai, B. Ru, Y. Zhao, X. Wang, G. Xiao, Z. Luo, Influence of torrefaction

on the characteristics and pyrolysis behavior of cellulose, Energy. 120 (2017) 864–871. https://doi.org/10.1016/j.energy.2016.11.135.

[76] C. Zhang, S.H. Ho, W.H. Chen, Y. Xie, Z. Liu, J.S. Chang, Torrefaction performance and energy usage of biomass wastes and their correlations with torrefaction severity index, Appl. Energy. 220 (2018) 598–604. https://doi.org/10.1016/j.apenergy.2018.03.129.

[77] Q.V. Bach, W.H. Chen, C.F. Eng, C.W. Wang, K.C. Liang, J.Y. Kuo, Pyrolysis characteristics and non-isothermal torrefaction kinetics of industrial solid wastes, Fuel. 251 (2019) 118–125. https://doi.org/10.1016/j.fuel.2019.04.024.

[78] O.D. Dacres, S. Tong, X. Li, X. Zhu, E.M.A. Edreis, H. Liu, G. Luo, N. Worasuwannarak, S. Kerdsuwan, B. Fungtammasan, H. Yao, Pyrolysis kinetics of biomasses pretreated by gas-pressurized torrefaction, Energy Convers. Manag. 182 (2019) 117–125. https://doi.org/10.1016/j.enconman.2018.12.055.

[79] L. Dai, Y. Wang, Y. Liu, R. Ruan, D. Duan, Y. Zhao, Z. Yu, L. Jiang, Catalytic fast pyrolysis of torrefied corn cob to aromatic hydrocarbons over Ni-modified hierarchical ZSM-5 catalyst, Bioresour. Technol. 272 (2019) 407–414. https://doi.org/10.1016/j.biortech.2018.10.062.

[80] S. Singh, J. Prasad Chakraborty, M. Kumar Mondal, Intrinsic kinetics, thermodynamic parameters and reaction mechanism of non-isothermal degradation of torrefied Acacia nilotica using isoconversional methods, Fuel. 259 (2020) 116263. https://doi.org/10.1016/j.fuel.2019.116263.

[81] Y.Y. Gan, W.H. Chen, H.C. Ong, Y.Y. Lin, H.K. Sheen, J.S. Chang, T.C. Ling, Effect of wet torrefaction on pyrolysis kinetics and conversion of microalgae carbohydrates, proteins, and lipids, Energy Convers. Manag. 227 (2021) 113609.

https://doi.org/10.1016/j.enconman.2020.113609.

[82] J. Liang, Z. Yu, L. Chen, S. Fang, X. Ma, Microwave pretreatment power and duration time effects on the catalytic pyrolysis behaviors and kinetics of water hyacinth, Bioresour. Technol. 286 (2019) 121369. https://doi.org/10.1016/j.biortech.2019.121369.

[83] A.K. Vuppaladadiyam, M.Z. Memon, G. Ji, A. Raheem, T.Z. Jia, V. Dupont, M. Zhao, Thermal Characteristics and Kinetic Analysis of Woody Biomass Pyrolysis in the Presence of Bifunctional Alkali Metal Ceramics, ACS Sustain. Chem. Eng. 7 (2019) 238–248. https://doi.org/10.1021/acssuschemeng.8b02967.

[84] Q. Song, H. Zhao, J. Jia, L. Yang, W. Lv, J. Bao, X. Shu, Q. Gu, P. Zhang, Pyrolysis of municipal solid waste with iron-based additives: A study on the kinetic, product distribution and catalytic mechanisms, J. Clean. Prod. 258 (2020) 120682. https://doi.org/10.1016/j.jclepro.2020.120682.

[85] S. Gupta, P. Mondal, Catalytic pyrolysis of pine needles with nickel doped gamma-alumina: Reaction kinetics, mechanism, thermodynamics and products analysis, J. Clean. Prod. 286 (2021) 124930. https://doi.org/10.1016/j.jclepro.2020.124930.

[86] B.L.F. Chin, S. Yusup, A. Al Shoaibi, P. Kannan, C. Srinivasakannan, S.A. Sulaiman, Kinetic studies of co-pyrolysis of rubber seed shell with high density polyethylene, Energy Convers. Manag. 87 (2014) 746–753. https://doi.org/10.1016/j.enconman.2014.07.043.

[87] Z. Wu, S. Wang, J. Zhao, L. Chen, H. Meng, Synergistic effect on thermal behavior during co-pyrolysis of lignocellulosic biomass model components blend with bituminous coal, Bioresour. Technol. 169 (2014) 220–228. https://doi.org/10.1016/j.biortech.2014.06.105.

[88] A.O. Oyedun, C.Z. Tee, S. Hanson, C.W. Hui, Thermogravimetric analysis of the pyrolysis characteristics and kinetics of plastics and biomass blends, Fuel Process. Technol. 128 (2014) 471–481. https://doi.org/10.1016/j.fuproc.2014.08.010.

[89] S.D. Gunasee, M. Carrier, J.F. Gorgens, R. Mohee, Pyrolysis and combustion of municipal solid wastes: Evaluation of synergistic effects using TGA-MS, J. Anal. Appl. Pyrolysis. 121 (2016) 50–61. https://doi.org/10.1016/j.jaap.2016.07.001.

[90] K.G. Burra, A.K. Gupta, Kinetics of synergistic effects in co-pyrolysis of biomass with plastic wastes, Appl. Energy. 220 (2018) 408–418. https://doi.org/10.1016/j.apenergy.2018.03.117.

[91] M.U. Garba, A. Inalegwu, U. Musa, A.A. Aboje, Thermogravimetric characteristic and kinetic of catalytic co-pyrolysis of biomass with low- and high-density polyethylenes, Biomass Conv. Bioref. 8 (2018) 143–150. https://doi.org/10.1007/s13399-017-0261-y.

[92] R. Chen, J. Zhang, L. Lun, Q. Li, Y. Zhang, Comparative study on synergistic effects in co-pyrolysis of tobacco stalk with polymer wastes: Thermal behavior, gas formation, and kinetics, Bioresour. Technol. 292 (2019) 121970. https://doi.org/10.1016/j.biortech.2019.121970.

[93] X. Kai, T. Yang, S. Shen, R. Li, TG-FTIR-MS study of synergistic effects during co-pyrolysis of corn stalk and high-density polyethylene (HDPE), Energy Convers. Manag. 181 (2019) 202–213. https://doi.org/10.1016/j.enconman.2018.11.065.

[94] C. Sun, C. Li, H. Tan, Y. Zhang, Synergistic effects of wood fiber and polylactic acid during co-pyrolysis using TG-FTIR-MS and Py-GC/MS, Energy Convers. Manag. 202 (2019) 112212. https://doi.org/10.1016/j.enconman.2019.112212.

[95] W. Wang, K. Sun, M. Ali, X. Liu, Q. Huang, Copyrolysis behavior of xylan and

polyvinyl chloride plastic, Energy and Fuels. 33 (2019) 8727–8734. https://doi.org/10.1021/acs.energyfuels.9b01734.

[96] S. Wang, X. Lin, Z. Li, W. Yi, X. Bai, Thermal and Kinetic Behaviors of Corn Stover and Polyethylene in Catalytic Co-pyrolysis, BioResources. 13 (2018) 4102–4117. https://doi.org/10.15376/biores.13.2.4102-4117.

[97] R. Chen, S. Zhang, X. Yang, G. Li, H. Zhou, Q. Li, Y. Zhang, Thermal behaviour and kinetic study of co-pyrolysis of microalgae with different plastics, Waste Manag. 126 (2021) 331–339. https://doi.org/10.1016/j.wasman.2021.03.001.

[98] B.L.F. Chin, S. Yusup, A. Al Shoaibi, P. Kannan, C. Srinivasakannan, S.A. Sulaiman, Comparative studies on catalytic and non-catalytic co-gasification of rubber seed shell and high density polyethylene mixtures, J. Clean. Prod. 70 (2014) 303–314. https://doi.org/10.1016/j.jclepro.2014.02.039.

[99] W. Jin, D. Shen, Q. Liu, R. Xiao, Evaluation of the co-pyrolysis of lignin with plastic polymers by TG-FTIR and Py-GC/MS, Polym. Degrad. Stab. 133 (2016) 65–74. https://doi.org/10.1016/j.polymdegradstab.2016.08.001.

[100] P. Lu, Q. Huang, A.C.T. Bourtsalas, Y. Chi, J. Yan, Synergistic e ff ects on char and oil produced by the co-pyrolysis of pine wood , polyethylene and polyvinyl chloride, Fuel. 230 (2018) 359–367. https://doi.org/10.1016/j.fuel.2018.05.072.

[101] G. Özsin, A.E. Pütün, Co-pyrolytic behaviors of biomass and polystyrene : Kinetics , thermodynamics and evolved gas analysis, Korean J. Chem. Eng. 35 (2018) 428–437. https://doi.org/10.1007/s11814-017-0308-6.

[102] Y. Zheng, L. Tao, X. Yang, Y. Huang, C. Liu, Z. Zheng, Study of the thermal behavior , kinetics , and product characterization of biomass and low-density polyethylene co-

pyrolysis by thermogravimetric analysis and pyrolysis-GC / MS, J. Anal. Appl. Pyrolysis. 133 (2018) 185–197. https://doi.org/10.1016/j.jaap.2018.04.001.

[103] X. Gou, X. Zhao, S. Singh, D. Qiao, Tri-pyrolysis: A thermo-kinetic characterisation of polyethylene, cornstalk, and anthracite coal using TGA-FTIR analysis, Fuel. 252 (2019) 393–402. https://doi.org/10.1016/j.fuel.2019.03.143.

[104] X. Kai, T. Yang, S. Shen, R. Li, TG-FTIR-MS study of synergistic e ff ects during co-pyrolysis of corn stalk and high-density polyethylene (HDPE), Energy Convers. Manag. 181 (2019) 202–213. https://doi.org/10.1016/j.enconman.2018.11.065.

[105] S.R. Naqvi, Z. Hameed, R. Tariq, S.A. Taqvi, I. Ali, M.B.K. Niazi, T. Noor, A. Hussain, N. Iqbal, M. Shahbaz, Synergistic effect on co-pyrolysis of rice husk and sewage sludge by thermal behavior, kinetics, thermodynamic parameters and artificial neural network, Waste Manag. 85 (2019) 131–140. https://doi.org/10.1016/j.wasman.2018.12.031.

[106] A.K. Varma, N. Lal, A.K. Rathore, R. Katiyar, L.S. Thakur, R. Shankar, P. Mondal, Thermal, kinetic and thermodynamic study for co-pyrolysis of pine needles and styrofoam using thermogravimetric analysis, Energy. 218 (2021) 119404. https://doi.org/10.1016/j.energy.2020.119404.

[107] A. Toptas, Y. Yildirim, G. Duman, J. Yanik, Combustion behavior of different kinds of torrefied biomass and their blends with lignite, Bioresour. Technol. 177 (2015) 328–336. https://doi.org/10.1016/j.biortech.2014.11.072.

[108] L. Cao, X. Yuan, L. Jiang, C. Li, Z. Xiao, Z. Huang, Thermogravimetric characteristics and kinetics analysis of oil cake and torrefied biomass blends, Fuel. 175 (2016) 129–136.

[109] Q. Bu, K. Chen, W. Xie, Y. Liu, M. Cao, X. Kong, Q. Chu, Hydrocarbon rich bio-oil production , thermal behavior analysis and kinetic study of microwave-assisted co-pyrolysis of microwave-torre fi ed lignin with low density polyethylene, Bioresour. Technol. 291 (2019) 121860. https://doi.org/10.1016/j.biortech.2019.121860.

[110] P. Keliona, W. Likun, H. Zhang, Insights into pyrolysis of torrefied-biomass , plastics / tire and blends : Thermochemical behaviors , kinetics and evolved gas analyses, Biomass and Bioenergy. 143 (2020) 105852. https://doi.org/10.1016/j.biombioe.2020.105852.

[111] H.W. Lee, Y.M. Kim, J. Jae, J.K. Jeon, S.C. Jung, S.C. Kim, Y.K. Park, Production of aromatic hydrocarbons via catalytic co-pyrolysis of torrefied cellulose and polypropylene, Energy Convers. Manag. 129 (2016) 81–88. https://doi.org/10.1016/j.enconman.2016.10.001.

[112] L. Zhou, H. Zou, Y. Wang, Z. Le, Z. Liu, A.A. Adesina, Effect of potassium on thermogravimetric behavior and co-pyrolytic kinetics of wood biomass and low density polyethylene, Renew. Energy. 102 (2017) 134–141. https://doi.org/10.1016/j.renene.2016.10.028.

[113] Z. Xiang, J. Liang, H.M. Morgan, Y. Liu, H. Mao, Q. Bu, Thermal behavior and kinetic study for co-pyrolysis of lignocellulosic biomass with polyethylene over Cobalt modified ZSM-5 catalyst by thermogravimetric analysis, Bioresour. Technol. 247 (2018) 804–811. https://doi.org/10.1016/j.biortech.2017.09.178.

[114] Z. Wang, D. Shen, C. Wu, S. Gu, Thermal behavior and kinetics of co-pyrolysis of cellulose and polyethylene with the addition of transition metals, Energy Convers. Manag. 172 (2018) 32–38. https://doi.org/10.1016/j.enconman.2018.07.010.

[115] Y. Chi, J. Xue, J. Zhuo, D. Zhang, M. Liu, Q. Yao, Catalytic co-pyrolysis of cellulose

and polypropylene over all-silica mesoporous catalyst MCM-41 and Al-MCM-41, Sci. Total Environ. 633 (2018) 1105–1113. https://doi.org/10.1016/j.scitotenv.2018.03.239.

[116] K. Praveen Kumar, S. Srinivas, Catalytic Co-pyrolysis of Biomass and Plastics (Polypropylene and Polystyrene) Using Spent FCC Catalyst, Energy and Fuels. 34 (2020) 460–473. https://doi.org/10.1021/acs.energyfuels.9b03135.

[117] S. Xu, B. Cao, B.B. Uzoejinwa, E.A. Odey, S. Wang, H. Shang, C. Li, Y. Hu, Q. Wang, J.N. Nwakaire, Synergistic effects of catalytic co-pyrolysis of macroalgae with waste plastics, Process Saf. Environ. Prot. 137 (2020) 34–48. https://doi.org/10.1016/j.psep.2020.02.001.

[118] Y. Zhao, X. Yang, Z. Fu, R. Li, Y. Wu, Synergistic effect of catalytic co-pyrolysis of cellulose and polyethylene over HZSM-5, J. Therm. Anal. Calorim. 140 (2020) 363–371. https://doi.org/10.1007/s10973-019-08633-7.

[119] S. Zhong, B. Zhang, C. Liu, A. Shujaa aldeen, Mechanism of synergistic effects and kinetics analysis in catalytic co-pyrolysis of water hyacinth and HDPE, Energy Convers. Manag. 228 (2021) 113717. https://doi.org/10.1016/j.enconman.2020.113717.

[120] X. Lin, L. Kong, X. Ren, D. Zhang, H. Cai, H. Lei, Catalytic co-pyrolysis of torrefied poplar wood and high-density polyethylene over hierarchical HZSM-5 for mono-aromatics production, Renew. Energy. 164 (2021) 87–95. https://doi.org/10.1016/j.renene.2020.09.071.

[121] Y. Zheng, L. Tao, X. Yang, Y. Huang, C. Liu, Z. Zheng, Study of the thermal behavior, kinetics, and product characterization of biomass and low-density polyethylene co-pyrolysis by thermogravimetric analysis and pyrolysis-GC/MS, J. Anal. Appl. Pyrolysis. 133 (2018) 185–197.

https://doi.org/10.1016/j.jaap.2018.04.001.

[122] Z. Wang, G. Liu, D. Shen, C. Wu, S. Gu, Co-pyrolysis of lignin and polyethylene with the addition of transition metals - Part I : Thermal behavior and kinetics analysis, J. Energy Inst. 93 (2020) 281–291. https://doi.org/10.1016/j.joei.2019.03.003.

[123] P. Keliona, W. Likun, H. Zhang, R. Xiao, Online Vapors Separation of Torre fi ed-Bagasse / HDPE Co-pyrolysis into Three Grades of Bio-oils, Energy & Fuels. 34 (2020) 8376–836.

[124] K. Wang, J. Zhang, B.H. Shanks, R.C. Brown, The deleterious effect of inorganic salts on hydrocarbon yields from catalytic pyrolysis of lignocellulosic biomass and its mitigation, Appl. Energy. 148 (2015) 115–120. https://doi.org/10.1016/j.apenergy.2015.03.034.

[125] N. Zhao, B. Li, The effect of sodium chloride on the pyrolysis of rice husk, Appl. Energy. 178 (2016) 346–352.

[126] J.S. Arora, J.W. Chew, S.H. Mushrif, Influence of Alkali and Alkaline-Earth Metals on the Cleavage of Glycosidic Bond in Biomass Pyrolysis: A DFT Study Using Cellobiose as a Model Compound, J. Phys. Chem. A. 122 (2018) 7646–7658. https://doi.org/10.1021/acs.jpca.8b06083.

[127] M. Safar, B.J. Lin, W.H. Chen, D. Langauer, J.S. Chang, H. Raclavska, A. Pétrissans, P. Rousset, M. Pétrissans, Catalytic effects of potassium on biomass pyrolysis, combustion and torrefaction, Appl. Energy. 235 (2019) 346–355. https://doi.org/10.1016/j.apenergy.2018.10.065.

[128] M. Iwamoto, A. Shimatai, M. Honda, M. Matsukata, Depolymerization of Cellulose with Superheated Steam: Remarkable Obstruction Effects of Sodium and High

Reactivity of Crystalline Cellulose, ACS Sustain. Chem. Eng. 6 (2018) 6570–6576. https://doi.org/10.1021/acssuschemeng.8b00375.

[129] S. Wang, Z. Li, X. Bai, W. Yi, P. Fu, Influence of inherent hierarchical porous char with alkali and alkaline earth metallic species on lignin pyrolysis, Bioresour. Technol. 268 (2018) 323–331. https://doi.org/10.1016/j.biortech.2018.07.117.

[130] P. Giudicianni, V. Gargiulo, M. Alfè, R. Ragucci, A.I. Ferreiro, M. Rabaçal, M. Costa, Slow pyrolysis of xylan as pentose model compound for hardwood hemicellulose: A study of the catalytic effect of Na ions, J. Anal. Appl. Pyrolysis. 137 (2019) 266–275. https://doi.org/10.1016/j.jaap.2018.12.004.

[131] H. Nan, L. Zhao, F. Yang, Y. Liu, Z. Xiao, X. Cao, H. Qiu, Different alkaline minerals interacted with biomass carbon during pyrolysis: Which one improved biochar carbon sequestration?, J. Clean. Prod. 255 (2020) 120162. https://doi.org/10.1016/j.jclepro.2020.120162.

[132] X. Lin, D. Zhang, X. Ren, Q. Zhang, H. Cai, W. Yi, H. Lei, Catalytic co-pyrolysis of waste corn stover and high-density polyethylene for hydrocarbon production: The coupling effect of potassium and HZSM-5 zeolite, J. Anal. Appl. Pyrolysis. 150 (2020) 104895. https://doi.org/10.1016/j.jaap.2020.104895.

[133] Y. Wei, C. Shen, J. Xie, Q. Bu, Study on reaction mechanism of superior bamboo biochar catalyst production by molten alkali carbonates pyrolysis and its application for cellulose hydrolysis, Sci. Total Environ. 712 (2020) 136435. https://doi.org/10.1016/j.scitotenv.2019.136435.

[134] X. Tian, Y. Wang, Z. Zeng, L. Dai, Y. Peng, L. Jiang, X. Yang, L. Yue, Y. Liu, R. Ruan, Study on the mechanism of co-catalyzed pyrolysis of biomass by potassium and calcium, Bioresour. Technol. 320 (2021) 124415.

https://doi.org/10.1016/j.biortech.2020.124415.

[135] S. Tewari, H. Negi, R. Kaushal, Status of Bamboo in India, Int. J. Econ. Plants. 6 (2019) 030–039. https://doi.org/10.23910/ijep/2019.6.1.0288.

[136] A.D. Sawarkar, D.D. Shrimankar, A. Kumar, A. Kumar, E. Singh, L. Singh, S. Kumar, R. Kumar, Commercial clustering of sustainable bamboo species in India, Ind. Crops Prod. 154 (2020) 112693. https://doi.org/10.1016/j.indcrop.2020.112693.

Chapter 2

Materials and Methods

This chapter details the experimental investigations, procedures, and the methods of analyses followed throughout the study. It includes the determination of physicochemical properties, such as functional groups structural morphology, size, and crystallinity of biomass as well as torrefied biomass along with catalyst activities of zeolites. Specifications of all reagents and chemicals are documented in this chapter. Any specific change or deviation from what is stated here is detailed in the respective section(s) / chapter(s).

2.1 Materials and Reagents

The xylose (99.5%), fructose (99%), glucose (99.5%), lactic acid (85.9%) were obtained from Himedia, India. The cellobiose (99.5%), 5-hydroxymethylfurfural (99%) were from Sigma Aldrich, USA. The formic acid (85%) and levulinic acid (99%) were from Merck, Germany. The linear low-density polyethylene (LLDPE) was provided by Haldia petrochemical limited, India. The complete details of materials used in this research work are summarized in the Table 2.1. Deionized (DI) water (conductivity 0.055 µS cm^{-1}) of Millipore Filtration Unit (Elix-3, USA) was used to prepare all the reagents and solutions. All the plastic wares used were made of polypropylene procured from Tarson Products Pvt. Ltd., Kolkata (India). Glassware with a low coefficient of thermal expansion was mostly obtained from Borosil, Mumbai (India).

Table 2.1. List of chemical and reagents to carry out experiment

Reagents/chemicals	Purity (%)	Grade	Make
5-HMF ($C_6H_6O_3$)	99	GR	Sigma Aldrich (India)
Cellobiose ($C_{12}H_{22}O_{11}$)	99.5	AR	Sigma Aldrich (India)
Fructose ($C_6H_{12}O_6$)	99.5	AR	Hi-media (India)
Glucose ($C_6H_{12}O_6$)	99.5	AR	
Xylose ($C_5H_{10}O_5$)	99.5	AR	
Lactic acid ($C_3H_6O_3$)	99.6	AR	
Formic acid (CH_2O_2)	85	GR	Merck (India)
Furfural ($C_5H_4O_2$)	98.5	GR	
Levulinic acid ($C_5H_8O_3$)	99	GR	
1,4 Dioxane ($C_4H_8O_2$)	99.5	AR	
Levulinic acid ($C_3H_8O_3$)	97	GR	
Acetone (C_3H_6O)	≥ 99.8	AR	
Silicone oil	–	–	
Potassium bromide (KBr)	99.5	GR	
Sodium chloride (NaCl)	99.5	GR	
Sulphuric acid (H_2SO_4)	98	AR	
HZSM-5 (SAR:80)	–	–	Alfa-Aesar (now Thermo Fisher)
MesoHY (SAR:80)	–	–	Alfa-Aesar (now Thermo Fisher)

2.2 Sample preparation

Bamboo biomass (Bambusa *tulda*), harvested in the state of Assam, north-eastern India (26°14' 38" N and 92° 32' 16" E), was employed as a feedstock for this study. The biomass, obtained from a bamboo processing mill (Guwahati city, Assam, India), was washed with water to remove impurities, and dried to remove moisture. Further, the sample was ground and sieved, to obtain particle size range of 105–250 µm. To prepare the wet-torrefied bamboo sawdust the following procedure was adopted. In a typical wet torrefaction experiment, 10 wt% of BSD (particle size distribution: 150–300 µm) was suspended in 2 ml DI water in a glass reactor (model: CG4920–01, Chemglass, USA). To this suspension, NaCl and formic acid (FA) were added such that BSD:NaCl ratio 1:3 w/w and BSD:FA ratio 1:1 w/w. The wet torrefaction was carried out at the desired pre-set temperature (120–150°C) and for the desired duration (30–90 min) under stirring. After completion of the experiment, the reaction mixture was filtered using a 0.2 µm nylon membrane filter. The solid residue was thoroughly washed for multiple times with DI water to remove all the leftover NaCl and dried at room temperature under vacuum for further analysis/use. The filtrate was analysed by high-pressure liquid chromatography (HPLC).

To prepare LLDPE powder from beads, the following procedure was adopted. The beads and the solvent (toluene) were added into a flask connected to a condenser and heated at around 80°C for 1 h, to ensure complete dissolution of the LLDPE polymer. Then, the polymer solution from the cooled flask was poured into the non-solvent (ethyl alcohol) to re-precipitate the polymer. The re-precipitated polymer was then washed, filtrated and dried in an oven at 80°C for 10 h.

2.3 Product analysis

The quantities of Pentoses (xylose + arabinose), hexoses (glucose + galactose + mannose), acetic acid, furfural, 5-hydroxymethylfurfural (HMF) and levulinic acid formed during the wet-torrefaction were determined by using HPLC (Model: LC-20AD, MAKE: Shimadzu, Japan) equipped RID (Model: RID-20A, MAKE: Shimadzu, Japan) detector and HPLC column (Model: Aminex HPX-87H; Make: Bio-Rad, The USA). The mobile phase was an aqueous sulphuric acid solution (0.005 M) at a flow rate of 0.6 mL min^{-1}. The column temperature was set at 60°C. It is pertinent to note that the hemicellulose of bamboo biomass consists of xylose, arabinose, galactose, mannose and glucose. The sugar profile of hemicellulose is as follows: xylose was the highest (87.6 wt.%) followed by arabinose (8.7 wt.%), glucose (2.1 wt.%), mannose (0.9 wt.%) and galactose (0.7 wt.%).[1] Here, the xylose and arabinose are pentose isomers and glucose, mannose and galactose are hexose isomers. The Aminex HPX-87H column detected the xylose and arabinose as a single peak (named as "pentoses") and the glucose, mannose and galactose as a single peak (named as "hexoses"). The yields of the compounds were calculated using the following formulae:

$$Yield\ of\ i\ (mole\ \%) = \frac{\text{moles of i formed}}{\text{Initial moles of cellulose + hemicellulose present}} \times 100 \ldots\ldots\ldots\ldots\ldots 2.1$$

where i is hexoses (glucose + galactose + mannose), HMF, or levulinic acid. The moles of cellulose were based on the equivalent hexose (e.g., glucose) units (molecular weight = 162.14 g mol^{-1}).[2]

$$Yield\ of\ m\ (mole\ \%) = \frac{\text{moles of m formed}}{\text{Initial moles of hemicellulose present}} \times 100 \ldots\ldots\ldots\ldots\ldots\ldots\ldots\ldots 2.2$$

where m is pentoses (xylose + arabinose), acetic acid, or furfural. The moles of hemicellulose were based on the equivalent pentose (e.g., xylose) units (molecular weight = 132.14 g mol^{-1}).

The concentrations of cellulose (31 wt%) and hemicellulose (23.1 wt%) were taken from our previous study.[2]

2.4 Material characterisation

The proximate and ultimate analysis of pure BSD and plastic (LLDPE) are given in Table 2.2. The quality of solid fuel was characterized by four parameters i.e. fixed carbon, volatile matter, ash and moisture content.[3] The volatile matter was determined in accordance with ASTM E872 standard method. One-gram of dried sample was kept in a muffle furnace (VBCC-14/15-FF), pre-stabilized at a temperature of 950°C, and heated for 7 min exactly. The sample was removed from the furnace and allowed to cool in a desiccator. The difference in weight before and after heating gives the amount of volatile matter present in the sample. Moisture content experiment was performed according to ASTM 871-82: 1 g of sun-dried sample was placed in the oven at 103±1°C for 16 h. The moisture content was calculated by subtracting the final weight of the sample form the initial weight.

The mineral content and inorganic matter comes under the category of ash. [4] The ash content was determined by ASTM E1534-93 Standard Test Method. The fixed-carbon content was determined by subtracting the moisture, volatile matter, and ash contents (wt.%) from 100 wt.%. Channiwala and Parikh presented an equation (eq. 2.3) to evaluate the high heating value of various biomasses having different chemical composition.

$$HHV\ (MJ/kg) = 0.3491C + 1.1783H + 0.105S - 0.1034O - 0.015N - 0.0211A \quad \ldots\ldots\ldots\ldots 2.3$$

Where, C, H, O, N, S and A represent Carbon, Hydrogen, Oxygen, Nitrogen, Sulphur and Ash contents of sample, wt.% on dry basis.

Elemental analysis of the BSD, TBSD and plastic samples (C, H & N) was carried out by using the CHNS analyzer (Thermo scientific flash 2000, Thermo Fisher Scientific, USA). The calorific value of BSD was calculated by Bomb Calorimeter (Parr 6400, Parr instrument company, USA).

Table 2.2. Proximate and ultimate analysis of BSD, TBSD and LLDPE

Sample	PA[#] (wt.% dry basis)			UA[*] (wt.% ash-free and dry basis)				HHV (MJ/kg)		H/C	O/C	MC
	FC	VM	Ash	C	H	N	O	Cal.	Exp.			
BSD	9.2	74.9	5.8	46.73	6.18	0	47.66	18.55	17.04	0.132	1.02	10.1
TBSD[$]	30	66	0.3	51.4	6.5	0.02	42.04	21.32	24.02	0.127	0.82	4.5
LLDPE	0.5	99.5	0.0	75.96	13.45	0	10.59	41.27	NA	0.18	0.14	Neg.

[#]PA & [*]UA: Proximate and Ultimate analysis data of BSD and LLDPE
[$]The proximate and ultimate analysis data of TBSD sample that is prepared by wet torrefaction of BSD at 140°C and 30 min (optimum conditions).
FC: Fixed carbon; VM: Volatile matter; Cal.: Calculated; Exp.: Experimental; MC: Moisture Content
NA: Not available; Neg.: Negligible

2.4.1 Surface characterization of bamboo biomass and Catalyst

The functional groups of BSD and TBSD were analysed by Fourier-transformed infrared spectroscopy (FTIR, Model: IR Affinity, MAKE: Shimadzu, Japan). The spectra were collected in the wavenumber range of 400–4000 cm^{-1}. The sample pellets were prepared by blending 1% finely ground BSD/TBSD with KBr. The X-ray powder diffractometer (XRD; Model: Smart Lab; Make: Rigaku, Japan) was used to determine the crystallinity of biomass. The Ni filtered Cu K_α radiation (λ: 0.15418 nm, 45 kv, and 112 mA) was employed in the range of 5–70° (2Θ) with a step size of 0.01° and a scan rate of 20° min^{-1}. The morphology of BSD and TBSD was determined using Field Emission Scanning Electron Microscopy (FESEM, Model: JSM-7610F, MAKE: JEOL, Japan). Prior to analysis, the samples were gold-coated in an argon atmosphere, to avoid charging. Prior to analysis, the samples were gold-coated in an argon atmosphere, to avoid charging**.** The porosity of zeolites was evaluated by N_2-sorption process (Model: Autosorb-1QMP, Make: Quanta chrome, USA) at -196°C. Before analysis, the sample was degassed at 200°C for 6 h to remove moisture or unwanted materials under

vacuum. The Barrette-Joyner-Halenda (BJH) method was used to characterize pore size distribution and average pore width. The textural properties of zeolites (HZMS-5 and MesoHY) were shown in Table 2.3.

Table 2.3. Physicochemical properties of MesoHY and HZSM-5 zeolites

Sample	IZA code	S_{BET}*	S_{MICRO}#	$S_{MESO}$$	V_T&	V_{MICRO}%	V_{MESO}@	APS£	Py FTIR¥	
									C_{BAS}©	C_{LAS}§
MesoHY	FAU¢ (100) ***12*** 7.4 x 7.4 IPS (Å)Θ : 11.24	773	440	333	0.58	0.23	0.35	3.79	78.4	2236.4
HZSM-5	MFIø (100) ***10*** 5.1 x 5.5 ↔ (010) ***10*** 5.3 x 5.6 IPS (Å)Θ: 5.6	382	316	66	0.30	0.17	0.13	1.40	130.5	869.9

Note: ΘIPS: Internal pore space in Å, ¢FAU: Plane with pore size and number of rings present in zeolites [5]; S: Specific surface area; *S_{BET}, (BET: Brunauer, Emmett and Teller) specific surface area, $m^2\ g^{-1}$; #S_{MICRO} : specific surface area of micropore, $m^2\ g^{-1}$; $$S_{MESO}$: specific surface area of mesopore, $m^2\ g^{-1}$; &V_T: Total pore volume, $cm^3\ g^{-1}$; &V_T: Total pore volume calculated at p/p_o (0.99) , $cm^3\ g^{-1}$; %V_{MICRO}: t-plot micropore volume, $cm^3\ g^{-1}$; @V_{MESO}: mesopore volume, $cm^3\ g^{-1}$; £APS: Average pore size (nm) of zeolites; ¥Py FTIR: FTIR Spectroscopy after pyridine adsorption [6]; ©C_{BAS}: Concentration of Brønsted acidic sites, μ mol g^{-1}; and §C_{LAS}: Concentration of Lewis acidic sites, μ mol g^{-1}

2.5 Thermogravimetric analysis

The thermal decomposition behaviour of solid raw or torrefied biomass, LLDPE and their blends, under non-isothermal conditions, was analysed in the thermogravimetric analyser (Model: TG209F1, Make: Netzsch, Germany). Approximately 10 mg of individual or blended sample was taken in an alumina crucible and heated with different heating ramps (5–40°C min^{-1}) and weight loss was recorded as a function of temperature (30–900°C). To maintain the inert atmosphere, the argon gas was used at a flowrate of 20 mL min^{-1}. The raw data obtained from TG analyzer was used to determine the synergism, kinetics, and reaction mechanism.

The blends (raw or torrefied biomass + plastic) were prepared by taking appropriate mass ratios in a mortar and pestle and blended thoroughly to homogeneity as shown in Table 2.4. To prepare the samples for catalytic co-pyrolysis, 60 wt% of the catalyst (HZSM-5 or MesoHY) was added to each sample and mixed well to homogeneity.

Table 2.4: The code and the composition of TBSD + LLDPE blends

Code	The weight % of each component in mixed samples	
	Raw or Torrefied bamboo sawdust	LLDPE
BSD or TBSD	100	0
BP3:1 or TBP3:1	75	25
BP1:1 or TBP1:1	50	50
BP1:3 or TBP1:3	25	75
LLDPE	0	100

2.6 Synergism analysis

To understand the synergistic effects in co-pyrolysis of blends, an additive formula was used, assuming no interaction between the two compounds (BSD or TBSD and LLDPE) present in the blend. The thermal profile was calculated using the additive formula and was compared with that obtained from the experiment. From the difference between the two profiles, the synergistic effects were deduced. The extent of synergistic effect (ΔW) during co-pyrolysis was calculated using the following formula. [7–10]

$$\Delta W = W_{EXP} - W_{CAL} \dots\dots\dots\dots\dots\dots\dots\dots\dots\dots\dots\dots\dots\dots\dots\dots 2.4$$

The following additive formula was used to calculate W_{CAL},

$$W_{CAL} = X_1 W_1 + X_2 W_2 \dots\dots\dots\dots\dots\dots\dots\dots\dots\dots\dots\dots\dots\dots\dots\dots 2.5$$

Where X_1 and X_2 are the mass fraction of BSD/TBSD and LLDPE in the blend and W_1 and W_2 are the weight % from TGA of BSD and LLDPE, respectively. According to this equation, the

total weight at a certain temperature is the sum of the weights of individual components multiplied by the corresponding weight fraction in the blend.[11–13]

Substituting the value of W_{CAL} in equation 2.1, we get following equation

$$\Delta W = W_{EXP} - (X_1 W_1 + X_2 W_2) \ldots\ldots\ldots\ldots\ldots\ldots\ldots\ldots\ldots\ldots\ldots\ldots 2.6$$

If the ΔW is positive, the synergistic effect is passive or inhibitive and if the ΔW is negative then the synergistic effect is positive.

2.7 Kinetic analysis

The apparent activation energies (E_α) of catalytic or non-catalytic (co-)pyrolysis of BSD/TBSD, LLDPE and their blends were calculated from the slope (E_α/R) of the graph between $ln\left[\frac{\beta}{T_{\alpha_i}^2}\right] vs \frac{1}{T_{\alpha_i}}$ at conversion rate α and various heating rates i = 5, 10, 20 and 40°C min^{-1} by Kissinger-Akahira-Sunose model (equation 1.11). In a similar manner, E_α were evaluated by FWO (equation 1.12) and FM (equation 1.13) models from the slope of the curves: $\ln(\beta_i) vs \frac{1}{T_{\alpha_i}}$, and $ln\left[\frac{d\alpha}{dt}\right]_{\alpha_i} vs \frac{1}{T_{\alpha_i}}$, respectively.

2.8 Criado's master plots

The Master plots for individual and blended samples were derived from equation 1.23 at ramp rate of 10 by using apparent activation energy from FM model. The RHS of equation 1.23 is known as reduced rate. A comparison between experimental results obtained from equation 1.23 with the theoretical master plot allows identifying the best reaction mechanism for the degradation process.[14]

References:

[1] L. Hu, H. Peng, Q. Xia, Y. Zhang, R. Ruan, W. Zhou, Effect of ionic liquid pretreatment on the physicochemical properties of hemicellulose from bamboo, J. Mol. Struct. 1210 (2020) 1–8. https://doi.org/10.1016/j.molstruc.2020.128067.

[2] B. Velaga, R.P. Parde, J. Soni, N.R. Peela, Synthesized hierarchical mordenite zeolites for the biomass conversion to levulinic acid and the mechanistic insights into humins formation, Microporous Mesoporous Mater. 287 (2019) 18–28. https://doi.org/10.1016/j.micromeso.2019.05.049.

[3] A. Demirbas, Combustion characteristics of different biomass fuels, Process Energy Combust. Sci. 30 (2004) 219–230. https://doi.org/10.1016/j.pecs.2003.10.004.

[4] A. Monti, N. Di Virgilio, G. Venturi, Mineral composition and ash content of six major energy crops, Biomass and Bioenergy. 32 (2008) 216–223. https://doi.org/10.1016/j.biombioe.2007.09.012.

[5] B.S. Kim, Y.M. Kim, H.W. Lee, J. Jae, D.H. Kim, S.C. Jung, C. Watanabe, Y.K. Park, Catalytic Copyrolysis of Cellulose and Thermoplastics over HZSM-5 and HY, ACS Sustain. Chem. Eng. 4 (2016) 1354–1363. https://doi.org/10.1021/acssuschemeng.5b01381.

[6] N.R. Peela, S.K. Yedla, B. Velaga, A. Kumar, A.K. Golder, Choline chloride functionalized zeolites for the conversion of biomass derivatives to 5-hydroxymethylfurfural, Appl. Catal. A Gen. 580 (2019) 59–70. https://doi.org/10.1016/j.apcata.2019.05.005.

[7] D.K. Park, S.D. Kim, S.H. Lee, J.G. Lee, Co-pyrolysis characteristics of sawdust and coal blend in TGA and a fixed bed reactor, Bioresour. Technol. 101 (2010) 6151–6156. https://doi.org/10.1016/j.biortech.2010.02.087.

[8] B. Han, Y. Chen, Y. Wu, D. Hua, Z. Chen, W. Feng, M. Yang, Q. Xie, Co-pyrolysis behaviors and kinetics of plastics-biomass blends through thermogravimetric analysis, J. Therm. Anal. Calorim. 115 (2014) 227–235. https://doi.org/10.1007/s10973-013-3228-7.

[9] Z. Wu, S. Wang, J. Zhao, L. Chen, H. Meng, Synergistic effect on thermal behavior during co-pyrolysis of lignocellulosic biomass model components blend with bituminous coal, Bioresour. Technol. 169 (2014) 220–228. https://doi.org/10.1016/j.biortech.2014.06.105.

[10] L. Zhou, Y. Wang, Q. Huang, J. Cai, Thermogravimetric characteristics and kinetic of plastic and biomass blends co-pyrolysis, Fuel Process. Technol. 87 (2006) 963–969. https://doi.org/10.1016/j.fuproc.2006.07.002.

[11] K. Azizi, M. Keshavarz, H. Abedini, Characteristics and kinetics study of simultaneous pyrolysis of microalgae Chlorella vulgaris , wood and polypropylene through TGA, Bioresour. Technol. 243 (2017) 481–491.

[12] X. Kai, T. Yang, S. Shen, R. Li, TG-FTIR-MS study of synergistic e ff ects during co-pyrolysis of corn stalk and high-density polyethylene (HDPE), Energy Convers. Manag. 181 (2019) 202–213. https://doi.org/10.1016/j.enconman.2018.11.065.

[13] Y.Y. Chong, S. Thangalazhy-gopakumar, S. Gan, H.K. Ng, L.Y. Lee, Kinetics and Mechanisms for Copyrolysis of Palm Empty Fruit Bunch Fiber (EFBF) with Palm Oil Mill E ffl uent (POME) Sludge, Energy & Fuels. 31 (2017) 8217–8227. https://doi.org/10.1021/acs.energyfuels.7b00877.

[14] D. Irmak, P. Parthasarathy, J.L. Goldfarb, S. Ceylan, Pyrolysis reaction models of waste tires : Application of Master-Plots method for energy conversion via devolatilization, Waste Manag. 68 (2019) 405–411.

Chapter 3

Copyrolysis of Bamboo Saw Dust and Linear Low Density Polyethylene

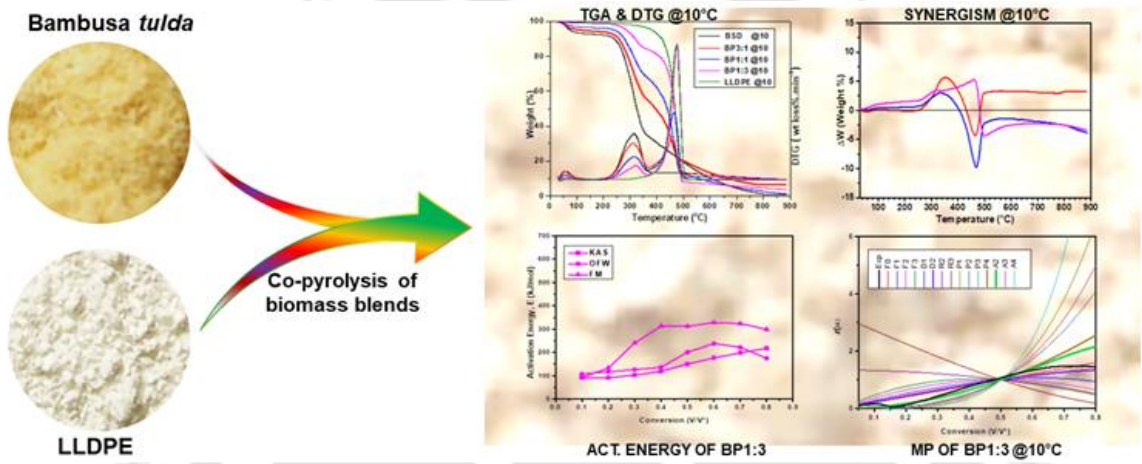

Highlights

- The co-pyrolysis of bamboo biomass and LLDPE is studied using thermogravimetry
- The highest synergism and an $\bar{E}_\alpha$ drop of 36% with the blend 1:3 biomass: plastic
- Master plot: A2, and D2 mechanisms at lower and higher conversions, respectively
- The $\bar{E}_\alpha$ for the blends 3:1, 1:1 and 1:3 are 397, 376, and 188 kJ mol^{-1}, respectively
- The mean reactivity order of blends is found to be 1:3>1:1>3:1 at all heating rates

3.1 Objectives

This chapter focuses on the kinetics and the synergistic effects of the co-pyrolysis of bamboo sawdust (BSD) and linear low-density polyethylene (LLDPE) using thermogravimetric

analysis (TGA). The kinetic parameters were determined utilizing three models based on the isoconversional method: Kissinger-Akahira-Sunose **(**KAS), Flynn-Wall-Ozawa (FWO), and Friedman (FM) models. The reaction mechanism was deduced using the Criado's master plot. To the best of our knowledge, no reports available on the co-pyrolysis of BSD+LLDPE blend.

3.2 Results and discussion

3.2.1 Thermal degradation of BSD and LLDPE blends

The TGA and DTG curves for pure BSD, LLDPE and their blends BP3:1, BP1:1 and BP1:3 at three heating rates (5, 10 and 20°C min^{-1}) are shown in Fig. 3.1 and deconvoluted plots fitted with Gaussian function are illustrated in Fig. A1.1– A1.3. In case of pure BSD and LLDPE, the thermal degradation occurred in three stages and two stages, respectively. While, their blends BP3:1, BP1:1 and BP1:3 showed four stages of degradation. The peak temperature (T_{max}), weight loss (W_{loss}), and the maximum rate of degradation (DR_{max}) in each stage, and the residual weight after 800°C and the mean reactivity for all the samples at different heating rates are presented in Table 3.1. The weight loss from BSD (e.g., 6.10 % at heating rate 20°C min^{-1}), corresponding to the first stage (25–150°C), is due to the removal of moisture and a marginal loss of light volatiles. [1,2] Structural water present in the form of hydrogen and hydroxyl moieties is stripped out from the equatorial position of cellulose in the temperature range of 140–150°C.[3] The very small weight loss (e.g., 0.46 wt.% at a heating rate of 20°C min^{-1}) from LLDPE in the first stage is due to moisture removal. [4,5]

The second stage of weight loss occurred in the temperature range of 180–400°C and 280–520°C from BSD and LLDPE, respectively. For both the samples this is the maximum degradation range and is termed as active pyrolysis. The third stage of weight loss from BSD occurred in the temperature range of 405–800°C and could be attributed to the decomposition of lignin and carbonaceous material. Maximum peak temperature (T_{max}) and the decomposition rate (DR_{max}) of LLDPE were higher as compared to those of BSD at all the heating rates (5

(Table S2), 10 (Table S3) and 20°C min^{-1} (Table 3.1)). For example, in the second stage, DR_{max} of LLDPE was 2.12 mg min^{-1} at a T_{max} of 474°C, while that of BSD was 0.73 mg min^{-1} at a T_{max} of 316°C, for 10°C min^{-1} ramp rate. Moreover, the second stage starting temperature for decomposition of LLDPE (280°C at 10°C min^{-1}) was higher as compared to that of BSD (180°C at 10°C min^{-1}). Weak ether bond (360–420 kJ mol^{-1}) in BSD is responsible for the lower T_{max}. On the other hand, the hard-to-break bonds (C−H; 414 kJ mol^{-1}, C−C; 344 kJ mol^{-1} and C=C; 611 kJ mol^{-1}) present in LLDPE make its T_{max} higher. [6,7] The width of weight loss peak (in DTG) from BSD, in the second stage, was wider as compared to that of LLDPE. For example, the decomposition of BSD and LLDPE in the second stage occurred in the range 180–400°C (width was 220°C) and 340–520°C (width was 180°C), respectively, at 20°C min^{-1} (Fig. 3.1 and Table 3.1). This is because of structural differences of lignocellulosic materials and LLDPE. The small hump (260–290°C) appeared on the left side of the main degradation peak from pure BSD and blended samples could be attributed to the degradation of hemicellulose. [8] Interestingly, the hump was clearly visible at 5 and 20°C min^{-1} ramp rates but was not completely distinguishable at 10°C min^{-1}, indicating that the degradation of hemicellulose is overlapped with that of cellulose and lignin [9,10].

The rate of decomposition in the second and third stages depended upon the composition of the blend (Fig.s 3.1a2, 3.1b2 and 3.1c2). In the second stage (180–410°C), the decomposition of cellulose and hemicellulose occurred and was slightly affected by presence of LLDPE. Whereas, in the third stage (380–520°C), the decomposition of LLDPE dominates. The free radicals formed from LLDPE helps in the decomposition of lignin in this stage. In blended samples, the PE pyrolyzates traverse to the lignin layer and interacts with the lignin pyrolysis intermediates. A series of radical intermediates such as benzyl, benzoyl, phenyl and acyl radicals were formed from thermal degradation of lignin as shown in scheme 1. Owing to effective mass transfer and quick interaction between lignin intermediates and PE pyrolyzates,

phenolic monomers were formed. In the absence of plastic pyrolyzates, the lignin derived radicals produce coke by coupling and rearrangement reactions.[11] Therefore, the free radicals formed from the LLDPE helps in the decomposition of lignin, as depicted by Scheme. A1.1 (Annexure A1). [12–18] Volatiles formation from the blends was due to breaking of various bonds (C–C, C=C, β–(C_1↔C_4), α–(C_1↔C_4 & C_1↔C_6), etc.) and involvement of various functional groups (–OH, –OR, >CO, –CHO, –COOH, etc.) in different reactions (cracking, condensation polymerization, depolymerisation, ring opening, etc.). Softening of LLDPE occurs at around 300°C, comes under the plastic state and inhibits the evolution of volatile matter at this (second) stage. [4,10] With the increase of LLDPE composition from 25 to 75 wt.% in BSD, DR_{max} in second stage was decreased at all the heating rates (5–20°C min^{-1}). For example, in the blend BP1:3, DR_{max} in second stage diminishes to 0.458 mg min^{-1} at 339°C at 20°C min^{-1} (Table 3.1). While in third stage, the pattern of DR_{max} was reversed. For example, the value of DR_{max} of BP1:3 (5.479 mg min^{-1} at 20°C min^{-1}) was the highest as compared to other mixed samples, because it contains the maximum amount of LLDPE (75%). The change in DR_{max} showed a similar trend with other two heating rates. The thermal behavior of these peaks for blended samples in second and third stage can be attributed to the disintegration of lignocellulosic materials (cellulose, hemicellulose, and lignin) and LLDPE, respectively. [19]

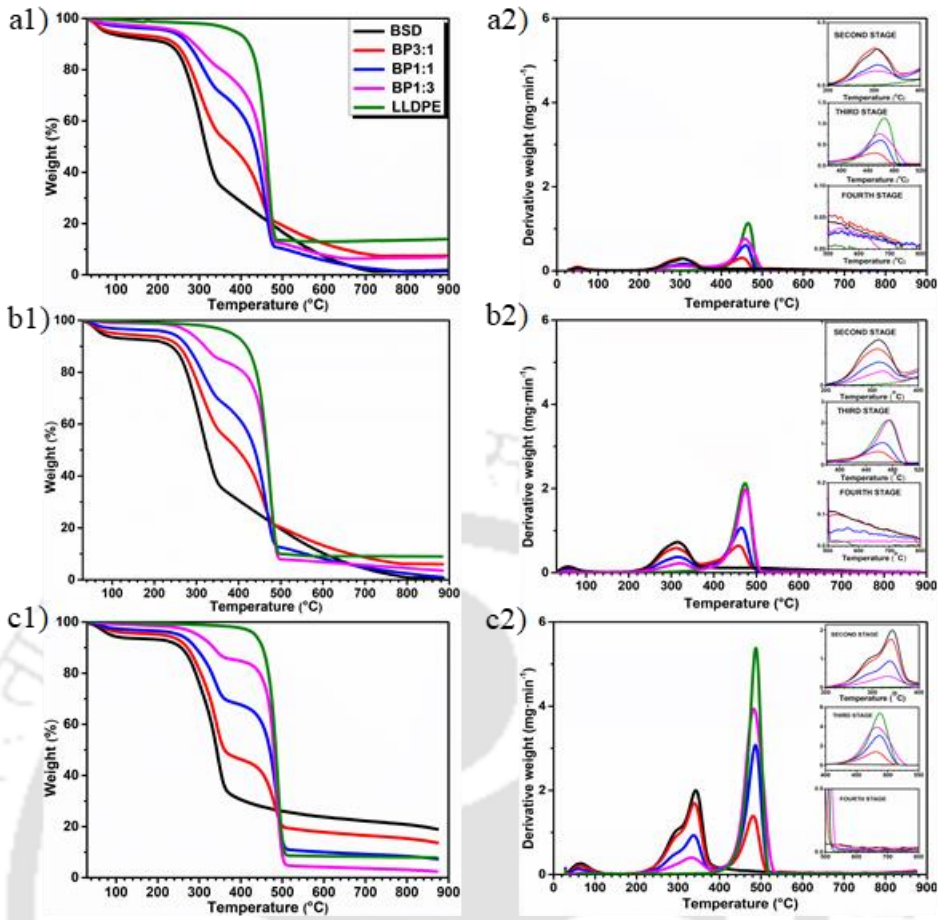

Figure 3.1. TG analysis of BSD+LLDPE blends at three different heating rates of (a) 5, (b) 10 and (c) 20°C min^{-1}: Weight loss as a function of temperature (a1, b1 and c1) and DTG (a2, b2, and c2). (The legend given in subfigure a1 is applicable to all the other subfigures).

The mean reactivity (R_M) was calculated based on the method developed by Ghetti et al.[20], which suggests that the mean reactivity depends on two parameters: peak height (R) and corresponding peak temperature (T_p) in DTG. The R_M is directly proportional to the peak height and inversely proportional to the corresponding peak temperature.[20,21] For blends, the peak height increased in the second stage with weight percentage of bamboo biomass in the second stage of DTG while it was reversed in the third stage. The order of M_R of blends was found to be BP1:3 > BP1:1 > BP3:1 at heating rates 10 and 20°C min^{-1}. The M_R of all the three blends were nearly equal at heating rate 5°C min^{-1}.

3.2.2 Effect of heating rate

The thermal degradation profiles of BSD, LLDPE and their blends at heating rates of 5, 10 and 20°C min^{-1} are shown in Fig. 3.2. The DTG peaks shifted to higher temperature with heating rate. The M_R and DR_{max} of mixed samples were increased with the increase of heating rate from 5 to 20°C min^{-1} (Tables 3.1, A1.1 and A1.2), which is a usual non-isothermal behavior as also reported by other researchers.[22,23] The poor thermal conductivity of BSD creates a temperature gradient across the BSD particles, which is responsible for peak shifting in DTG curves. A constant temperature across the BSD particle can be assumed at lower heating rate (5°C min^{-1}), where sufficient time was given for heating, while at the higher heating rates (10 and 20°C min^{-1}) a substantial temperature gradient exists across the biomass particle.[24] The secondary reactions may change with heating rate.[25] A better heat transfer inside the particle can be ensured at a lower heating rate.[26] The higher rate of decomposition was observed at higher heating rate because of the higher thermal energy.[27]

Similar studies conducted under non-isothermal conditions, demonstrated that TGA curves shifted to higher temperature zone with heating rate.[28,29] The initial and final degradation temperatures were increased with heating rate. The overall release of volatiles in the second and third stage of co-pyrolysis process was found to increase with heating rate and plastic content. In the second stage of BSD and LLDPE, the release of volatiles increased with heating rate (5–20°C min^{-1}), while the volatile components from the BSD decreased in the third stage (Fig. 3.2a and c). The generation of free radicals from volatiles depends upon heating rate. A lesser amount of free radicals forms at low ramp rate (5°C min^{-1}) and is responsible for the char formation by polymerization, cracking, recondensation, etc.[24] The thermal degradation of BSD follows complicated kinetics which could be attributed to the structural composition of hemicellulose, cellulose and lignin. At low heating rate, mass and heat transfer between particles is inhibited by cellulose and interface of hemicellulose and cellulose because

of crystalline nature of cellulose.[30] Heat flux is more at higher heating rate as compared to that at lower heating rate which brings down the viscosity of solid materials and initiates the reaction for volatile formation. [33, 34]

Table 3.1. Degradation parameters at different stages of degradation of pure BSD, LLDPE and their blends at a heating rate of 20°C min^{-1}.

Stages	Parameters	BSD	BP3:1	BP1:1	BP1:3	LLDPE
First stage	T_{Range} (°C)	25–150	25–150	25–150	25–150	25–150
	W_{Loss} (%)	6.075	4.121	2.879	1.436	0.463
	DR_{max} (mg min^{-1})	0.2608	0.207	0.133	0.039	–
	T_{max} (°C)	63	69	58	53	–
Second stage	T_{Range} (°C)	180–400	180–395	180–390	180–390	340–520
	W_{Loss} (%)	62.891	49.123	28.681	13.384	89.558
	DR_{max} (mg min^{-1})	1.997	1.685	0.927	0.458	5.382
	T_{max} (°C)	343	341	334	339	488
Third stage	T_{Range} (°C)	405–800	400–530	390–540	395–530	520–800
	W_{Loss} (%)	9.774	27.260	57.480	80.770	0.580
	DR_{max} (mg min^{-1})	–	1.389	3.054	5.479	–
	T_{max} (°C)	–	481	485	486	–
Fourth stage	T_{Range} (°C)	–	520–800	520–800	520–800	–
	W_{Loss} (%)	–	4.097	2.404	1.803	–
Reactivity (mg min^{-1} $°C^{-1}$) x10^3		4.98	3.691	3.788	4.453	11.028
% Residual weight at 800°C		20.770	15.04	8.051	3.071	7.98

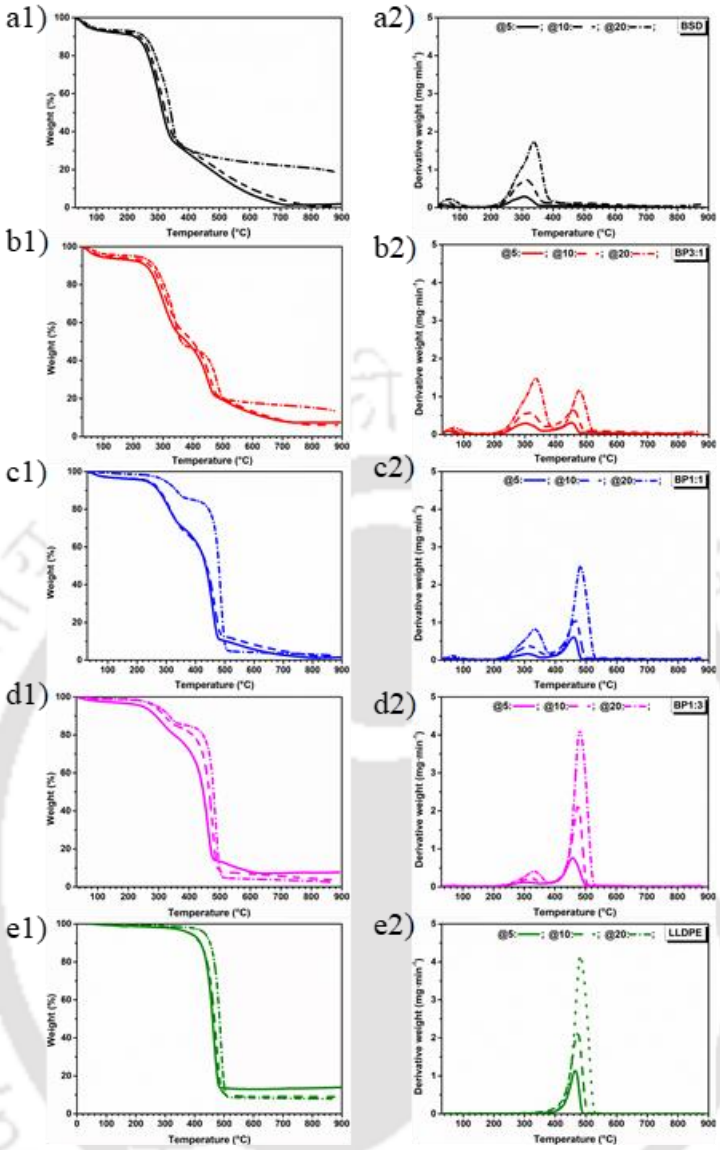

Figure3.2.TG analysis of three different BSD+LLDPE blends (a) BSD (b) BP3:1, (c) BP1:1, (d) BP1:3, and (e) LLDPE: Weight loss as a function of temperature (a1, b1, c1, d1 and e1) and DTG (a2, b2, c2, d2 and e2).

3.2.3 Synergistic effect

The BSD and LLDPE showed different thermal behaviour (Fig. 3.1) due to differences in their structural and chemical properties.

The residual weight (W_{CAL} (equation 2.5) at highest temperature) was higher in the case of calculated blend as compared to that (W_{EXP} at highest temperature) of experimental blend (Fig. 3.3a1, 3.3b1 and 3.3c1). This could be due to the higher liquid formation in the case of experimental blend, which in-turn could be attributed to the hydrogen rich atmosphere (resulted from the LLDPE) of the blend.[33] The LLDPE (with H/C_{eff} :0.18 w/w) acts as a hydrogen donor during co-pyrolysis process which inhibits the recombination and cross linking reactions that increase char formation. [34,35] In other words, in the absence of such atmosphere (biomass alone), the char formation was favoured and the residual weight was higher.

ΔW (equation 2.6) < 0 indicates an accelerated co-pyrolysis process and a positive synergistic effect. While, ΔW > 0 indicates a passive synergistic effect. For all the three blends, the ΔW was approximately zero below 280°C (Fig. 3.3), because, below this temperature, LLDPE is in plastic state and does not start decomposition/interaction with BSD. In the temperature range of 300 to 500°C, $W_{EXP} < W_{CAL}$ for BP1:3 implying that the weight loss was more in the case of experimental blend. This indicates a positive synergistic effect between BSD and LLDPE during the co-pyrolysis. For BP1:1 and BP3:1, the value of ΔW was positive at low temperatures and then decreased sharply at 430–500°C, peaking at 460°C. While, for BP1:3, the ΔW was started to decline at 320°C and increased sharply at 500°C after peaking at 450°C. This characteristic behaviour of blend can be explained by the physical state of LLDPE. First it gets softened at about 280°C followed by a plastic state which inhibits the release of volatiles from BSD by the formation of a coating layer on the surface of BSD. The internal pressure of volatiles from BSD and plastic increases with increase in temperature. This is beneficial for dispersal of residue of biomass formed by secondary reactions.[10,33,36,37]. This behaviour is pictorially shown in Fig. 3.4. This could be the reason for the higher liquid production (or lower residual mass) during the thermal degradation of the blends. Rapid generation of volatiles from LLDPE in mixed samples was occurred upon further heating (>

280°C) which ruptures the coating on BSD and causes the ΔW to decrease quickly. Furthermore, it was observed that the values of ΔW of BP1:3 (-11.68) and BP1:1 (-11.08) are much higher than that of BP3:1 (-4.75) at 5°C min^{-1}, suggesting that BP1:3 and BP1:1 showed a strong positive synergism than BP3:1. The synergism was examined during copyrolysis of biomass and plastic, biomass accelerated the chain scission of polyethylene to short carbon chain length while PE promoted the decomposition of biomass to carbohydrate derived light oxygenates (for examples furan). Therefore, Diels-Alder reaction occurred between light oxygenate furan from biomass and olefins from PE to form aromatic components and inhibit coke formation. Zhang et al. explored the synergism between biomass and plastic. Primary free radicals are formed from biomass which react with PE derived hydrocarbons to form volatile substances which not only accelerated biomass decomposition but also inhibit free radical repolymerization to form coke. The blend containing higher amount of plastic which produce higher number of olefin chain which react further oxygenates derived from biomass saw dust or torrefied biomass saw dust during copyrolysis process to exhibit highest synergism as compared to other blends (BP3:1 and BP1:1 or TBP3:1 and TBP1:1). The ΔW of all the blends was approximately constant above 500°C since the devolatilization process has essentially been completed.

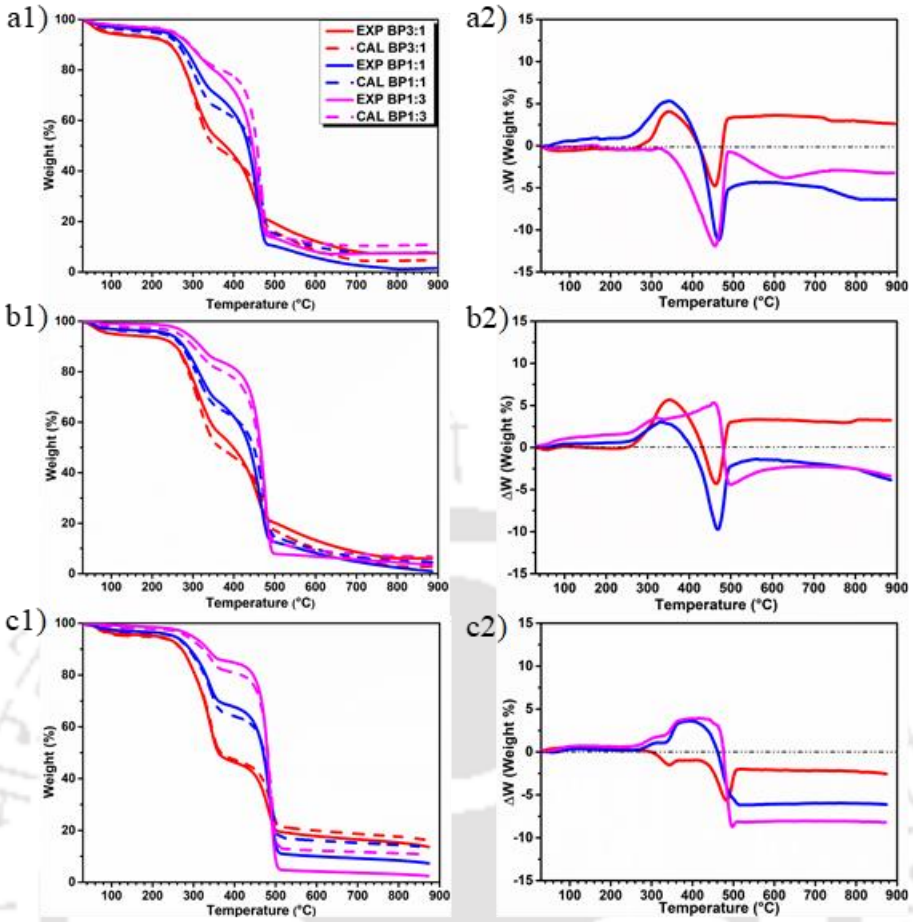

Figure 3.3. Experimental and calculated (from equation 18) TG curves for three different BSD+LLDPE blends (BP3:1, BP1:1, and BP1:3) at three different heating rates of (a) 5, (b) 10 and (c) 20°C min^{-1}: Weight loss as a function of temperature (a1, b1 and c1) and ΔW (a2, b2, and c2). (The legend given in subfigure a1 is applicable to all other sub figures).

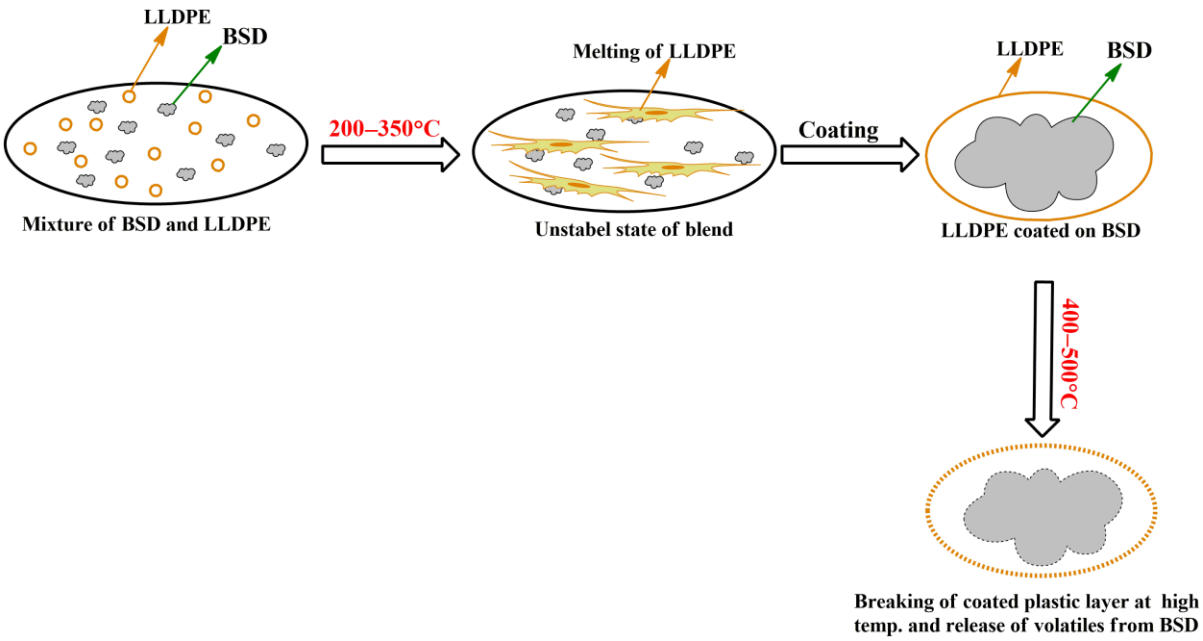

Figure 3.4. Schematic representation of co-pyrolysis process of BSD and LLDPE at lower temperatures.

The thermal degradation of polyolefin occurs via a radical chain process. It consists of three steps i.e. initiation, propagation and termination [4,33,38]. A large number of free radicals are evolved from lignocellulosic materials during co-pyrolysis. These free radicals accelerate the decomposition of plastic involving many reactions such as cracking, depolymerisation and crosslinking reaction.

3.2.4 Kinetic analysis

For the estimation of kinetic parameters (E_α and A) of the co-pyrolysis process, two integral isoconversional models (KAS and FWO) and one differential (FM) model were used. In these models, decomposition was assumed to be first order reaction. The apparent activation energy (E_α) determined by these isoconversional models is independent of the reaction mechanism. [32] The master plot was used to identify the order and mechanism of the reaction.

The equations 1.11, 1.12 and 1.13 were plotted, at constant conversion, to estimate the activation energy and frequency factor from KAS, FWO and FM models, respectively, as

shown in Fig. A1.1 (Annexure A1). For kinetic analysis, a temperature range of 150–700°C was used at all the three heating rates. Moisture was removed below 150°C and there was no weight loss above 700°C, as shown by the TGA graph (Fig. 3.1). The values of E_α, A and the correlation coefficient (R^2) for the thermal degradation of blended biomass are presented in Tables A1.3–A1.7 (Annexure A1). The apparent activation energy increased with conversion as shown in Fig. 3.5, indicating that the solid-state reactions follow multi-step reactions. For example, the apparent activation energies in the conversion range from 0.1 to 0.7 varied in the range of 92–324 kJ mol^{-1} and subsequently decreased towards the end of the reaction. The cleavage of weak bonds and elimination of volatile molecules occurs at the beginning of pyrolysis process which requires low activation energy. Decomposition of the stronger bonds and bigger stable molecules requires higher apparent activation energy. [39] The mean values of apparent activation energy ($\bar{E}_\alpha$) for the decomposition of blends (BP3:1, BP1:1 and BP1:3) were determined to be 357, 371, and 143 kJ mol^{-1} from KAS, 368, 400 and 165 kJ mol^{-1} from FWO and 468, 356 and 255 kJ mol^{-1} from FM models, respectively (Table 3.2). In addition, the mean $\bar{E}_\alpha$ value of individual sample such as BSD and LLDPE was found as 265 and 207 kJ mol^{-1} from KAS, 265 and 230 kJ mol^{-1} from FWO and 353 and 175 kJ mol^{-1} from FM model, respectively. Overall, the BSD degradation involves the cracking and condensation reactions of cellulose, hemicellulose and lignin. While, the LLDPE consists of C–C bonds in linear fashion with short chain lengths and only cracking occurs during its degradation. Hence, the activation energy of BSD was higher as compared to that of LLDPE.[40–44] The E_α of blends obtained from KAS and FWO models were first increased then decreased, while, those obtained from FM model decreased continuously, with LLDPE concentration. The pattern of mean apparent activation energy (E_α) as discussed above was collectively due to composition variation, polymeric structure (hemicellulose, cellulose, lignin and LLDPE), types of chemical bonds of bamboo biomass and plastic and temperature. The apparent activation energies

obtained by FM model were noisy as compared to those from the other two models (KAS and FWO). The KAS and FWO models are derived based on the assumption of constant activation energy, which may introduce a systematic error in the treatment.[45,46] In FM model, approximations and boundary conditions are not required to calculate apparent activation energy.[45,46] Scattered values of apparent activation energy and noisy data obtained by FM method were because of the differential method applied to integral data.[46,47] For calculating kinetic parameters, the FM model can be the best method among three methods (KAS, FWO, and FM) for solid state reactions.[48] The BP1:3 is the potentially efficient blend for co-pyrolysis as compared to other two blends because of its lower mean apparent activation energy. The values of R^2 over the entire conversion range (0.1–0.8) were close to 1 (> 0.97) for all the three models tested indicating a good fit of the experimental data to all three models.

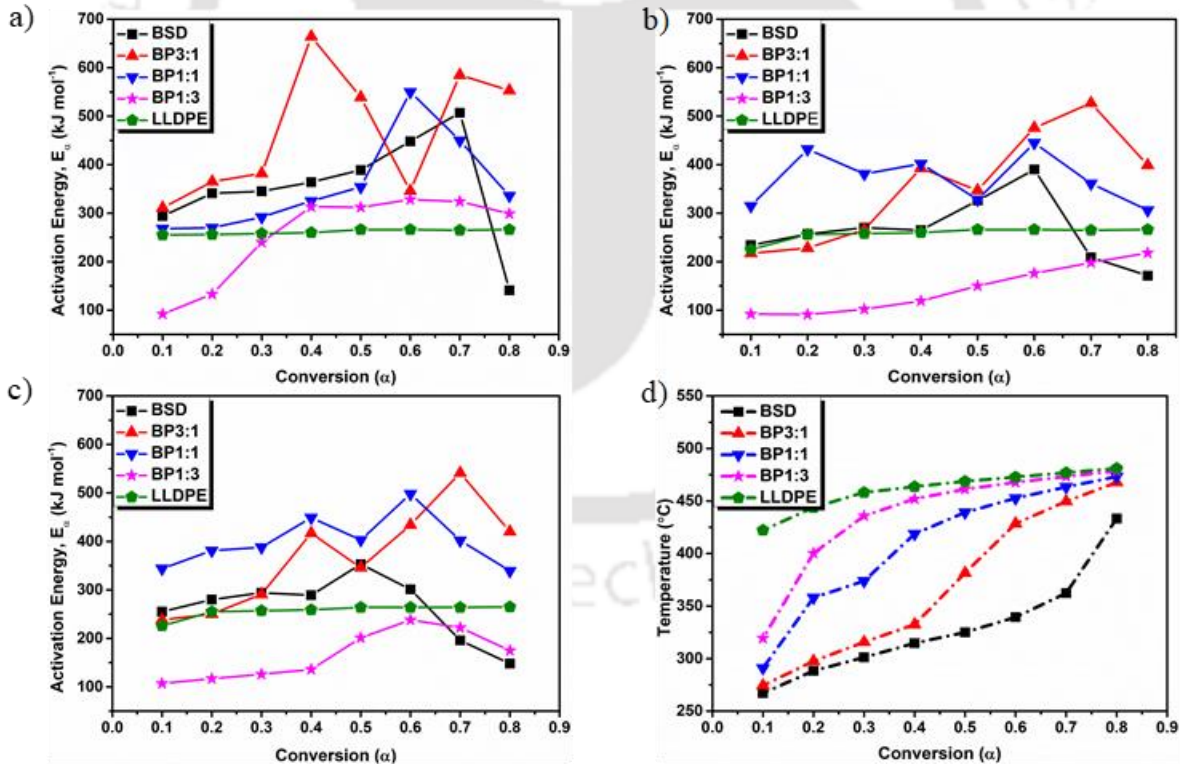

Figure 3.5. Variation of E_α and temperature with conversion of BSD+LLDPE blends: a) FM model, b) KAS, c) FWO model with mixed and individual sample d) Temperature profile of mixed samples

Table 3.2. Average apparent activation energy from isoconversional methods of BSD, LLDPE and BSD + LLDPE blends.

Code	KAS Model		FWO Model		FM Model	
	$\bar{E}_\alpha$, (kJ mol^{-1})	Avg. R^2	$\bar{E}_\alpha$, (kJ mol^{-1})	Avg. R^2	$\bar{E}_\alpha$, (kJ mol^{-1})	Avg. R^2
BSD	265	0.982	265	0.976	353	0.970
BP3:1	357	0.979	368	0.981	468	0.956
BP1:1	371	0.976	400	0.978	356	0.993
BP1:3	143	0.988	165	0.990	255	0.982
LLDPE	207	0.970	230	0.975	175	0.990

3.2.5 Master plot method for determination of reaction mechanism

For kinetic studies, determination of mechanism is a fundamental step which helps to improve understanding of the reaction. In the previous sections, a first order reaction was assumed in isoconversional methods [31,49–52] but it is not a recommended assumption without prior knowledge of master plots because other orders may also be suitable to describe the reaction. The average values of apparent activation energy ($\bar{E}_\alpha$) of thermal degradation of BSD, LLDPE and blends calculated using FM model are used to construct an experimental master plot at 10°C min^{-1} by using equation 1.23 to find out reaction mechanism. The experimental master plot ($Z(\alpha)$ against α) at 10°C min^{-1} ramp rate is shown in Fig. 3.6. Theoretical master plots obtained with various reaction mechanisms [32,53–56] are also shown in the same figure. The experimental master plot of BSD in the conversion range from 0.05 to 0.5 followed an F3 model (3rd order reaction) while that in the conversion range from 0.5 to 0.8 was close to contraction volume R3 model (Fig. 3.6a). The experimental master plot of BP1:1 in the conversion range of 0.3 to 0.8 was close to the theoretical master plot of random nucleation and growth mechanism (A_2, n:2) (Fig. 3.6b). When the conversion value less than 0.3, the same experimental graph follow the trend of F3 model. For the blend BP1:3, in 0.05 to 0.5 conversion range, the master plot was close to the theoretical master plot of random nucleation and growth mechanism (A_2, n:2) (Fig. 3.6c). When the conversion value was graeter than 0.5 to 0.8, the

same experimental graph followed the trend of D2 model. These findings are in-line with the previous studies. [57–59] By diffusion controlled mechanism, the breakdown of hemicellulose and extractives occurs more vigorously at a low temperature which creates more volatile components. These components promote the degradation of cellulose. [60–62]. The theoretical master plot of the F1 model (n^{th} order reaction; α value from 0.05 to 0.8) was the best suited to the experimental master plot of LLDPE (Fig. 3.6d). The experimental conversion ranges and their corresponding theoretical master plots models are summarized in Table 3.3.

In literature, no study reported the co-pyrolysis of BSD and LLDPE. Therefore, the data obtained in this study was compared with the similar blends such as biomass (pine saw dust, bagasse, empty fruit bunch etc.) and LDPE, HDPE, PS or PP reported in the literature (Table S9).[10,63–69] The thermal reactivity of BSD is lower as compared to that of LLDPE because of high mean activation energy of BSD in pyrolysis process (Tables A1.3 and A1.7). Similar results are also reported in various other studies.[4,63,70] The peak temperature (T_{max}) is related to material structure, plastics such as LDPE, HDPE and PP having similar structure therefore they have almost same T_{max} (486–505°C) but LLDPE has different structural arrangement (polyethylene and α olefins i.e. hexane-1 and octane-1). The physical characteristics of olefin polymers are discussed in the introduction part of this thesis. The variations of mean activation energies of blends (Tables A1.4–A1.6) with weight ratio show that they possess different pyrolysis reactivity. The activation energies vary with raw material structures, weight ratio between biomass and plastic, operating conditions and methods. The mean activation energy of the blend BP1:3 (188 kJ $mole^{-1}$) lie below that of both BSD and LLDPE and was 36% lower with respect to BSD which is a clear indication of synergism. Moreover, the synergistic effect was much higher with the BP1:3 blend as compared to that from most of the other studies (Table 1.3). Therefore, LLDPE is a good choice to blend with the BSD. The high synergism could be explained based on the favourable properties of the

LLDPE as compared to LDPE and HDPE. Typical characteristics of LLDPE such as structural components (polyethylene and α olefins) and arrangements, lower lamellar thickness, lower melting point range (125–128°C) and high frequency of shorter side chain are responsible for higher thermal reactivity [40,41,71] which, in turn, provides the higher reactivity when blended with biomass.

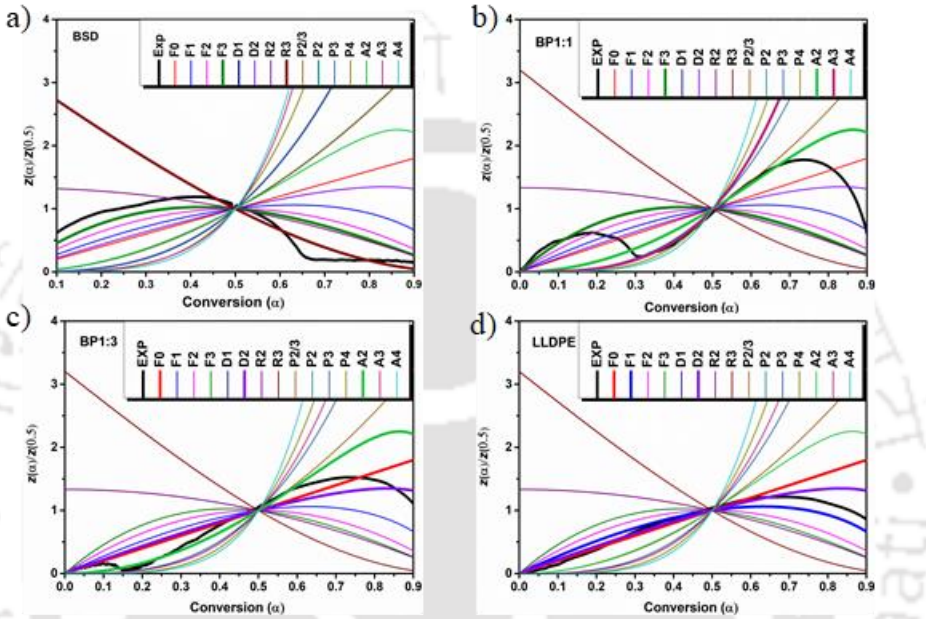

Figure 3.6. Master plot Z (α) of BSD+LLDPE blends at a heating rate of 10°C min^{-1}: a) BSD b) BP 1:1, c) BP 1:3 and d) LLDPE.

Table 3.3. Determination of kinetic model by Criadios-Master plots method for pure BSD, plastic and blended samples at 10°C min^{-1}

BSD			**BP1:1**			**BP1:3**			**LLDPE**		
α	**M**	**M^n**	**α**	**M**	**M^n**	**α**	**M**	**M^n**	**α**	**M**	**M^n**
0.05–0.5	F3	RO	0.05–0.3	F3	RO	0.05–0.5	A2	NM	0.05–0.4	P3	PL
0.5–0.8	R3	GC	0.3–0.8	A2	NM	0.5–0.8	D2	DN	0.4–0.8	F1	RO
Note: M^n: Mechanism; M: Model (RO: Reaction order, GC: Geometrical Contraction, DN: Diffusion model and NM: Nucleation model); α: Conversion											

3.3 Conclusions

The co-pyrolysis of BSD+LLDPE blends occurs in four stages. The highest synergistic interaction between BSD and LLDPE was occurred with the blend BP1:3 (25 wt.% BSD and 75 wt.% LLDPE). In addition, an activation energy drops of 36% (with respect to biomass) was observed with the same blend. The average apparent activation energy of pure BSD, LLDPE and the blends BP3:1, BP1:1 and BP1:3 as obtained from isoconversional method were 265, 207, 357, 371, and 143 kJ mol^{-1}, respectively, from KAS model. The order of mean reactivity of blends was found to be BP1:3 > BP1:1 > BP3:1 at all the heating rates (5, 10, 20°C min^{-1}) studied. Multistep reactions were found to be responsible for a large variation of apparent activation energy of co-pyrolysis, as depicted by the master plot. The decomposition of the blend BP1:3 followed a nucleation growth (A2) model in the lower conversion range and diffusion (D2) model in the higher conversion range.

References

[1] J. Chen, Y. Wang, X. Lang, X. Ren, S. Fan, Evaluation of agricultural residues pyrolysis under non-isothermal conditions: Thermal behaviors, kinetics, and thermodynamics, Bioresour. Technol. 241 (2017) 340–348. https://doi.org/10.1016/j.biortech.2017.05.036.

[2] S. Munir, S.S. Daood, W. Nimmo, A.M. Cunliffe, B.M. Gibbs, Thermal analysis and devolatilization kinetics of cotton stalk, sugar cane bagasse and shea meal under nitrogen and air atmospheres, Bioresour. Technol. 100 (2009) 1413–1418. https://doi.org/10.1016/j.biortech.2008.07.065.

[3] M.. Tang, R. Bacon, Carbonization of cellulose fibers—I. Low temperature pyrolysis, Carbon N. Y. 2 (1964) 211–220.

https://doi.org/10.1016/0008-6223(64)90035-1.

[4] L. Zhou, Y. Wang, Q. Huang, J. Cai, Thermogravimetric characteristics and kinetic of plastic and biomass blends co-pyrolysis, Fuel Process. Technol. 87 (2006) 963–969. https://doi.org/10.1016/j.fuproc.2006.07.002.

[5] S.M. Al-Salem, A. Antelava, A. Constantinou, G. Manos, A. Dutta, A review on thermal and catalytic pyrolysis of plastic solid waste (PSW), J. Environ. Manage. 197 (2017) 177–198. https://doi.org/10.1016/j.jenvman.2017.03.084.

[6] L. Sørum, M.G. Grønli, J.E.I. Hustad, Pyrolysis characteristics and kinetics of municipal solid wastes, Fuel. 80 (2001) 1217–1227. https://doi.org/10.1016/S0016-2361(00)00218-0.

[7] Z. Wu, S. Wang, J. Zhao, L. Chen, H. Meng, Synergistic effect on thermal behavior during co-pyrolysis of lignocellulosic biomass model components blend with bituminous coal, Bioresour. Technol. 169 (2014) 220–228. https://doi.org/10.1016/j.biortech.2014.06.105.

[8] F.X. Collard, J. Blin, A review on pyrolysis of biomass constituents: Mechanisms and composition of the products obtained from the conversion of cellulose, hemicelluloses and lignin, Renew. Sustain. Energy Rev. 38 (2014) 594–608.

https://doi.org/10.1016/j.rser.2014.06.013.

[9] Y. Ma, Y. Guan, K. Zhang, G. Xu, Y. Yang, P. Stevenson, Dependency of the combustion behavior of energy grass and three other types of biomass upon lignocellulosic composition, Environ. Prog. Sustain. Energy. 37 (2018) 815–823. https://doi.org/10.1002/ep.12705.

[10] A.O. Oyedun, C.Z. Tee, S. Hanson, C.W. Hui, Thermogravimetric analysis of the pyrolysis characteristics and kinetics of plastics and biomass blends, Fuel Process. Technol. 128 (2014) 471–481. https://doi.org/10.1016/j.fuproc.2014.08.010.

[11] Y. Fan, C. Liu, X. Kong, Y. Han, M. Lei, R. Xiao, A new perspective on polyethylene-promoted lignin pyrolysis with mass transfer and radical explanation, Green Energy Environ. (2021) 2–10. https://doi.org/10.1016/j.gee.2021.02.004.

[12] G. Lopez, M. Artetxe, M. Amutio, J. Bilbao, M. Olazar, Thermochemical routes for the valorization of waste polyolefinic plastics to produce fuels and chemicals. A review, Renew. Sustain. Energy Rev. 73 (2017) 346–368. https://doi.org/10.1016/j.rser.2017.01.142.

[13] M. El Moustaqim, A. El Kaihal, M. El Marouani, S. Men-La-Yakhaf, M. Taibi, S. Sebbahi, S. El Hajjaji, F. Kifani-Sahban, Thermal and thermomechanical analyses of lignin, Sustain. Chem. Pharm. 9 (2018) 63–

68. https://doi.org/10.1016/j.scp.2018.06.002.

[14] Z. Wang, K.G. Burra, T. Lei, A.K. Gupta, Co-pyrolysis of waste plastic and solid biomass for synergistic production of biofuels and chemicals-A review, Prog. Energy Combust. Sci. 84 (2021) 100899. https://doi.org/10.1016/j.pecs.2020.100899.

[15] O. Dogu, M. Pelucchi, R. Van de Vijver, P.H.M. Van Steenberge, D.R. D'hooge, A. Cuoci, M. Mehl, A. Frassoldati, T. Faravelli, K.M. Van Geem, The chemistry of chemical recycling of solid plastic waste via pyrolysis and gasification: State-of-the-art, challenges, and future directions, Prog. Energy Combust. Sci. 84 (2021) 100901. https://doi.org/10.1016/j.pecs.2020.100901.

[16] V. Mortezaeikia, O. Tavakoli, M.S. Khodaparasti, A review on kinetic study approach for pyrolysis of plastic wastes using thermogravimetric analysis, J. Anal. Appl. Pyrolysis. 160 (2021) 105340. https://doi.org/10.1016/j.jaap.2021.105340.

[17] N. Li, H. Liu, Z. Cheng, B. Yan, G. Chen, S. Wang, Conversion of plastic waste into fuels: A critical review, J. Hazard. Mater. 424 (2022) 127460. https://doi.org/10.1016/j.jhazmat.2021.127460.

[18] X. Zhao, M. Korey, K. Li, K. Copenhaver, H. Tekinalp, S. Celik, K. Kalaitzidou, R. Ruan, A.J. Ragauskas, S. Ozcan, Plastic waste upcycling

toward a circular economy, Chem. Eng. J. 428 (2022) 131928. https://doi.org/10.1016/j.cej.2021.131928.

[19] Z. Wu, S. Wang, J. Zhao, L. Chen, H. Meng, Thermal behavior and char structure evolution of bituminous coal blends with edible fungi residue during co-pyrolysis, in: Energy and Fuels, 2014: pp. 1792–1801. https://doi.org/10.1021/ef500261q.

[20] P. Ghetti, L. Ricca, L. Angelini, 96/03972 Thermal analysis of biomass and corresponding pyrolysis products, Fuel Energy Abstr. 37 (1996) 278. https://doi.org/10.1016/0140-6701(96)82268-5.

[21] S. Shawalliah, N. Abd, K. Ismail, A. Bahari, Z. Abd, Bioresource Technology Investigation on thermochemical behaviour of low rank Malaysian coal , oil palm biomass and their blends during pyrolysis via thermogravimetric analysis (TGA), Bioresour. Technol. 101 (2010) 4584–4592. https://doi.org/10.1016/j.biortech.2010.01.059.

[22] H.-X. Yan, F.-F. Hou, H. Zhao, H.-N. Wang, S. Gao, M. Wu, P.-Y. Yu, J.-F. Liu, N. Li, Y.-W. Sun, W. Jiang, K.-X. Fan, T. He, S. Qin, Pyrolysis kinetics of invasive coastal plant *Spartina anglica* using thermogravimetric analysis, Energy Sources, Part A Recover. Util. Environ. Eff. 38 (2016) 2867–2875. https://doi.org/10.1080/15567036.2015.1120825.

[23] C. Chen, X. Ma, Y. He, Co-pyrolysis characteristics of microalgae Chlorella vulgaris and coal through TGA, Bioresour. Technol. 117 (2012) 264–273. https://doi.org/10.1016/j.biortech.2012.04.077.

[24] S. Maiti, S. Purakayastha, B. Ghosh, Thermal characterization of mustard straw and stalk in nitrogen at different heating rates, Fuel. 86 (2007) 1513–1518. https://doi.org/10.1016/j.fuel.2006.11.016.

[25] H. Jüntgen, Review of the kinetics of pyrolysis and hydropyrolysis in relation to the chemical constitution of coal, Fuel. 63 (1984) 731–737. https://doi.org/10.1016/0016-2361(84)90058-9.

[26] R.S. Chutia, R. Kataki, T. Bhaskar, Thermogravimetric and decomposition kinetic studies of Mesua ferrea L. deoiled cake, Bioresour. Technol. 139 (2013) 66–72. https://doi.org/10.1016/j.biortech.2013.03.191.

[27] S.S. Kim, H.V. Ly, J. Kim, J.H. Choi, H.C. Woo, Thermogravimetric characteristics and pyrolysis kinetics of Alga Sagarssum sp. biomass, Bioresour. Technol. 139 (2013) 242–248. https://doi.org/10.1016/j.biortech.2013.03.192.

[28] L.N. Samuelsson, M.U. Babler, R. Moriana, A single model-free rate expression describing both non-isothermal and isothermal pyrolysis of Norway Spruce, Fuel. 161 (2015) 59–67.

https://doi.org/10.1016/j.fuel.2015.08.019.

[29] A. Chandrasekaran, S. Ramachandran, S. Subbiah, Determination of kinetic parameters in the pyrolysis operation and thermal behavior of Prosopis juliflora using thermogravimetric analysis, Bioresour. Technol. 233 (2017) 413–422. https://doi.org/10.1016/j.biortech.2017.02.119.

[30] N. Zhang, S. Li, L. Xiong, Y. Hong, Y. Chen, Cellulose-hemicellulose interaction in wood secondary cell-wall, Model. Simul. Mater. Sci. Eng. 23 (2015) 1–15. https://doi.org/10.1088/0965-0393/23/8/085010.

[31] T. Damartzis, D. Vamvuka, S. Sfakiotakis, A. Zabaniotou, Thermal degradation studies and kinetic modeling of cardoon (Cynara cardunculus) pyrolysis using thermogravimetric analysis (TGA), Bioresour. Technol. 102 (2011) 6230–6238. https://doi.org/10.1016/j.biortech.2011.02.060.

[32] Y. He, C. Chang, P. Li, X. Han, H. Li, S. Fang, J. Chen, X. Ma, Thermal decomposition and kinetics of coal and fermented cornstalk using thermogravimetric analysis, Bioresour. Technol. 259 (2018) 294–303. https://doi.org/10.1016/j.biortech.2018.03.043.

[33] J. Chattopadhyay, C. Kim, R. Kim, D. Pak, Thermogravimetric characteristics and kinetic study of biomass co-pyrolysis with plastics, Korean J. Chem. Eng. 25 (2008) 1047–1053. https://doi.org/10.1007/s11814-008-0171-6.

[34] T. Sonobe, N. Worasuwannarak, S. Pipatmanomai, Synergies in co-pyrolysis of Thai lignite and corncob, Fuel Process. Technol. 89 (2008) 1371–1378. https://doi.org/10.1016/j.fuproc.2008.06.006.

[35] D.K. Park, S.D. Kim, S.H. Lee, J.G. Lee, Co-pyrolysis characteristics of sawdust and coal blend in TGA and a fixed bed reactor, Bioresour. Technol. 101 (2010) 6151–6156. https://doi.org/10.1016/j.biortech.2010.02.087.

[36] H. Wu, Z., Eang, S., Zhao, J., Chen, L., Meng, Thermal Behavior and Char Structure Evolution of Bituminous Coal Blends with Edible Fungi Residue during Co-Pyrolysis, Energy and Fuels. 28 (2014) 1792–1801.

[37] Z. Wu, S. Wang, J. Zhao, L. Chen, H. Meng, Synergistic effect on thermal behavior during co-pyrolysis of lignocellulosic biomass model components blend with bituminous coal, Bioresour. Technol. 169 (2014) 220–228. https://doi.org/10.1016/j.biortech.2014.06.105.

[38] H. Bockhorn, A. Hornung, U. Hornung, D. Schawaller, Kinetic study on the thermal degradation of polypropylene and polyethylene, J. Anal. Appl. Pyrolysis. 48 (1999) 93–109.

[39] M. Heydrai, M. Raman, R. Gupta, Kinetic Study and Thermal Decomposition Behavior of Lignite Coal, Int. J. Chem. Eng. 2015 (2015) 1–9. https://doi.org/http://dx.doi.org/10.1155/2015/481739.

[40] M.Y. Gelfer, H.H. Winter, Effect of Branch Distribution on Rheology of LLDPE during Early Stages of Crystallization, Macromolecules. 32 (1999) 8974–8981.

[41] S.M. Al-Salem, A. Bumajdad, A.R. Khan, B.K. Sharma, S.R. Chandrasekaran, F.A. Al-Turki, F.H. Jassem, A.T. Al-Dhafeeri, Non-isothermal degradation kinetics of virgin linear low density polyethylene (LLDPE) and biodegradable polymer blends, J. Polym. Res. 25 (2018). https://doi.org/10.1007/s10965-018-1513-7.

[42] J.B. Huang, G.S. Zeng, X.S. Li, X.C. Cheng, H. Tong, Theoretical studies on bond dissociation enthalpies for model compounds of typical plastic polymers, IOP Conf. Ser. Earth Environ. Sci. 167 (2018). https://doi.org/10.1088/1755-1315/167/1/012029.

[43] H. Yang, M. Gong, J. Hu, B. Liu, Y. Chen, J. Xiao, S. Li, Z. Dong, H. Chen, Cellulose Pyrolysis Mechanism Based on Functional Group Evolutions by Two-Dimensional Perturbation Correlation Infrared Spectroscopy, Energy & Fuels. 34 (2020) 3412–3421. https://doi.org/10.1021/acs.energyfuels.0c00134.

[44] H. Yang, Z. Dong, B. Liu, Y. Chen, M. Gong, S. Li, H. Chen, A new insight of lignin pyrolysis mechanism based on functional group evolutions of solid char, Fuel. 288 (2021) 119719. https://doi.org/10.1016/j.fuel.2020.119719.

[45] W. Wu, J. Cai, R. Liu, Isoconversional kinetic analysis of distributed activation energy model processes for pyrolysis of solid fuels, Ind. Eng. Chem. Res. 52 (2013) 14376–14383. https://doi.org/10.1021/ie4021123.

[46] S. Vyazovkin, N. Sbirrazzuoli, Isoconversional kinetic analysis of thermally stimulated processes in polymers, Macromol. Rapid Commun. 27 (2006) 1515–1532. https://doi.org/10.1002/marc.200600404.

[47] G. Mishra, J. Kumar, T. Bhaskar, Kinetic studies on the pyrolysis of pinewood, Bioresour. Technol. 182 (2015) 282–288. https://doi.org/10.1016/j.biortech.2015.01.087.

[48] S. Vyazovkin, Isoconversional kinetics of thermally stimulated processes, Macromol. Rapid Commun. 18 (2006) 1505–1616. https://doi.org/10.1007/978-3-319-14175-6.

[49] É.D.G. Baroni, K. Tannous, Y.J. Rueda-Ordóñez, L.K. Tinoco-Navarro, The applicability of isoconversional models in estimating the kinetic parameters of biomass pyrolysis, J. Therm. Anal. Calorim. 123 (2016) 909–917. https://doi.org/10.1007/s10973-015-4707-9.

[50] K. Slopiecka, P. Bartocci, F. Fantozzi, Thermogravimetric analysis and kinetic study of poplar wood pyrolysis, Appl. Energy. 97 (2012) 491–497. https://doi.org/10.1016/j.apenergy.2011.12.056.

[51] S. Ceylan, Y. Topçu, Pyrolysis kinetics of hazelnut husk using

thermogravimetric analysis, Bioresour. Technol. 156 (2014) 182–188. https://doi.org/10.1016/j.biortech.2014.01.040.

[52] Y.J. Rueda-Ord????ez, K. Tannous, Isoconversional kinetic study of the thermal decomposition of sugarcane straw for thermal conversion processes, Bioresour. Technol. 196 (2015) 1–9. https://doi.org/10.1016/j.biortech.2015.07.062.

[53] J. Cai, R. Liu, Kinetic analysis of solid-state reactions: A general empirical kinetic model, Ind. Eng. Chem. Res. 48 (2009) 3249–3253. https://doi.org/10.1021/ie8018615.

[54] S.C. Turmanova, S.D. Genieva, A.S. Dimitrova, L.T. Vlaev, Non-isothermal degradation kinetics of filled with rise husk ash polypropene composites, Express Polym. Lett. 2 (2008) 133–146. https://doi.org/10.3144/expresspolymlett.2008.18.

[55] Z. Shuping, W. Yulong, Y. Mingde, L. Chun, T. Junmao, Pyrolysis characteristics and kinetics of the marine microalgae Dunaliella tertiolecta using thermogravimetric analyzer, Bioresour. Technol. 101 (2010) 359–365. https://doi.org/10.1016/j.biortech.2009.08.020.

[56] A. Aboulkas, K. El harfi, A. El Bouadili, Thermal degradation behaviors of polyethylene and polypropylene. Part I: Pyrolysis kinetics and mechanisms, Energy Convers. Manag. 51 (2010) 1363–1369.

https://doi.org/10.1016/j.enconman.2009.12.017.

[57] G. Mishra, T. Bhaskar, Non isothermal model free kinetics for pyrolysis of rice straw, Bioresour. Technol. 169 (2014) 614–621. https://doi.org/10.1016/j.biortech.2014.07.045.

[58] Poletto, J.A. Zattera, M.C.R. Santana, Thermal decomposition of wood: Kinetics and degradation mechanisms, Bioresour. Technol. 126 (2012) 7–12. https://doi.org/10.1016/j.biortech.2012.08.133.

[59] L.T. Vlaev, I.G. Markovska, L.A. Lyubchev, Non-isothermal kinetics of pyrolysis of rice husk, Thermochim. Acta. 406 (2003) 1–7. https://doi.org/10.1016/S0040-6031(03)00222-3.

[60] G.C. Collazzo, C.C. Broetto, D. Perondi, J. Junges, A. Dettmer, A.A. Dornelles Filho, E.L. Foletto, M. Godinho, A detailed non-isothermal kinetic study of elephant grass pyrolysis from different models, Appl. Therm. Eng. 110 (2017) 1200–1211. https://doi.org/10.1016/j.applthermaleng.2016.09.012.

[61] J. Wang, G. Wang, M. Zhang, M. Chen, D. Li, F. Min, M. Chen, S. Zhang, Z. Ren, Y. Yan, A comparative study of thermolysis characteristics and kinetics of seaweeds and fir wood, Process Biochem. 41 (2006) 1883–1886. https://doi.org/10.1016/j.procbio.2006.03.018.

[62] R. Saikia, B. Baruah, D. Kalita, K.K. Pant, N. Gogoi, R. Kataki, Pyrolysis

and kinetic analyses of a perennial grass (Saccharum ravannae L.) from north-east India: Optimization through response surface methodology and product characterization, Bioresour. Technol. 253 (2018) 304–314. https://doi.org/10.1016/j.biortech.2018.01.054.

[63] M.U. Garba, A. Inalegwu, U. Musa, A.A. Aboje, Thermogravimetric characteristic and kinetic of catalytic co-pyrolysis of biomass with low- and high-density polyethylenes, Biomass Conv. Bioref. 8 (2018) 143–150. https://doi.org/10.1007/s13399-017-0261-y.

[64] P. Lu, Q. Huang, A.C.T. Bourtsalas, Y. Chi, J. Yan, Synergistic e ff ects on char and oil produced by the co-pyrolysis of pine wood , polyethylene and polyvinyl chloride, Fuel. 230 (2018) 359–367. https://doi.org/10.1016/j.fuel.2018.05.072.

[65] D. Mallick, M. Kumar, P. Mahanta, V.S. Moholkar, Bioresource Technology Discernment of synergism in pyrolysis of biomass blends using thermogravimetric analysis, Bioresour. Technol. 261 (2018) 294–305. https://doi.org/10.1016/j.biortech.2018.04.011.

[66] Y. Zheng, L. Tao, X. Yang, Y. Huang, C. Liu, Z. Zheng, Study of the thermal behavior , kinetics , and product characterization of biomass and low-density polyethylene co-pyrolysis by thermogravimetric analysis and pyrolysis-GC / MS, J. Anal. Appl. Pyrolysis. 133 (2018) 185–197. https://doi.org/10.1016/j.jaap.2018.04.001.

[67] G. Özsin, A.E. Pütün, Co-pyrolytic behaviors of biomass and polystyrene : Kinetics , thermodynamics and evolved gas analysis, Korean J. Chem. Eng. 35 (2018) 428–437. https://doi.org/10.1007/s11814-017-0308-6.

[68] X. Kai, T. Yang, S. Shen, R. Li, TG-FTIR-MS study of synergistic e ff ects during co-pyrolysis of corn stalk and high-density polyethylene (HDPE), Energy Convers. Manag. 181 (2019) 202–213. https://doi.org/10.1016/j.enconman.2018.11.065.

[69] R.K. Mishra, A. Sahoo, K. Mohanty, Pyrolysis kinetics and synergistic effect in co-pyrolysis of Samanea saman seeds and polyethylene terephthalate using thermogravimetric analyser, Bioresour. Technol. 289 (2019) 1–11. https://doi.org/10.1016/j.biortech.2019.121608.

[70] B. Han, Y. Chen, Y. Wu, D. Hua, Co-pyrolysis behaviors and kinetics of plastics – biomass blends through thermogravimetric analysis Co-pyrolysis behaviors and kinetics of plastics – biomass blends through thermogravimetric analysis, J Therm. Anal Calorim. 115 (2013) 227–235. https://doi.org/10.1007/s10973-013-3228-7.

[71] D. V Suriapparao, D.K. Ojha, T. Ray, R. Vinu, Kinetic analysis of co-pyrolysis of cellulose and polypropylene, J Therm. Anal Calorim. 117 (2014) 1441–1451. https://doi.org/10.1007/s10973-014-3866-4.

Chapter 4

Wet Torrefaction of Bamboo Saw Dust and Its Co-Pyrolysis with Plastic

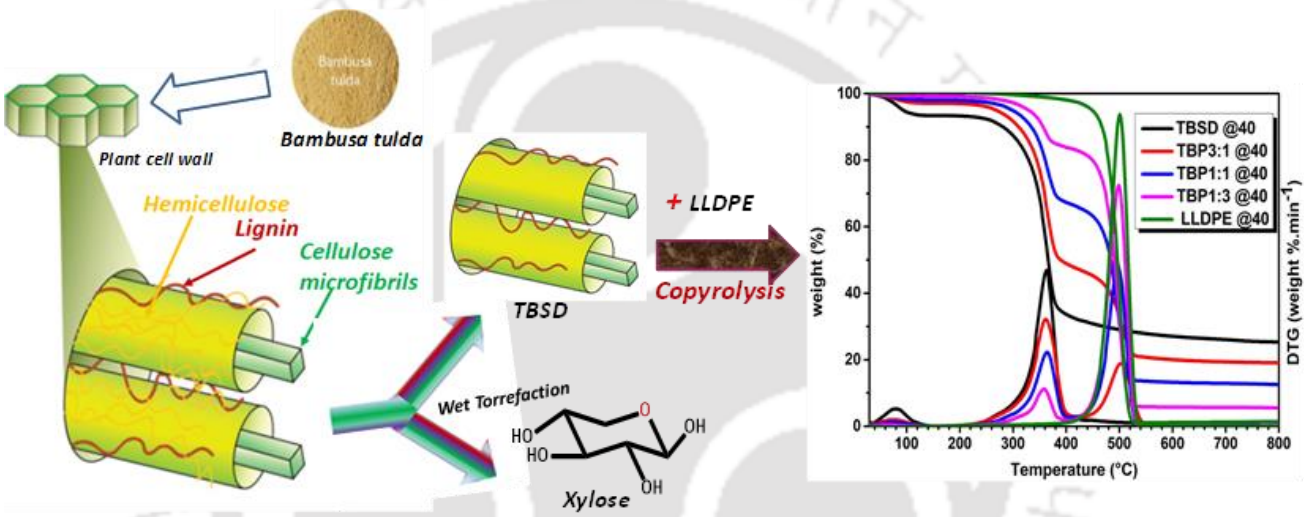

Highlights

- The wet torrefaction selectively removes hemicellulose as xylose (yield 85%)
- The catalyst in wet torrefaction reduces the temperature and time of operation
- The wet torrefied biomass shows better pyrolysis characteristics
- The blend with 1:3 weight ratio of TBSD to LLDPE gives the highest synergism
- The co-pyrolysis follows the multi-step reaction mechanism (Criado's master plot)

4.1 Objectives

In this chapter, the bamboo sawdust (BSD) was wet torrefied using salt and organic acid as catalysts to produce platform chemicals (xylose + arabinose) and torrefied bamboo sawdust (TBSD) or also known as hydrochar. The wet torrefaction was used to reduce the moisture content, increase the H/C ratio and HHV and improve the grindability and hydrophobicity of BSD. The co-pyrolysis of the blends (TBSD + LLDPE) was studied using thermogravimetric analysis (TGA) at heating rates 5–40°C min^{-1}. The kinetics and the synergistic effects of the co-pyrolysis were studied in detail. The kinetic parameters were estimated using isoconversional methods and the reaction mechanism was deduced using the Criado's master plot. To the best of our knowledge, the co-pyrolysis of TBSD and LLDPE is not reported in the literature. Moreover, the quantification of the platform chemicals from the wet torrefaction of BSD is reported for the first time in this study.

4.2 Results and discussion

4.2.1 Hemicellulose removal from bamboo biomass by wet torrefaction

The variation of product yields of wet torrefaction of BSD as a function of the concentrations of NaCl, and formic acid, temperature and time is shown in Fig. 4.1. As the temperature increased from 120 to 150°C at constant reaction time (30 min), the pentoses (xylose + arabinose) and acetic acid yields were first increased and then decreased passing through a maximum at 140°C. The maximum yields of pentoses and acetic acid at 140°C were 85 and 38%, respectively. It is worth mentioning that the total yield of the products from hemicellulose is more than 100%. This is because the molar yields were calculated based on the pentose molar-equivalent of hemicellulose weight (see methods section) and the molecular weight of acetic acid is lower as compared to that of pentose. Hemicellulose being the complex polymer of various components, this is the best one can do. At 150°C, pentoses and acetic acid yields were decreased from 85 to 60% and 38 to 34%, respectively, and the furfural yield was increased from 5 to 25%. It indicates that the pentoses convert into furfural in the presence of

Brønsted acid, at higher temperatures [1]. The yield of acetic acid decreased due to reactions such as decarboxylation of carboxylic (–COOH), and acetyl groups, reforming of ketonic groups (>C=O), cracking and condensation, at high temperature [2]. With reaction time, the pentoses yield was gradually decreased, hexoses, HMF, and acetic acid yields were nearly constant and the furfural yield was increased.

The effect of NaCl concentration on wet torrefaction of bamboo sawdust (BSD) was studied in the range NaCl: BSD ratio of 0:1 to 3:1 w/w at 140°C, 30 min and FA: BSD ratio of 1:1 w/w (Fig. 4.1c). The NaCl concentration of 30% is in DI water close to its saturation limit and therefore the NaCl concentration was varied only up to 30% (NaCl:BSD ratio 3:1 w/w). The pentoses (xylose + arabinose) and acetic acid yields were increased linearly with NaCl from 30.7 and 14.3%, respectively, at NaCl:BSD ratio 0:1 w/w to 85.7 and 38.5% at 3:1 w/w (Fig. 4.1c). The yields of other compounds such as hexoses (glucose + mannose + galactose), 5-hydroxymethylfurfural (HMF) and furfural were marginal (less than 5%), at all the NaCl concentrations studied. This result testifies that the cellulose part of the BSD was intact and the hemicellulose part was selectively converted to pentoses and acetic acid, under the torrefaction conditions used. The xylose conversion to furfural was also negligible. The Fig. 4.1d shows the yields of various compounds in the presence and absence of FA at 140°C, 30 min and an NaCl:BSD ratio of 3 w/w. The FA addition has a great effect on the torrefaction reaction. In the absence of FA, the acetic acid only was formed in reasonable quantity (4%) and the yields of all other products (pentoses, hexoses, HMF and furfural) were negligible (< 2%). However, upon the addition of formic acid at a FA:BSD ratio of 1:1 w/w, the yields of pentoses and the acetic acid were increased significantly. Overall, the yields were very low in the absence of either NaCl or FA and were highest when both NaCl and FA were present in right quantity. This indicates a synergistic effect between the NaCl and FA.

The highest pentoses yield (85%) was obtained at 140°C for 30 min in presence of NaCl (NaCl:BSD :: 3:1 w/w) and FA (FA:BSD :: 1:1 w/w). At these optimum wet torrefaction conditions, approximately 96 wt.% of hemicellulose was removed predominantly in the form of pentoses (xylose and arabinose) and acetic acid. The formic acid and NaCl can be recycled after the separation of solids and the pentoses products. The same aqueous solution (containing NaCl, formic acid, and predominantly pentoses) after separation of solids can be used to further convert the pentoses to valuable products such as furfural or levulinic acid. The low concentration of reactant (10 wt.%) results in high energy demand and hampers the economic feasibility. The concentration of the reactant should be increased to improve the economics. These are the on-going works in our research group.

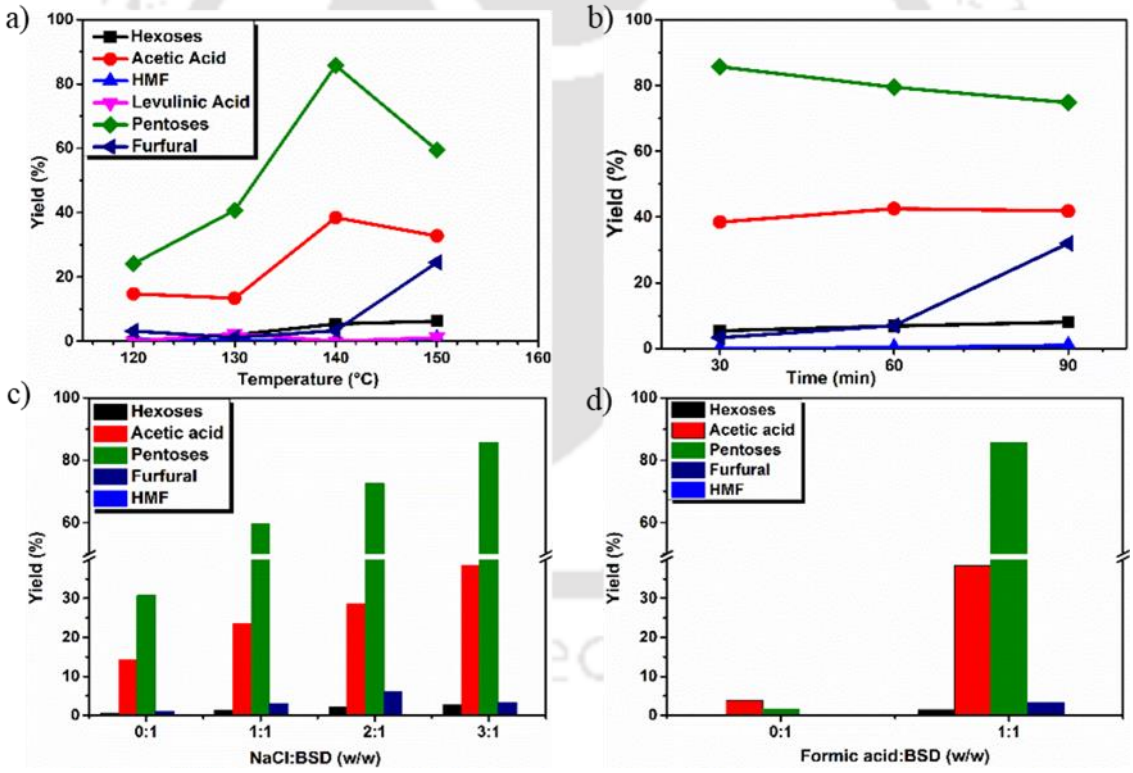

Figure 4.1. The variation of product yields as a function of (a) temperature, (b) time (c) NaCl:BSD ratio w/w and (d) FA:BSD ratio w/w, during wet-torrefaction of BSD. (Other reaction conditions (other than the variable in a particular graph): 140°C temperature, 30 min reaction time, 10 wt.% of BSD in 2 ml DI water, NaCl:BSD 3:1 w/w and FA:BSD 1:1 w/w)

(Pentoses majorly contain xylose and arabinose and hexoses contain glucose, mannose and galactose).

The xyloglucan is a form of hemicellulose, amorphous in nature, consist of pentose rings (xylose, arabinose, etc.) by glycosidic linkage, acetyl units also attached with C–2 or C–3 position in xylose units and glucuronic acid also attached with side chain backbone of xyloglucan [1]. The xyloglucuran a form of hemicellulose bonds randomly (physically), or covalently or in bridge form to the cellulose [3]. It also connects to lignin through different types of linkages (β–O–4 or γ–ester) and forms the lignin-carbohydrate complex [4]. In the WT process, initially, the alkali salt (NaCl) solubilizes the xyloglucuran by breaking-down the ether linkage and ester bonds between hemicellulose and lignin and also disrupt the hydrogen bonding between hemicellulose and cellulose [5,6]. It also breaks down the cellulose partially and lignin marginally. The sodium chloride brings down the activation energy barrier of biomass degradation by forming a metal complex with xyloglucuran [7]. The chloride ions from sodium chloride improve the activity of H^+ ions. These H^+ and H_3O^+ ($HCOOH \rightarrow H^+ + HCOO^-$; $H^+ + H_2O \rightarrow H_3O^+$) ions attack on xylan units having acetyl groups (–COR) and glucuronic acid which further break down into xylose, acetic acid via oxonium ion by series of reactions including dehydration, decarboxylation, decarbonylation and rearrangement reactions (Fig. 4.2). Therefore, the yields of pentose sugars and acetic acid were increased with the concentration of NaCl. Further, Brønsted acidic site (H_3O^+) attacks the oxygen atom in acetyl groups having lone-pair to produce acetic acid and formic acid. The elementary steps (path 1 & 2) for the conversion of xylose into furfural were shown in Fig. A2.1, Annexure A2. The $(H_3O)^+$ attacks O5 of pyranose ring and converts the xylopyranose to furan derivatives, which immediately dehydrates to form furfural. The Brønsted acidic site (H_3O^+) also partially degraded the cellulose into glucose which further converted into HMF at high temperature (150°C).[8]

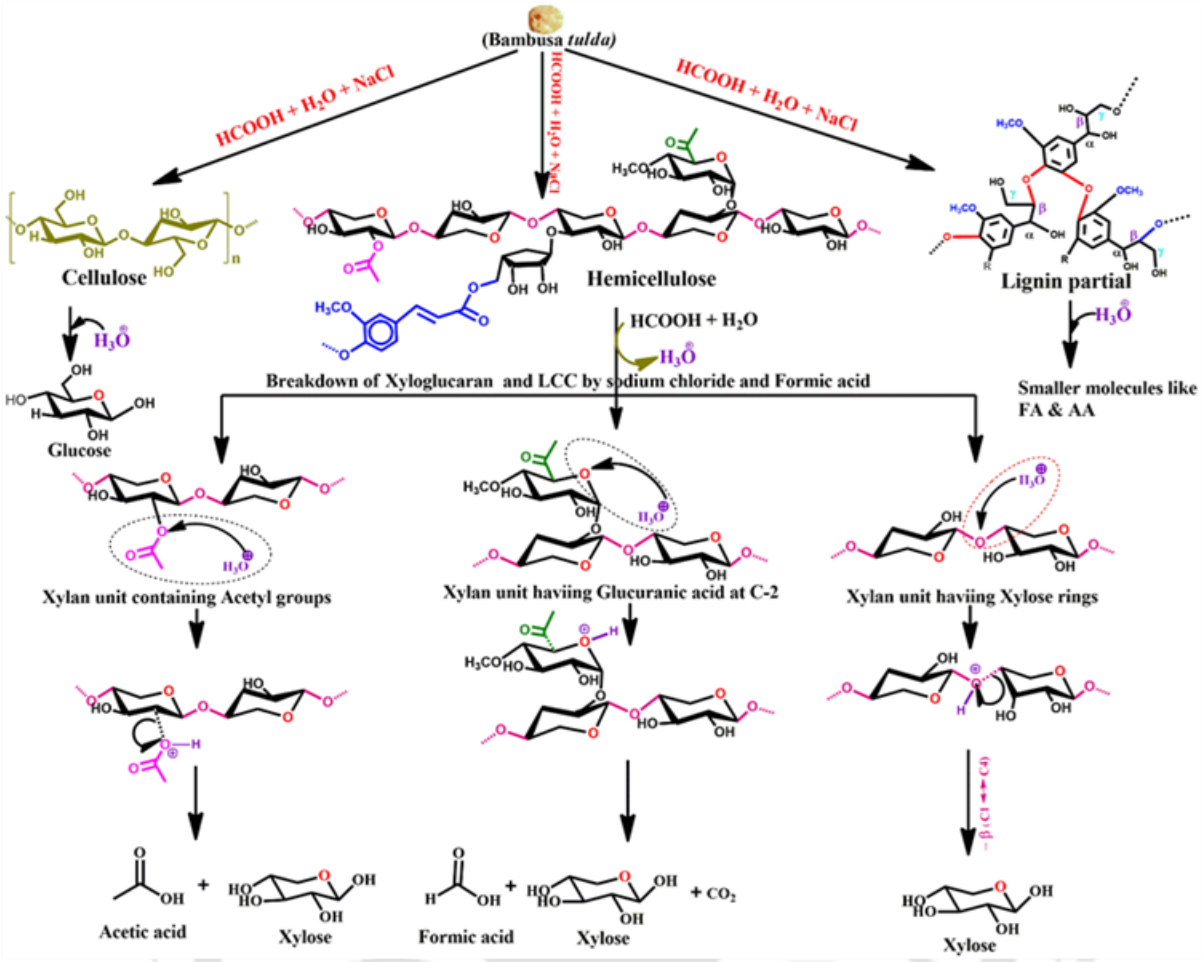

Figure 4.2. Formation of Acetic acid, formic acid, and xylose from hemicellulose containing bamboo sawdust by Formic acid (10%) and sodium chloride (30%) at 140°C.

4.2.2 Chemical and structural properties of biomass sawdust (BSD) and torrefied bamboo sawdust (TBSD)

The FTIR spectra of BSD and TBSD are shown in Fig. 4.3**.** Various functional groups such as alcohol, aldehyde, carbonyls, carboxylic, esters, alkyls, and alkoxy groups, are found in both BSD and TBSD [9]. The intensity of absorption peaks of the –OH group and oxygen-containing functional group in TBSD was lower as compared to that in BSD signifying the hydrophobic nature of TBSD. The decrease of the peak of hydrophilic oxygen-containing functional groups clearly indicates that the reduction of functional groups in the surface of

hydrochar or TBSD (Fig. 4.3f: 1750–1650 cm^{-1} and 1650–1600 cm^{-1}) and finally resulted in a significant decrease in hygroscopicity of hydrochar, that is the hydrophobicity of TBSD is enhanced. The hydrophobicity of biomass was determined by equilibrium moisture content (EMC) and contact angle.[10] A similar observation was found by wet torrefaction of woody and herbaceous and grassy biomass by many researchers, intensity of C=O band decreased after wet torrefaction.[10–14] The peak absorption intensity of unconjugated carbonyl groups (1738 cm^{-1}) in TBSD was lower as compared to that of BSD, a clear degradation of hemicellulose (Fig. 3f). The peak range 1500–1560 cm^{-1} is responsible for C=O group vibration in hemicellulose and lignin (Fig. 4.3g). In TBSD, the absorbance of these peaks decreased because of the removal of hemicellulose and a minor amount of cellulose. The lower absorbance of different peaks ranges such as 1750–1650 cm^{-1} in TBSD as compared to BSD was a clear indication of the release of aldehydes, ketones, carboxylic and phenolic functional groups. The peak at 1000 cm^{-1} shown by BSD having higher absorbance as compared to TBSD which could be due to the structural vibration of –C–O and –C–O–C groups. Therefore, it gives an idea of breaking of functional groups to alcohols, carboxylic acids, ethers, and esters during wet torrefaction [15]**.** In BSD, a 1730 cm^{-1} peak was found due to the presence of benzyl ester lignin-carbohydrate bonds. While in TBSD it disappears, which could be due to the rupture of ester linkages between lignin and carbohydrate. Five types of linkages were found in the association of lignin with carbohydrates [4]. The XRD graph of BSD, TBSD, and the corresponding parameters are shown in Fig. 4.4. The diffraction peaks at 16° (101) and 22° (002) represent the crystalline structures, cellulose I_α (triclinic) and cellulose I_β (monoclinic), respectively [16]. The crystallinity index (CrI) and the intensity of major peak (2Θ: 22.4°) of TBSD were higher as compared to those of BSD. This could be due to several reasons such as removal of amorphous hemicellulose, rearrangement of cellulose macromolecules, and dehydration

and decarboxylation reactions. A more ordered and graphite-like hydrochar forms in the presence of NaCl as compared to other salts such as sodium bicarbonate and sodium acetate [17,18].

The FESEM images of BSD and TBSD are shown in Fig. A2.2. The surface of the BSD showed the bundles and tubular structure. After wet torrefaction, bundles deformed and more tubular structure appeared (Fig. A2.2a and b) due to the removal of hemicellulose. Tubules made up of cellulose in BSD degraded after wet torrefaction as shown in Fig. A2.2c and d, indicating a small amount of cellulose also degraded in WT [19].

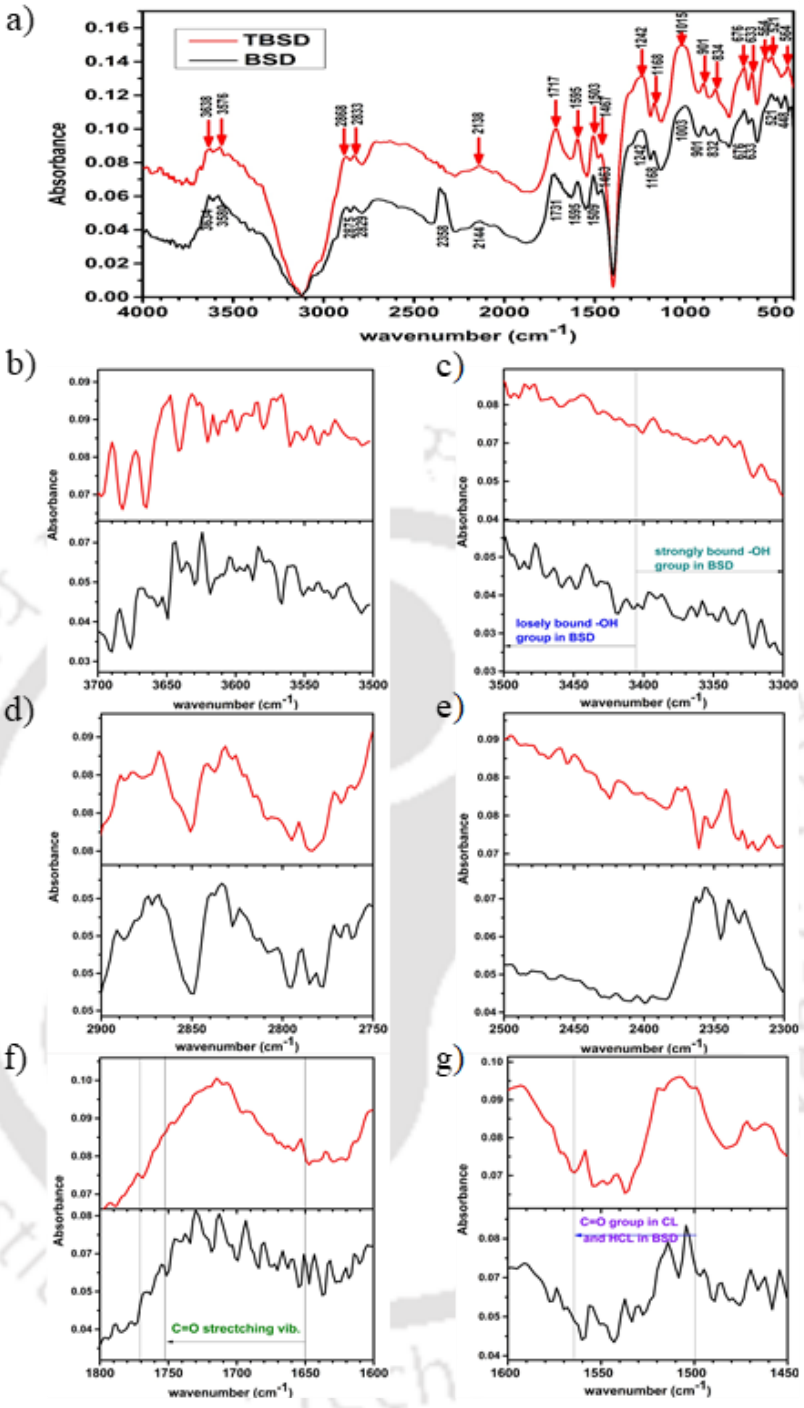

Figure 4.3. FTIR spectra of BSD and TBSD (a) and the spectra of some specific functional groups were plotted separately (b-g). (HCL: hemicellulose; LIG: lignin).

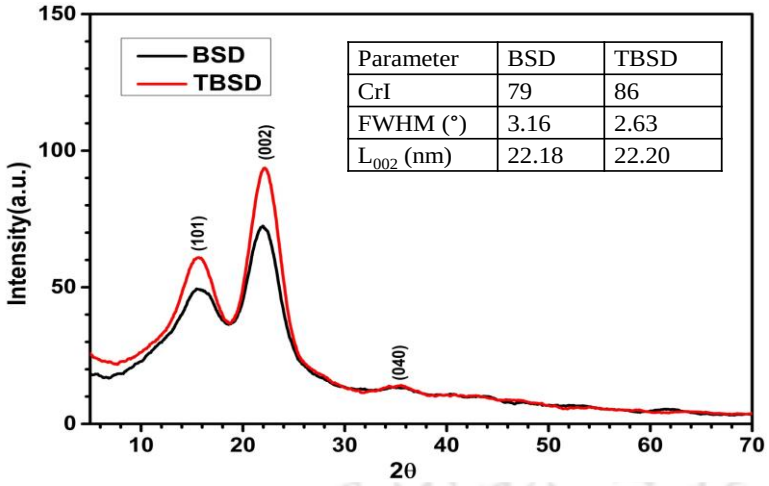

Parameter	BSD	TBSD
CrI	79	86
FWHM (°)	3.16	2.63
L_{002} (nm)	22.18	22.20

Figure 4.4. The XRD patterns of BSD and TBSD.

4.2.3 Role of torrefaction and NaCl in the pyrolysis of TBSD

The effect of torrefaction and the role of NaCl on the degradation behavior of TBSD in the pyrolysis process are shown in Fig. 4.5. To check catalytic activity of NaCl in the pyrolysis and co-pyrolysis, 10 wt.% NaCl was added to TBSD. To better understand the hemicellulose removal and lignin decomposition, the decomposition peaks in DTG were deconvoluted using cumulative fit peak (CFP) with Gaussian function in plotting software ORIGIN Pro 9.0. From the TG and DTG curves, it was observed that the degradation of BSD and TBSD occurred in two stages. The first stage corresponds to moisture removal and light volatiles. The deconvolution of second stage of the DTG of BSD (Fig. 4.5b) shows three peaks (b*, c* & d*) corresponding to degradation of hemicellulose, cellulose, and lignin, respectively. The second stage of TBSD deconvoluted into two peaks (Peaks 2 and 3). The peak 2 corresponds to cellulose and peak 3 to lignin degradation. The degradation of lignin occurred between 150 and 580°C due to its complex structure having different linkages (α, β, γ, ether, and ester) and functional groups (Fig. 1.2c).

The degradation of hemicellulose, cellulose, and lignin in BSD started at 180, 260, and 180°C and ended at 425, 410 and 660°C, respectively (Fig. 4.5b). In torrefied samples, the cellulose and lignin decomposition started at 260 and 150°C and ended at 400 and 580°C,

respectively, in the presence of NaCl (Fig. 4.5d). While, their decomposition started at 275 and 380°C and ended at 440 and 500°C, respectively, in the absence of NaCl (Fig. 4.5f). The start temperature of the main active pyrolysis was lower and the end temperature was higher in the presence of NaCl (Tables A2.1 and A2.2, column: 4; stage_3). This indicates that the presence of NaCl not only hastens the start of pyrolysis but also delays its end. The delay of the reaction in presence of NaCl provides some insights on efficient degradation of lignin, which is also evident from the deconvoluted DTG plot of TBSD + NaCl (Fig. 4.5d). According to Fig. 4.5, the lignin decomposition was the highest in presence of NaCl as compared to both BSD or pure TBSD. The efficient degradation of lignin results in higher fraction of aromatics in the pyrolysis oil obtained. A similar effect was reported with other metal halides in the literature. The detailed function of alkali, alkaline-earth, or transition metal halides on the pyrolysis of lignocellulosic biomass is given in Table 1.5. The residual weight was higher in the pyrolysis of TBSD with NaCl (Tables A2.1 and A2.2) because of the formation of char through cross-linking and poly-condensation reactions. Other researchers also reported similar results [5,17,20,21]. However, the residue formation was lower with sodium as compared to the other alkali and alkaline earth metals [20].

In the second stage of the BSD degradation process, the shoulder peak was observed at all heating rates which indicates the presence of hemicellulose [22]. The shoulder peak was absent in TBSD pyrolysis which confirms the absence of hemicellulose in the TBSD (Fig. 4.5). The thermal stability of the TBSD was higher as compared to that of BSD. This could be attributed to the removal of hemicellulose and extractives, which in turn results in an increase of crystallinity of cellulose by bringing cellulose microfibrils close to each other. In TBSD the ash content was almost removed (Table 2.2). From the thermograms and corresponding data (Fig. 4.5 and Tables A2.1 and A2.2), it was also observed that the degradation rate of TBSD

was higher compared to that of BSD but mean reactivity was lower, indicating the possible change in the reaction mechanism [23].

The alkali metal ions (Na^+) in NaCl would pierce through the texture of TBSD and acts on cellulose and lignin materials altering the reaction pathways [24]. Inorganic salt is less corrosive than acid and can be recycled, it is more economically viable if inorganic salt in aqueous solution can be directly used in the pre-treatment of lignocellulosic biomass. Mass yield and energy densification of hydrochar are higher because of chloride ion interaction with biomass to remove only lower HHV components while leaving lignin and other higher HHV components in the biomass. It also catalyse the lower HHV components to higher fuel value products by cross linking reaction. The sodium chloride solubilizes the xyloglucan by breaking ether linkage and ester bond between hemicellulose and lignin and also disrupt hydrogen bonding between hemicellulose and cellulose.[25–30] The salts also accelerates the hydrogen production by reforming of C=C and C-H groups in lignin.[6][7] The Mg^{2+} ions bring down activation energy barrier of glycosylation, ring contraction and mannose pathways requiring activation enthalpies of 32–52 kcal mol^{-1}. The Mg^{2+} and Ca^{2+} also inhibit dehydration pathway.[8] The role of metal salts (mono, bi and trivalent metals) were expressed as scheme 1 (Annexure A2).

It enhances the homolytic cleavage of several bonds in pyranose rings leading to the decomposition of smaller molecules in addition to hetrolytic cleavage of glycosidic linkages [31]. It also suppresses levoglucosan formation and promotes the breakdown of cellulose and lignin into smaller fragments by ring scission, isomerization, dehydration, decarboxylation, decarbonylation, cross-linking, and rearrangement reactions [32]. Because of the above reasons, the co-pyrolysis experiments were performed in the presence of NaCl.

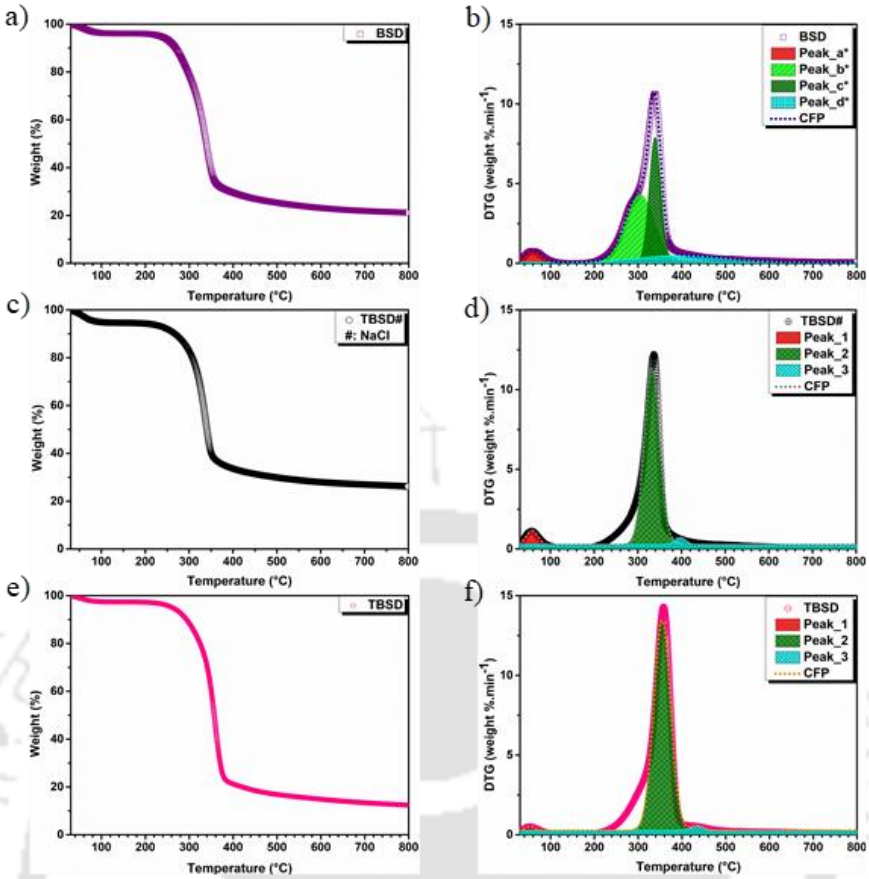

Figure 4.5. The TGA (a, c, and e) and DTG, along with CFP, plots (b, d, and f) of BSD (a and b), TBSD + NaCl (c and d) and TBSD (e and f) at 10°C min^{-1} (CFP: Cumulative fit peak with Gaussian function for peak deconvolution).

4.2.4 Thermogravimetric analysis on Co-pyrolysis of TBSD and LLDPE

Thermogravimetric analysis was conducted with various combinations (1:0, 3:1, 1:1, 1:3 and 0:1) of TBSD and LLDPE at different heating rates (5, 10, 20, 40°C min^{-1}) in presence of 10% NaCl (with respect to TBSD) in an inert atmosphere to understand the thermal degradation behavior and reaction mechanism of co-pyrolysis process.

The co-pyrolysis characteristics of TBSD, LLDPE, and their blends are shown in Fig. 4.6 and the deconvoluted plots, fitted by the Gaussian function, are presented in Fig.s A2.3–A2.6. The degradation of LLDPE occurred in a single stage. The degradation behavior of TBSD was already discussed in the above section. The degradation of blends (TBSD+LLDPE)

occurred in three stages. The complete degradation of cellulose and the partial degradation of lignin occurred during the second stage. During the third stage, mainly lignin and plastic degrade [22]. The degradation parameters for different stages of TBSD, LLDPE, and their blends are given in Table 4.1 (for 10°C min^{-1}) and Tables A2.3–A2.5 (for 5, 20 and 40°C min^{-1} heating rates). The degradation of TBSD has occurred in the temperature range of 180–460°C and that of LLDPE was 350–510°C at 5°C min^{-1}. Similarly, at 10°C min^{-1}, the TBSD degradation temperature range was 180–450°C and that of LLDPE 380–520°C. The DR_{max} (25.70 wt % min^{-1}) of LLDPE was higher by a factor of 2 as compared to that of TBSD (13.55 wt% min^{-1}) at 10°C min^{-1}. The degradation rate and mean reactivity of TBP was significantly increased with the heating rate (Fig. A2.7). Due to the poor thermal conductivity of TBSD, peak shifting of DTG to higher temperatures occurred with the heating rate (5–20°C min^{-1}). Based on cell wall composition, lignin-carbohydrate complex and cellulose hinder the heat and mass transfer between torrefied biomass particles at a high heating rate (40°C min^{-1}) as a comparison to that at a low heating rate (5°C min^{-1}) [4,33]. The LLDPE improves the effective H/C ratio of the blend and acts as a hydrogen source, which in turn enhances the mean reactivity (M_R) of blends in the co-pyrolysis process. The Mean reactivity is directly proportional to peak height and inversely proportional to the corresponding peak temperature. The M_R values for various combinations of TBP (3:1, 1:1, and 1:3) were observed as 3.77, 4.46, 4.52 wt % min^{-1} $°C^{-1}$, respectively, at 10°C min^{-1}. The percentage residual weights at 790°C were in the order of TBSD > TBP3:1 > TBP1:1 >TBP1:3 > LLDPE.

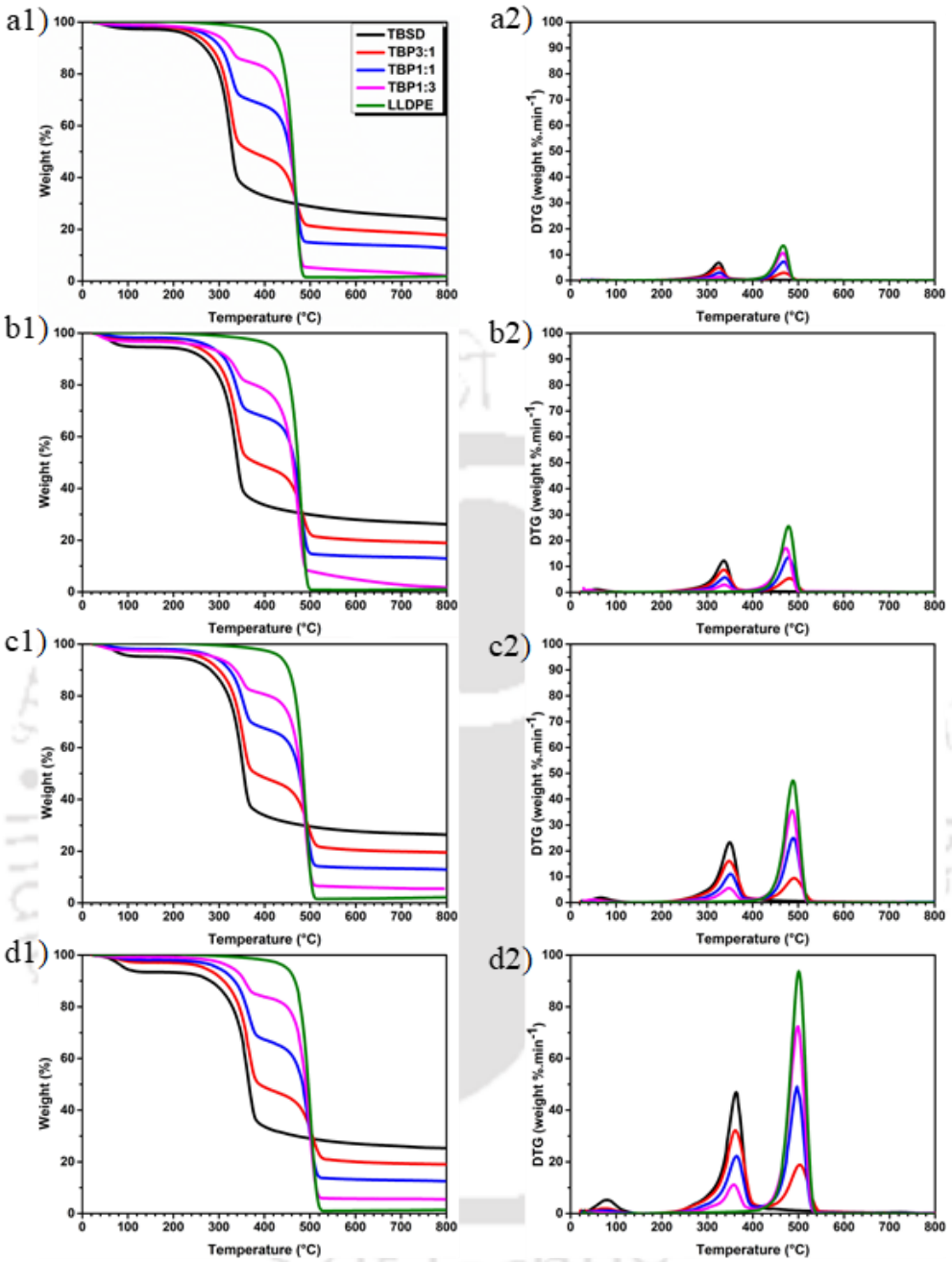

Figure 4.6. TG analysis of TBSD+LLDPE blends at four different heating rates of a) 5, b) 10, c) 20 and d) 40°C min^{-1}: Weight loss as a function of temperature (a1, b1, c1 and d1) and DTG (a2, b2, c2 and d2). (The legend given in subfigure a1 is applicable to all the other subfigures).

Table 4.1. Degradation parameters at different stages of degradation of TBSD, LLDPE and their blends at a heating rate of 10°C min^{-1}

Stages	Parameters	TBSD	TBP3:1	TBP1:1	TBP1:3	LLDPE
Stage_1 (Moisture removal)	T_{range} (°C)	30–120	30–110	30–95	30–80	–
	DR_{max} (wt% ·min^{-1})	*1.22*	*0.6*	*0.43*	*0.9*	–
	T_{max} (°C)	56	55	53	40	–
	W_{loss} (%)	4.82	2.67	0.53	2.49	–
Stage_2	T_{range} (°C)	180–450	250–410	200–385	210–370	380–520
	DR_{max} (wt% ·min^{-1})	*12.36*	*8.81*	*5.82*	*3.0*	*25.70*
	T_{max} (°C)	335	334	337	335	476
	W_{loss} (%)	63.35	46.29	29.5	15.85	96.1
Stage_3	T_{range} (°C)	–	405–540	395–525	375–520	–
	DR_{max} (wt% ·min^{-1})	–	*5.44*	*13.45*	*17.14*	–
	T_{max} (°C)	–	481	477	473	–
	W_{loss} (%)	–	20.73	53.02	73.17	–
Mean Reactivity (M_R) x 10^2 (wt % min^{-1} °C^{-1})		3.69	3.77	4.46	4.52	5.40
% Residual weight after 790°C		26.13	18.20	13.27	2.03	1.50

4.2.5 Synergistic effect

The synergistic effect between the TBSD and LLDPE in co-pyrolysis process was determined by calculating the difference of weight loss (ΔW) from equation 2.6. The values of ΔW_{max} (wt%) of all blends were positive at temperatures below 400°C at all ramp rates (5–40°C min^{-1}), with only a few exceptions (Fig. 4.7 and Table 4.2). This observation suggests that the decomposition of TBSD was inhibited with the addition of LLDPE, in most of the cases, at lower temperatures. The possible reason for the inhibition is that the LLDPE forms a coating on the TBSD because the LLDPE first softens in the temperature range 180–300°C (Fig. 4.6) and release of volatiles from the TBSD becomes difficult. At above 400°C, the ΔW_{max} values were negative for all the blends at 40°C min^{-1} ramp rate, and for TBP1:3 at all the ramp rates (Table 4.3), indicating that the decomposition of TBSD was promoted with the addition

of LLDPE [34]. Various structural rearrangements of biopolymer (cellulose: linear and lignin: amorphous) and LLDPE (ethylene with α–olefin), the orientation of dispersed phase, nature of the interaction, density, glass transition temperature, and biomass composition are responsible for positive and passive synergistic effects between TBSD and LLDPE [22,35,36]**.** At temperatures above 400°C, the thermal degradation of polyolefin (LLDPE) occurs via a radical chain process consisting of three steps (initiation, propagation, and termination). This process produces several smaller fragments (propyl, isopropyl, hexyl, iso-pentyl, and neo-butyl) which react with volatiles from TBSD or with TBSD itself and enhance the overall degradation process synergistically [37,38]. The ΔW of all the blends at ramp rates 5–40°C min^{-1} was approximately constant above 600°C since the devolatilization process has essentially been completed. The TBP1:3 has more positive synergistic effect as compared to the other two blends (TBP3:1 and TBP1:1) at all ramp rates (Fig. 4.7), majorly due to the higher concentration of LLDPE in this blend. Various structural rearrangements of biopolymer (cellulose: linear and lignin: amorphous) and LLDPE (ethylene with α–olefin), the orientation of dispersed phase, nature of the interaction, density, glass transition temperature, and biomass composition are responsible for positive and passive synergistic effects between TBSD and LLDPE [22,35,36]**.** In the co-pyrolysis process, the biomass first degrades (at temperatures below 400°C) and generates free radicals, which may react with LLDPE and initiates its degradation reactions.[37] The LLDPE donates protons (hydrogen) and stabilizes the co-pyrolysis products.[39] The char produced from the biomass (TBSD) catalyses the pyrolysis of LLDPE.[40] Thus, the presence of both TBSD and LLDPE in the right quantities synergistically help each other in their degradation process.

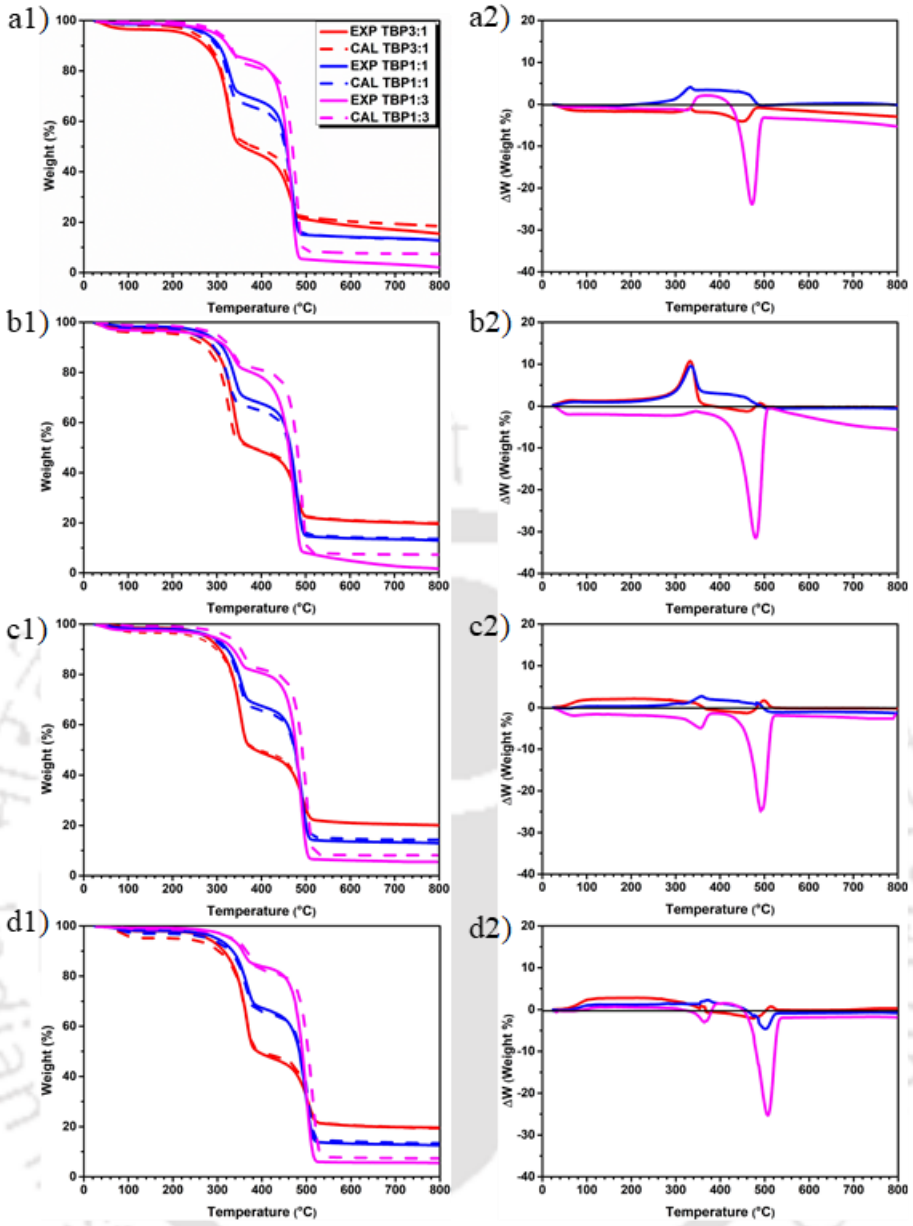

Figure 4.7. Experimental and calculated TG curves for three different TBSD+LLDPE blends (TBP3:1, TBP1:1, and TBP1:3) at four different heating rates of (a) 5, (b) 10, (c) 20 and (d) 40°C min^{-1}: Weight loss as a function of temperature (a1, b1, c1 and d1) and ΔW (a2, b2, c2 and d2). (The legend given in subfigure a1 applies to all other subfigures).

Table 4.2. Synergistic effect of mixed samples with different heating rates (5–40°C min^{-1})

RR	Extent of Synergism											
	TBP3:1				TBP1:1				TBP1:3			
	ΔW^{*}	T^{a}	$\Delta W^{\#}$	T^{b}	ΔW^{*}	T^{a}	$\Delta W^{\#}$	T^{b}	ΔW^{*}	T^{a}	$\Delta W^{\#}$	T^{b}
5	3.92	450	–	–	–	–	4.25	333	23.58	471	2.38	368

10	1.33	459	10.57	333	0.56	510	9.42	335	31.33	480	–	–
20	– –	– –	2.10 1.86	197 499	– –	– –	2.82 1.17	358 482	4.64 24.58	355 494	– –	– –
40	1.92	477	3.10	182	4.55	502	2.39	372	25.30	507	0.53	162

RR: Ramp rate; ΔW^{*}: Maximum weight percentage difference (negative values); $\Delta W^{\#}$: Maximum weight percentage difference (positive values); T^{a}: Maximum temperature (°C) for ΔW^{*}; T^{b}: Maximum temperature (°C) for $\Delta W^{\#}$.

4.2.6 kinetic analysis

The apparent activation energy (E_α) of the co-pyrolysis was estimated by isoconversional models (KAS (equation 1.11), FWO (equation 1.12), and FM (equation 1.13)) [41]. These kinetic models use the experimental data generated from the thermogravimetric analysis. For kinetic analysis, temperature range from 150–700°C was taken because below 150°C most of the weight loss was due to moisture removal and above 700°C, the weight loss was marginal. The variation of activation energy (E_α) and temperature profile with conversion (α) for co-pyrolysis of various blends (3:1, 1:1, and 1:3) of TBSD and LLDPE and the pyrolysis of BSD, TBSD and LLDPE are shown in Fig. 4.8 and Tables A2.6–2.11. The R^2 (correlation coefficient) values in most cases were greater than 0.99, indicating that all the models fit well for the co-pyrolysis and pyrolysis processes (Table 4.3). [41] The average apparent activation energy for the pyrolysis of TBSD was lower than that of BSD (Table 4.3), indicating less energy required for the pyrolysis of torrefied biomass. The reason for the lower activation energy of TBSD pyrolysis as compared to that of BSD could be the weaker bonds of lignin (–ether (C–O–C) and >C=O), which bring down the activation energy. Other reasons for the lower activation energy of TBSD may be a removal of xylan from BSD [15].

The $\bar{E}_{\alpha\ \text{for}}$ co-pyrolysis of (TBSD+LLDPE) blends (3:1, 1:1 and 1:3) were observed to be 207, 264, and 245 kJ mol^{-1} from KAS model; 229, 261, and 244 kJ mol^{-1} from FWO model; 258, 254, and 256 kJ mol^{-1} from Friedman model, respectively. The $\bar{E}_\alpha$ of pyrolysis of LLDPE from KAS, FWO, and Friedman model were 210, 256, and 259 kJ mol^{-1}, respectively. From

the above results, it was observed that the apparent activation energies of the co-pyrolysis of blends fell in between those of pyrolysis of TBSD and LLDPE. The E_α calculated for all the 6 samples from all the three models fall within a standard error of ≤10 kJ mol^{-1} (Table 4.3). In most of the cases, the E_α was significantly higher from FM model as compared to those form KAS and FWO models, because of the differential form of FM model [22]. Therefore, the FM model was the most contributor for the higher standard error. The standard error was the highest for the BSD sample (10 kJ mol^{-1}) and was the lowest for the TBP1:1 (2 kJ mol^{-1}). The blends have the lowest standard error, indicating that any of the three models can be used to estimate the activation energies. Moreover, the trends of activation energy variation with conversion were similar from all the three models (Fig.s 4.8a, b and c).

The E_α of TBSD and BSD (estimated from all the three models) was nearly constant with conversion, at lower conversions (α: 0.1–0.6) and increased at higher conversions (Fig.s 4.8a, b and c). While the E_α of LLDPE followed an opposite trend, it was increased with conversion, at lower conversions (α: 0.1–0.3) and remained nearly constant at higher conversions (α: 0.3–0.8). The profile of E_α of blends with the conversion was similar to that of TBSD and LLDPE at lower (e.g., TBP3:1) and higher (e.g., TBP1:3) concentrations of LLDPE, respectively. For example, the E_α of TBP3:1 was nearly constant with α, at $\alpha \leq 0.5$, and then increased and passed through a maximum at $\alpha = 0.7$ (KAS and FWO models) and 0.6 (FM model). The co-pyrolysis of blends can be divided into three stages. The first stage of TBP3:1 occurred from conversion range 0.1 to 0.3 at the temperature range 300–335°C. At this stage, the cleavage of weak bonds (β–, ether and –COOH in lignin) and the elimination of volatile molecules from cellulose and LLDPE occur in the co-pyrolysis of mixed samples, which requires low E_α. The second stage was in the conversion range 0.3–0.5 at higher temperatures from 335 to 350°C. In this temperature range, degradation of functional groups having higher bond energy (such as glycosidic bonds [β–(C1↔C4)], ether bonds (α–O–4), $–OCH_3$ and

biphenyls, etc.) occurred. The sudden change in E_α at 0.5–0.7 conversions could be attributed to the degradation of resinol, and phenyl–coumarane-type linkages in lignin. Stage three was occurred in the temperature range from 454 to 476°C and at conversion from 0.7 to 0.8. At this stage, the condensed molecules having aromatic rings, which act as precursors for char, degrades with higher activation energy.

The E_α of TBP3:1 was increased (with a small dip at α: 0.2) and levelled off (became constant) at $\alpha \geq 0.5$. The dip in activation energy at α: 0.2 could be due to the synergistic effects, which was discussed in detail in the Section 4.2.5. A positive synergistic effect was observed in the temperature range of 320–380°C for TBD1:3 (Fig. 4.7). The fractional conversion was increased from 0.1 to 0.2 in the temperature range of 340–420°C. Which indicates that the dip in activation energy was due to synergism between TBSD and LLDPE of this blend. For this blend, the trend of E_α variation with conversion was similar from all the three models used. The trend of E_α variation of TBP1:1 with conversion was more like in-between that of TBP3:1 and TBP1:3.

The Arrhenius plots (Fig. A2.8) generated from different kinetic models and at various conversions (0.1 to 0.9) indicate that the reactions of co-pyrolysis are multistep. The blends TBP3:1 and TBP1:3 are the potentially efficient blends for co-pyrolysis as compared to the TBP1:1 blend because of the lower mean apparent activation energy. The degradation mechanism was determined by plotting the master plots using Criado's method in the next section.

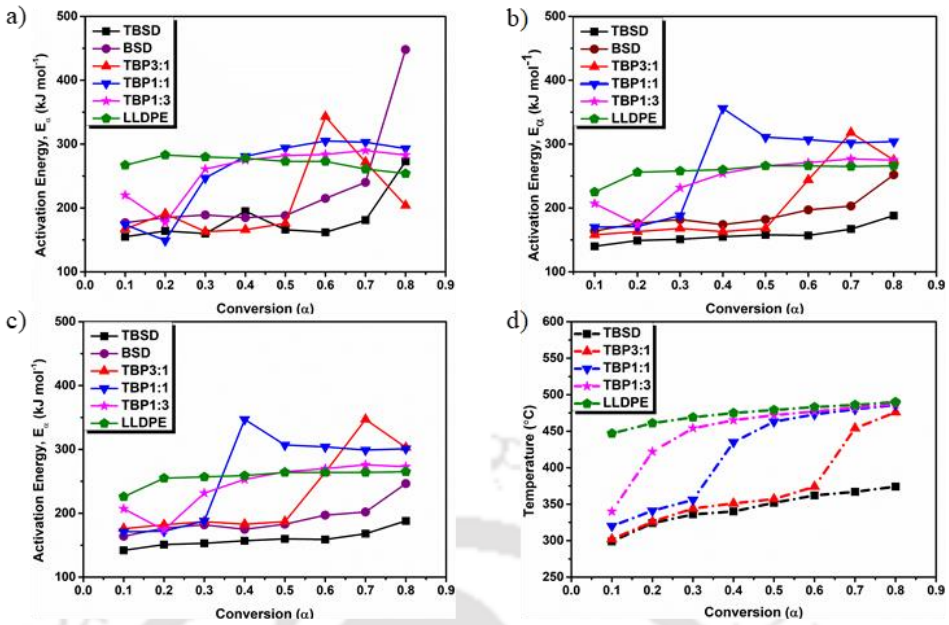

Figure 4.8. Variation of apparent activation energy (a, b and c) with the conversion, obtained from FM (a), KAS (b), FWO (c) models for both blends and individual samples. The temperature profile of blends as a function of conversion (d). The temperature was averaged over all the four heating rates

Table 4.3. Average apparent activation energy of pyrolysis of TBSD, and LLDPE and co-pyrolysis of TBSD+LLDPE blends from isoconversional methods

Code	KAS MODEL		FWO MODEL		FM MODEL	
	$\bar{E}_\alpha$, (kJ mol^{-1})	Avg. R^2	$\bar{E}_\alpha$, (kJ mol^{-1})	Avg. R^2	$\bar{E}_\alpha$, (kJ mol^{-1})	Avg. R^2
BSD	191	0.996	191	0.974	228	0.985
TBSD	155	0.998	157	0.996	180	0.988
TBP3:1	207	0.994	229	0.995	210	0.971
TBP1:1	264	0.992	261	0.996	256	0.989
TBP1:3	245	0.960	244	0.965	260	0.984
LLDPE	258	0.999	257	0.999	271	0.998

4.2.7 Determination of reaction model by Master plot

The FM model was used to construct an experimental master plot [23]. The experimental master curves (equation 1.23) were plotted from TGA data at the heating rate of 10°C min^{-1} (Fig. 4.9). The experimental data was matched with the theoretical curves to evaluate the

reaction mechanism of solid decomposition (co-pyrolysis). The theoretical models such as nucleation (A and P), diffusion (D), geometrical contraction (R) and reaction order (F) models were used for the evaluation.[42] Avrami-Erofeyev (A) and power law (P) models come under the category of nucleation model, which is related to the phase transformation that depends upon temperature, time and heterogeneity of materials (edge dislocation, defects, surfaces, impurities).[42,43] The reaction between reactants from two different crystal lattices is often controlled by diffusion and its mechanism follows the diffusion (D) model.[42] The LLDPE degradation followed a first-order reaction (F1) at all the conversions (Fig. 4.9f). The TBSD degradation followed a zero-order reaction (F0) at conversions from 0.1 to 0.55 and first-order reaction (F1) at 0.55 to 0.7 conversions (Fig. 4.9b).

The co-pyrolysis of TBSD + LLDPE blends did not follow a single reaction mechanism instead it followed the mixed reaction mechanisms because of the complex composition of the blends. The co-pyrolysis of the blend TBP3:1 initially followed third order reaction (F3) from 0.1 to 0.6 and at further conversions (0.6-0.9) the reaction followed the trend of two-dimensional Avrami-Erofeyev model (A2). The co-pyrolysis of the blend TBP1:1 also followed third order reaction (F3) from conversions 0.1 to 0.3 and at higher conversions, the reaction followed the trend of two-dimensional Avrami-Erofeyev model (A2). The blend TBP1:3 followed the trend of two-dimensional Avrami-Erofeyev model (A2) at lower conversions (0.1–0.55) in temperature range of 300–450°C. The volatiles generated from lignin and extractives at low-temperature (300–450°C) help in the fragmentation of cellulose. At higher conversions, it followed the diffusion-reaction model (D2) but the degradation trend seems to end with following first-order reaction mechanism (F1). At temperature >450°C, the fragments initially formed move from one location/lattice to another location/lattice by diffusion-controlled mechanism.

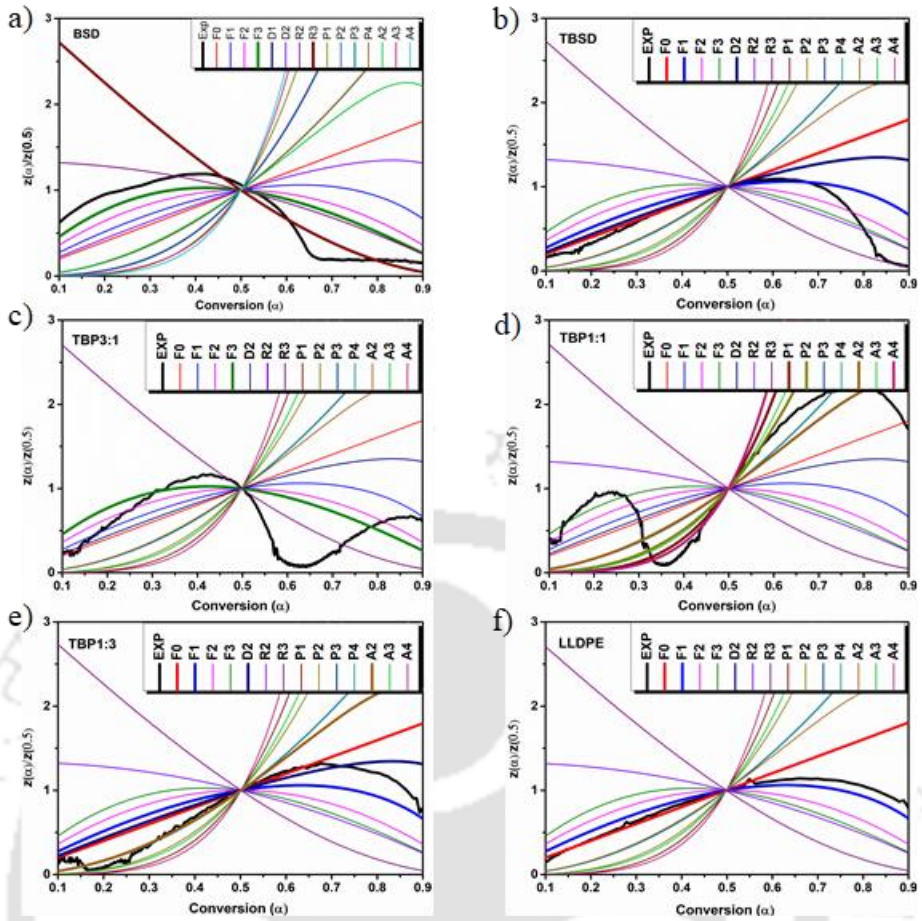

Figure 4.9. Master plot [Z(α): z(α)/z(0.5)] of TBSD+LLDPE blends at a heating rate of 10°C min^{-1}: a) BSD, b) TBSD, c) TBP 3:1, d) TBP 1:1, e) TBP 1:3 and f) LLDPE

4.3 Conclusions

The hydrochar and pentoses (xylose + arabinose) were selectively produced from bamboo biomass using catalytic wet torrefaction (WT). The hemicellulose was selectively removed in the form of pentoses (xylose + arabinose), during the WT. The produced hydrochar (TBSD) was hydrophobic in nature, having high heating value (HHV) 24.02 MJ kg^{-1}, comparable to that of low-rank coal, lignite (25.10 MJ kg^{-1}). The best torrefaction activity, with pentose sugar yields of 85% and complete removal of hemicellulose (> 95%), was obtained with formic acid:BSD ratio of 1:1 w/w and NaCl:BSD ratio of 3:1 w/w at 140°C for 30 min. In the co-pyrolysis of TBSD+LLDPE blends, the blend TBP1:3 has more positive synergistic effect compared to TBP1:1 and TBP3:1. The activation energy of TBSD was lower by 20% as

compared to that of BSD. The average apparent activation energies of samples TBSD, TBP3:1, TBP1:1 TBP1:3, and LLDPE were 155, 207, 264, 245, and 258 kJ mol^{-1}, respectively. The multistep reactions were found to be responsible for a large variation of apparent activation energy of co-pyrolysis with conversion, as shown by the master plot. The decomposition of the blend TBP1:3 follows a nucleation growth (A2) model in the conversion range of 0.1 to 0.5 and diffusion-reaction (D2) model in the higher conversion range (0.5 to 0.8).

References

[1] L.Z. Wang S, Dai G, Yang H, Lignocellulosic biomass pyrolysis mechanism : A state-of-the-art review, Prog. Energy Combust. Sci. 62 (2017) 33–86. https://doi.org/10.1016/j.pecs.2017.05.004.

[2] D. Shen, W. Jin, J. Hu, R. Xiao, K. Luo, An overview on fast pyrolysis of the main constituents in lignocellulosic biomass to valued-added chemicals : Structures , pathways and interactions, Renew. Sustain. Energy Rev. 51 (2015) 761–774. https://doi.org/10.1016/j.rser.2015.06.054.

[3] J. Zhang, Y.S. Choi, C.G. Yoo, T.H. Kim, R.C. Brown, B.H. Shanks, Cellulose − Hemicellulose and Cellulose − Lignin Interactions during Fast Pyrolysis, ACS Sustain. Chem. Eng. 3 (2015) 293–301. https://doi.org/10.1021/sc500664h.

[4] N. Giummarella, M. Lawoko, A.J. Ragauskas, A critical review on the analysis of lignin carbohydrate bonds, Green Chem. 21 (2019) 1573–1595. https://doi.org/10.1039/c8gc03606c.

[5] M. Safar, B.J. Lin, W.H. Chen, D. Langauer, J.S. Chang, H. Raclavska, A. Pétrissans, P. Rousset, M. Pétrissans, Catalytic effects of potassium on biomass pyrolysis, combustion and torrefaction, Appl. Energy. 235 (2019) 346–355. https://doi.org/10.1016/j.apenergy.2018.10.065.

[6] J. Wen, L. Xiao, Y. Sun, S.N. Sun, Comparative study of alkali-soluble hemicelluloses

isolated from bamboo (Bambusa rigida), Carbohydr. Res. 346 (2011) 111–120. https://doi.org/10.1016/j.carres.2010.10.006.

[7] J.S. Arora, K.B. Ansari, J.W. Chew, P.J. Dauenhauer, S.H. Mushrif, Unravelling the catalytic influence of naturally occurring salts on biomass pyrolysis chemistry using glucose as a model compound : a combined experimental and DFT study, Catal. Sci. Technol. 9 (2019) 3504–3524. https://doi.org/10.1039/C9CY00005D.

[8] M. Alam, D. Rammohan, A. Bhavanam, N.R. Peela, Wet torrefaction of bamboo saw dust and its co-pyrolysis with plastic, Fuel. 285 (2021). https://doi.org/10.1016/j.fuel.2020.119188.

[9] D. Chen, Z. Zheng, K. Fu, Z. Zeng, J. Wang, M. Lu, Torrefaction of biomass stalk and its effect on the yield and quality of pyrolysis products, Fuel. 159 (2015) 27–32. https://doi.org/10.1016/j.fuel.2015.06.078.

[10] W.H. Chen, B.J. Lin, B. Colin, J.S. Chang, A. Pétrissans, X. Bi, M. Pétrissans, Hygroscopic transformation of woody biomass torrefaction for carbon storage, Appl. Energy. 231 (2018) 768–776. https://doi.org/10.1016/j.apenergy.2018.09.135.

[11] Y. Zhang, K. Song, Thermal and chemical characteristics of torrefied biomass derived from a generated volatile atmosphere, Energy. 165 (2018) 235–245. https://doi.org/10.1016/j.energy.2018.09.006.

[12] M.N. Cahyanti, T.R.K.C. Doddapaneni, T. Kikas, Biomass torrefaction: An overview on process parameters, economic and environmental aspects and recent advancements, Bioresour. Technol. 301 (2020) 122737. https://doi.org/10.1016/j.biortech.2020.122737.

[13] H.C. Ong, W.H. Chen, Y. Singh, Y.Y. Gan, C.Y. Chen, P.L. Show, A state-of-the-art review on thermochemical conversion of biomass for biofuel production: A TG-FTIR approach, Energy Convers. Manag. 209 (2020) 112634.

https://doi.org/10.1016/j.enconman.2020.112634.

[14] H. Jiang, Y. Ye, P. Lu, M. Zhao, G. Xu, D. Chen, T. Song, Effects of torrefaction conditions on the hygroscopicity of biochars, J. Energy Inst. 96 (2021) 260–268. https://doi.org/10.1016/j.joei.2021.03.018.

[15] S. Raza, R. Tariq, Z. Hameed, I. Ali, M. Naqvi, W. Chen, S. Ceylan, H. Rashid, J. Ahmad, S.A. Taqvi, M. Shahbaz, Pyrolysis of high ash sewage sludge : Kinetics and thermodynamic analysis using Coats-Redfern method, Renew. Energy. 131 (2019) 854–860. https://doi.org/10.1016/j.renene.2018.07.094.

[16] Z. Ma, Y. Yang, Q. Ma, H. Zhou, X. Luo, X. Liu, S. Wang, Evolution of the chemical composition , functional group , pore structure and crystallographic structure of bio-char from palm kernel shell pyrolysis under di ff erent temperatures, J. Anal. Appl. Pyrolysis. 127 (2017) 350–359. https://doi.org/10.1016/j.jaap.2017.07.015.

[17] M. Iwamoto, A. Shimatai, M. Honda, M. Matsukata, Depolymerization of Cellulose with Superheated Steam: Remarkable Obstruction Effects of Sodium and High Reactivity of Crystalline Cellulose, ACS Sustain. Chem. Eng. 6 (2018) 6570–6576. https://doi.org/10.1021/acssuschemeng.8b00375.

[18] B. Hu, Q. Huang, A.C.T. Bourtsalas, M. Ali, Y. Chi, J. Yan, Effect of Chlorine on the Structure and Reactivity of Char Derived from Solid Waste, Energy & Fuels. 31 (2017). https://doi.org/10.1021/acs.energyfuels.7b01042.

[19] Y. Zhang, J. Zhao, Z. Ma, F. Yang, F. Cheng, Effect of oxygen concentration on oxy-fuel combustion characteristic and interactions of coal gangue and pine sawdust, Waste Manag. 87 (2019) 288–294. https://doi.org/10.1016/j.wasman.2019.01.040.

[20] N. Shimada, H. Kawamoto, S. Saka, Different action of alkali/alkaline earth metal chlorides on cellulose pyrolysis, J. Anal. Appl. Pyrolysis. 81 (2008) 80–87. https://doi.org/10.1016/j.jaap.2007.09.005.

[21] J.G. Lynam, M. Toufiq Reza, V.R. Vasquez, C.J. Coronella, Effect of salt addition on hydrothermal carbonization of lignocellulosic biomass, Fuel. 99 (2012) 271–273. https://doi.org/10.1016/j.fuel.2012.04.035.

[22] M. Alam, A. Bhavanam, A. Jana, J. kumar S. Viroja, N.R. Peela, Co-pyrolysis of bamboo sawdust and plastic: Synergistic effects and kinetics, Renew. Energy. 149 (2020) 1133–1145. https://doi.org/10.1016/J.RENENE.2019.10.103.

[23] S. Vyazovkin, N. Sbirrazzuoli, Isoconversional kinetic analysis of thermally stimulated processes in polymers, Macromol. Rapid Commun. 27 (2006) 1515–1532. https://doi.org/10.1002/marc.200600404.

[24] N. Zhao, B. Li, The effect of sodium chloride on the pyrolysis of rice husk, Appl. Energy. 178 (2016) 346–352.

[25] N. Zhao, B.X. Li, The effect of sodium chloride on the pyrolysis of rice husk, Appl. Energy. 178 (2016) 346–352. https://doi.org/10.1016/j.apenergy.2016.06.082.

[26] J.S. Arora, J.W. Chew, S.H. Mushrif, Influence of Alkali and Alkaline-Earth Metals on the Cleavage of Glycosidic Bond in Biomass Pyrolysis: A DFT Study Using Cellobiose as a Model Compound, J. Phys. Chem. A. 122 (2018) 7646–7658. https://doi.org/10.1021/acs.jpca.8b06083.

[27] Y. Wei, C. Shen, J. Xie, Q. Bu, Study on reaction mechanism of superior bamboo biochar catalyst production by molten alkali carbonates pyrolysis and its application for cellulose hydrolysis, Sci. Total Environ. 712 (2020) 136435. https://doi.org/10.1016/j.scitotenv.2019.136435.

[28] Y. Zhang, X. Xie, J. Zhao, X. Wei, The alkali metal occurrence characteristics and its release and conversion during wheat straw pyrolysis, Renew. Energy. 151 (2020) 255–262. https://doi.org/10.1016/j.renene.2019.11.013.

[29] Y. Fang, L. Yin, H. Yang, X. Gong, Y. Chen, H. Chen, Catalytic mechanisms of

potassium salts on pyrolysis of β-O-4 type lignin model polymer based on DFT study, Proc. Combust. Inst. 38 (2021) 3969–3976. https://doi.org/10.1016/j.proci.2020.07.038.

[30] X. Tian, Y. Wang, Z. Zeng, L. Dai, Y. Peng, L. Jiang, X. Yang, L. Yue, Y. Liu, R. Ruan, Study on the mechanism of co-catalyzed pyrolysis of biomass by potassium and calcium, Bioresour. Technol. 320 (2021) 124415. https://doi.org/10.1016/j.biortech.2020.124415.

[31] C. Conditioning, M.T. Reza, University of Nevada , Reno Upgrading Biomass by Hydrothermal and Chemical Conditioning, (2013).

[32] Z. Xiang, J. Liang, H. Marion, M. Jr, Y. Liu, Bioresource Technology Thermal behavior and kinetic study for co-pyrolysis of lignocellulosic biomass with polyethylene over Cobalt modi fi ed ZSM-5 catalyst by thermogravimetric analysis, Bioresour. Technol. J. 247 (2018) 804–811. https://doi.org/10.1016/j.biortech.2017.09.178.

[33] N. Zhang, S. Li, L. Xiong, Y. Hong, Y. Chen, Cellulose-hemicellulose interaction in wood secondary cell-wall, Model. Simul. Mater. Sci. Eng. 23 (2015) 1–15. https://doi.org/10.1088/0965-0393/23/8/085010.

[34] W. Cao, J. Li, L. Lue, X. Zhang, Release of alkali metals during biomass thermal conversion ., Arch Ind Biotechnol. 1 (2016) 2–4.

[35] Y. Lin, Y. Liao, Z. Yu, S. Fang, Y. Lin, Y. Fan, X. Peng, Co-pyrolysis kinetics of sewage sludge and oil shale thermal decomposition using TGA – FTIR analysis, Energy Convers. Manag. J. 118 (2016) 345–352.

[36] C. Liu, J. Wang, J. He, Rheological and thermal properties of m-LLDPE blends with m-HDPE and LDPE, Polymer (Guildf). 43 (2002) 3811–3818.

[37] L. Zhou, Y. Wang, Q. Huang, J. Cai, Thermogravimetric characteristics and kinetic of plastic and biomass blends co-pyrolysis, Fuel Process. Technol. 87 (2006) 963–969. https://doi.org/10.1016/j.fuproc.2006.07.002.

[38] H. Bockhorn, A. Hornung, U. Hornung, D. Schawaller, Kinetic study on the thermal degradation of polypropylene and polyethylene, J. Anal. Appl. Pyrolysis. 48 (1999) 93–109.

[39] S.D. Gunasee, B. Danon, J.F. Görgens, R. Mohee, Co-pyrolysis of LDPE and cellulose: Synergies during devolatilization and condensation, J. Anal. Appl. Pyrolysis. 126 (2017) 307–314. https://doi.org/10.1016/j.jaap.2017.05.016.

[40] E. Jakab, G. Várhegyi, O. Faix, Thermal decomposition of polypropylene in the presence of wood-derived materials, J. Anal. Appl. Pyrolysis. 56 (2000) 273–285. https://doi.org/10.1016/S0165-2370(00)00101-7.

[41] Y. He, C. Chang, P. Li, X. Han, H. Li, S. Fang, J. Chen, X. Ma, Thermal decomposition and kinetics of coal and fermented cornstalk using thermogravimetric analysis, Bioresour. Technol. 259 (2018) 294–303. https://doi.org/10.1016/j.biortech.2018.03.043.

[42] A. Khawam, D.R. Flanagan, Solid-State Kinetic Models : Basics and Mathematical Fundamentals Solid-State Kinetic Models : Basics and Mathematical Fundamentals, J. Phys. Chem. B. 110 (2006) 17315–17328. https://doi.org/10.1021/jp062746a.

[43] M. Avrami, Granulation, phase change, and microstructure kinetics of phase change. III, J. Chem. Phys. 9 (1941) 177–184. https://doi.org/10.1063/1.1750872.

Chapter 5

Catalytic Co-pyrolysis of Wet-Torrefied Bamboo Sawdust and Plastic over the Zeolite H-ZSM-5: Synergistic Effects and Kinetics

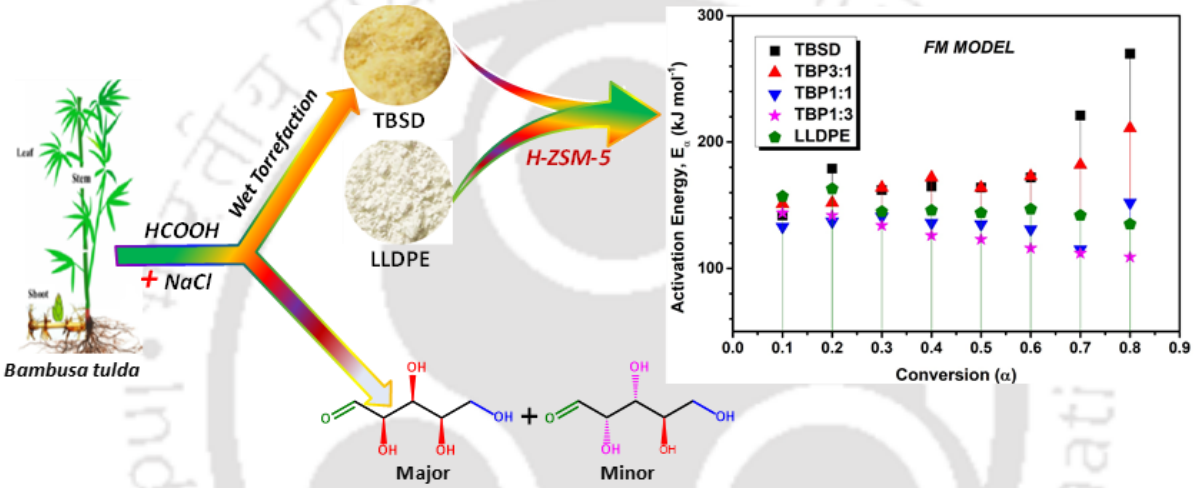

Highlights

- Torrefied bamboo sawdust (TBSD) was co-pyrolyzed with LLDPE over HZSM-5
- The catalytic co-pyrolysis of the blend 1:3 TBSD: LLDPE has the least activation energy
- The catalytic (co-)pyrolysis outperformed the (co-)pyrolysis of TBSD and/or LLDPE
- The catalytic co-pyrolysis (CCP) of the TBSD: LLDPE blends showed the synergism.
- The CCP mechanism was more complex with samples having higher fraction of TBSD

5.1 Objectives

In this study, the catalytic co-pyrolysis of wet-torrefied BSD (TBSD) with plastic (LLDPE) over HZSM-5 was then investigated, using thermogravimetric analysis (TGA) at heating rates 5–40°C min^{-1}. The effect of presence of NaCl on the catalytic pyrolysis of TBSD and catalytic co-

pyrolysis of TBP1:3 was studied. The kinetic parameters were estimated and the reaction mechanism was predicted using isoconversional methods and the Criado's master plot, respectively. To the best of our knowledge, the catalytic co-pyrolysis of wet-torrefied biomass and LLDPE is not reported in the literature.

5.2 Results and Discussion

5.2.1 Catalytic pyrolysis of TBSD and LLDPE and catalytic co-pyrolysis of blends

The TG and DTG curves for the catalytic pyrolysis (CP) of TBSD and LLDPE and the catalytic co-pyrolysis (CCP) of their (TBSD and LLDPE) blends at heating rates 5–40°C min^{-1} are shown in Fig. 5.1. According to our previous study, presence of NaCl in TBSD enhances the pyrolysis activity[1] and therefore, 10 wt.% of NaCl with respect to TBSD was added to each sample. The CP of TBSD and CCP of TBP3:1 and TBP1:1 occurred in three stages and at all the heating rates. Those of LLDPE and TBP1:3 occurred in two stages. The first stage (30–150°C), in both cases (for all the five samples), was corresponded to the loss of moisture and low molecular weight compounds. The shoulder peak corresponding to hemicellulose (which typically occurs in the range of 200–290°C) was not observed in the decomposition of both TBSD and its blends, a clear indication of removal of hemicellulose during wet-torrefaction.

The second stage, observed in the range 150–450°C, was majorly due to degradation of cellulose and some lignin. This region is also known as active pyrolysis region. The TBP3:1 and TBP1:1 showed a broad hump and a shoulder peak at higher temperatures (in the range 380–500°C), respectively. The tailing (from the samples with high fraction of TBSD) in the high-temperature region (500–720°C) was due to charring and condensation reactions of lignin having bonds such as α–O–4, β–O–4, γ–O–4 and benzene rings, which need more energy to rupture [2,3]. In the CCP of blends (TBP3:1 and TBP1:1), shorter tailing was observed as compared to

that in CP of TBSD. No hump/shoulder was observed in the CP of TBSD. Moreover, the peak decomposition temperature was lowered with the increase of LLDPE fraction in the blend (insets of DTG graphs of Fig. 5.1). These facts indicate that the presence of LLDPE helps in the effective degradation of TBSD (particularly the lignin portion). Moreover, the synergy between biomass and LLDPE also could be positively affected by the catalyst acidity.[4,5] It is worth noting that the hump/shoulder/tailing disappear in the case of TBP1:3 blend. The peak degradation temperature (365°C) of TBSD was similar in presence and absence of the catalyst.[1]

The CP of LLDPE showed a sharp DTG peak centered at 300–340°C, the peak temperature was increased with heating rate (Fig. A3.1). At heating rate 40°C min^{-1}, the CP of LLDPE exhibited a shoulder peak towards high temperature side, centered at 410°C. As compared to non-catalytic pyrolysis, the CP of LLDPE showed a lower decomposition temperature. The decomposition temperature in the former process was 480°C[1] and that in the later process was 320°C. Other works also reported a decrease in the peak temperature of pyrolysis of polyethylene's (PEs) in presence of catalyst [6,7]. This could be due to the presence of acidic sites (Brønsted and Lewis) in HZSM-5, which enhances the rate of cracking reactions.

The thermal behavior of TBSD, LLDPE and their blends are presented in Table 5.1 (10°C min^{-1}) and Tables A3.1–A3.3 (for 5, 20 and 40°C min^{-1}). The second stage peak degradation temperature and mean reactivity for all the samples were increased with heating rate (5–40°C min^{-1}). The LLDPE possessed higher H/C_{eff} ratio as compared to TBSD and acted as hydrogen source in blended samples, which enhanced the mean reactivity of blends (except TBP1:1) with respect to TBSD. For example, the mean reactivity of blends TBP3:1, TBP1:1 and TBP1:3 were 13.1, 10.0 and 14.5 wt.% min^{-1} $°C^{-1}$, respectively, at 10°C min^{-1}. In CP of TBSD, the formation of solid residue at 790°C was higher than that in CP of LLDPE and CCP of blends. The solid residue in CCP of blends was decreased with increase of LLDPE fraction in the blend. This could be attributed to lower H/C_{eff} ratio of TBSD as compared to that of LLDPE.[1] The lower H/C_{eff}

ratio of TBSD produce hydrocarbon pools inside the catalyst pores and due to hydrogen deficiency these pools form larger molecules. These molecules act as precursors of solid residue or char. However, in presence of hydrogen-rich reactants such as LLDPE, these hydrocarbon pools undergo reactions such as Diels-Alders and form more aromatic hydrocarbons.[8] Overall, in catalytic pyrolysis (CP) and co-pyrolysis (CCP), the zeolite catalyst reduced the decomposition temperature of LLDPE and blends (TBSD+LLDPE) by providing alternate path because of unique pore dimensions and (Brønsted and Lewis) acidity.

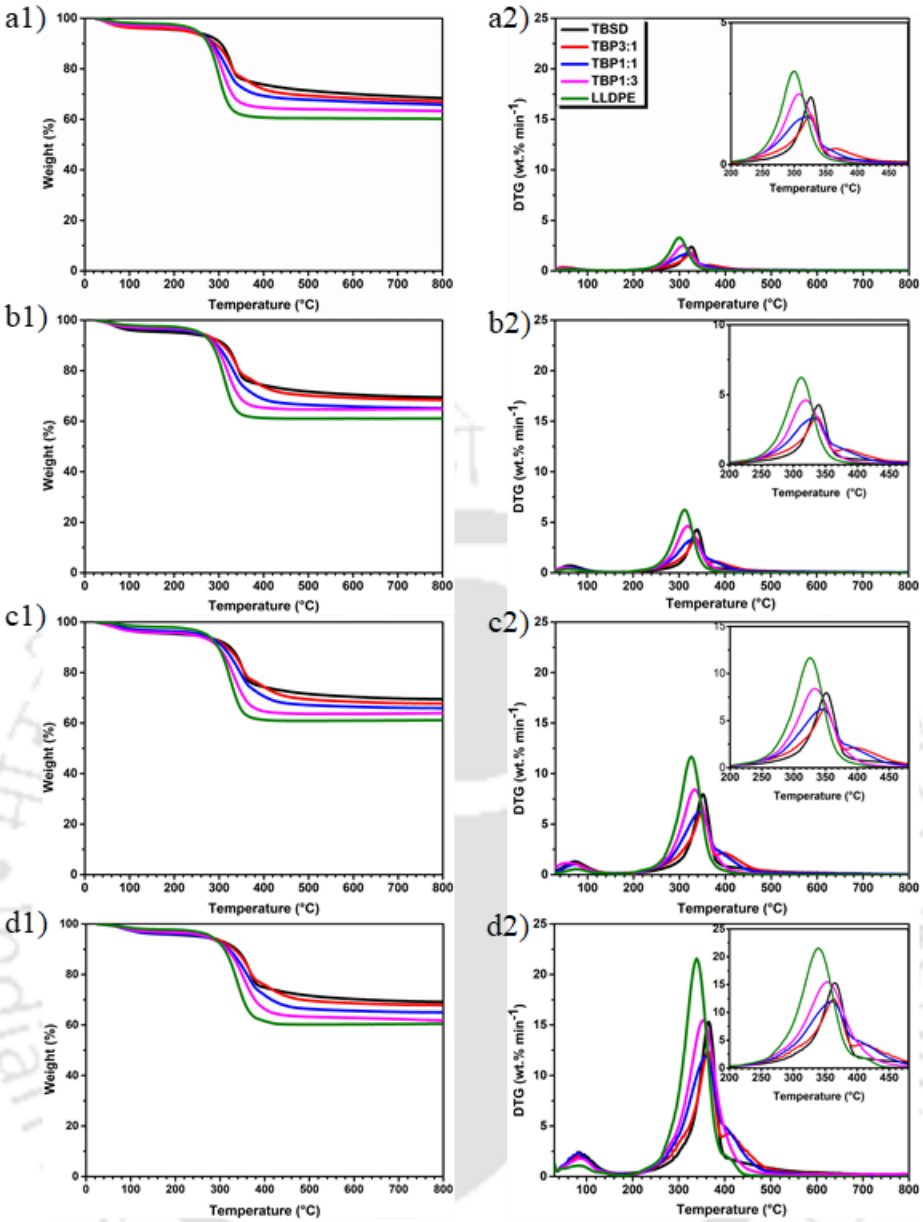

Figure 5.1. TG analysis of catalytic pyrolysis of Torrefied Bamboo Saw Dust and Linear Low-Density Polyethylene and catalytic co-pyrolysis of blends TBP3:1, TBP1:1 and TBP1:3, in presence of HZSM-5, at heating rates (a) 5, (b) 10 (c) 20 and (d) 40°C min^{-1}: Weight loss as a function of temperature (a1, b1, c1 and d1) and DTG (a2, b2, c2 and d2). The legend given in subfigure a1 is applicable to all the other subfigures.

Table 5.1. Degradation parameters and stages of catalytic pyrolysis of Torrefied Bamboo Saw Dust and Linear Low-Density Polyethylene and catalytic co-pyrolysis of blends TBP3:1, TBP1:1 and TBP1:3, in presence of HZSM-5, at a heating rate of 10°C min^{-1}.

Stages	Parameters	TBSD	TBP3:1	TBP1:1	TBP1:3	LLDPE
Moisture removal Stage 1	T_{range} (°C)	30–150	30–150	30–150	30–150	30–150
	DR_{max} (wt.% min^{-1})	0.72	0.52	0.55	0.52	0.38
	T_{max} (°C)	62	63	61	52	58
	W_{loss} (%)	4.3	2.84	2.85	2.68	1.08
Stage 2	T_{range} (°C)	150–385	150–360	180–360	180–430	180–405
	DR_{max} (wt.% min^{-1})	4.29	3.44	3.33	4.62	6.25
	T_{max} (°C)	339	337	332	319	311
	W_{loss} (%)	22.55	19.22	23.87	31.71	35.95
Stage 3	T_{range} (°C)	385–610	365–590	360–487	–	–
	DR_{max} (wt.% min^{-1})	–	1.11	–	–	–
	T_{max} (°C)	–	380	–	–	–
	W_{loss} (%)	3.72	8.01	6.04	–	–
Mean Reactivity (M_R) x 10^3 (wt.% min^{-1} $°C^{-1}$)		12.66	13.13	10.03	14.48	20.10
% Residual weight[#] at 790°C		69.46	68.52	65.27	64.75	61.21
[#]The residual weight includes the catalyst weight also.						

5.2.2 Interaction between materials (synergism) during the catalytic co-pyrolysis

The blend TBP3:1 showed synergism (ΔW (equation 2.6) was negative) only at low heating rate (5°C min^{-1}) at temperatures below 280°C. The blends TBP1:1 and TBP1:3 exhibited positive synergism at all the heating rates, except at 5°C min^{-1} for TBP1:1 (Fig. 5.2). The blend TBP1:3 showed the positive synergism with ΔW: -1.47 (Table 5.2). When temperature increases above 280°C, the decomposition of LLDPE begins and volatile hydrocarbon radicals form by free radical reaction mechanism. These radicals react with oxygenated species formed from the pyrolysis of TBSD instead of attacking LLDPE chain [9], resulting in the passive synergism in

the temperature range 280–500°C. A similar synergistic effects were observed by other researchers.[10–14]

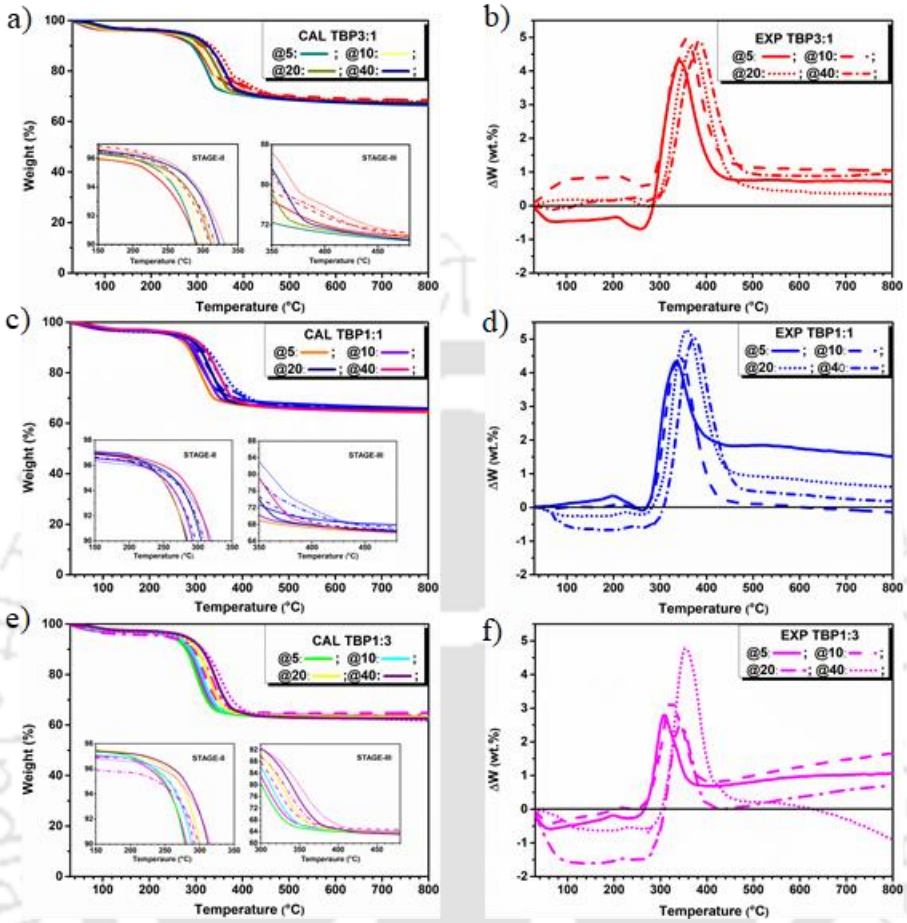

Figure 5.2. Experimental and calculated TG curves for three different Torrefied Bamboo Saw Dust and Linear Low Density Polyethylene blends (TBP3:1 (a & b); TBP1:1 (c & d); and TBP1:3 (e & f) at four different heating rates (5–40°C min^{-1}): Weight as a function of temperature (a, c and e) and ΔW (b, d and f) in presence of HZSM-5

Table 5.2. Synergistic effect of mixed samples with different heating rates (5 – 40 °C min^{-1}) in presence of HZSM-5

RR	Extent of synergism											
	TBP3:1				TBP1:1				TBP1:3			
	ΔW^{*}	T^{a}	$\Delta W^{\#}$	T^{b}	ΔW^{*}	T^{a}	$\Delta W^{\#}$	T^{b}	ΔW^{*}	T^{a}	$\Delta W^{\#}$	T^{b}
5	-0.70	260	4.31	344	–	–	4.34	333	-0.24	248	2.80	308
10	–	–	5.0	356	–	–	4.34	342	-0.43	264	3.24	323

20	–	–	4.81	372	-0.21	263	5.30	357	-1.47	300	2.46	344
40	–	–	4.87	387	-0.66	194	5.06	373	-0.59	181	4.76	354
RR: Ramp rate (°C min^{-1}); ΔW^{*}: Maximum weight percentage difference (at temperature T^{a}); $\Delta W^{\#}$: Maximum weight percentage difference (at temperature T^{b}).												

5.2.3 Role of salt on catalytic (co-)pyrolysis of biomass and plastic

To determine the effect of NaCl on the pyrolysis rate, the activation energies catalytic CP of TBSD and CCP of TBP1:3 blend in presence and absence of NaCl were compared (Fig. 5.3). The * represents the absence of salt. For example, the sample *TBSD is the torrefied biomass sawdust sample without NaCl and TBSD represents torrefied biomass sawdust with NaCl. It can clearly be seen that the activation energy of catalytic and non-catalytic (co-)pyrolysis of both TBSD and TBP1:3 samples was lower in the presence of NaCl. This is because of combined effect of catalysts (alkali metal or salt and HZSM-5). The glycosidic linkages [β–{C1↔C4}] between glucose units in cellulose macromolecules can be broken by alkali metal or salt (Table 1.5). The braking of ester linkages (–COOR) in lignin[2] and ring opening reactions are favorable in presence of alkali metal or salt.[7] In CCP of blended sample, the combined effect of catalysts (alkali metal and HZSM-5) generates the free radicals from biomass. The free radicals generated from LLDPE by Brønsted acid sites of HZSM-5 help in stabilizing the biomass-derived radicals (Schemes A3.1–A3.4) to form various oxygenates and aromatic compounds. These products form through various reactions such as Diels-Alder reaction, hydro deoxygenation, dehydration, decarboxylation, decarbonylation and cracking,[15] and brings down the $\bar{E}_{\alpha}$ of individual or blended samples. The activation energies of CP and of CCP at various conversions in the absence of NaCl from the three different methods are tabulated in Table A3.4 (for *TBSD) and Table A3.5 (for *TBP1:3).

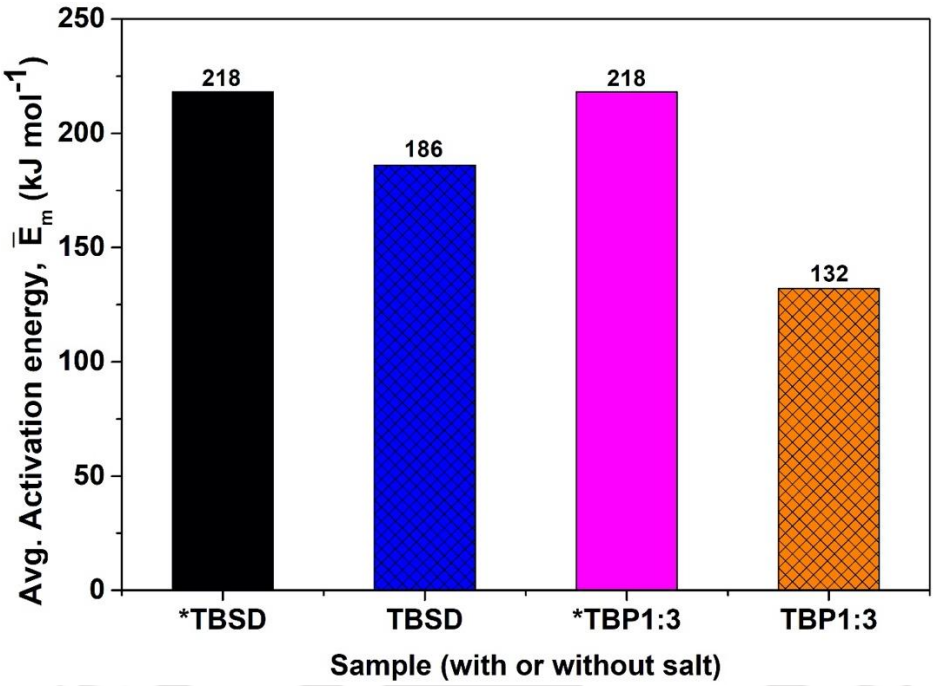

Figure 5.3. Activation energies of catalytic co-pyrolysis of Torrefied Bamboo Saw Dust and the 1:3 blend of torrefied biomass sawdust and Linear Low-Density Polyethylene (TBP1:3) in presence (samples TBSD and TBP1:3) and absence (samples *TBSD and *TBP1:3) of NaCl.

5.2.4 kinetic analysis of catalytic (co-)pyrolysis of TBSD, LLDPE and their blends

To evaluate the apparent activation energy (E_α) of CP of TBSD and LLDPE and CCP of their blends, three iso-conversional methods (KAS (equation 1.11), OFW (equation 1.12) and FM (equation 1.13)) were applied on the corresponding TGA experimental data. The decomposition data in the temperature range of 150–700°C was considered for the analysis.[1] The typical Arrhenius plots for the E_α determination are shown in Fig. A3.2. Both the CP of individual and CCP of blended samples followed a multistep reaction. The data from FM model was scattered as compared to that from other two models due to differential form of the kinetic equation used in the FM model. The variation of E_α from all the three models and temperature

profile with conversion (α), for CP of TBSD and LLDPE and CCP of their blends (TBP3:1, TPB1:1, and TBP1:3) is shown in Fig. 5.4 and Tables A3.6–A3.10.

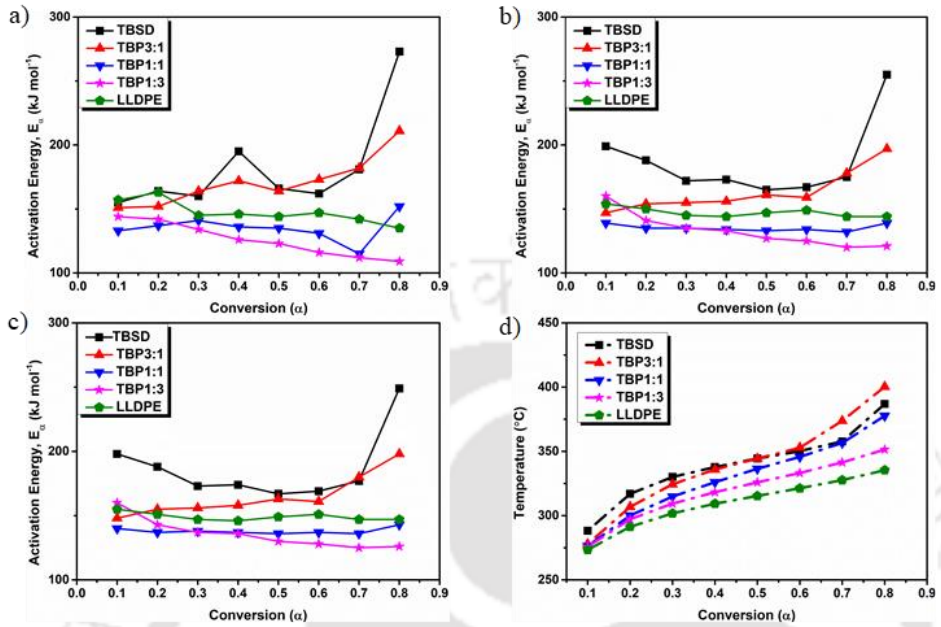

Figure 5.4. Variation of apparent activation energy (from (a) FM, (b) KAS and (c) OFW models) and temperature (d) with conversion in catalytic pyrolysis of Torrefied Bamboo Saw Dust and Linear Low-Density Polyethylene and catalytic co-pyrolysis of blends TBP3:1, TBP1:1 and TBP1:3, in presence of HZSM-5.

The $\bar{E}_\alpha$ for CCP of blends TBP3:1, TBP1:1 and TBP1:3 were found to be 163, 135, and 133 kJ mol^{-1} from KAS model; 165, 137, and 136 kJ mol^{-1} from OFW model; 171, 135, and 126 kJ mol^{-1} from FM model, respectively (Table 5.3). The $\bar{E}_\alpha$ of CP of LLDPE from KAS, FWO, and FM model were 147, 149, and 148 kJ mol^{-1}, respectively, and those of TBSD were 187,187 and 184 kJ mol^{-1}, respectively. The R^2 (the coefficient of determination) values were determined and compared for all the three models at each conversion level. The R^2 values obtained in the calculation of activation energy from KAS, FWO and FM models were higher than 0.99, indicating a good applicability of these models to the experimental data. The R^2 values from KAS and FWO models were always higher than those from FM model, since the FM is a

differential model and KAS and FWO are integral models. The experimental data that we obtain is integral data and, in MF model case, we are applying the differential model to the integral experimental data. All the three models gave similar trends of the variation of the activation energies with the blend concentration. Therefore, the $\bar{E}_\alpha$ obtained from KAS model were used for the discussion.

Surprisingly, the $\bar{E}_\alpha$ of CP of LLDPE was lower than that of TBSD, indicating that the TBSD is less reactive as compared to LLDPE, in presence of HZSM-5 catalyst. However, the trend is usually opposite in the absence of catalyst.[1] The $\bar{E}_\alpha$ of CP and CCP were lower as compared to those of non-catalytic pyrolysis (except for TBSD) and co-pyrolysis, respectively.[1] This could be attributed to the presence of Brønsted and Lewis acid sites in the zeolite HZSM-5, which are responsible for enhancing the rates of cracking, ring opening, cyclization and deoxygenation reactions [7]. The $\bar{E}_\alpha$ of CP of TBSD was slightly higher as compared to that of non-catalytic pyrolysis of TBSD, indicating that the CP of TBSD was not enhanced by the HZSM-5. A similar effect was observed with $MnFeO_3$ catalyst for the CP of poplar wood.[16] The $\bar{E}_\alpha$ of the CCP of blends were decreased with LLDPE concentration and (except TBP3:1) were lower than those of CP of TBSD and LLDPE, indicating a clear synergism.

The activation energy (E_α) calculated from KAS model for CP of TBSD was higher at lower conversions (α), decreased with α up to α 0.5 (to 165 kJ mol^{-1}) and then increased (to 255 kJ mol^{-1} at α 0.8). The increase was rapid at higher conversions: The E_α was increased from 175 to 255 kJ mol^{-1} as conversion increased from 0.7 to 0.8. For TBP1:3, the E_α, after a slight increase from α: 0.1–0.2, was constant (at 157±2.4 kJ mol^{-1}) up to α 0.6 and then increased with α (to 197 kJ mol^{-1} at α 0.8). For TBP1:1, the E_α is nearly constant (at 135±1.9 kJ mol^{-1}) with α at all conversions. For TBP1:3, the E_α decreased with α from 160–120 kJ mol^{-1}. The decrease was higher at lower conversions (decreased from 160–135 kJ mol^{-1} with α increase from 0.1–0.3) and was marginal at higher conversions. For LLDPE, the activation energy was first decreased, then

increased, again decreased and finally leveled-off (at 144 kJ mol^{-1}) at the higher conversions (0.7–0.8). The trends of E_α variation with conversion from FWO and FM models (with a few exceptions) were similar to those of KAS. For example, the trend of E_α of CP of TBSD was similar to that of KAS model except at conversion 0.1. That of TBP3:1 was also similar except a hump at conversion 0.4. The trend of E_α of CCP of TBP1:1 from FM model was completely different than that from KAS and FWO models: E_α was increased up to α 0.3, then decreased up to α 0.7 and finally increased. The activation energy values calculated from KAS and OFW models were nearly the same with deviation < 2%.

The variation of apparent activation energy (E_α) with conversion can be divided into three stages in CP of TBSD and in CCP of blends (TBP3:1 and TBP1:1) containing higher fraction of TBSD (Fig. 5.4). The first stage ($0.1 \leq \alpha \leq 0.3$) occurred in the temperature range of 288–330°C. At this stage, the activation energy was the highest at lower conversion and decreased with conversion. The second stage ($0.3 \leq \alpha \leq 0.7$) was in the temperature range of 330–358°C. In this stage, also known as active pyrolysis stage, the reaction rate was the highest. The acidic sites of HZSM-5 enhance the reaction rate of various reactions, such as dehydration, decarbonylation, deoxygenation and ring opening reactions, and promotes the degradation of cellulose and partial degradation of lignin. In the third stage ($0.7 \leq \alpha \leq 0.8$), the temperature required was the highest (258–387°C) and the activation energy was also the highest. This could be attributed to the degradation of bigger molecules (condensed: 3–4 benzene fused rings) and different linkages in the lignin (resinol type and coumarane linkage).[2,17] The trend of temperature variation with conversion for the blends TBP3:1 and TBP1:1 were similar to that of TBSD (all the three stages can be seen). However, for the samples TBP1:3 and LLDPE, only first two stages were observed (Fig. 5.4d). The temperature required to reach a particular conversion was increased with increasing the TBSD concentration in the sample, at lower conversions up to 0.5. The trend was similar at high conversions except that the sample TBP3:1 required higher temperature than

TBSD. The temperature required to reach a particular conversion was the lowest for LLDPE followed by TBP1:3 and TBP1:1, in the entire conversion range. However, the $\bar{E}_\alpha$ followed a different trend: $\bar{E}_\alpha$ (TBP1:3) < $\bar{E}_\alpha$ (TBP1:1) < $\bar{E}_\alpha$ (TBP3:1). This could be due to the synergism between the TBSD and the LLDPE of the blended samples. Usually, it is advantageous to complete the degradation in a shorter temperature range.[18] The temperature difference to reach conversion from 0.1 to 0.8 was the lowest with LLDPE (62°C), followed by TBP1:3 (76°C), and was the highest with TBP3:1 (122°C). The trends of activation energy and temperature variation with conversion can better be understood by analyzing the reaction mechanism using the master plots. Therefore, the Criado's master plots were presented for all the blends in the next section.

The results indicate that the blend containing 25 wt.% TBSD and 75 wt.% LLDPE (TBP1:3) showed the best catalytic co-pyrolysis characteristics with the least activation energy. Other literature reports also indicated the similar results with ZSM-5 [19] and other catalysts (MgO/C) [20]. The Diels-Alder reactions between furanic groups of biomass and the hydrocarbons of LLDPE results in the formation of additional aromatics [20]. The HZSM-5 catalyzed co-pyrolysis of 1:3 blend of raw bamboo biomass and LLDPE also resulted in the highest aromatic content [19]. Therefore, it can be concluded, from our experimental data and the literature reports, that the presence of HZSM-5 results in lower activation energy and higher aromatic content.

Table 5.3. Average apparent activation energy, and corresponding R^2 value, of catalytic pyrolysis of Torrefied Bamboo Saw Dust and Linear Low-Density Polyethylene and catalytic co-pyrolysis of blends TBP3:1, TBP1:1 and TBP1:3, in presence of HZSM-5, from isoconversional (KAS, OFW and FM) methods.

Code	KAS Model		OFW Model		FM Model	
	$\bar{E}_\alpha$, (kJ mol^{-1})	Avg. R^2	$\bar{E}_\alpha$, (kJ mol^{-1})	Avg. R^2	$\bar{E}_\alpha$, (kJ mol^{-1})	Avg. R^2
TBSD	187±6	0.998	187±6	0.997	184±9	0.989

TBP3:1	163±2	0.999	165±2	0.999	171±3	0.992
TBP1:1	135±1	0.997	137±1	0.998	135±2	0.986
TBP1:3	133±6	0.987	136±6	0.989	126±2	0.971
LLDPE	147±2	0.995	149±2	0.995	148±4	0.990

5.2.5 Determination of reaction mechanism by Criado's master plot

The mechanism of solid-state reactions can be represented by various models.[1,9,21,22] The reaction mechanism was determined using the master plots and was used to understand the reaction kinetics obtained from the isoconversional methods.

The $\bar{E}_\alpha$ calculated from FM model was used to construct master plot at 10°C min^{-1}, since no approximation is needed with FM model. The equation 1.23 was used to plot the reaction models of CP of TBSD, and LLDPE and CCP of their blends (TBP3:1, TBP1:1, and TBP1:3). The master plots of all the samples were presented in Fig. 5.5 and compared with theoretical models [9]. The models which were followed by the experimental data at various conversion ranges are summarized in Table 5.4. The CP of TBSD followed different models, namely zero order reaction (with α 0.1–0.3), second order diffusion (α 0.3–0.4), first and second order reactions (α 0.4–0.65) and geometrical contraction (α > 0.7). The CP of LLDPE followed a first order reaction for α 0–0.65 and tends to second order reaction (F2) model at α above 0.65.

The CCP of TBP3:1, initially (with α 0.1–0.45) followed a zero-order reaction (F0), then followed first (F1) and second order reactions (F2) in a brief conversion range of 0.45–0.55. The mechanism finally changed to third order geometrical contraction (R3) for conversions above 0.55 with corresponding temperature 350–400°C (Table 5.4). While, the CCP of TBP1:1 followed the first order reaction (F1) in the conversion range 0.1–0.5, then the second order reaction (F2) for α 0.5–0.65. Finally, it tends to a second order geometrical contraction at α > 0.65, with decomposition temperature between 340 and 380°C. The CCP of TBP1:3 followed first (F1) and second order (F2) reactions at lower (0.1–0.5) and higher (> 0.5) conversions,

respectively. Overall, the mechanism of CP and CCP at lower conversions (< 0.5) transitioned from "F0 followed by D2" to "F0 followed by F1 and F2" and to "just F1" at no, lower and higher fractions of LLDPE, respectively. That at higher conversions (> 0.5) transitioned from "F2 followed by R3" to "F2 followed by R2" and to "just F2" at no, lower and higher fractions of LLDPE, respectively. The reaction mechanism from master plot correlates well with the kinetics presented in the previous section. The CP and CCP of samples with higher fraction of TBSD followed a three-stage degradation and those with higher fraction of LLDPE followed a two-stage degradation. This was clearly reflected from the master plot also, which determined that the mechanism is more complex (containing more steps) in the case of samples with higher fraction of TBSD as compared to those with lower fraction of TBSD.

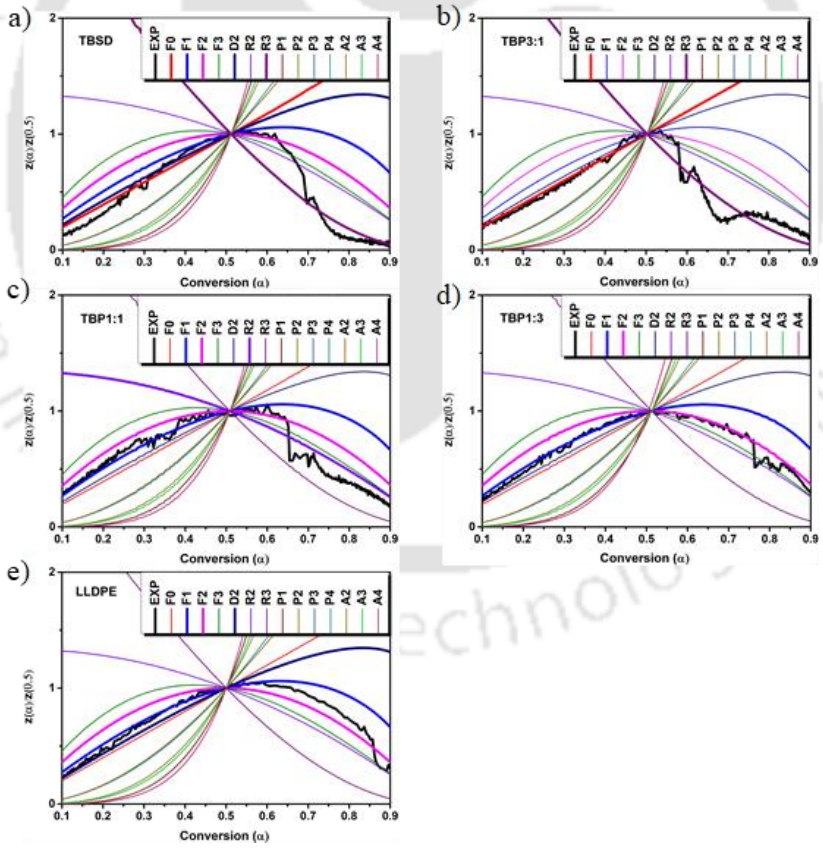

Figure 5.5. Master plot [Z(α): z(α)/z (0.5)] of TBSD (a) TBP3:1 (b) TBP1:1 (c) TBP1:3 (d) and LLDPE (e), in presence of HZSM-5 at a heating rate of 10°C min^{-1}.

Table 5.4. The kinetic models from Criado's master plot for catalytic pyrolysis of Torrefied Bamboo Saw Dust and Linear Low Density Polyethylene and catalytic co-pyrolysis of blends TBP3:1, TBP1:1 and TBP1:3 at 10°C min^{-1} heating rate, in presence of HZSM-5.

TBSD			**TBP3:1**			**TBP1:1**			**TBP1:3**			**LLDPE**		
α	**M**	**M^n**	**α**	**M**	**M^n**	**α**	**M**	**M^n**	**α**	**M**	**M^n**	**α**	**M**	**M^n**
0.1–0.3	F0	RO	0.1–0.45	F0	RO	0.1–0.5	F1	RO	0.1–0.50	F1	RO	0.1–0.65	F1	RO
0.3–0.4	D2	DN	0.45–0.55	F1	RO	0.5–0.65	F2	RO	>0.5	F2	RO	>0.65	F2 (C)	RO
0.4–0.5	F1	RO	>0.55	R3	GC	>0.65	R2 (C)	GC	–	–	–	–	–	–
0.5–0.65	F2	RO	–	–	–	–	–	–	–	–	–	–	–	–
>0.7	R3	GC	–	–	–	–	–	–	–	–	–	–	–	–

Note: M: Model; M^n: Mechanism (RO: Reaction order model, DN: diffusion and GC: Geometrical Contraction model); α: Conversion; (C) indicates tending towards (close to) that mechanism but not exactly matching.

5.2.6 Probable reaction pathways of CP of TBSD and LLDPE and CCP of the blends (TBP)

CCP is a set of complex reactions involving a significant number of species, such as free radicals and carbocation. As per the FTIR analysis carried out in our previous study, the major functional groups present on the TBSD surface are carboxylic, carbonyl, ester, alcohol, aldehyde, and alkoxy groups.[1] The TBSD (consisting of cellulose, lignin, and a minor amount of hemicellulose) broke down into different oligomers by cracking reaction in presence of zeolite containing (Brønsted and Lewis) acidic sites and at temperatures in the range of 200–400°C as shown in Fig. 5d. Further, the macromolecule cellulose consists of D-glucose units joined by glycosidic bonds [β–{C1↔C4}] which thermally degraded into oligosaccharides and monosaccharides on the external surface of zeolite by cleaving of glycosidic linkages. These anhydrosugars further break down into light and heavy oxygenates. Acetic acid, ketones, and acetaldehydes come under the category of light oxygenates while furans and their derivatives under heavy oxygenates. Further, these oxygenates move into the pores of HZSM-5 zeolite where reactions such as deoxygenation and rearrangement (Grob type) occur on catalytic

(Brønsted and Lewis) sites of the zeolite to form various aromatics (scheme A3.1).[1,7,17,23–28] The production of phenol and its derivatives with different kinetic diameters (phenol: 0.45-0.54 nm and its derivatives: > 0.54 nm) from lignin pyrolysis adsorbed on the surface of zeolites (HZSM-5) which recombine and rearrange to form a precursor of coke that reduce catalytic activity (scheme A3.2).[29,30] [31] The plastic polymer, predominantly consisting of C–C and C–H bonds, degraded into different fragments by the catalytic activity of zeolite (on the external surface) at high temperatures (280–400°C) by various session processes (β, random, end chain and mid-chain).[1] Further, these fragments move into the pores of zeolite which convert into olefins (C2−C4), wax-like materials, aromatics (minor amount) (Scheme A3.3) [1,9,32], hydrogen radicals and hydrogen ions (H^+) over Brønsted and Lewis acid sites through cracking reactions.[29] The hydrogen radicals further react with lignin and cellulose derivatives to from oxygenates (Schemes A3.1−A3.4) and enhances the catalytic activity by reducing the coke formation. The oxygenates (furanic and phenolic derivatives) may also further react in hydrocarbon pools in zeolite pores (HZSM-5) during co-pyrolysis to form mono aromatic hydrocarbons by Diels-Alder reaction and polyaromatic hydrocarbons by multiple reactions, as shown in Scheme A3.4.[15]

5.3 Conclusions

The bamboo sawdust (BSD) was torrefied to selectively produce pentose sugars (predominantly xylose) and acetic acid from the hemicellulose portion of the BSD. The best torrefaction activity, with pentose sugar yields of 85% and complete removal of hemicellulose, was obtained with formic acid:BSD ratio of 1:1 w/w and NaCl:BSD ratio of 3:1 w/w. The catalytic co-pyrolysis (CCP) of blends containing higher (TBP3:1 and TBP1:1) and lower (TBP1:3) fractions of torrefied BSD (TBSD) occurred in three and two stages, respectively. The average apparent activation energies (E_m) of samples TBSD, TBP3:1, TBP1:1 TBP1:3, and LLDPE for KAS model were found to be 187, 163, 135, 133, and 147 kJ mol^{-1}, respectively. The

CCP of blends TBP1:3 and TBP1:1 showed synergism in terms of apparent activation energy. The values of $\bar{E}_\alpha$ of CP and CCP were lower as compared to those of non-catalytic pyrolysis (except for TBSD) and co-pyrolysis, respectively. The blend containing 25 wt.% TBSD and 75 wt.% LLDPE (TBP1:3) showed the best CCP characteristics with the least $\bar{E}_\alpha$. In CCP, the temperature difference to reach conversion from 0.1 to 0.8 was the lowest with TBP1:3 (76°C) and was the highest with TBP3:1 (122°C). The reaction mechanism from the master plot correlates well with the kinetics, i.e., the mechanism is more complex (containing more steps) in the case of CCP of samples with a higher fraction of TBSD as compared to those with a lower fraction of TBSD.

References

[1] M. Alam, D. Rammohan, A. Bhavanam, N.R. Peela, Wet torrefaction of bamboo saw dust and its co-pyrolysis with plastic, Fuel. 285 (2021) 119188. doi:10.1016/j.fuel.2020.119188.

[2] N. Giummarella, M. Lawoko, A.J. Ragauskas, A critical review on the analysis of lignin carbohydrate bonds, Green Chemistry. 21 (2019) 1573–1595. doi:10.1039/c8gc03606c.

[3] L.Z. Wang S, Dai G, Yang H, Lignocellulosic biomass pyrolysis mechanism : A state-of-the-art review, Progress in Energy and Combustion Science. 62 (2017) 33–86. doi:10.1016/j.pecs.2017.05.004.

[4] H. Shafaghat, H.W. Lee, L. Yang, D. Oh, S.C. Jung, G.H. Rhee, J. Jae, Y.K. Park, Catalytic co-conversion of Kraft lignin and linear low-density polyethylene over mesoZSM-5 and Al-SBA-15 catalysts, Catalysis Today. (2019). doi:10.1016/j.cattod.2019.04.052.

[5] Y.M. Kim, H.W. Lee, J. Jae, K. Bin Jung, S.C. Jung, A. Watanabe, Y.K. Park, Catalytic

co-pyrolysis of biomass carbohydrates with LLDPE over Al-SBA-15 and mesoporous ZSM-5, Catalysis Today. 298 (2017) 46–52. doi:10.1016/j.cattod.2017.06.006.

[6] X. Zhang, H. Lei, L. Zhu, X. Zhu, M. Qian, G. Yadavalli, J. Wu, S. Chen, Thermal behavior and kinetic study for catalytic co-pyrolysis of biomass with plastics, Bioresource Technology. 220 (2016) 233–238. doi:10.1016/j.biortech.2016.08.068.

[7] Y.M. Kim, J. Jae, B.S. Kim, Y. Hong, S.C. Jung, Y.K. Park, Catalytic co-pyrolysis of torrefied yellow poplar and high-density polyethylene using microporous HZSM-5 and mesoporous Al-MCM-41 catalysts, Energy Conversion and Management. 149 (2017) 966–973. doi:10.1016/j.enconman.2017.04.033.

[8] Z. Sun, B. Xu, A.H. Rony, S. Toan, S. Chen, K.A.M. Gasem, H. Adidharma, M. Fan, W. Xiang, Thermogravimetric and kinetics investigation of pine wood pyrolysis catalyzed with alkali-treated CaO/ZSM-5, Energy Conversion and Management. 146 (2017) 182–194. doi:10.1016/j.enconman.2017.04.104.

[9] M. Alam, A. Bhavanam, A. Jana, J. kumar S. Viroja, N.R. Peela, Co-pyrolysis of bamboo sawdust and plastic: Synergistic effects and kinetics, Renewable Energy. 149 (2020) 1133–1145. doi:10.1016/J.RENENE.2019.10.103.

[10] Z. Wu, S. Wang, J. Zhao, L. Chen, H. Meng, Synergistic effect on thermal behavior during co-pyrolysis of lignocellulosic biomass model components blend with bituminous coal, Bioresource Technology. 169 (2014) 220–228. doi:10.1016/j.biortech.2014.06.105.

[11] J. Nikko, V. Salvilla, B. Ivan, G. Ofrasio, A.P. Rollon, F.G. Manegdeg, R. Ruffel, M. Abarca, M. Daniel, G. De Luna, Synergistic co-pyrolysıs of polyolefin plastics with wood and agricultural wastes for biofuel production ☆, Applied Energy. 279 (2020)

115668. doi:10.1016/j.apenergy.2020.115668.

[12] Z. Wang, G. Liu, D. Shen, C. Wu, S. Gu, Co-pyrolysis of lignin and polyethylene with the addition of transition metals - Part I: Thermal behavior and kinetics analysis, Journal of the Energy Institute. 93 (2020) 281–291. doi:10.1016/j.joei.2019.03.003.

[13] X. Liu, K.R.G. Burra, Z. Wang, J. Li, D. Che, A.K. Gupta, Towards enhanced understanding of synergistic effects in co-pyrolysis of pinewood and polycarbonatee, Applied Energy. 143 (2021) 116662. doi:10.1115/1.4049464.

[14] S. Zhong, B. Zhang, C. Liu, A. Shujaa aldeen, Mechanism of synergistic effects and kinetics analysis in catalytic co-pyrolysis of water hyacinth and HDPE, Energy Conversion and Management. 228 (2021) 113717. doi:10.1016/j.enconman.2020.113717.

[15] J. Wang, Z. Zhong, K. Ding, B. Zhang, A. Deng, M. Min, P. Chen, R. Ruan, Co-pyrolysis of bamboo residual with waste tire over dual catalytic stage of CaO and co-modi fi ed HZSM-5, Energy. 133 (2017) 90–98. doi:10.1016/j.energy.2017.05.146.

[16] H. Wang, Q. Yao, C. Wang, B. Fan, Y. Xiong, Y. Chen, Q. Sun, C. Jin, Z. Ma, New Insight on Promoted thermostability of poplar wood modified by MnFe2O4 nanoparticles through the pyrolysis behaviors and kinetic study, Scientific Reports. 7 (2017) 1–12. doi:10.1038/s41598-017-01597-4.

[17] H. Kawamoto, Lignin pyrolysis reactions, J of Wood Sciennec. (2017) 117–132. doi:10.1007/s10086-016-1606-z.

[18] B.S. Kim, Y.M. Kim, H.W. Lee, J. Jae, D.H. Kim, S.C. Jung, C. Watanabe, Y.K. Park, Catalytic Copyrolysis of Cellulose and Thermoplastics over HZSM-5 and HY, ACS Sustainable Chemistry and Engineering. 4 (2016) 1354–1363.

doi:10.1021/acssuschemeng.5b01381.

[19] J. Wang, J. Jiang, Z. Zhong, K. Wang, X. Wang, B. Zhang, R. Ruan, M. Li, A.J. Ragauskas, Catalytic fast co-pyrolysis of bamboo sawdust and waste plastics for enhanced aromatic hydrocarbons production using synthesized CeO2/Γ-Al2O3 and HZSM-5, Energy Conversion and Management. 196 (2019) 759–767. doi:10.1016/j.enconman.2019.06.009.

[20] H.W. Ryu, Y.F. Tsang, H.W. Lee, J. Jae, S.C. Jung, S.S. Lam, E.D. Park, Y.K. Park, Catalytic co-pyrolysis of cellulose and linear low-density polyethylene over MgO-impregnated catalysts with different acid-base properties, Chemical Engineering Journal. 373 (2019) 375–381. doi:10.1016/j.cej.2019.05.049.

[21] A. Khawam, D.R. Flanagan, Solid-state kinetic models: Basics and mathematical fundamentals, Journal of Physical Chemistry B. 110 (2006) 17315–17328. doi:10.1021/jp062746a.

[22] M. Avrami, Granulation, phase change, and microstructure kinetics of phase change. III, The Journal of Chemical Physics. 9 (1941) 177–184. doi:10.1063/1.1750872.

[23] J. Xue, J. Zhuo, M. Liu, Y. Chi, D. Zhang, Q. Yao, Synergetic E ff ect of Co-pyrolysis of Cellulose and Polypropylene over an All-Silica Mesoporous Catalyst MCM-41 Using Thermogravimetry − Fourier Transform Infrared Spectroscopy and Pyrolysis − Gas Chromatography − Mass Spectrometry, Energy & Fuels. 31 (2017) 9576–954. doi:10.1021/acs.energyfuels.7b01651.

[24] P.S. Rezaei, D. Oh, Y. Hong, Y.M. Kim, J. Jae, S.C. Jung, J.K. Jeon, Y.K. Park, In-situ catalytic co-pyrolysis of yellow poplar and high-density polyethylene over mesoporous catalysts, Energy Conversion and Management. 151 (2017) 116–122.

doi:10.1016/j.enconman.2017.08.073.

[25] S. Zhang, Xuesong;Lei, Hanwu; Chen, Catalytic co-pyrolysis of lignocellulosic biomass with polymers: a critical review, Green Chem. 18 (2016). doi:10.1039/c6gc00911e.

[26] P.R. Patwardhan, Understanding the product distribution from biomass fast pyrolysis, (2010).

[27] J.S. Arora, J.W. Chew, S.H. Mushrif, In fl uence of Alkali and Alkaline-Earth Metals on the Cleavage of Glycosidic Bond in Biomass Pyrolysis : A DFT Study Using Cellobiose as a Model Compound, The Journal of Physical Chemistry A. 122 (2018) 7646–7658. doi:10.1021/acs.jpca.8b06083.

[28] P. Keliona, W. Likun, H. Zhang, R. Xiao, Online Vapors Separation of Torre fi ed-Bagasse / HDPE Co-pyrolysis into Three Grades of Bio-oils, Energy & Fuels. 34 (2020) 8376–836.

[29] Z. Wang, K.G. Burra, T. Lei, A.K. Gupta, Co-pyrolysis of waste plastic and solid biomass for synergistic production of biofuels and chemicals-A review, Progress in Energy and Combustion Science. 84 (2021) 100899. doi:10.1016/j.pecs.2020.100899.

[30] H. Yang, Z. Dong, B. Liu, Y. Chen, M. Gong, S. Li, H. Chen, A new insight of lignin pyrolysis mechanism based on functional group evolutions of solid char, Fuel. 288 (2021) 119719. doi:10.1016/j.fuel.2020.119719.

[31] E. Lorenc-Grabowska, Effect of micropore size distribution on phenol adsorption on steam activated carbons, Adsorption. 22 (2016) 599–607. doi:10.1007/s10450-015-9737-x.

[32] K. Pyra, K.A. Tarach, A. Śrębowata, I. Melián-cabrera, K. Góra-marek, Applied Catalysis B : Environmental Pd-modified beta zeolite for modulated hydro-cracking of

low-density polyethylene into a paraffinic-rich hydrocarbon fuel, Applied Catalysis B: Environmental. 277 (2020) 119070. doi:10.1016/j.apcatb.2020.119070.

Chapter 6

Catalytic Co-Pyrolysis of Wet-Torrefied Bamboo Sawdust and Plastic over the Zeolite HY: Synergism and Kinetics

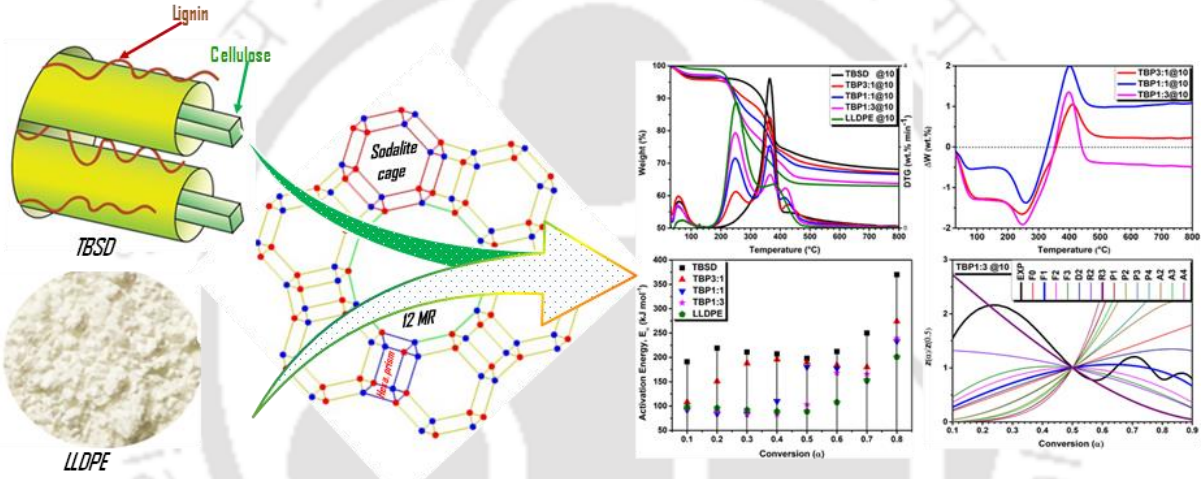

Highlights

- The catalytic co-pyrolysis (CCP) of wet-torrefied bamboo sawdust (TBSD) and LLDPE.
- A clear synergism between TBSD and LLDPE in CCP at lower temperatures.
- Blend (25 wt% TBSD and 75 wt% LLDPE): Highest synergism and lowest $\bar{E}_\alpha$ (117 kJ mol^{-1})
- E_α of blends was lower than that of torrefied bamboo, supporting the synergistic effects.
- CCP of TBP1:3 followed R3 and F1 models at low and high conversions, respectively.

6.1 Objectives

The aim of this study was to explore the potential of mesoporous MesoHY zeolite (with SAR 80) in the co-pyrolysis of torrefied bamboo biomass (TBSD) and plastic (linear low-density polyethylene). The TBSD was prepared using wet-torrefaction process in presence of formic acid and sodium chloride. The effect of heating rate and blend concentrations on the synergism and kinetics was studied in detail. The reaction mechanism of CCP was understood using Criado's master plots. To the best of knowledge, no work is reported in the open literature that is related to catalytic co-pyrolysis (CCP) of torrefied bamboo sawdust (TBSD) and linear low-density polyethylene (LLDPE) over MesoHY zeolite.

6.2 Results and discussion

6.2.1 Catalyst characterization

From the N_2-sorption studies, the MesoHY and HZSM-5 were found to follow Type IV isotherm, indicating the mesoporous nature of the materials by IUPAC classification. In addition, an H4 type of hysteresis loop was observed with MesoHY zeolite (Fig. 6.1a and Table 2.3) implying the presence of narrow slit-like pore. The BET surface area and total pore volume of zeolite MesoHY were determined to be 773 $m^2\ g^{-1}$ and 0.58 $cm^3\ g^{-1}$, respectively. The mesoporous texture was confirmed by average pore diameter (3.79 nm) with pore diameter ranging up to 30 nm as shown in Fig. 6.1b. The HZSM-5 exhibited typical MFI structure with diffraction planes at 2θ of 7.9° (111), 8.8°(020), 23.6°(151), 23.9°(303), and 29.1°(352). Similarly, the HY also showed typical FAU structure with diffraction planes at 2θ of 6.2°(111), 10.2°(220), 12.2° (311), 15.5°(331), 23.4°(533), and 26.8°(642).[1,2] Both the zeolites exhibited good crystallinity (Fig. 6.1c).

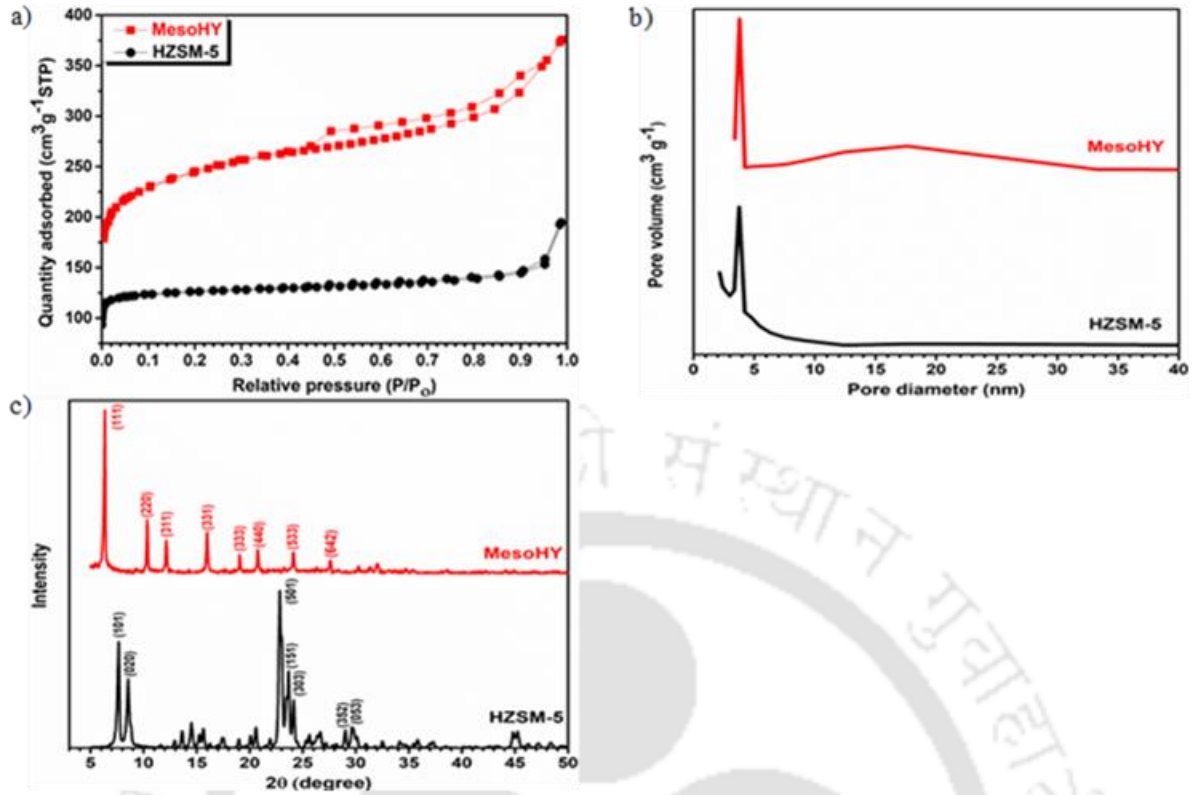

Figure 6.1. Catalytic characterization of zeolites a) N_2 adsorption-desorption b) Pore size distribution by BJH method and c) XRD of MesoHY and HZSM-5 catalyst.

6.2.2 TG analysis of an individual and mixed sample of TBSD and LLDPE over MesoHY catalyst

The thermal profiles of the CP of individuals and the CCP of blends over MesoHY are shown in Fig. 6.2. The thermal degradation parameters at ramp rates 5, 10, 20, and 40°C min^{-1} are summarized in Tables A4.1, 4.1, A4.2, and A4.3, respectively. The deconvoluted plots of TGA of TB and blends at the heating rate 10°C min^{-1} are depicted in Fig. 6.3. The thermal degradation of TBSD over MesoHY occurred in three stages including moisture removal. The moisture removal is stage I which occurred in the temperature range of 30–150°C. In the second stage (180–405°C), the devolatilization of wet torrefied biomass occurred by degradation of cellulose and a minor amount of hemicellulose which was left over after the wet torrefaction process. This stage is also known as the active pyrolysis stage of biomass. The lignin

degradation occurred in the third stage in the temperature range of 410–670°C. The lignin with a complicated structure started to degrade at 180°C (Fig. 6.3).[3] At temperatures above 500°C, charring and condensation reactions occur in biomass polymer.[4] To summarize, in CP of TB, the degradation of cellulose occurred at temperatures between 180°C and 405°C (active pyrolysis) and that of lignin in the range of 410–670°C.

The peak temperature (T_{max}) in this study was defined as the temperature at which the decomposition rate was maximum in that particular stage (Table 6.1). The peak temperature (T_{max}) of DTG curve of non-catalytic TBSD pyrolysis was occurred at 336°C and was shifted to a higher temperature (364°C) when the TBSD was pyrolyzed in presence of MesoHY zeolite (Fig. 6.4). The shift was higher in presence of HY (28°C) as compared to that in presence of HZSM-5 (3°C) (Fig. 6.5). Alteration of the maximum degradation temperature (T_{max}) of torrefied biomass saw dust (TBSD) over MesoHY during pyrolysis was because of the catalyst deactivation. The catalyst deactivation was in turn caused by char/coke formation which deposited on the catalyst of the surface. The MesoHY zeolite allows larger sized oxygenates to be diffused into its pores and undergo further conversion or recombine to condensed molecules which act as precursor of coke. The T_{max} of the catalytic pyrolysis of TBSD in presence of HZSM-5 was similar to that of non-catalytic pyrolysis because of its medium sized pores (5.1 x 5.5 ↔ 5.3 x 5.6 Å) and lower internal pore space (6.36 Å). The kinetic diameter of cellulose and lignin are much larger than the micro-pore size of HZSM-5 zeolite. Therefore, the diffusional limitations play an important role on the degradation of cellulose and lignin over different zeolites.[5–10] Moreover, the peak height of degradation of TBSD over MesoHY was lower compared to that of over HZSM-5 because of the accumulation of coke on the surface of the catalyst.

The catalytic pyrolysis of LLDPE over MesoHY revealed a broader peak (180–480°C), as shown in Fig. 6.3e. The pyrolysis of plastic (LLDPE) over MesoHY occurred at a lower

temperature (T_{max} :251°C) as compared to that without catalyst (T_{max} :478°C). The LLDPE derived components, such as isobutane (kinetic diameter 0.528 nm [7–9,11]), can easily diffuse into the pores of the catalyst and undergo further catalytic transformations over the acidic sites located inside catalyst channel to form aromatic hydrocarbons without re-polymerization. Therefore, the lowest char/coke formation was occurred with the LLDPE feedstock (Fig. 6.4). The pyrolysis temperature of LLDPE (T_{max} :251°C) over MesoHY catalyst was lower than that over HZSM-5 (T_{max} :313°C), as shown in Fig. 6.5. This could be attributed to the larger surface area, mesoporosity and larger average pore size of HY (Table 2.3).

The catalytic co-pyrolysis (CCP) of blends (of TBSD and LLDPE) over MesoHY showed four stages including moisture removal (30–150°C). The maximum degradation temperature (T_{max}) of each stage in a given mixture was different depending on their composition. The weight loss regions of thermal decomposition of blends (TBP3:1, TBP1:1, and TBP1:3) over MesoHY catalyst at heating rate 10°C min^{-1} are shown in Table 6.1 and at 5, 20, and 40°C min^{-1} are shown in Tables A4.1-A4.3. For TBP3:1, the weight loss regions were: second stage 160–290°C, the third stage 295–405°C, and fourth stage 405–640°C. Similarly, for TBP1:1: second stage 160–310°C, the third stage 310–400°C, and fourth stage 400–570°C. For TBP1:3: second stage 160–325°C, the third stage 325–395°C, and fourth stage 400–510°C.

The second decomposition stage of CCP of blends was majorly due to the decomposition of the LLDPE (Fig. 6.3). The decomposition of both plastic and cellulose part of the TBSD contributed to the third stage. The fourth stage was majorly due to the decomposition of lignin. The T_{max} of the catalytic co-pyrolysis of blends was shifted to lower temperatures as compared to the corresponding non-catalytic co-pyrolysis. Further, the catalytic co-pyrolysis temperature was lower over MesoHY as compared to that over HZSM-5. For example, T_{max} of CCP for the blend TBP1:3 over HY was 249°C and that over HZSM-5 was 320°C. The T_{max} values of CCP in presence of catalysts MesoHY and HZSM-5 were lower as compared to those in the absence

of catalyst (339°C), as shown in Fig.s 6.4 and 6.5. Due to the large cavities of MesoHY zeolite, the primary (1°) pyrolyzates can easily reach to the internal acidic sites, making the co-pyrolysis reaction over MesoHY zeolite more efficient than that over HZSM-5.[12,13]

The mean reactivity, which is inversely proportional to the T_{max},[14] followed the order $MR_{LLDPE} > MR_{TBP1:3} > MR_{TBP1:1} > MR_{TBP3:1} > MR_{TBSD}$, at all four different heating rates, over MesoHY zeolite.

The residual weight of TBP3:1, TBP1:1, and TBP1:3 was found to be 7.3, 6.6, and 4.1 wt.% (excluding catalyst weight), respectively, at 790°C and ramp rate 10°C min^{-1} (Table 6.1). The residual weight obtained from CCP of TBP1:3 was the lowest. This could be attributed to the higher plastic content of the blend, which provides a hydrogen-rich atmosphere (H/C_{eff} = 0.18) and prevents the polymerization of fragmented species.[15] The heating rate affects the decomposition of individual and mixed samples over MesoHY zeolite (Fig. A4.1). The DTG peak shifted to a higher temperature region as the heating rate increased from 5 to 40°C min^{-1}. In other words, the sample decomposition required high temperature at high heating rates, indicating that the heat and mass transfer resistances intruded the decomposition process. Moreover, the temperature and pressure gradients across the particle increase with the heating rate.

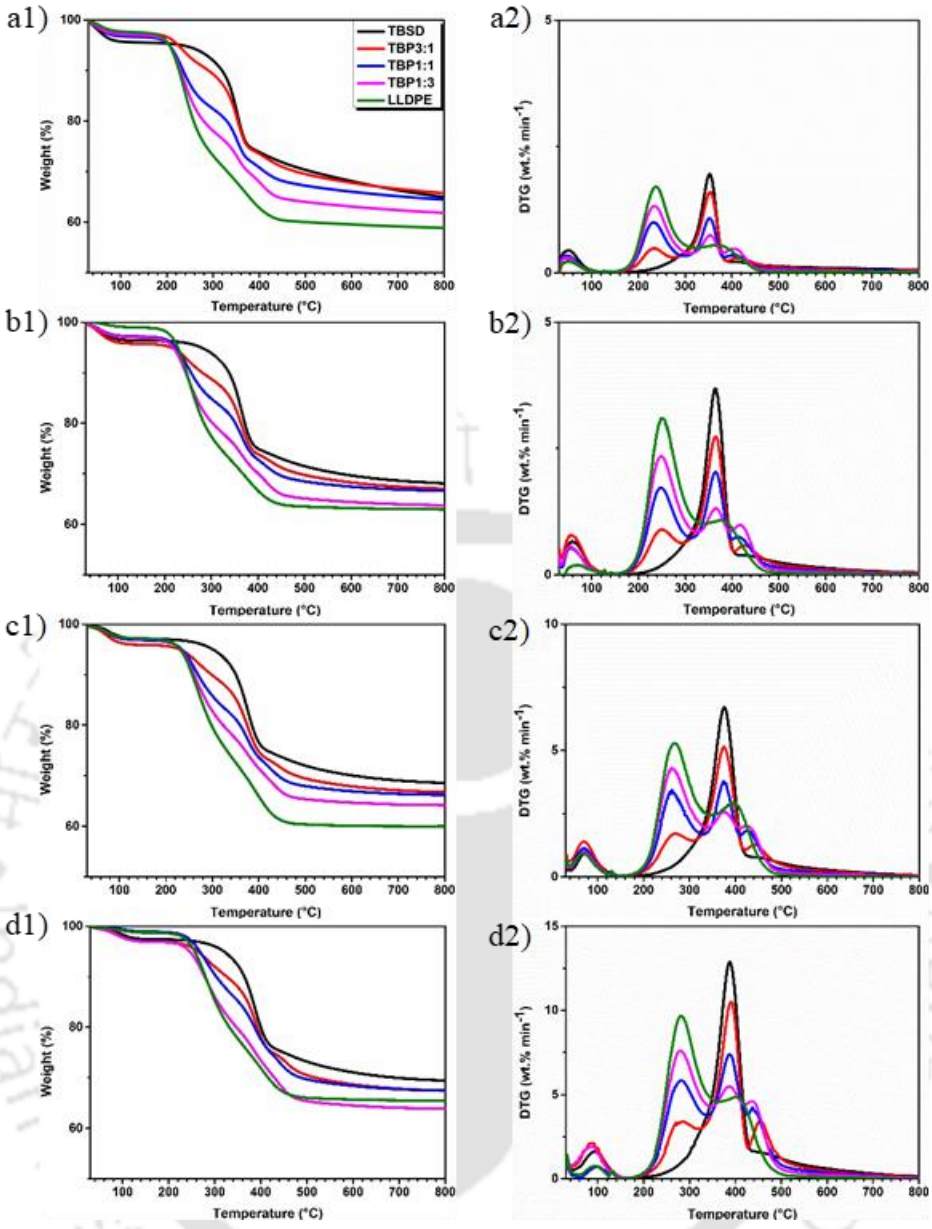

Figure 6.2. Catalytic pyrolysis and co-pyrolysis of individual and blended samples at (a) 5, (b) 10 and (c) 20 and d) 40°C min^{-1}: Mass variation with temperature (a1, b1, c1 and d1) and DTG (a2, b2, c2, and d2), in presence of MesoHY zeolite

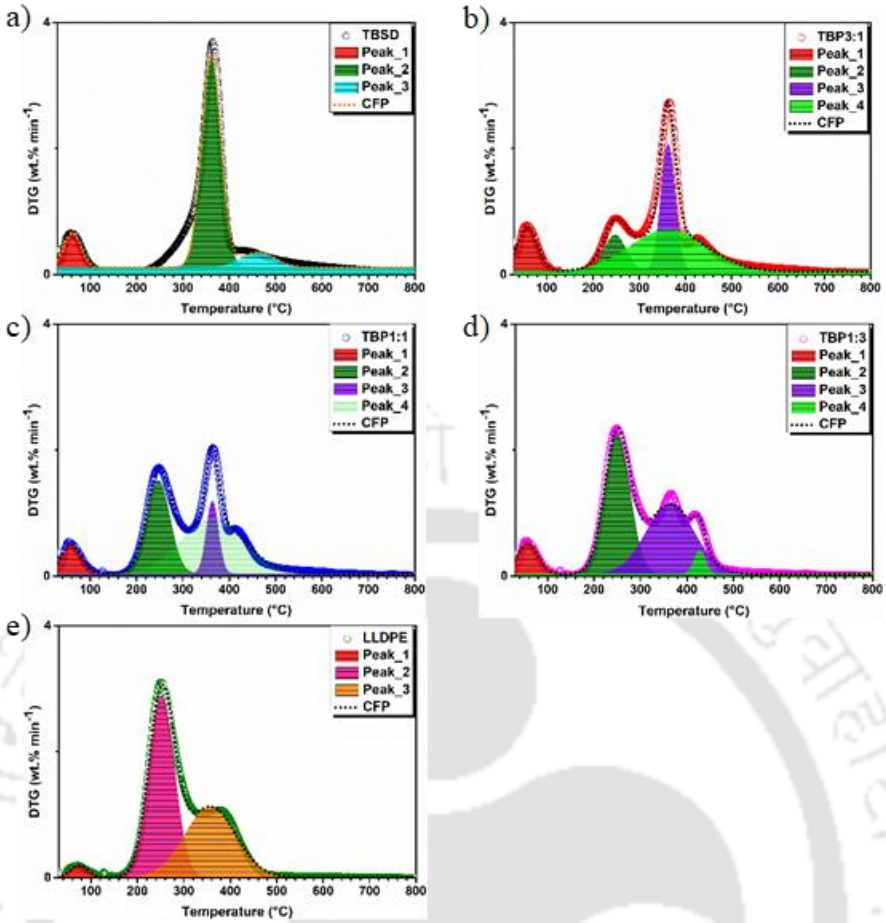

Figure 6.3. The deconvolution of DTG graph along with CFP, plots of TBSD (a), TBP3:1 (b), TBP1:1 (c), TBP1:3 (d) and LLDPE (e) at 10°C min-1 over MesoHY zeolite (CFP: Cumulative fit peak with Gaussian function for peak deconvolution: Origin pro 9.0).

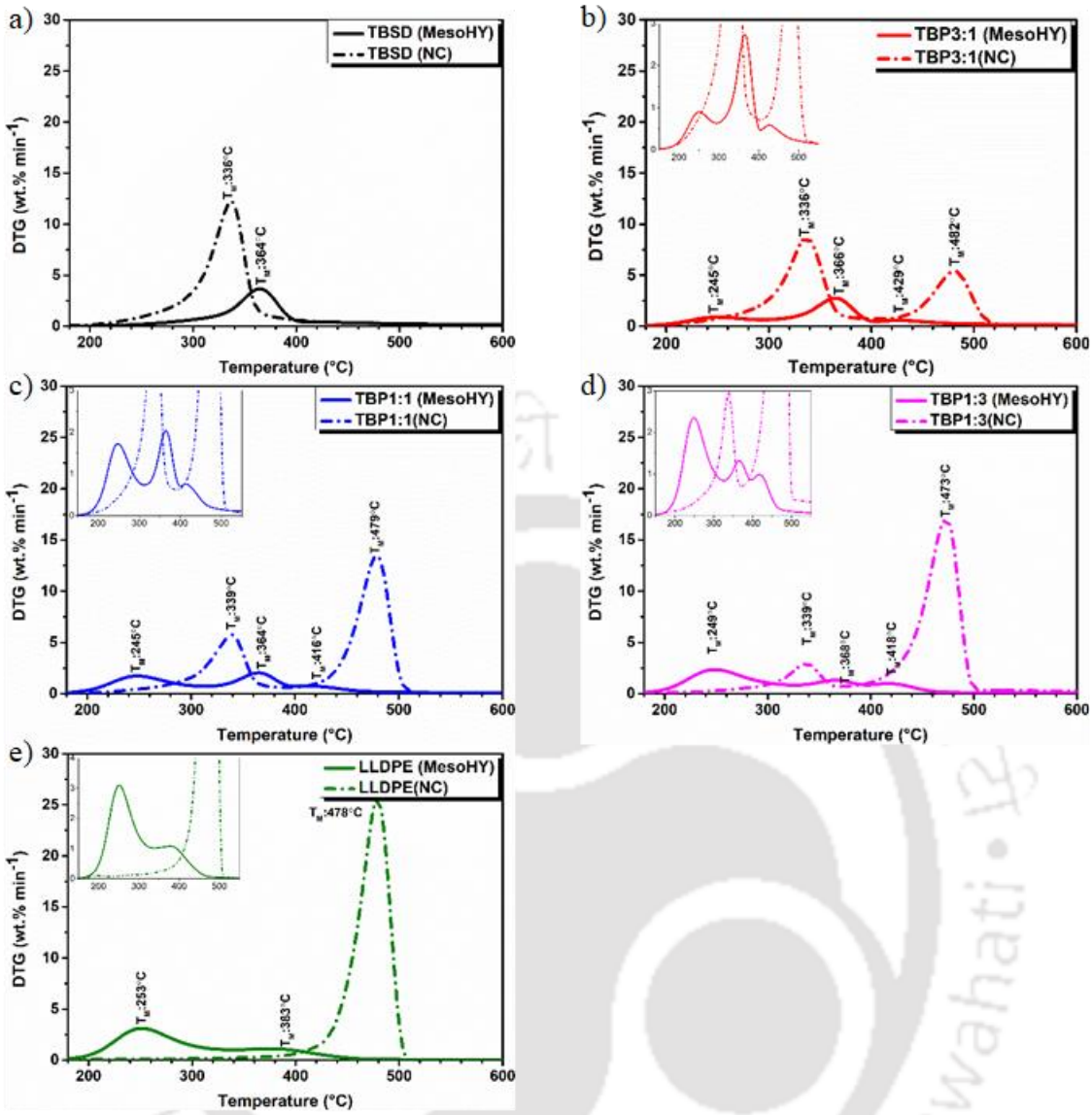

Figure 6.4. Comparison of the DTG profiles of catalytic (over MesoHY) and non-catalytic (NC) pyrolysis of torrefied bamboo sawdust (TBSD) (a) and LLDPE (e) and catalytic (over MesoHY) and non-catalytic co-pyrolysis of TBSD with LLDPE with various weight ratios of TBSD and LLDPE (TBP3:1 (b), TBP1:1 (c) and TBP1:3 (d)), at a ramp rate of 10°C min^{-1}.

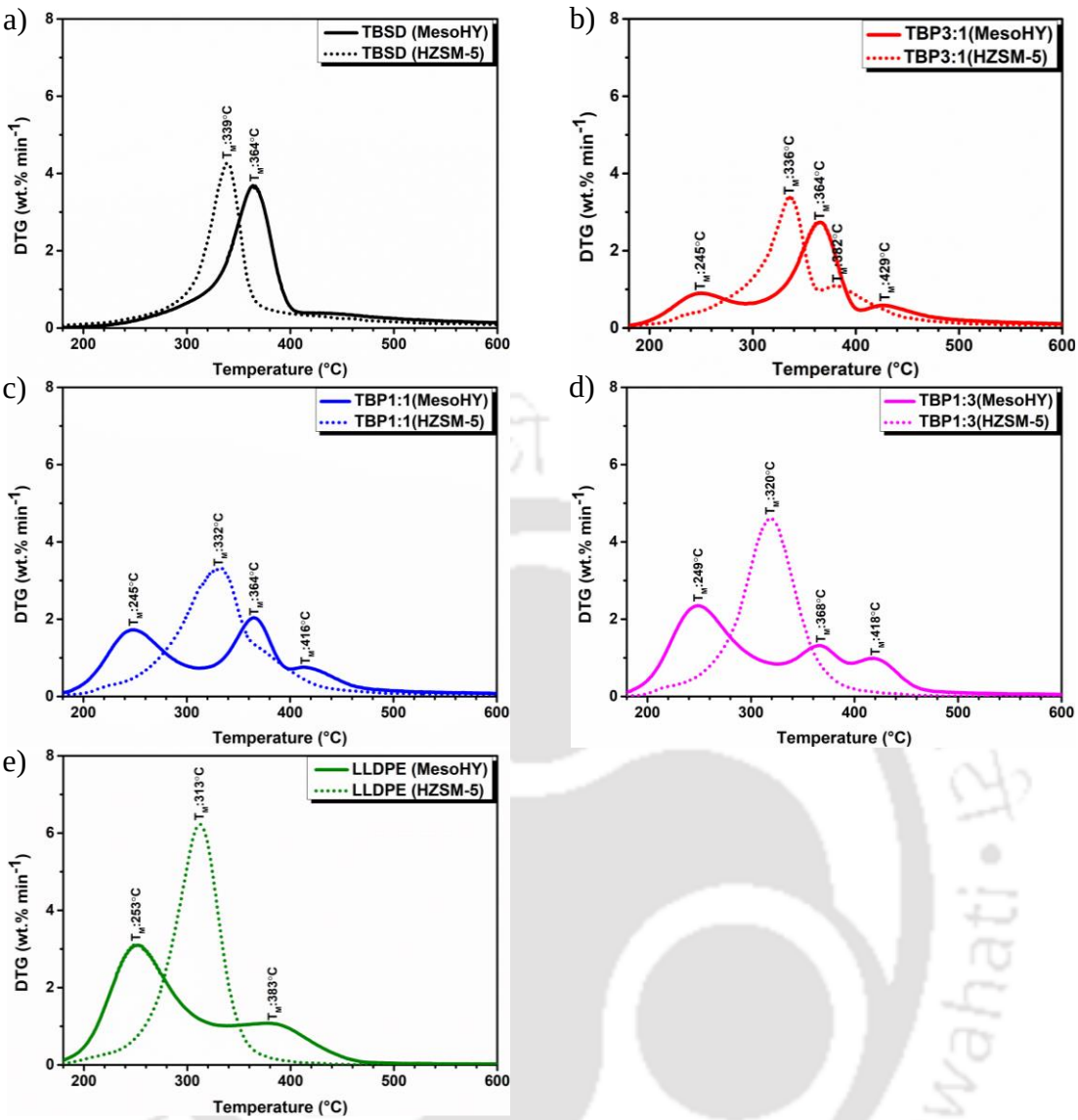

Figure 6.5. Comparison of the DTG profiles of catalytic pyrolysis of torrefied bamboo sawdust (TBSD) (a) and LLDPE (e) and catalytic co-pyrolysis of TBSD with LLDPE with various weight ratios of TB and LLDPE (TBP3:1 (b), TBP1:1 (c) and TBP1:3 (d)) over MesoHY and HZSM-5 catalysts, at a ramp rate of 10°C min^{-1}.

Table 6.1. The catalytic (co)pyrolysis reaction parameters of TBSD, LLDPE and their blends at 10°C min^{-1} ramp rate.

Stages	Parameters	TBSD	TBP3:1	TBP1:1	TBP1:3	LLDPE
Moisture removal Stage_1	T_{range} (°C)	30–140	30–140	30–140	30–150	40–120
	DR_{max} (wt% min^{-1})	*0.68*	*0.79*	*0.55*	*0.57*	*0.21*
	T_{max} (°C)	60	57	54	55	69
	W_{loss} (%)	3.02	4.28	2.40	2.75	0.87
Stage_2	T_{range} (°C)	180–405	160–290	160–310	160–325	150–335
	DR_{max} (wt% min^{-1})	*3.70*	*0.91*	*1.74*	*2.36*	*3.11*
	T_{max} (°C)	363	250	248	249	251
	W_{loss} (%)	21.72	6.45	12.83	18.88	25.32
Stage_3	T_{range} (°C)	410–670	295–405	310–400	325–395	330–470
	DR_{max} (wt% min^{-1})	*0.41*	*2.75*	*2.05*	1.33	*1.10*
	T_{max} (°C)	435	364	365	365	380
	W_{loss} (%)	5.52	15.62	11.38	7.49	9.76
Stage_4	T_{range} (°C)	–	405–640	400–570	400–510	–
	DR_{max} (wt% min^{-1})	–	0.60	*0.76*	*0.99*	–
	T_{max} (°C)	–	428	414	418	–
	W_{loss} (%)	–	5.75	5.17	5.11	–
Mean Reactivity x 10^2 (wt % min^{-1} $°C^{-1}$)		1.11	1.26	1.45	1.34	1.83
% Residual weight* at 790°C		68.12	67.25	66.55	64.05	63.18
Calculated residual weight[#]		8.12	6.89	5.65	4.42	3.18

6.2.3 Interaction between TBSD and LLDPE over MesoHY catalyst

The interaction between TBSD and LLDPE during CCP over MesoHY may lead to synergism. The understanding of synergism is useful to improve the quality and/or quantity of bio-oil produced during the catalytic co-pyrolysis.[16] The synergism relies on many factors such as composition and contact between volatiles, removal or equilibrium of volatiles generated from individual polymers in the blends, operating conditions (temperature, duration of co-pyrolysis, and heating rates), the addition of catalysts and hydrogen donors.[17] To evaluate the existence

of synergism between TBSD and LLDPE of the blends, the theoretical and experimental weight losses of blends during CCP over MesoHY were compared (Fig. 6.6).

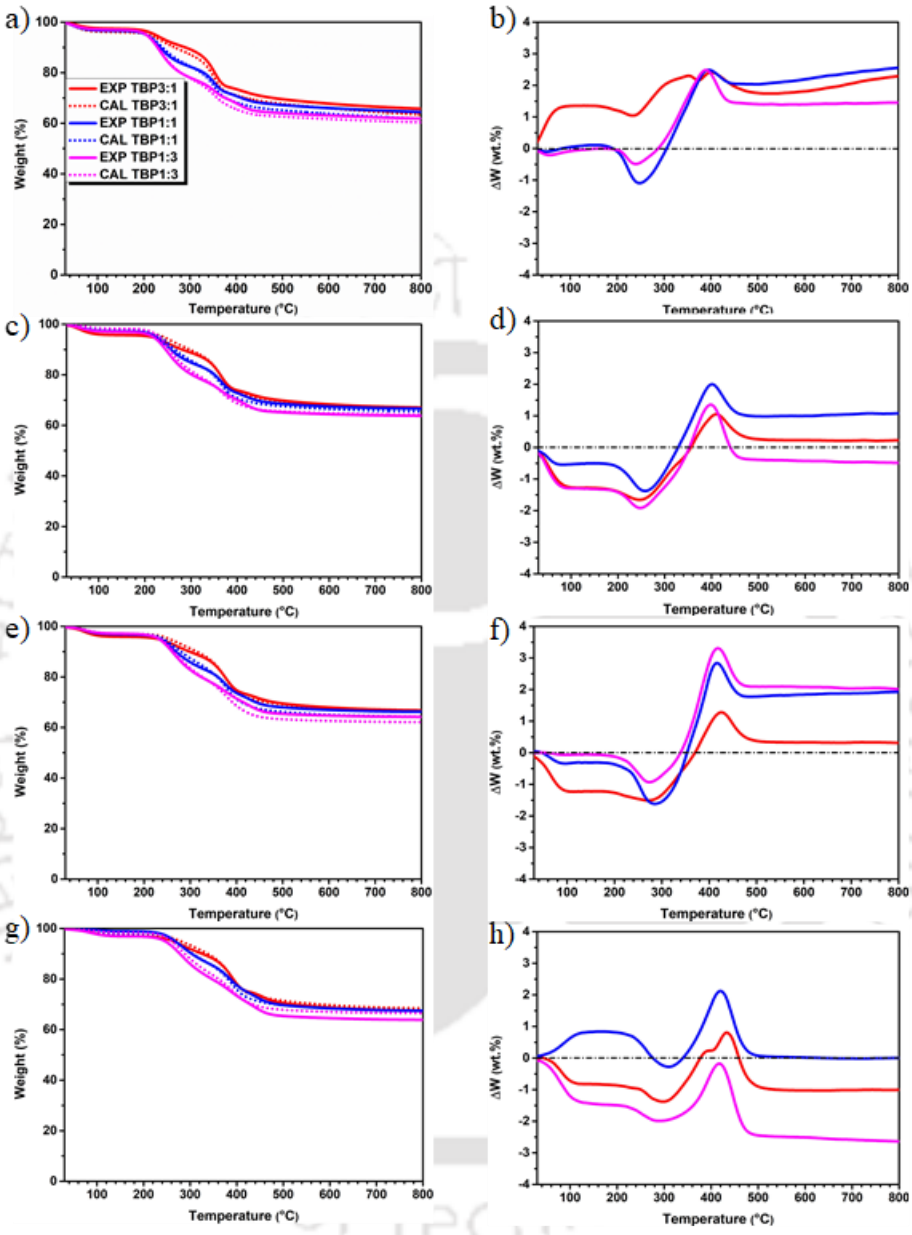

Figure 6.6. Experimental and calculated TG curves for three blends (TBP3:1, TBP1:1, and TBP1:3) at the ramp of (a) 5, (c) 10, (e) 20 and (g) 40°C·min^{-1}: Variation of weight loss as a function of temperature (a, c, e, and g) and ΔW (b, d, f, and h) in environment of MesoHY zeolite.

The majority of blends showed positive synergism (ΔW (equation 2.6) negative) in the temperature range 50−300°C at ramp rates 5, 10, 20 and 40°C min^{-1} (Fig. 6.6d and f). In this temperature range, the sidechain and backbone (to lesser extent) of LLDPE breaks down to form smaller fragments. These fragments help in decomposing the sidechain functional groups such as COOH and COOR from the torrefied biomass over MesoHY catalyst during CCP process. All blends in CCP over MesoHY showed a passive synergism in the temperature range of 350–500°C. The positive synergistic effect was increased with TBSD content in the blends in the lower temperature range 50−250°C at heating rate 20°C min^{-1} and followed the order of $\Delta W_{TBP3:1} > \Delta W_{TBP1:1} > \Delta W_{TBP1:3}$ (Table A4.4). While, the reverse trend was observed in the temperature range of 350−480°C and reflected the order as $\Delta W_{TBP3:1} < \Delta W_{TBP1:1} < \Delta W_{TBP1:3}$. The backbone of LLDPE further decomposes and forms volatile hydrocarbon radicals (ethyl, propyl, butyl, isobutyl, and neopentyl) at higher temperature. The catalytic copyrolysis induces the formation of secondary (2°) radicals. The secondary radicals initiate various reactions, such as depolymerization, inter and intramolecular hydrogen transfer, monomer formation, and isomerization via vinyl groups. These radicals selectively react with oxygen-containing species of TBSD instead of attacking the LLDPE chain, which retards the cracking reaction of LLDPE.[18] In addition, at above 300°C, the degradation of cellulose and lignin (linkage: α/β-O4, γ-ester) occurs to form various pyrolyzates (derivatives of furanic and phenolic compounds). The pyrolyzates react with hydrocarbon radicals over HY to form aromatic hydrocarbons (AHCs) by Diels-Alder reaction.[19–24] Therefore, the passive synergism at high temperatures can be attributed to the reaction of secondary radicals with oxygenated compounds, retarding the overall reaction. The devolatilization of all blends was nearly complete at 500°C (Fig. 6.6). However, a constant difference in experimental and calculated weights was observed above 500°C, which can be attributed to the difference in experimental and calculated residual weight. For example, the experimental residual weight (4%) of the

blend TBP1:3 after CCP at ramp rate 10°C min^{-1} was lower than that calculated, 4.4% (Table 1). In addition, all blends at heating rate of 40°C min^{-1} showed positive synergism at 780°C with ΔW -2.62, -1.01 and -0.02wt% for TBP1:3, TBP3:1 and TBP1:1, respectively. This indicates that the catalytic copyrolysis reduces the solid residue. Lower solid residues are favorable for the stable furnace operation. This is in good agreement with previous studies.[20,24–27]

6.2.4 Kinetic Analysis of Torrefied biomass, Plastic and mixed samples

The apparent activation energy values were calculated using iso-conversional models (equations 1.11, 1.12, and 1.13) in the conversion range of 0.1–0.8 over MesoHY catalyst (Fig. 6.7 and Tables A4.5–A4.9). A correlation coefficient of 0.99 in most cases indicates that the proposed models fit very well to the experimental data. The average apparent activation energy ($\bar{E}_\alpha$) of CCP of the blends TBP3:1, TBP1:1, and TBP1:3 over MesoHY zeolite was found to be 171, 128 and 117 kJ mol^{-1} from KAS; 172, 131 and 120 kJ mol^{-1} from OFW; and 184, 139 and 128 kJ mol^{-1} from FM model, respectively (Table 6.2). Similarly, the $\bar{E}_\alpha$ of CP of LLDPE were 107, 111, and 116 kJ mol^{-1} from KAS, OFW, and FM models, respectively, and those of TBSD were 216, 214, and 232 kJ mol^{-1}.

In CP of TBSD, the E_α was first increased (from 176 to 208 kJ mol^{-1}) in the conversion range of 0.1 to 0.2 and then nearly constant (208±4 kJ mol^{-1}) for the α range of 0.2 to 0.6. Thereafter, the E_α was decreased to 171 kJ mol^{-1} at α: 0.7 and increased significantly to 343 kJ mol^{-1} at high conversions (α: 0.8). At conversion 0.1, the E_α was lower because of the degradation of molecules having lower bond energy. The E_α increased with conversion due to degradation of glycosidic linkages (300–350°C) which connect glucose monomer in cellulose macromolecules. The fragmentation of lignin possesses higher E_α because of the complicated structure (linkages: α/β–O4; condensed (C–C) and coumarane). While side-chain degraded to

lower molecular components such as methanol and acetic acid at a lower temperature.[14,28] the CP of LLDPE, the E_α decreased from 98 to 90 kJ mol^{-1} in the first stage ($0.1 \leq \alpha \leq 0.5$), with a corresponding temperature of 230–290°C. In this temperature range, the backbone of LLDPE breaks down into smaller fragments over-acidic sites of MesoHY catalyst which further converted into free radicals as shown in Scheme A4.3. In the second stage ($0.5 \leq \alpha \leq 0.8$), the E_α increased from 90 to 161 kJ mol^{-1}.

The E_α of TBP3:1 increased from 105 to 193 kJ mol^{-1} (Fig. 6.7b) with the increase of conversion from 0.1 to 0.5, in the temperature range of 250–350°C (Fig. 6.7d). With further increase of conversion, the E_α decreased, reaching 183 kJ mol^{-1} at conversion 0.7 and temperature 390°C. Finally, the E_α was increased significantly at high conversion. For example, the E_α at 0.8 conversions (temperature 425°C) was 212 kJ mol^{-1}. The variation of E_α for CCP of both TBP1:1 and TBP3:1 followed a trend similar to that of LLDPE at lower conversions. For example, the E_α of TBP1:1 was decreased from 97 to 87 kJ mol^{-1} with the conversion from 0.1 to 0.3 and that of TBP1:3 was decreased from 99 to 87 kJ mol^{-1} with the conversion from 0.1 to 0.4. At higher conversions, the variation trend of E_α for CCP of TBP1:1 was similar to that of TBP3:1. The E_α of TBP1:3 was continuously increased with conversion at higher conversions. With both individual feedstock's (TBSD and LLDPE) and blends (TBP3:1, TBP1:1 and TBP1:3), an increase of E_α was observed towards higher conversions, which could be attributed to the formation of precursor molecules of coke.[29,30] In summary, the variation of the E_α of CCP of blends showed trends similar to those of TBSD at lower LLDPE concentration and those of LLDPE at higher LLDPE concentration. In addition, the variation of the E_α of the CCP of blends was similar to that of TBSD and LLDPE at higher and lower conversions, respectively.

As can be observed from Fig. 6.7d, the temperature required to reach a particular conversion in the blends was decreasing with the concentration of LLDPE in the blend. The decrease in temperature was significant at lower conversions. For example, upon addition of 50 wt.%

LLDPE to TB, the temperature was reduced from 355 to 275°C at 0.3 conversion level. The degradation temperature for LLDPE at the same conversion level was 260°C. This is a clear indication of synergy between the TBSD and LLDPE in the blend, at lower conversions. The trends of the variation of activation energy and temperature were in agreement with the synergism trend shown in Fig. 6.6.

The CP of individual samples and CCP of the blends over MesoHY follow a multistep reaction mechanism. as shown by the Arrhenius plot, obtained from isoconversional models (Fig. A4.2). The variation of activation energy with conversion (Fig. 6.7) indicates the multistep reaction mechanism. The only kinetic analysis is not sufficient to describe exact thermal decomposition behaviour because of the involvement of complex reactions. Therefore, Criado's master plot method was used to describe the reaction mechanism of CP of individual samples and CCP of the blends over MesoHY catalyst.

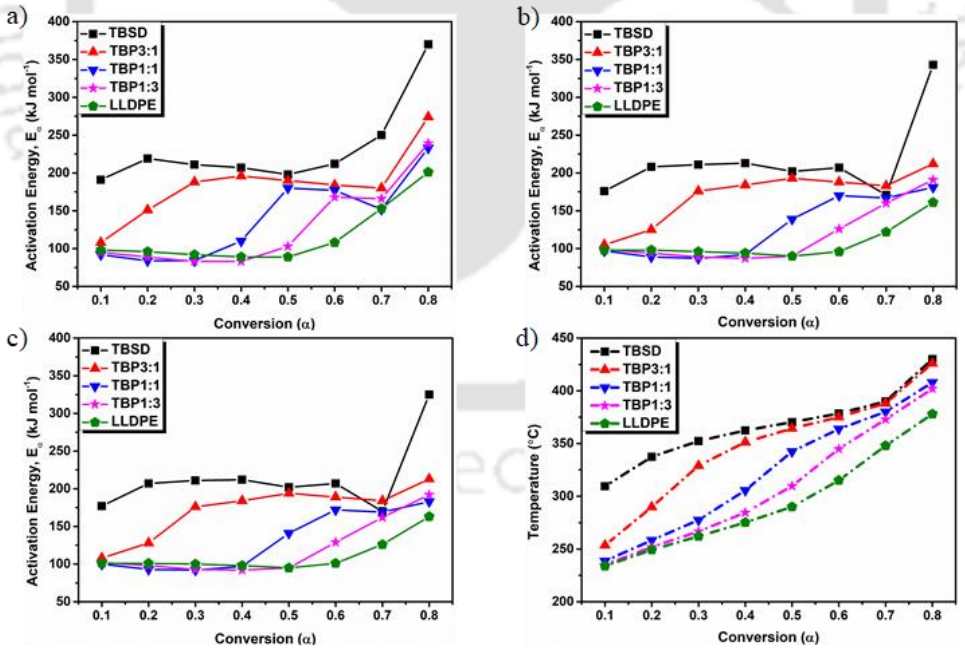

Figure 6.7. Variation of E_α and temperature with the conversion of TBSD+LLDPE blends: a) FM model, b) KAS, c) OFW model with mixed and individual sample d) Temperature profile of mixed samples in the presence of MesoHY zeolite.

Table 6.2. The average E_α from model-free methods of CP of TBSD, LLDPE, and CCP of blends (TBSD +LLDPE) over MesoHY zeolite

Code	KAS MODEL		OFW MODEL		FM MODEL	
	$\bar{E}_\alpha$, (kJ mol^{-1})	Avg. R^2	$\bar{E}_\alpha$, (kJ mol^{-1})	Avg. R^2	$\bar{E}_\alpha$, (kJ mol^{-1})	Avg. R^2
TBSD	216	0.9915	214	0.9915	232	0.9879
TBP3:1	171	0.9800	172	0.9820	184	0.9864
TBP1:1	128	0.9905	131	0.9918	139	0.9901
TBP1:3	117	0.9909	120	0.9923	128	0.9918
LLDPE	107	0.9667	111	0.9719	116	0.9610

6.2.5 Reaction Mechanism by Master plot method

The catalytic degradation of individual or blended samples is a process involving hundreds of complex reactions, making the prediction of its reaction mechanism difficult. However, mathematical models have been developed based on various approximations to predict the solid reaction mechanism (Table 1.1).[14,18,31] In the current study, the Z–Master plot (equation 1.23) was used to evaluate solid reaction mechanisms based on Criado's method. The E_α obtained from the FM model was used to construct the Z-Master plot [(Z(α)/Z (0.5)] at 10°C min^{-1} during pyrolysis/co-pyrolysis of individual/blended samples over MesoHY catalyst (Fig. 6.8). Based on the proximity, the theoretical curves obtained from equation (4) were compared with the experimental curves to obtain the reaction mechanism of the CP and CCP.[14]

For TBSD at α < 0.3, the experimental curve aligned with theoretical curve F0 (Table 1.1), demonstrating that the catalytic pyrolysis of TBSD followed the zero-order solid-state reaction (Fig. 6.8a). For α = 0.3–0.5, the experimental curve aligned with theoretical curves F1/F2, consistent with first (F1) and second (F2) order reaction models. The experimental curve of TBSD close to the theoretical curve F3 at α: 0.5–0.7, indicating that the CP of TBSD, in this conversion range, followed a third-order reaction (F3). Similarly, the TBSD also showed the

geometrical contraction (volume contraction) mechanism (R3) at α: 0.7–0.9. Overall, the CP of TBSD followed the reaction order models (zero, first, second, and third-order) and geometrical contraction model at different conversion ranges. This explains the reaction complexity of CP of TB, which in turn is due to the complex structure of the used wet-torrefied biomass. The pattern of experimental curves of LLDPE showed similar behavior with the theoretical curve of third-order reaction (F3) in the conversion range 0.10–0.45. Besides, in the conversion range 0.45–0.70, the experimental curve overlapped with the theoretical curve R3. These results indicate that the CP of LLDPE over MesoHY obeyed the third-order reaction and geometrical (volume) contraction mechanisms at low and high conversion ranges, respectively. By comparing the experimental curve with theoretical curves at α: 0.2–0.45, the CCP of TBP3:1 fluctuated between second-order Avrami–Erofeyev model (A2) and power law (P2/3) model. These models come under the category of nucleation mechanism (Table 1.1). At α: 0.45–0.55, the reaction mechanism shifted to first–order reaction model (F1). At lower ($\alpha < 0.2$) and higher conversions ($\alpha > 0.55$), the experimental curve crossed multiple curves of theoretical models indicating the poor fit.

The experimental curve for CCP of TBP1:1 closely overlapped with the theoretical curve (P4) at α: 0.45–0.60 indicating that the thermal degradation of TBP1:1 followed the power law (P4) model (under nucleation mechanism, Table 1.1). At lower conversions ($0.2 < \alpha < 0.45$), it followed the trend of geometric (volume) contraction (R3). At higher conversions (0.60–0.8), it crossed multiple theoretical curves, indicating a poor fit in this conversion range. At even higher conversions ($\alpha > 0.8$), it followed the trend of the first-order reaction (F1) model. The CCP of TBP1:3 followed approximately the geometrical (volume) contraction (R3) modal at α 0.2–0.6 and the first-order reaction (F1) model at α 0.6–0.9 (Table 6.3).

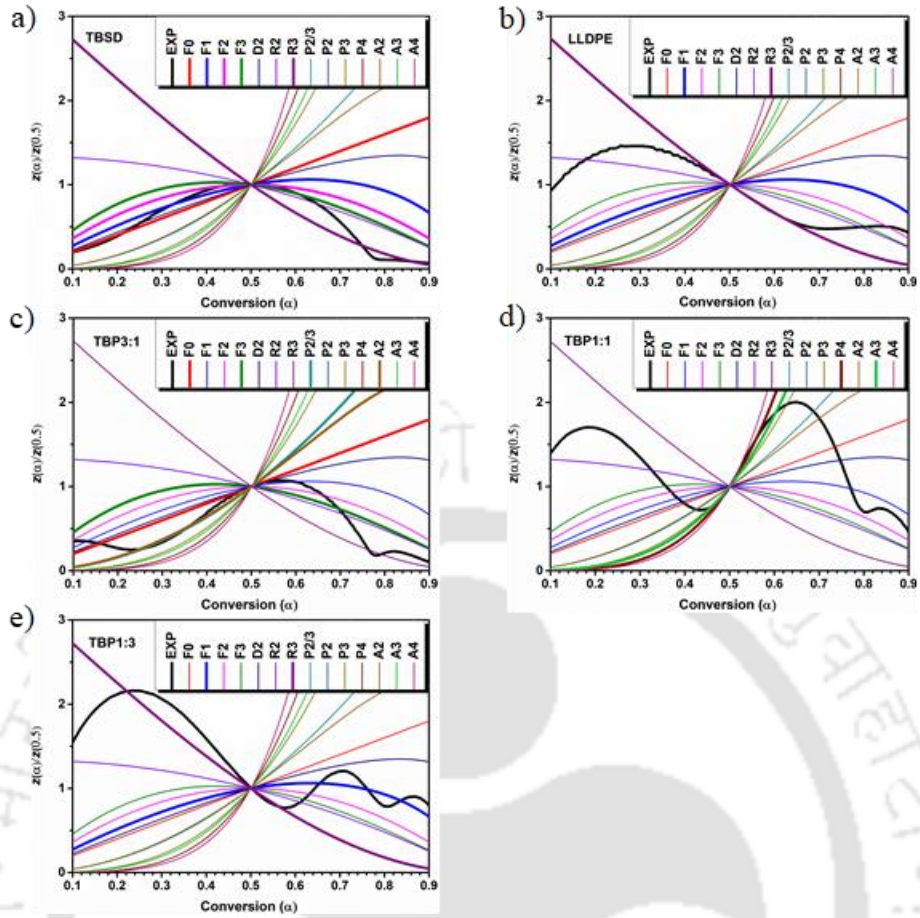

Figure 6.8. Master plot Z(α) of CP of a) TBSD and b) LLDPE and CCP of c) TBP3:1, d) TBP1:1 and e) TBP1:3 in presence of MesoHY, at ramp rate 10°C min^{-1}

Table 6.3. Determination of kinetic model by Criado's model- Master plot for TBSD, LLDPE, and mixed samples at 10°C. min^{-1} in presence of MesoHY zeolite

TBSD			**LLDPE**			**TBP3:1**			**TBP1:3**		
α	**M**	**M^n**	**α**	**M**	**M^n**	**α**	**M**	**M^n**	**α**	**M**	**M^n**
0.10–0.23	F0	RO	0.10–0.40	F3	RO	0.20–0.45	A2	NM	0.20–0.60	R3	GC
0.30–0.50	F1/F2	RO	0.40–0.70	R3	GC	0.20–0.45	P2/3	NM (C)	0.65–0.90	F1	RO (C)
0.50–0.70	F3	RO	–	–	–	0.50–0.65	F1	RO	–	–	–
0.70–0.90	R3	GC	–	–	–	–	–	–	–	–	–
Note: M: Model; M^n: Mechanism (RO: Reaction order, GC: Geometrical Contraction and NM: Nucleation model); α: Conversion; (C) indicates closer to curve but not exactly matching											

6.3 Conclusions

The catalytic (co)pyrolysis behavior and kinetics of TBSD, LLPDE, and their blends were studied in a thermogravimetric analyzer over MesoHY catalyst. The peak (maximum) decomposition temperature of LLDPE was lowered greatly over MesoHY as compared to that over HZSM-5, because of the larger pore size of the HY catalyst (7.4 Å). The bulky pyrolyzates derived from copyrolysis of TBSD and LLDPE easily diffuse into mesopores of MesoHY zeolite and convert into aromatic hydrocarbons by Diels-Alder reaction due to which coke or precursor of coke minimized in catalytic copyrolysis. While, the acidic sites present inside the microporous HZSM-5 are not accessible to the pyrolyzates. A clear synergism was observed in the catalytic co-pyrolysis of blends of TBSD and LLDPE over MesoHY zeolite, at low temperatures (<250°C). The blend TBP1:3 exhibited the lowest average apparent activation energy ($\bar{E}_\alpha$: 117 kJ mol^{-1}) from the KAS model. The mean activation energies ($\bar{E}_\alpha$) of the samples TBSD, LLDPE, TBP3:1, TBP1:1, and TBP1:3 were evaluated, using KAS model, to be 216, 107, 171, 128, and 117 kJ mol^{-1}, respectively. The order of the percentage of $\bar{E}_\alpha$ reduction of blends with respect to TBSD was as follows: TBP3:1 (20%) > TBP1:1 (40%) > TBP1:3 (45%). The multistep degradation mechanism was followed by both individual and blended samples, as identified by Criado's master plot. In CCP over MesoHY catalyst, the lowest average apparent activation energy, and highest synergism were observed with TBP1:3 among all the blends.

References

[1] D. Reinoso, M. Adrover, M. Pedernera, Green synthesis of nanocrystalline faujasite zeolite, Ultrason. Sonochem. 42 (2018) 303–309. https://doi.org/10.1016/j.ultsonch.2017.11.034.

[2] X. Lin, L. Kong, X. Ren, D. Zhang, H. Cai, H. Lei, Catalytic co-pyrolysis of torrefied

poplar wood and high-density polyethylene over hierarchical HZSM-5 for mono-aromatics production, Renew. Energy. 164 (2021) 87–95. https://doi.org/10.1016/j.renene.2020.09.071.

[3] P.S. Rezaei, D. Oh, Y. Hong, Y.M. Kim, J. Jae, S.C. Jung, J.K. Jeon, Y.K. Park, In-situ catalytic co-pyrolysis of yellow poplar and high-density polyethylene over mesoporous catalysts, Energy Convers. Manag. 151 (2017) 116–122. https://doi.org/10.1016/j.enconman.2017.08.073.

[4] Y.K. Park, J. Jung, S. Ryu, H.W. Lee, M.Z. Siddiqui, J. Jae, A. Watanabe, Y.M. Kim, Catalytic co-pyrolysis of yellow poplar wood and polyethylene terephthalate over two stage calcium oxide-ZSM-5, Appl. Energy. 250 (2019) 1706–1718. https://doi.org/10.1016/j.apenergy.2019.05.088.

[5] J. Jae, G.A. Tompsett, A.J. Foster, K.D. Hammond, S.M. Auerbach, R.F. Lobo, G.W. Huber, Investigation into the shape selectivity of zeolite catalysts for biomass conversion, J. Catal. 279 (2011) 257–268. https://doi.org/10.1016/j.jcat.2011.01.019.

[6] Y. Chi, J. Xue, J. Zhuo, D. Zhang, M. Liu, Q. Yao, Catalytic co-pyrolysis of cellulose and polypropylene over all-silica mesoporous catalyst MCM-41 and Al-MCM-41, Sci. Total Environ. 633 (2018) 1105–1113. https://doi.org/10.1016/j.scitotenv.2018.03.239.

[7] H. Shafaghat, H.W. Lee, L. Yang, D. Oh, S.C. Jung, G.H. Rhee, J. Jae, Y.K. Park, Catalytic co-conversion of Kraft lignin and linear low-density polyethylene over mesoZSM-5 and Al-SBA-15 catalysts, Catal. Today. (2019). https://doi.org/10.1016/j.cattod.2019.04.052.

[8] I. Muhammad, G. Manos, Intensification of co-pyrolysis of plastic with biomass via pretreatment, Process Saf. Environ. Prot. 146 (2021) 586–598. https://doi.org/10.1016/j.psep.2020.11.042.

[9] B.S. Kim, Y.M. Kim, H.W. Lee, J. Jae, D.H. Kim, S.C. Jung, C. Watanabe, Y.K. Park, Catalytic Copyrolysis of Cellulose and Thermoplastics over HZSM-5 and HY, ACS Sustain. Chem. Eng. 4 (2016) 1354–1363. https://doi.org/10.1021/acssuschemeng.5b01381.

[10] Y.M. Kim, J. Jae, B.S. Kim, Y. Hong, S.C. Jung, Y.K. Park, Catalytic co-pyrolysis of torrefied yellow poplar and high-density polyethylene using microporous HZSM-5 and mesoporous Al-MCM-41 catalysts, Energy Convers. Manag. 149 (2017) 966–973. https://doi.org/10.1016/j.enconman.2017.04.033.

[11] M. Gehre, Z. Guo, G. Rothenberg, S. Tanase, Sustainable Separations of C4-Hydrocarbons by Using Microporous Materials, ChemSusChem. 10 (2017) 3947–3963. https://doi.org/10.1002/cssc.201700657.

[12] Y.M. Kim, J. Jeong, S. Ryu, H.W. Lee, J.S. Jung, M.Z. Siddiqui, S.C. Jung, J.K. Jeon, J. Jae, Y.K. Park, Catalytic pyrolysis of wood polymer composites over hierarchical mesoporous zeolites, Energy Convers. Manag. 195 (2019) 727–737. https://doi.org/10.1016/j.enconman.2019.05.034.

[13] R. Cai, X. Pei, H. Pan, K. Wan, H. Chen, Z. Zhang, Y. Zhang, Biomass Catalytic Pyrolysis over Zeolite Catalysts with an Emphasis on Porosity and Acidity: A State-of-the-Art Review, Energy and Fuels. 34 (2020) 11771–11790. https://doi.org/10.1021/acs.energyfuels.0c02147.

[14] M. Alam, D. Rammohan, A. Bhavanam, N.R. Peela, Wet torrefaction of bamboo saw dust and its co-pyrolysis with plastic, Fuel. 285 (2021). https://doi.org/10.1016/j.fuel.2020.119188.

[15] H.W. Lee, Y.M. Kim, B. Lee, S. Kim, J. Jae, S.C. Jung, T.W. Kim, Y.K. Park, Catalytic copyrolysis of torrefied cork oak and high density polyethylene over a

mesoporous HY catalyst, Catal. Today. 307 (2018) 301–307. https://doi.org/10.1016/j.cattod.2017.01.036.

[16] X. Kai, T. Yang, S. Shen, R. Li, TG-FTIR-MS study of synergistic e ff ects during co-pyrolysis of corn stalk and high-density polyethylene (HDPE), Energy Convers. Manag. 181 (2019) 202–213. https://doi.org/10.1016/j.enconman.2018.11.065.

[17] Y.Y. Chong, S. Thangalazhy-gopakumar, S. Gan, H.K. Ng, L.Y. Lee, Kinetics and Mechanisms for Copyrolysis of Palm Empty Fruit Bunch Fiber (EFBF) with Palm Oil Mill E ffl uent (POME) Sludge, Energy & Fuels. 31 (2017) 8217–8227. https://doi.org/10.1021/acs.energyfuels.7b00877.

[18] M. Alam, A. Bhavanam, A. Jana, J. kumar S. Viroja, N.R. Peela, Co-pyrolysis of bamboo sawdust and plastic: Synergistic effects and kinetics, Renew. Energy. 149 (2020) 1133–1145. https://doi.org/10.1016/J.RENENE.2019.10.103.

[19] Z. Wu, S. Wang, J. Zhao, L. Chen, H. Meng, Synergistic effect on thermal behavior during co-pyrolysis of lignocellulosic biomass model components blend with bituminous coal, Bioresour. Technol. 169 (2014) 220–228. https://doi.org/10.1016/j.biortech.2014.06.105.

[20] X. Liu, K.R.G. Burra, Z. Wang, J. Li, D. Che, A.K. Gupta, Towards enhanced understanding of synergistic effects in co-pyrolysis of pinewood and polycarbonatee, Appl. Energy. 143 (2021) 116662. https://doi.org/10.1115/1.4049464.

[21] B. Han, Y. Chen, Y. Wu, D. Hua, Co-pyrolysis behaviors and kinetics of plastics – biomass blends through thermogravimetric analysis Co-pyrolysis behaviors and kinetics of plastics – biomass blends through thermogravimetric analysis, J Therm. Anal Calorim. 115 (2013) 227–235. https://doi.org/10.1007/s10973-013-3228-7.

[22] L. Zhou, Y. Wang, Q. Huang, J. Cai, Thermogravimetric characteristics and kinetic of plastic and biomass blends co-pyrolysis, Fuel Process. Technol. 87 (2006) 963–969. https://doi.org/10.1016/j.fuproc.2006.07.002.

[23] Z. Han, J. Li, T. Gu, B. Yan, G. Chen, The synergistic effects of polyvinyl chloride and biomass during combustible solid waste pyrolysis : Experimental investigation and modeling, Energy Convers. Manag. 222 (2020) 113237. https://doi.org/10.1016/j.enconman.2020.113237.

[24] J. Nikko, V. Salvilla, B. Ivan, G. Ofrasio, A.P. Rollon, F.G. Manegdeg, R. Ruffel, M. Abarca, M. Daniel, G. De Luna, Synergistic co-pyrolysıs of polyolefin plastics with wood and agricultural wastes for biofuel production ☆, Appl. Energy. 279 (2020) 115668. https://doi.org/10.1016/j.apenergy.2020.115668.

[25] Z. Wang, G. Liu, D. Shen, C. Wu, S. Gu, Co-pyrolysis of lignin and polyethylene with the addition of transition metals - Part I: Thermal behavior and kinetics analysis, J. Energy Inst. 93 (2020) 281–291. https://doi.org/10.1016/j.joei.2019.03.003.

[26] R. Chen, S. Zhang, X. Yang, G. Li, H. Zhou, Q. Li, Y. Zhang, Thermal behaviour and kinetic study of co-pyrolysis of microalgae with different plastics, Waste Manag. 126 (2021) 331–339. https://doi.org/10.1016/j.wasman.2021.03.001.

[27] S. Zhong, B. Zhang, C. Liu, A. Shujaa aldeen, Mechanism of synergistic effects and kinetics analysis in catalytic co-pyrolysis of water hyacinth and HDPE, Energy Convers. Manag. 228 (2021) 113717. https://doi.org/10.1016/j.enconman.2020.113717.

[28] H. Kawamoto, Lignin pyrolysis reactions, J. Wood Sci. 63 (2017) 117–132. https://doi.org/10.1007/s10086-016-1606-z.

[29] J.S. Arora, J.W. Chew, S.H. Mushrif, Influence of Alkali and Alkaline-Earth Metals on the Cleavage of Glycosidic Bond in Biomass Pyrolysis: A DFT Study Using Cellobiose as a Model Compound, J. Phys. Chem. A. 122 (2018) 7646–7658. https://doi.org/10.1021/acs.jpca.8b06083.

[30] K.B. Ansari, J.S. Arora, J.W. Chew, P.J. Dauenhauer, S.H. Mushrif, Fast Pyrolysis of Cellulose, Hemicellulose, and Lignin: Effect of Operating Temperature on Bio-oil Yield and Composition and Insights into the Intrinsic Pyrolysis Chemistry, Ind. Eng. Chem. Res. 58 (2019) 15838–15852. https://doi.org/10.1021/acs.iecr.9b00920.

[31] Poletto, J.A. Zattera, M.C.R. Santana, Thermal decomposition of wood: Kinetics and degradation mechanisms, Bioresour. Technol. 126 (2012) 7–12. https://doi.org/10.1016/j.biortech.2012.08.133.

Chapter 7

Major Findings and Future Directions

7.1 Major findings

Based on the investigations reported in Chapters 3, 4, 5, and 6, the following conclusions can be drawn:

Co-pyrolysis of BSD and LLDPE:

- The highest synergistic interaction between BSD and LLDPE was occurred and an activation energy drop of 36% (with respect to biomass) was observed with the blend BP1:3 (25 wt.% BSD and 75 wt.% LLDPE).
- The average apparent activation energy ($\bar{E}_\alpha$) of pure BSD, LLDPE and the blends BP3:1, BP1:1 and BP1:3 as obtained from isoconversional method are 294, 204, 397, 376, and 188 $kJ \cdot mol^{-1}$, respectively.
- The order of mean reactivity of blends was found to be BP1:3 > BP1:1 > BP3:1 at all the heating rates (5, 10, 20°C min^{-1}) studied.
- Multistep reactions are found to be responsible for a large variation of apparent activation energy of co-pyrolysis, as depicted by the master plot.
- The decomposition of the blend BP1:3 follows a nucleation growth (A2) model in the lower conversion range and diffusion (D2) model in the higher conversion range.

Wet-torrefaction of BSD and co-pyrolysis of torrefied BSD (TBSD) and LLDPE:

- The hemicellulose was selectively removed in the form of pentoses (xylose + arabinose) with 85% yield, during the wet torrefaction. The produced hydrochar (TBSD) was

hydrophobic in nature, having high heating value (HHV) of 24.02 MJ kg^{-1} which is comparable to that of low-rank coal, lignite (25.10 MJ kg^{-1}).

- The best torrefaction activity, with pentose sugar yields of 85% and complete removal of hemicellulose (> 95%), was obtained with formic acid:BSD ratio of 1:1 w/w and NaCl:BSD ratio of 3:1 w/w at 140°C for 30 min.
- The activation energy of TBSD was lower by 20% as compared to that of BSD.
- The average apparent activation energies of samples TBSD, TBP3:1, TBP1:1 TBP1:3, and LLDPE were 155, 207, 264, 245, and 258 kJ mol^{-1}, respectively.
- The decomposition of the blend TBP1:3 followed a nucleation growth (A2) model in the conversion range of 0.1 to 0.5 and diffusion-reaction (D2) model in the higher conversion range (0.5 to 0.8).

Catalytic co-pyrolysis of torrefied BSD and LLDPE over HZSM-5:

- The average apparent activation energies ($\bar{E}_\alpha$) of samples TBSD, TBP3:1, TBP1:1 TBP1:3, and LLDPE for KAS model were found to be 187, 163, 135, 133, and 147 kJ mol^{-1}, respectively.
- The CCP of blends TBP1:3 and TBP1:1 showed synergism in terms of apparent activation energy. The blend TBP1:3 showed the best CCP characteristics with the least $\bar{E}_\alpha$. The temperature difference to reach conversion from 0.1 to 0.8 was the lowest with TBP1:3 (76°C) and was the highest with TBP3:1 (122°C).
- The reaction mechanism from the master plot correlates well with the kinetics, i.e., the mechanism is more complex (containing more steps) in the case of CCP of samples with a higher fraction of TBSD as compared to those with a lower fraction of TBSD.

Catalytic co-pyrolysis of torrefied BSD and LLDPE over MesoHY:

- The peak (maximum) decomposition temperature of LLDPE was lowered greatly over MesoHY as compared to that over HZSM-5, due to larger pore size of the HY zeolite (7.4 Å).
- A clear synergism was observed in the catalytic co-pyrolysis of blends of TBSD and LLDPE over MesoHY zeolite, at low temperatures (<250°C).
- The blend TBP1:3 exhibited the lowest average apparent activation energy ($\bar{E}_\alpha$: 117 kJ mol^{-1}) from the KAS model.
- The mean activation energies ($\bar{E}_\alpha$) of the samples TBSD, LLDPE, TBP3:1, TBP1:1, and TBP1:3 were evaluated, using KAS model, to be 216, 107, 171, 128, and 117 kJ mol^{-1}, respectively.
- The order of the percentage of $\bar{E}_\alpha$ reduction of blends with respect to TBSD was as follows: TBP3:1 (20%) > TBP1:1 (40%) > TBP1:3 (45%).
- In CCP over MesoHY catalyst, the lowest average apparent activation energy, and highest synergism were observed with TBP1:3 among all the blends.

Overall summary:

- The catalytic co-pyrolysis of wet-torrefied bamboo biomass with LLDPE over MesoHY zeolite is the best process among all the processes studied in this thesis, due to higher synergism and lower activation energy.
- All the reactions (catalytic and non-catalytic pyrolysis of individual samples and catalytic and non-catalytic co-pyrolysis of blends) studied in this thesis followed the multistep degradation mechanism, as identified by Criado's master plot.
- The wet torrefaction process developed in this study improves the overall economics of the process due to the selective production of the additional valuable products (xylose).

- The improved CCP characteristics, in terms of both kinetics and synergism, of torrefied biomass and LLDPE leads to the generation of high-quality biofuels in a single step.
- This study is the path forward for better economics and better-quality biofuels.

7.2 Limitations of the thesis

- The lower concentration of reactant (10 wt.%) in wet-torrefaction process may result in high energy demand and hamper the economic feasibility.
- The product distribution from the catalytic and non-catalytic pyrolysis and co-pyrolysis processes was not determined.
- Advanced catalysts with precise pore structure were not studied.
- Only one biomass (bamboo sawdust) was tested in this study.

7.3 Future work directions

- The product distribution from the catalytic and non-catalytic pyrolysis and co-pyrolysis processes helps in designing better catalysts.
- Torrefaction study: The reactant concentration may be increased to improve the economics. Other organic acids, such as oxalic acid, as they provide more H^+ ions per mol and other alkali and alkaline-earth metals, such as Ca, Mg, and K, may be tested.
- Synthesis of hierarchical zeolites following advanced methods may help in controlling the pore size precisely, which in turn help in enhancing the catalytic (co-)pyrolysis process. Transition metal (3d and 4f elements) encapsulated zeolites may also be tested for the catalytic (co-)pyrolysis to produce benzene, toluene, ethyl benzene and p-xylene (BTEX) selectively.
- Use of operando methods to deduce the reaction mechanism would be highly helpful in designing the better catalysts for the process.

- Due to heterogenous nature of the lignocellulosic biomass, more biomass sources may be tested to understand the differences in their reactivity and robustness of the process.
- The hydrochar produced from wet-torrefaction can be tested for other applications such as adsorption, soil fertility, in battery electrodes.

Annexure A1

Table A1.1: Degradation parameters at different stages of degradation of pure BSD, LLDPE and their blends at a heating rate of 5°C.min^{-1}

Stages	Parameters	BSD	BP3:1	BP1:1	BP1:3	LLDPE
First stage	T_{Range} (°C)	25–150	25–150	25–150	25–150	25–150
	W_{Loss} (%)	7.770	6.447	3.606	2.895	1.042
	DR_{max} (mg·min^{-1})	*0.067*	*0.096*	*0.044*	*0.034*	–
	T_{max} (°C)	53	52	49	49	–
Second stage	T_{Range} (°C)	180–365	180–360	180–350	180–355	280–510
	W_{Loss} (%)	58.461	40.453	24.502	17.564	84.890
	DR_{max} (mg·min^{-1})	*0.292*	*0.168*	*0.118*	*0.114*	*1.144*
	T_{max} (°C)	306	309	383	306	467
Third stage	T_{Range} (°C)	375–800	360–485	355–495	360–510	520–800
	W_{Loss} (%)	30.486	32.714	59.547	67.578	0.580
	DR_{max} (mg·min^{-1})	–	*0.312*	*0.618*	*0.941*	–
	T_{max} (°C)	–	449	459	464	–
Fourth stage	T_{Range} (°C)	–	500–800	520–800	520–800	–
	W_{Loss} (%)	–	10.953	7.424	4.726	–
Reactivity (mg min^{-1} °C^{-1}) X 10^3		1.11	1.030	0.851	1.032	2.45
% Residual weight at 800°C		1.44	7.550	0.853	7.470	13.49

Table A1.2: Degradation parameters at different stages of degradation of pure BSD, LLDPE and their blends at a heating rate of 10°C.min^{-1}

Stages	Parameters	BSD	BP3:1	BP1:1	BP1:3	LLDPE
First stage	T_{range} (°C)	25–150	25–150	25–150	25–150	25–150
	W_{loss} (%)	7.194	5.163	3.103	1.042	0.463
	DR_{max} (mg·min^{-1})	*0.140*	*0.1404*	*0.0816*	*0.0333*	*0.0136*
	T_{max} (°C)	57	57	56	59	65
Second stage	T_{range} (°C)	180–400	180–365	180–360	180–365	280–520
	W_{loss} (%)	61.538	38.179	27.943	14.811	88.592
	DR_{max} (mg·min^{-1})	*0.7272*	*0.591*	*0.373*	*0.231*	*2.1244*
	T_{max} (°C)	316	314	315	325	474
Third stage	T_{range} (°C)	405–800	380–520	380–510	380–520	–

	W_{loss} (%)	29.037	35.636	54.825	76.359	–
	DR_{max} (mg·min^{-1})	*0.109*	*0.642*	*1.062*	*2.143*	–
	T_{max} (^{o}C),	509	458	465	476	–
Fourth stage	T_{range} (°C)	–	500–800	520–800	520–800	–
	W_{loss} (%)	–	13.750	8.410	2.929	–
Mean Reactivity (M_R) x 10^3 (mg·min^{-1}.^{o}C^{-1})		2.28	3.27	3.45	5.20	4.40
% Residual weight at 800°C		1.23	6.32	2.667	4.32	9.03

Table A1.3: Kinetic parameters (E_α and A) from model free methods (KAS, OFW and FM) for BSD and corresponding R^2 value.

α	KAS MODEL			OFW MODEL			FRIEDMAN MODEL		
	E_α (kJ.mol^{-1})	**A (min^{-1})**	**R^2**	**E_α (kJ.mol^{-1})**	**A (min^{-1})**	**R^2**	**E_α (kJ.mol^{-1})**	**A (min^{-1})**	**R^2**
0.1	234	3.881 E+18	0.9946	255	1.998 E+24	0.9449	294	9.160 E+27	0.9803
0.2	257	1.916 E+20	0.9996	280	8.799 E+25	0.9999	341	1.335 E+31	0.9952
0.3	270	9.911 E+20	0.9999	294	4.329 E+26	0.9999	345	5.844 E+30	0.968
0.4	265	1.227 E+20	0.9999	289	5.859 E+25	0.9999	364	3.804 E+31	0.9879
0.5	326	1.289 E+25	0.9709	353	4.223 E+30	0.9726	389	1.410 E+33	0.9943
0.6	390	1.277 E+30	0.9996	301	9.541 E+25	0.9772	448	2.237 E+37	0.9563
0.7	209	7.554 E+12	0.9554	196	1.882 E+16	0.9282	507	3.599 E+41	0.9304
0.8	171	2.342 E+9	0.9353	148	3.360 E+12	0.9813	141	5.204 E+8	0.9448
Avg.	**265**	**1.596 E+29**	**0.9819**	**265**	**5.280 E+29**	**0.975487**	**353**	**4.499 E+40**	**0.96965**

Table A1.4: Kinetic parameters (E_α and A) from model free methods (KAS, OFW and FM) for BP3:1 and corresponding R^2 value.

α	KAS MODEL			OFW MODEL			FRIEDMAN MODEL		
	E_α (kJ.mol^{-1})	**A (min^{-1})**	**R^2**	**E_α (kJ.mol^{-1})**	**A (min^{-1})**	**R^2**	**E_α (kJ.mol^{-1})**	**A (min^{-1})**	**R^2**
0.1	217	4.468 E+16	0.9624	238	2.727 E+22	0.9652	311	1.329 E+29	0.987
0.2	228	1.244 E+17	0.9497	250	7.518 E+22	0.9534	365	1.145 E+19	0.9422
0.3	266	1.175 E+20	0.9948	291	5.758 E+25	0.9964	382	1.232 E+33	0.9999
0.4	393	4.209 E+30	0.9798	417	2.921 E+35	0.9717	664	2.439 E+56	0.9958
0.5	347	2.603 E+24	0.9837	346	4.524 E+27	0.9969	539	4.36 E+41	0.977

0.6	476	1.902 E+32	0.9973	434	1.257 E+37	0.9995	346	1.874 E+4	0.8333
0.7	527	1.211 E+35	0.9712	541	1.228 E+44	0.9732	585	4.201 E+40	0.9885
0.8	399	3.768 E+25	0.9946	420	3.316 E+34	0.9949	553	6.156 E+37	0.926
Avg.	**357**	**1.516 E+34**	**0.9792**	**367**	**1.535 E+43**	**0.9814**	**468**	**3.049 E+55**	**0.9562**

Table A1.5: Kinetic parameters (E_α and A) from model free methods (KAS, OFW and FM) for BP1:1 and corresponding R^2 value

α	KAS MODEL			OFW MODEL			FRIEDMAN MODEL		
	E_α (kJ.mol^{-1})	A (min^{-1})	R^2	E_α (kJ.mol^{-1})	A (min^{-1})	R^2	E_α (kJ.mol^{-1})	A (min^{-1})	R^2
0.1	315	1.656 E+28	0.9617	344	1.004 E+28	0.9664	268	5.469 E+26	0.998
0.2	432	3.793 E+37	0.9758	381	2.084 E+27	0.9843	270	3.389 E+24	0.9999
0.3	381	1.078 E+31	0.9771	388	5.007 E+28	0.9828	292	5.158 E+26	0.9929
0.4	402	6.866 E+29	0.9975	449	1.943 E+30	0.9897	325	1.736 E+27	0.9676
0.5	328	4.893 E+23	0.9811	403	2.542 E+26	0.9698	354	1.323 E+29	0.9965
0.6	445	5.899 E+31	0.9638	498	2.384 E+32	0.9722	550	1.636 E+43	0.9992
0.7	361	2.122 E+25	0.9745	402	3.668 E+25	0.9799	450	3.885 E+35	0.9996
0.8	306	1.473 E+21	0.9727	339	1.565 E+21	0.9768	336	1.283 E+27	0.9945
Avg.	**371**	**4.741 E+36**	**0.9756**	**400**	**3.005 E+31**	**0.9777**	**356**	**2.046 E+42**	**0.9934**

Table A1.6: Kinetic parameters (E_α, and A) from model-free methods (KAS, OFW, and FM) for BP1:3 and corresponding R^2 value

α	KAS MODEL			OFW MODEL			FRIEDMAN MODEL		
	E_α (kJ.mol^{-1})	A (min^{-1})	R^2	E_α (kJ.mol^{-1})	A (min^{-1})	R^2	E_α (kJ.mol^{-1})	A (min^{-1})	R^2
0.1	92	4.025 E+6	0.9869	107	1.510 E+7	0.9891	92	4.025 E+5	0.9644
0.2	91	3.622 E+5	0.9919	117	8.131 E+6	0.9699	133	9.674 E+11	0.9799
0.3	102	3.231 E+6	0.9974	126	2.452 E+7	0.9993	240	1.426 E+20	0.9968
0.4	119	4.581 E+7	0.9998	136	1.0183 E+8	0.9825	313	4.510 E+25	0.997
0.5	150	7.294 E+9	0.9812	201	1.588 E+12	0.9971	312	3.401 E+25	0.9959
0.6	176	5.636 E+11	0.9826	238	4.452 E+14	0.9996	328	4.306 E+26	0.9669
0.7	198	2.313 E+13	0.9828	222	3.083 E+13	0.9847	324	2.871 E+26	0.9605
0.8	218	5.451 E+14	0.983	175	3.645 E+10	0.9992	299	4.098 E+24	0.9914
Avg.	**143**	**7.110 E+13**	**0.9882**	**165**	**5.970 E+13**	**0.9902**	**255**	**1.001 E+26**	**0.9816**

Table A1.7: Kinetic parameters (E_α and A) from model free methods (KAS, OFW and FM) for LLDPE and corresponding R^2 value.

α	KAS MODEL			OFW MODEL			FRIEDMAN MODEL		
	E_α (kJ.mol^{-1})	A (min^{-1})	R^2	E_α (kJ.mol^{-1})	A (min^{-1})	R^2	E_α (kJ.mol^{-1})	A (min^{-1})	R^2
0.1	99	6.328 E+5	0.9560	112	1.562 E+5	0.9724	168	1.183 E+12	0.9920
0.2	142	1.488 E+9	0.9664	159	2.237 E+9	0.9754	175	2.324 E+12	0.9640
0.3	211	1.725 E+14	0.9625	235	2.077 E+14	0.9694	256	8.4656 E+17	0.9993
0.4	216	3.913 E+14	0.9686	240	4.176 E+14	0.9738	260	1.181 E+18	0.9998
0.5	236	9.890 E+15	0.9862	261	9.404 E+15	0.989	255	6.112 E+17	0.9742
0.6	241	2.230 E+16	0.9605	266	2.055 E+16	0.9642	280	1.755 E+19	0.9996
0.7	252	1.291 E+17	0.9718	278	1.099 E+17	0.9744	247	5.010 E+16	0.9907
0.8	263	7.857 E+17	0.9834	290	6.187 E+17	0.9849	248	4.327 E+16	0.9999
Avg.	**207**	**1.185 E+17**	**0.9694**	**230**	**9.490 E+16**	**0.9754**	**175**	**2.536 E+18**	**0.9899**

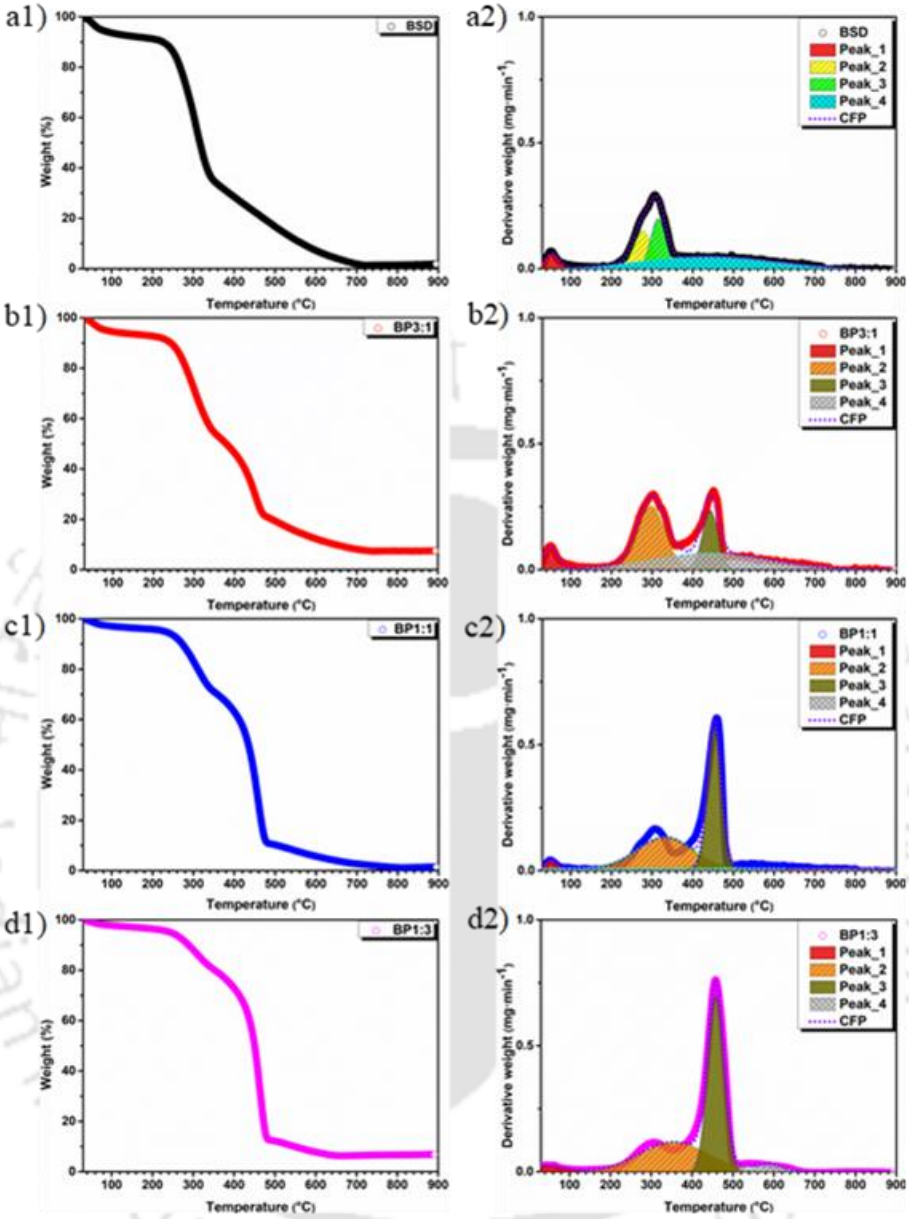

Figure A1.1. The deconvolution of DTG graph along with CFP, plots of BSD (a), BP3:1 (b), BP1:1 (c) and BP1:3 (d) at 5°C min-1 (CFP: Cumulative fit peak with Gaussian function for peak deconvolution: Origin pro 9.0).

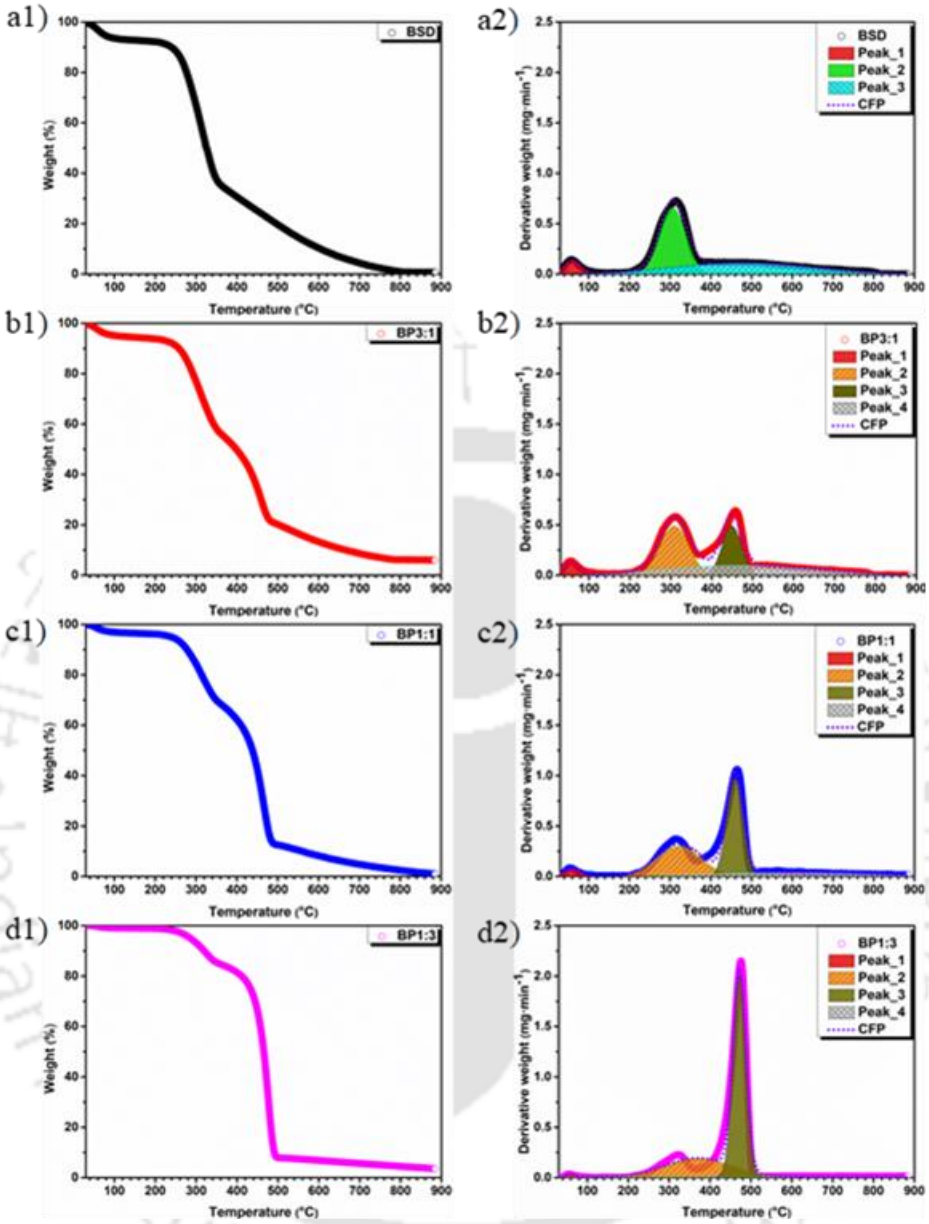

Figure A1.2. The deconvolution of DTG graph along with CFP, plots of BSD (a), BP3:1 (b), BP1:1 (c) and BP1:3 (d) at 10°C min-1 (CFP: Cumulative fit peak with Gaussian function for peak deconvolution: Origin pro 9.0).

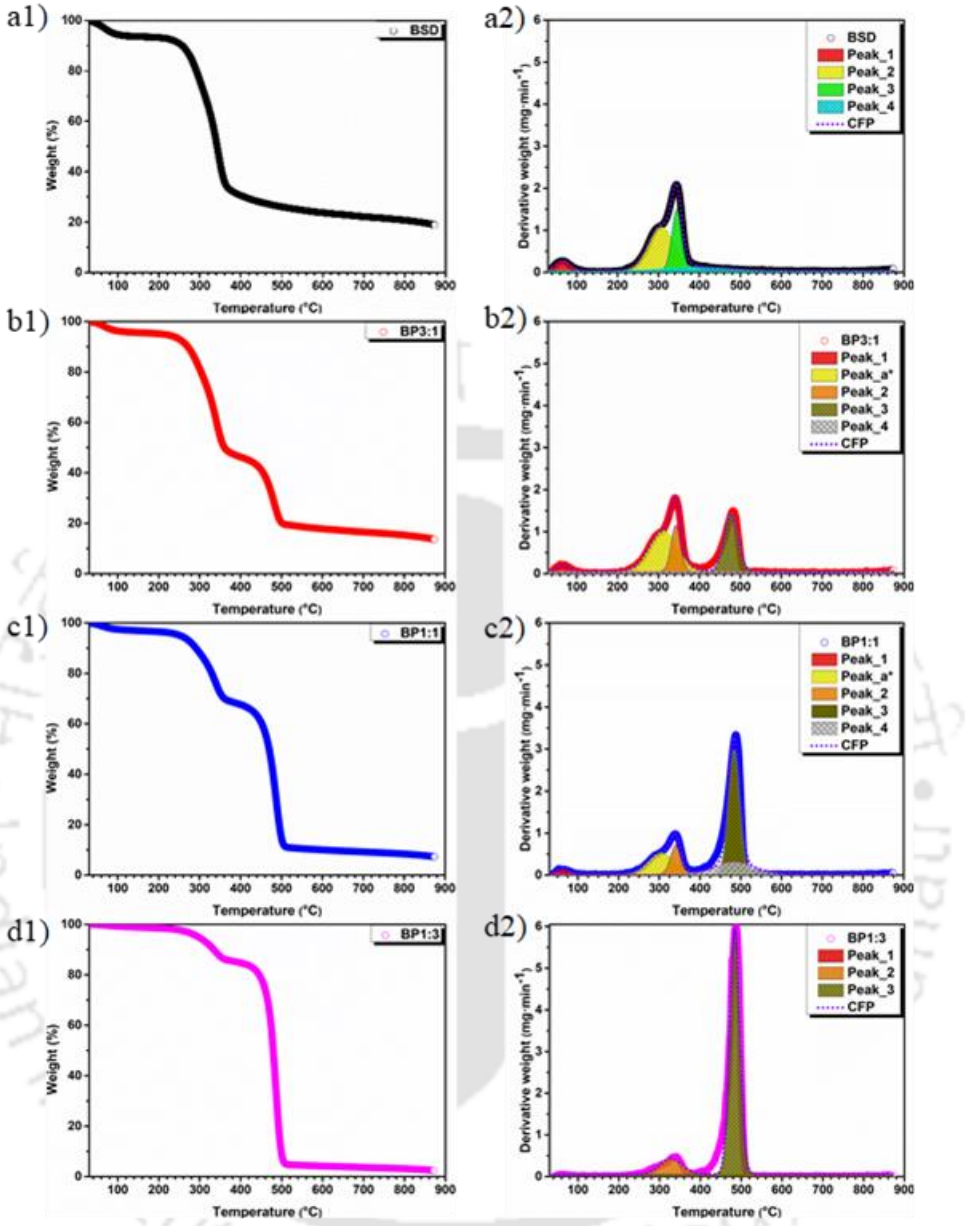

Figure A1.3. The deconvolution of DTG graph along with CFP, plots of BSD (a), BP3:1 (b), BP1:1 (c) and BP1:3 (d) at 20°C min-1 (CFP: Cumulative fit peak with Gaussian function for peak deconvolution: Origin pro 9.0).

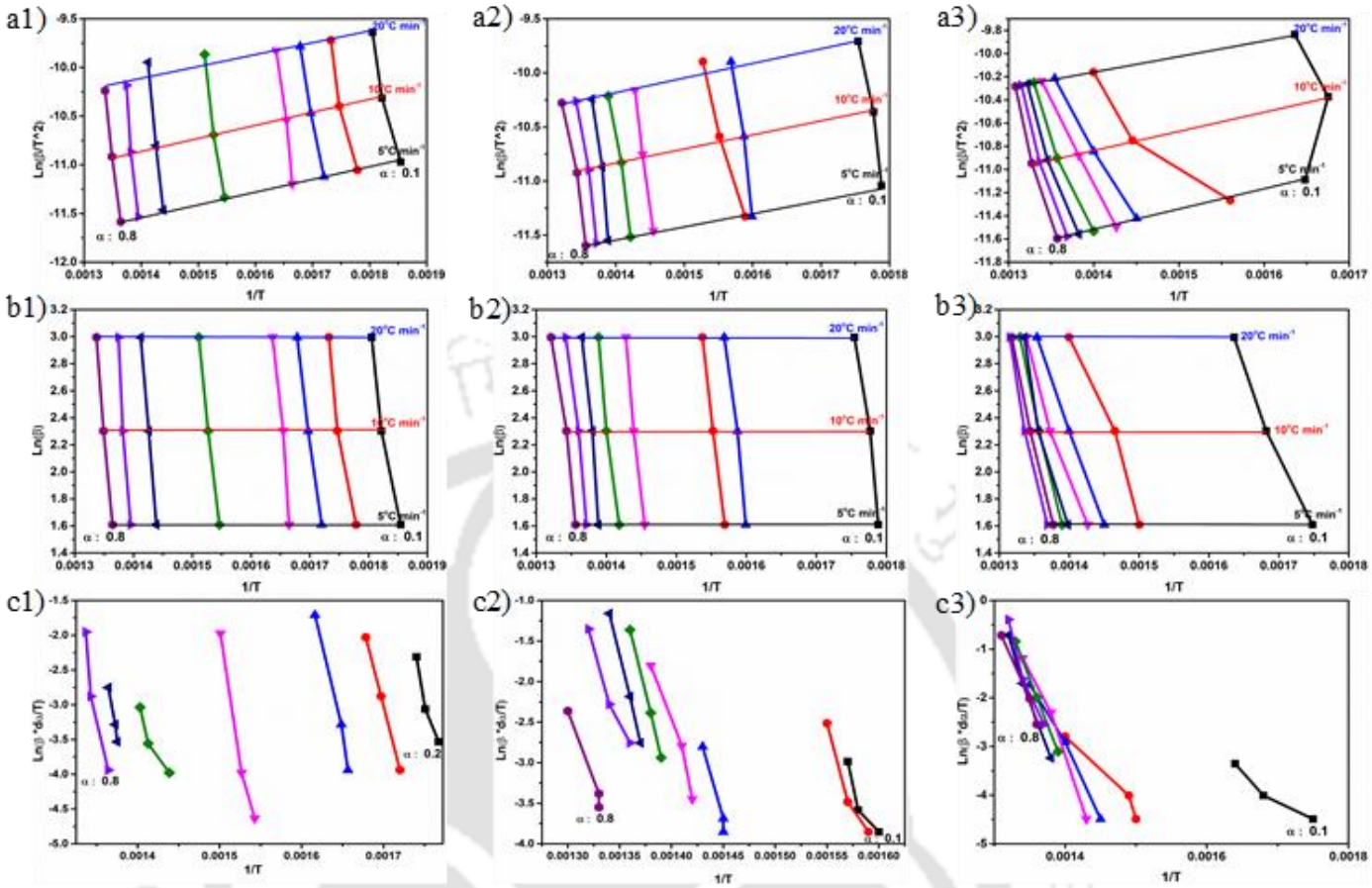

Figure A1.4. Determination of Activation energy using three different isoconversional models: KAS (a), OFW (b) and FM (c) of various BSD + LLDPE blends (BP3:1: a1 to c1; BP1:1: a2 to c2; and BP1:3: a3 to c3).

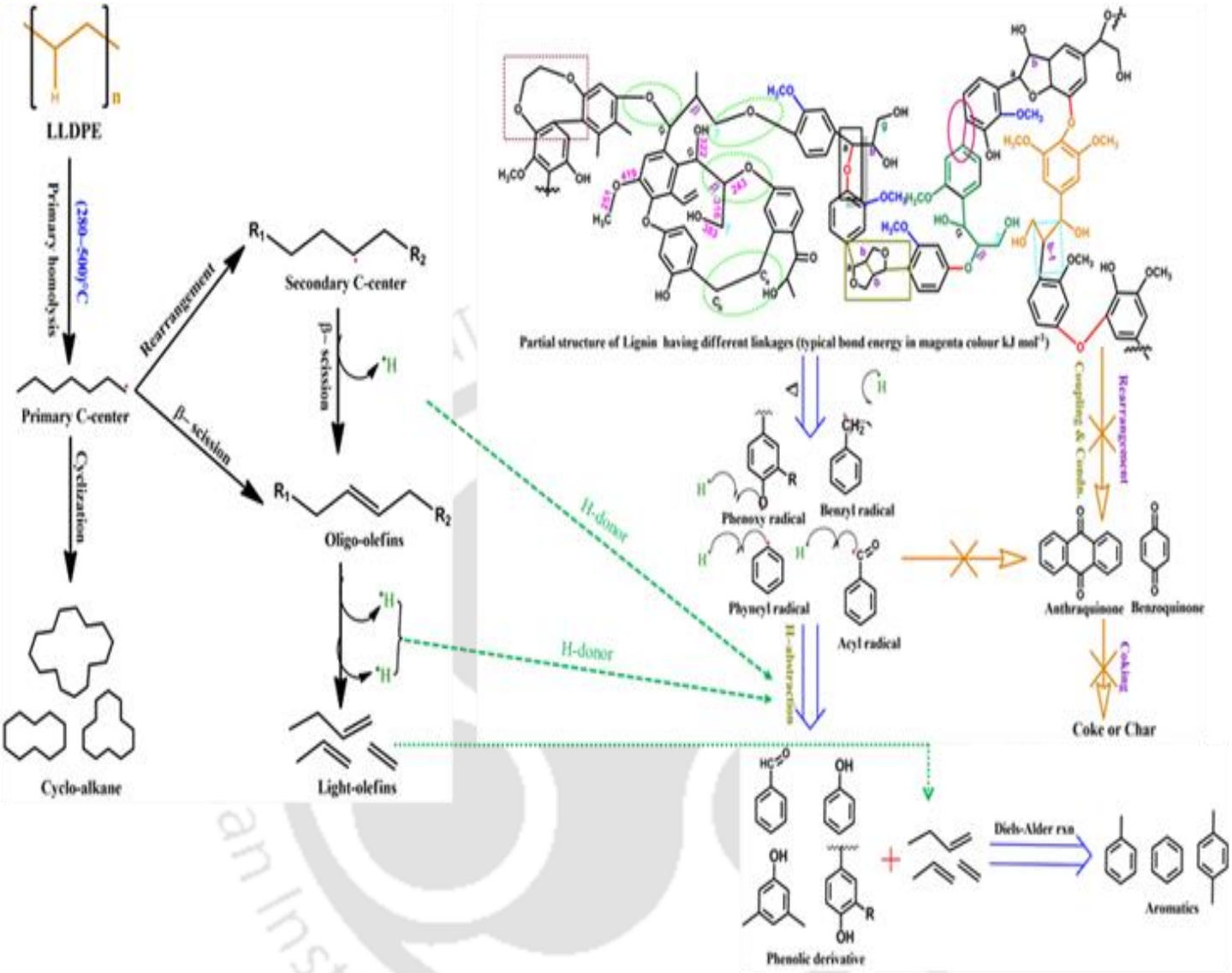

Scheme A1.1: Role of plastic during copyrolysis of Bamboo sawdust and LLDPE [1–5]

Annexure A2

Table A2.1: Degradation parameters at different stages of degradation of TBSD with or without salt at a heating rate of 10°C min^{-1}

Stages	Parameters	BSD	*TBSD (W) With NaCl	#TBSD (W) without NaCl
Stage_1 (Moisture removal)	T_{range} (°C)	30–120	30–110	30–95
	DR_{max} (wt% ·min^{-1})	*0.82*	*1.19*	*0.53*
	T_{max} (°C)	59	57	53
	W_{loss} (%)	3.24	4.26	1.64
Stage_2	T_{range} (°C)	260–295	–	–
	DR_{max} (wt% ·min^{-1})	*3.087*	–	–
	T_{max} (°C)	273	–	–
	W_{loss} (%)	11.46	–	–
Stage_3	T_{range} (°C)	290–500	180–500	200–500
	DR_{max} (wt% ·min^{-1})	*10.65*	*12.30*	*14.31*
	T_{max} (°C)	337	336	358
	W_{loss} (%)	57.45	64.27	80.47
Mean Reactivity (M_R) x 10^2 (wt % min^{-1} °C^{-1})		4.29	3.66	4.00
% Residual weight after 790°C		21.14	26.32	12.72

Table A2.2: Degradation parameters at different stages of degradation of TBSD with or without salt at a heating rate of 20°C min^{-1}

Stages	Parameters	BSD	TBSD (W) With NaCl	TBSD (W) without NaCl
Stage_1 (Moisture removal)	T_{range} (°C)	30–120	30–120	30–110
	DR_{max} (wt% ·min^{-1})	*1.90*	*1.98*	*1.10*
	T_{max} (°C)	67	68	62
	W_{loss} (%)	4.12	4.06	1.97
Stage_2	T_{range} (°C)	260–310	–	–
	DR_{max} (wt% ·min^{-1})	*5.80*	–	–
	T_{max} (°C)	282	–	–
	W_{loss} (%)	14.05	–	–
	T_{range} (°C)	290–500	180–500	200–500
	DR_{max} (wt% ·min^{-1})	*20.08*	*23.43*	*25.77*

Stage_3	T_{max} (°C)	348	350	359
	W_{loss} (%)	53.43	65.56	79.73
Mean Reactivity (M_R) x 10^2 (wt % min^{-1} $°C^{-1}$)		7.83	6.69	7.18
% Residual weight after 790°C		23.22	26.77	13.24

Table A2.3: Degradation parameters at different stages of degradation of TBSD, LLDPE blends at a heating rate of 5°C min^{-1}

Stages	Parameters	TBSD	TBP3:1	TBP1:1	TBP1:3	LLDPE
Stage_1 (Moisture removal)	T_{range} (°C)	30–100	30–110	30–90	30–80	–
	DR_{max} (wt% $\cdot min^{-1}$)	*0.3*	*0.22*	*0.21*	*0.12*	–
	T_{max} (°C)	48	55	53	40	–
	W_{loss} (%)	1.8	0.52	0.35	0.30	–
Stage_2	T_{range} (°C)	180–460	140–390	180–375	200–370	350–510
	DR_{max} (wt% $\cdot min^{-1}$)	*6.82*	*4.97*	*3.05*	*1.38*	*13.55*
	T_{max} (°C)	325	327	326	327	466
	W_{loss} (%)	67.30	49.88	29.03	13.88	96.64
Stage_3	T_{range} (°C)	–	390–540	380–520	370–510	–
	DR_{max} (wt% $\cdot min^{-1}$)	–	*2.94*	*7.29*	*10.61*	–
	T_{max} (°C)	–	468	467	466	–
	W_{loss} (%)	–	27.93	54.82	79.21	–
Mean Reactivity (M_R) x 10^2 (wt % min^{-1} $°C^{-1}$)		2.10	2.15	2.50	2.70	2.91
% Residual weight after 790°C		24.32	18.06	12.89	2.20	1.34

Table A2.4: Degradation parameters at different stages of degradation of TBSD, LLDPE blends at a heating rate of 20°C min^{-1}

Stages	Parameters	TBSD	TBP3:1	TBP1:1	TBP1:3	LLDPE
Stage_1 (Moisture removal)	T_{range} (°C)	30–120	30–110	30–100	30–95	–
	DR_{max} (wt% $\cdot min^{-1}$)	1.94	0.94	0.71	1.25	–
	T_{max} (°C)	65	65	60	48	–
	W_{loss} (%)	4.3	1.98	1.05	1.97	–
Stage_2	T_{range} (°C)	180–460	180–405	200–400	210–390	390–540
	DR_{max} (wt% $\cdot min^{-1}$)	23.38	16.10	11.08	5.59	47.27
	T_{max} (°C)	349	349	350	349	487
	W_{loss} (%)	64.28	49.65	30.37	16.56	96.11

Stage_3	T_{range} (°C)	–	405–560	400–540	395–530	–
	DR_{max} (wt% ·min^{-1})	–	9.44	25.04	35.84	–
	T_{max} (°C)	–	491	488	486	–
	W_{loss} (%)	–	26.9	53.78	74.39	–
Mean Reactivity (M_R) x 10^2 (wt % min^{-1} ·$°C^{-1}$)		6.70	6.54	8.30	8.98	9.71
% Residual weight after 790°C		26.30	19.39	13.12	5.40	2.40

Table A2.5: Degradation parameters at different stages of degradation of TBSD, LLDPE blends at a heating rate of 40°C min^{-1}

Stages	Parameters	TBSD	TBP3:1	TBP1:1	TBP1:3	LLDPE
Stage_1 (Moisture removal)	T_{range} (°C)	30–130	30–110	30–110	30–80	–
	DR_{max} (wt% ·min^{-1})	5.33	2.03	1.41	0.49	–
	T_{max} (°C)	79	77	74	60	–
	W_{loss} (%)	6.38	2.5	1.22	0.87	–
Stage_2	T_{range} (°C)	200–450	180–418	200–400	220–400	380–550
	DR_{max} (wt% ·min^{-1})	46.95	32.24	22.26	11.48	93.55
	T_{max} (°C)	363	361	362	357	501
	W_{loss} (%)	62.66	49.13	30.84	14.81	97.57
Stage_3	T_{range} (°C)	–	418–570	400–550	400–540	–
	DR_{max} (wt% ·min^{-1})	–	19.02	49.09	72.43	–
	T_{max} (°C)	–	503	496	500	–
	W_{loss} (%)	–	27.41	54.12	77.76	–
Mean Reactivity (M_R) x 10^2 (wt % min^{-1} ·$°C^{-1}$)		12.93	12.71	16.05	17.70	18.67
% Residual weight after 790°C		25.55	18.93	12.72	5.63	1.33

Table A2.6: Activation energy (E_α) from model-free methods (KAS, OFW, and FM) for TBSD and corresponding R^2 value.

α	KAS MODEL		OFW MODEL		FRIEDMAN MODEL	
	E_α (kJ.mol^{-1})	R^2	E_α (kJ.mol^{-1})	R^2	E_α (kJ.mol^{-1})	R^2
0.1	140	0.9983	142	0.9985	155	0.9627
0.2	149	0.9985	151	0.9987	164	0.9985
0.3	151	0.9974	153	0.9978	160	0.9984
0.4	155	0.9988	157	0.9989	195	0.9859
0.5	158	0.9988	160	0.9990	166	0.9996

0.6	157	0.9989	159	0.9991	162	0.9993
0.7	167	0.9995	168	0.99956	181	0.9975
0.8	188	0.9949	188	0.9954	273	0.9601
Avg.	**155**	**0.9981**	**157**	**0.9984**	**180**	**0.9878**

Table A2.7: Activation energy (E_α) from model-free methods (KAS, OFW, and FM) for TBP3:1 and corresponding R^2 value.

α	KAS MODEL		OFW MODEL		FRIEDMAN MODEL	
	E_α (kJ.mol^{-1})	R^2	E_α (kJ.mol^{-1})	R^2	E_α (kJ.mol^{-1})	R^2
0.1	158	0.9979	176	0.9982	167	0.9953
0.2	163	0.9992	182	0.9993	191	0.9865
0.3	168	0.9995	187	0.9995	163	0.9995
0.4	163	0.9997	183	0.9998	166	0.9994
0.5	168	0.9998	187	0.9998	176	0.9983
0.6	244	0.9868	264	0.9866	343	0.9909
0.7	318	0.9733	347	0.9752	272	0.9077
0.8	275	0.9981	303	0.9982	204	0.9144
Avg.	**207**	**0.9943**	**229**	**0.9946**	**210**	**0.9712**

Table A2.8: Activation energy (E_α) from model-free methods (KAS, OFW and FM) for TBP1:1 and corresponding R^2 value

α	KAS MODEL		OFW MODEL		FRIEDMAN MODEL	
	E_α (kJ.mol^{-1})	R^2	E_α (kJ.mol^{-1})	R^2	E_α (kJ.mol^{-1})	R^2
0.1	170	0.9997	171	0.9998	174	0.9997
0.2	171	0.9993	172	0.9994	149	0.9772
0.3	188	0.9996	188	0.9996	247	0.9909
0.4	356	0.9914	347	0.9915	281	0.9590
0.5	311	0.9973	307	0.9975	294	0.9936
0.6	307	0.9909	304	0.9915	305	0.9941
0.7	302	0.9954	299	0.9958	303	0.9973
0.8	304	0.9949	301	0.9953	293	0.9971
Avg.	**264**	**0.9923**	**261**	**0.9963**	**256**	**0.9886**

Table A2.9: Activation energy (E_α) from model-free methods (KAS, OFW, and FM) for TBP1:3 and corresponding R^2 value

α	KAS MODEL		OFW MODEL		FRIEDMAN MODEL	
	E_α (kJ.mol^{-1})	R^2	E_α (kJ.mol^{-1})	R^2	E_α (kJ.mol^{-1})	R^2
0.1	207	0.9802	207	0.9817	220	0.9467
0.2	173.7	0.9354	173.9	0.9510	177	0.9633
0.3	237.8	0.9201	237.7	0.9289	267	0.9935
0.4	254	0.9419	253	0.9469	275	0.9929
0.5	266	0.9625	265	0.9657	282	0.9953
0.6	271	0.9792	270	0.9810	284	0.9964
0.7	277	0.9841	276	0.9854	290	0.9966
0.8	275	0.9914	273	0.9922	283	0.9994
Avg.	**245**	**0.9598**	**244**	**0.9647**	**260**	**0.9843**

Table A2.10: Activation energy (E_α) from model-free methods (KAS, OFW, and FM) for LLDPE and corresponding R^2 value.

α	KAS MODEL		OFW MODEL		FRIEDMAN MODEL	
	E_α (kJ.mol^{-1})	R^2	E_α (kJ.mol^{-1})	R^2	E_α (kJ.mol^{-1})	R^2
0.1	225	0.9970	226	0.9973	267	0.9922
0.2	256	0.9997	255	0.9997	283	0.9994
0.3	258	0.9998	257	0.9998	280	0.9984
0.4	260	0.9996	259	0.9996	278	0.9985
0.5	266	0.9989	264	0.9990	273	0.9983
0.6	266	0.9996	264	0.9996	273	0.9996
0.7	265	0.9987	264	0.9988	261	0.9996
0.8	266	0.9985	265	0.9987	254	0.9979
Avg.	**258**	**0.9989**	**257**	**0.9991**	**271**	**0.9980**

Table A2.11: Activation energy (E_α) from model-free methods (KAS, OFW, and FM) for BSD and corresponding R^2 value.

α	KAS MODEL		OFW MODEL		FRIEDMAN MODEL	
	E_α (kJ.mol^{-1})	R^2	E_α (kJ.mol^{-1})	R^2	E_α (kJ.mol^{-1})	R^2

0.1	164	0.9971	164	0.9974	177	0.9624
0.2	176	0.9972	177	0.9974	185	0.9960
0.3	182	0.9901	182	0.9910	189	0.9945
0.4	174	0.9961	175	0.9965	185	0.9978
0.5	182	0.9961	183	0.9964	188	0.9972
0.6	197	0.9935	197	0.9941	215	0.9989
0.7	203	0.9992	202	0.9993	240	0.9929
0.8	252	0.9967	246.5	0.9949	448	0.9432
Avg.	**191.3**	**0.9957**	**190.9**	**0.9738**	**228**	**0.9854**

Biomass composition

Bamboo comes under the family of *Poaceae* or *Gramineae* and Bambusa genera, monocot plants and rarely flowering and irregular cycle known as grass. It is the fastest-growing plant on earth, grows on poor soil conditions or degrade lands, high productivity and self-regeneration ability which make it one of the best-known Bioresource. [6] Plant cell wall of Bambusa *tulda* consists majorly of biopolymers, namely cellulose, hemicellulose and lignin, and non-structural components, extractives and ash in minor amounts. [7] Hexose monomers are the building blocks of cellulose (I) which join by glycosidic bonds in regular array to form microfibrils that act as a skeleton in the cell wall. Due to inter and intramolecular hydrogen bonding, these microfibrils also connected with hemicellulose and lignin. [8] It is crystalline. Based on crystallographic configuration, two types of crystalline cellulose (I_α and I_β) occur in lignocellulosic biomass having triclinic, with one chain, and monoclinic, with two chain, structures. [9]

Hemicellulose is a heteropolysaccharide, amorphous in nature and lower degree of polymerization compare to cellulose. Its backbones consist of pentose units (xylose and arabinose), and these units also attached with oligosaccharides chain having hexose monomers such as galactose, mannose, glucose and fructose. [7] Acetyl units are attached with C2 or C3 in xylose ring and glucuronic acid also attached with xylose ring in xylan backbone, shown in Fig. A 2.1b. It acts as linking

materials, connected through lignin and cellulose by hydrogen and covalent bonds. The linkage or bond between lignin and carbohydrate (LCC) were categorized into five categories including phenyl glycosides (C_6H_5–O–C1), benzyl ether (α–O–4 or β–O–4), alkyl benzyl ether, γ–ester or ester linkages with glucuronic acid and acetal bonds shown in Fig. A 2.1d. [10]

Lignin is tridimensional polymer, amorphous in nature and composition varies from species to species. The hardwood, softwood, and grasses contain 20–25, 25–35 and 10–15% lignin, respectively. [7] The strength and rigidity of the cell wall depend upon the extent of the lignin matrix which consists of three basic units p–hydroxyphenyl (H), guaiacyl (G) and syryngyl (S). These units are differentiated based on the number of methoxy groups they contain. The H, G and S units possess zero, one and two methoxy groups, respectively. [11] These monomers are joined to each other by different linkages such as ether (β–O–4, α–O–4 and γ–O–4), carbon-carbon linkage in aromatic and alkylated carbon (β–5, β–1, 5–5), resinol type (β–β, α –O–γ′, γ–O–α′) and phenyl-coumarane (β–5, α–O4) [12]**,** shown in Fig. A2.1c.

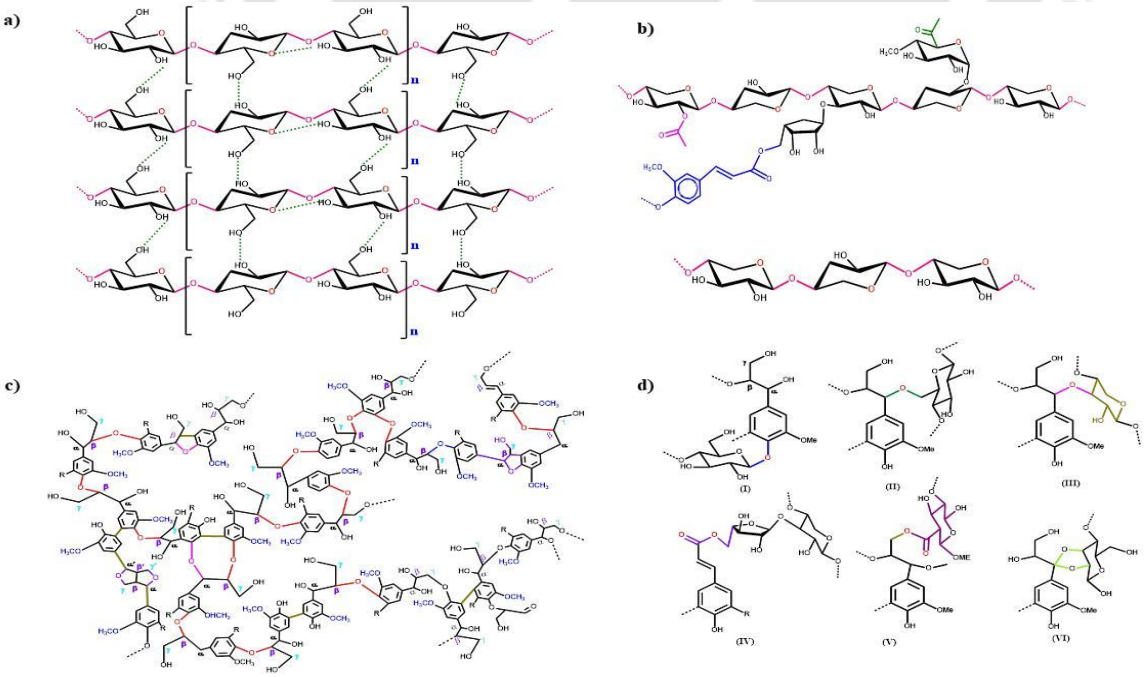

Figure A2.1. Schematic illustration of cellulose (a), hemicellulose (b) and lignin (c) in cell wall of bambusa *tulda* and lignin carbohydrate complex having different bonds [glycosidic (I), benzyl ether (II), γ–ester (III), acetal (IV), etc.] (d).

Conversion of xylose into furfural

The elementary steps related to the conversion of xylose into furfural are presented in two paths in Fig. A2.2. An insignificant amount of levulinic acid also formed from glucose through 5–hydroxymethylfurfural in the presence of Brønsted acid sites. [8]

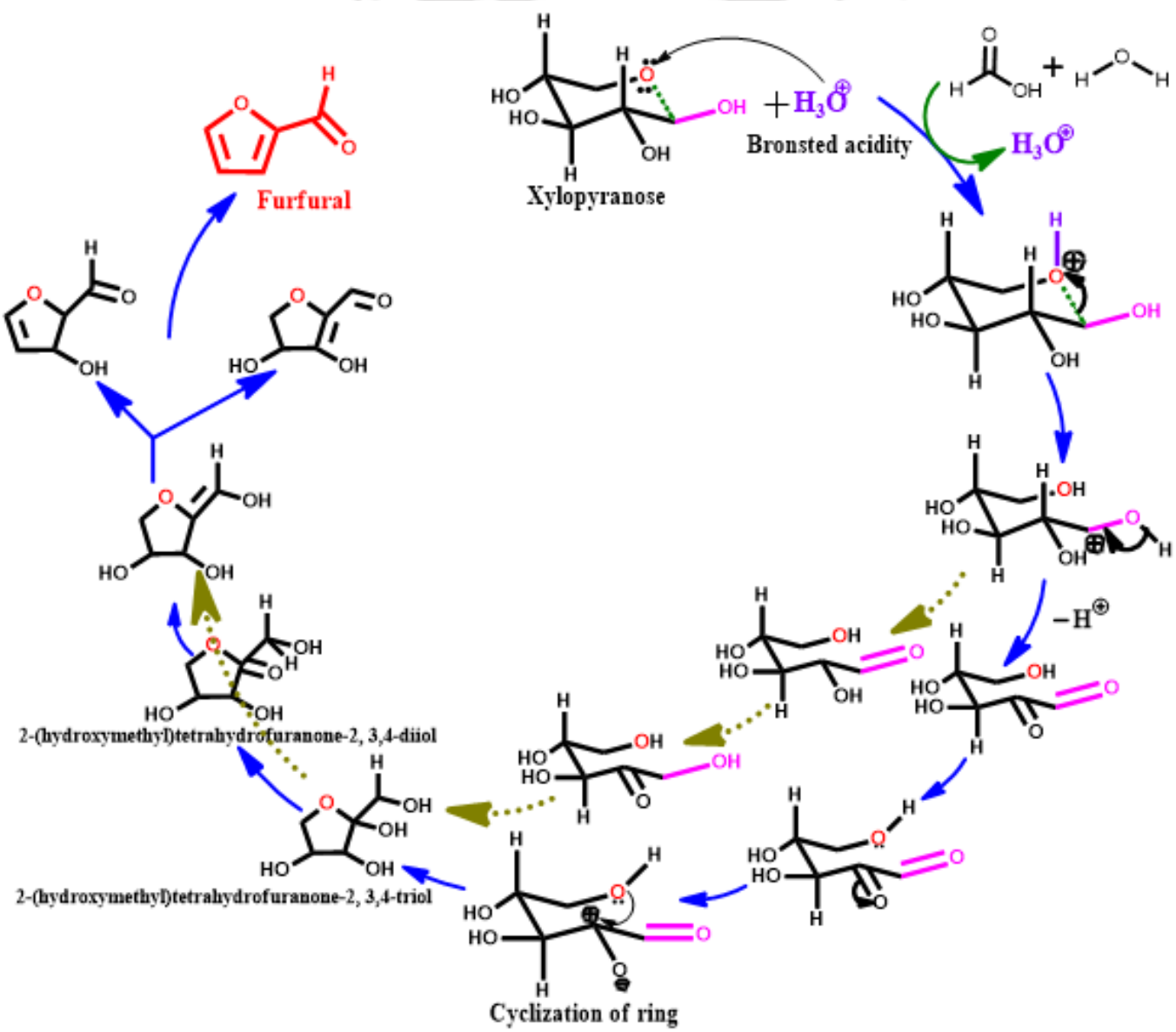

Figure A2.2. The conversion of Furfural from β–D–xylose by most favourable pathways (represented in blue and golden arrows)

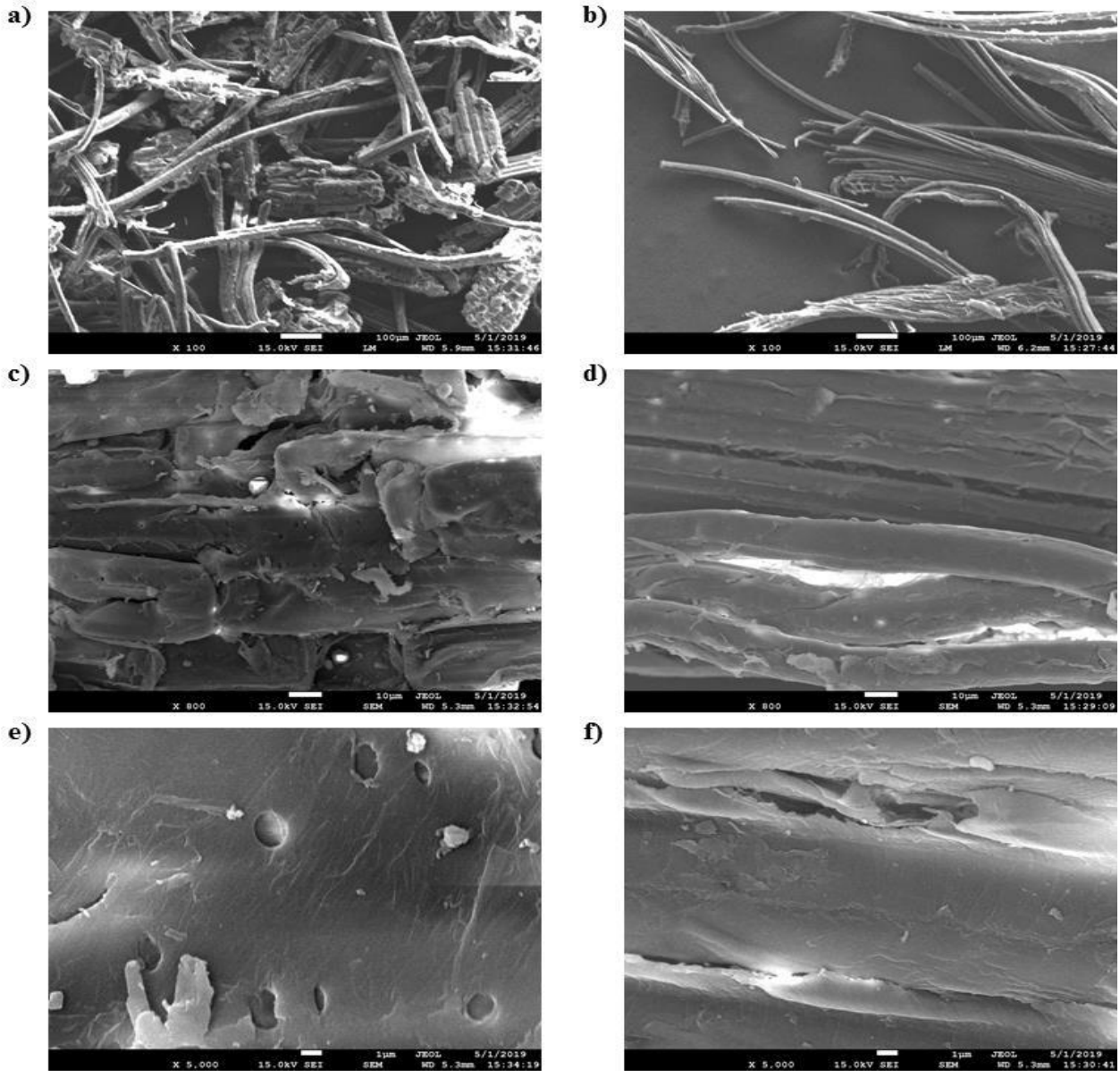

Figure A2.3. FESEM images of bamboo saw dust (a, c & e) and torrefied BSD (b, d & f).

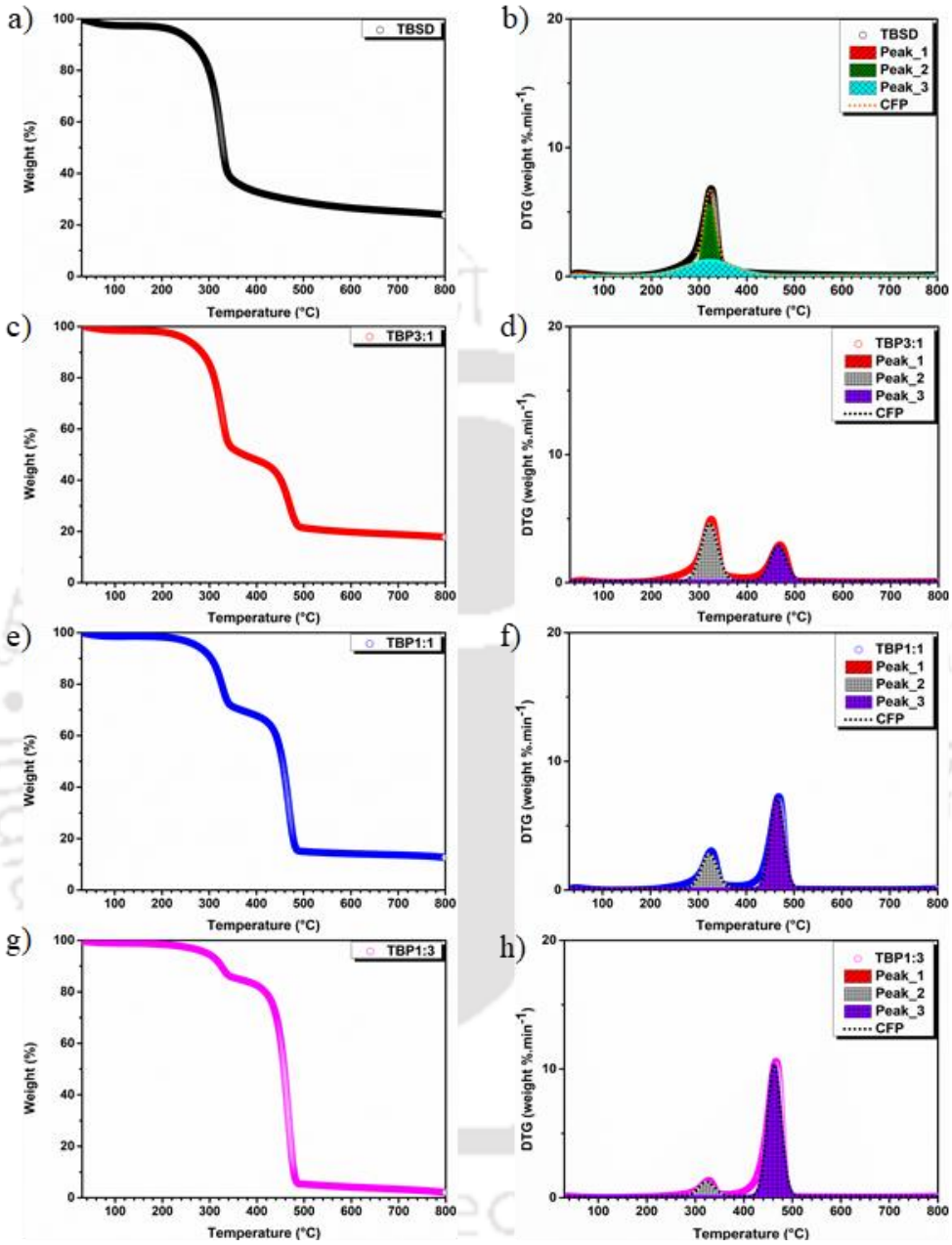

Figure A2.4. The TGA (a, c, e and g) and DTG, along with CFP, plots (b, d, f and h) of TBSD (a and b), TBP3:1 (c and d), TBP1:1 (e and f) and TBP1:3 (g and h) at 5°C min^{-1} (CFP: Cumulative fit peak with Gaussian function for peak deconvolution).

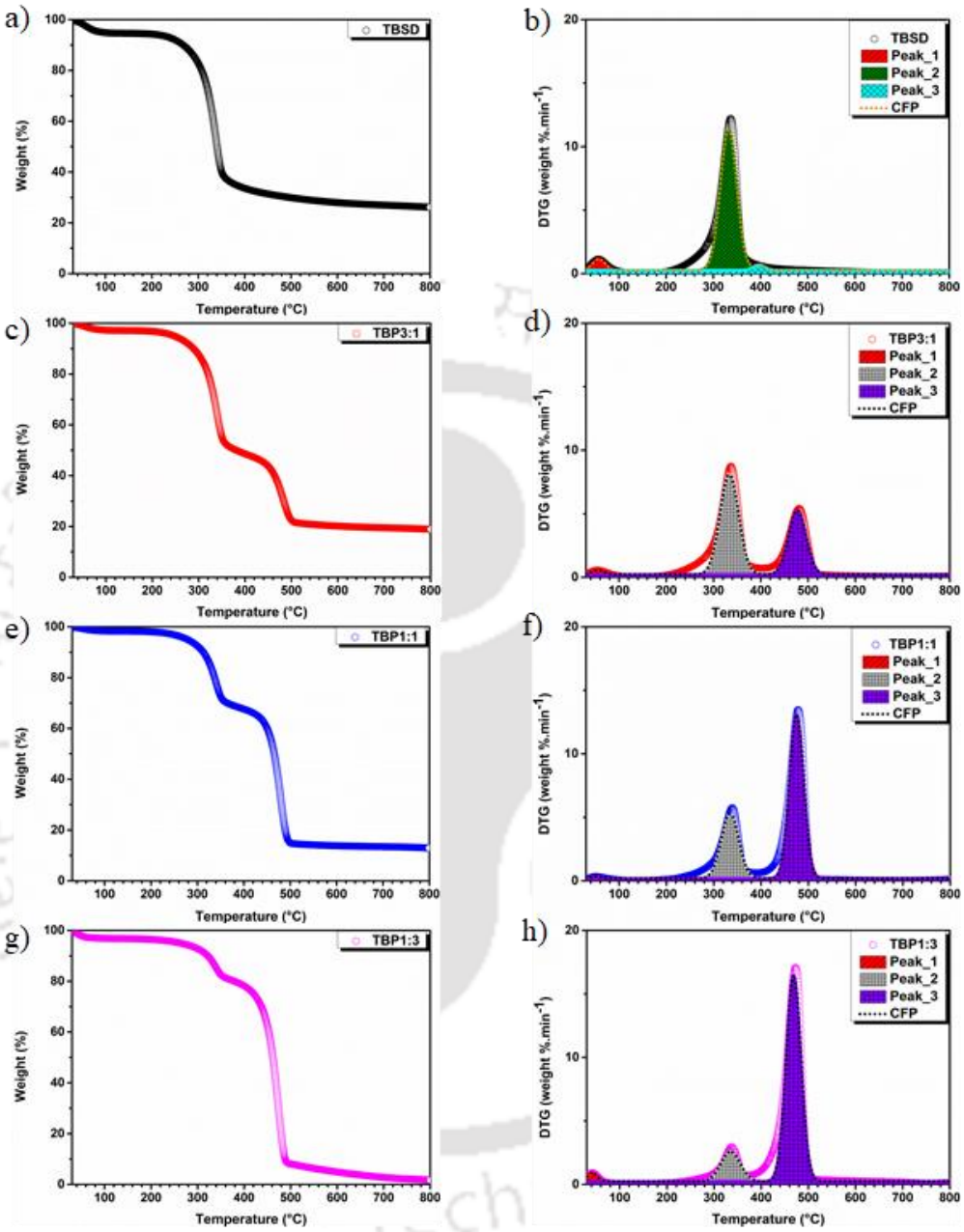

Figure A2.5. The TGA (a, c, e and g) and DTG, along with CFP, plots (b, d, f and h) of TBSD (a and b), TBP3:1 (c and d), TBP1:1 (e and f) and TBP1:3 (g and h) at 10°C min^{-1} (CFP: Cumulative fit peak with Gaussian function for peak deconvolution).

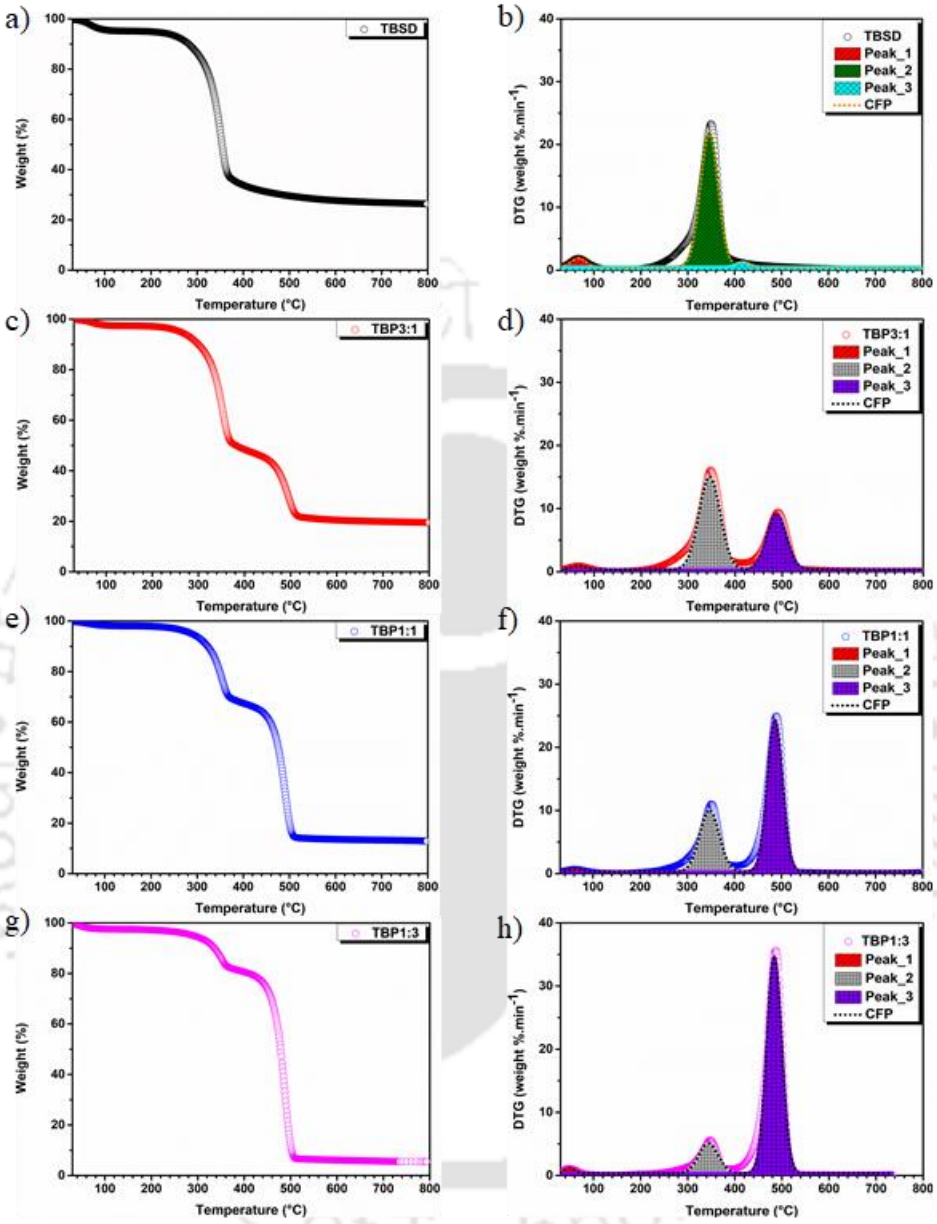

Figure A2.6. The TGA (a, c, e and g) and DTG, along with CFP, plots (b, d, f and h) of TBSD (a and b), TBP3:1 (c and d), TBP1:1 (e and f) and TBP1:3 (g and h) at 20°C min^{-1} (CFP: Cumulative fit peak with Gaussian function for peak deconvolution).

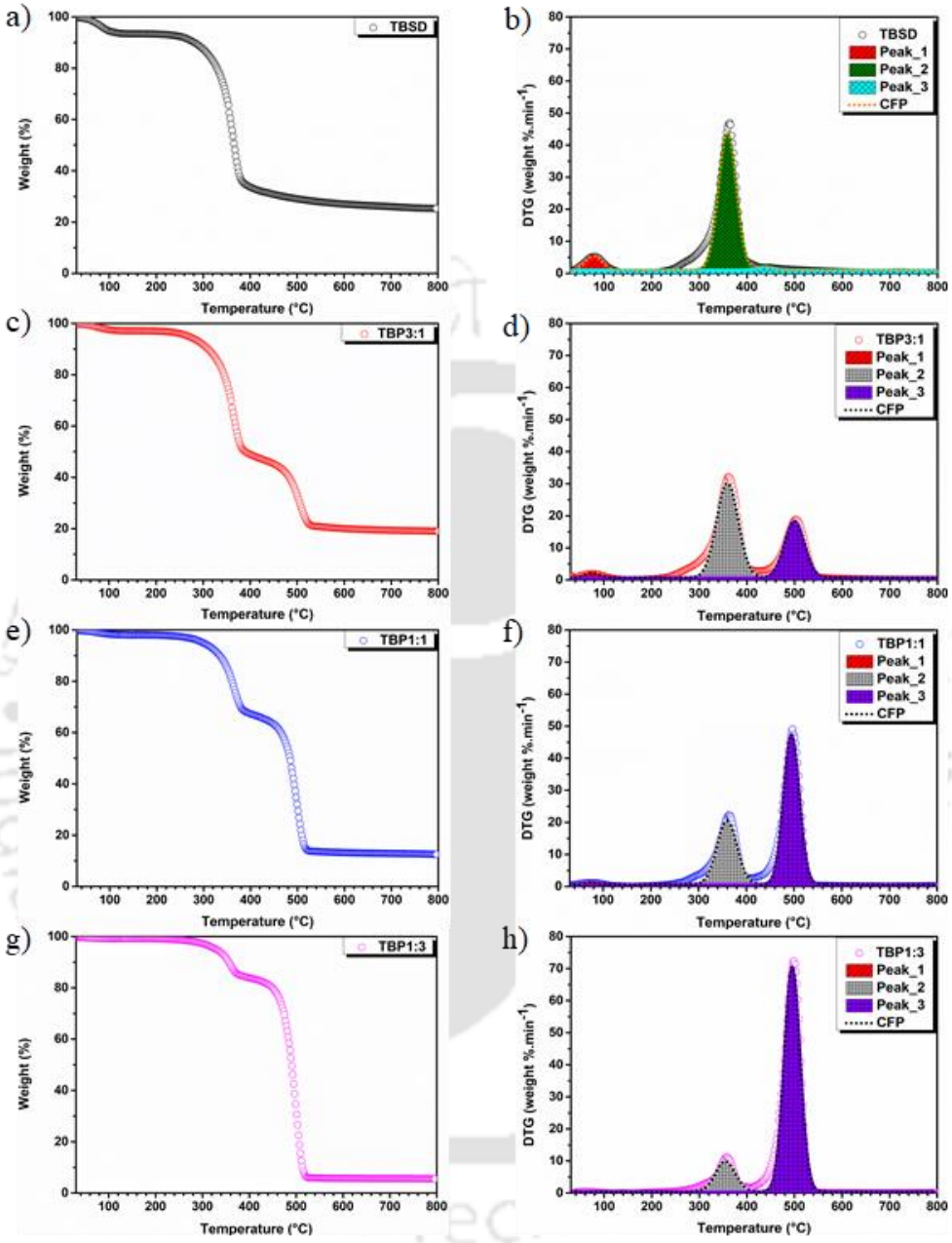

Figure A2.7. The TGA (a, c, e and g) and DTG, along with CFP, plots (b, d, f and h) of TBSD (a and b), TBP3:1 (c and d), TBP1:1 (e and f) and TBP1:3 (g and h) at 40°C min^{-1} (CFP: Cumulative fit peak with Gaussian function for peak deconvolution).

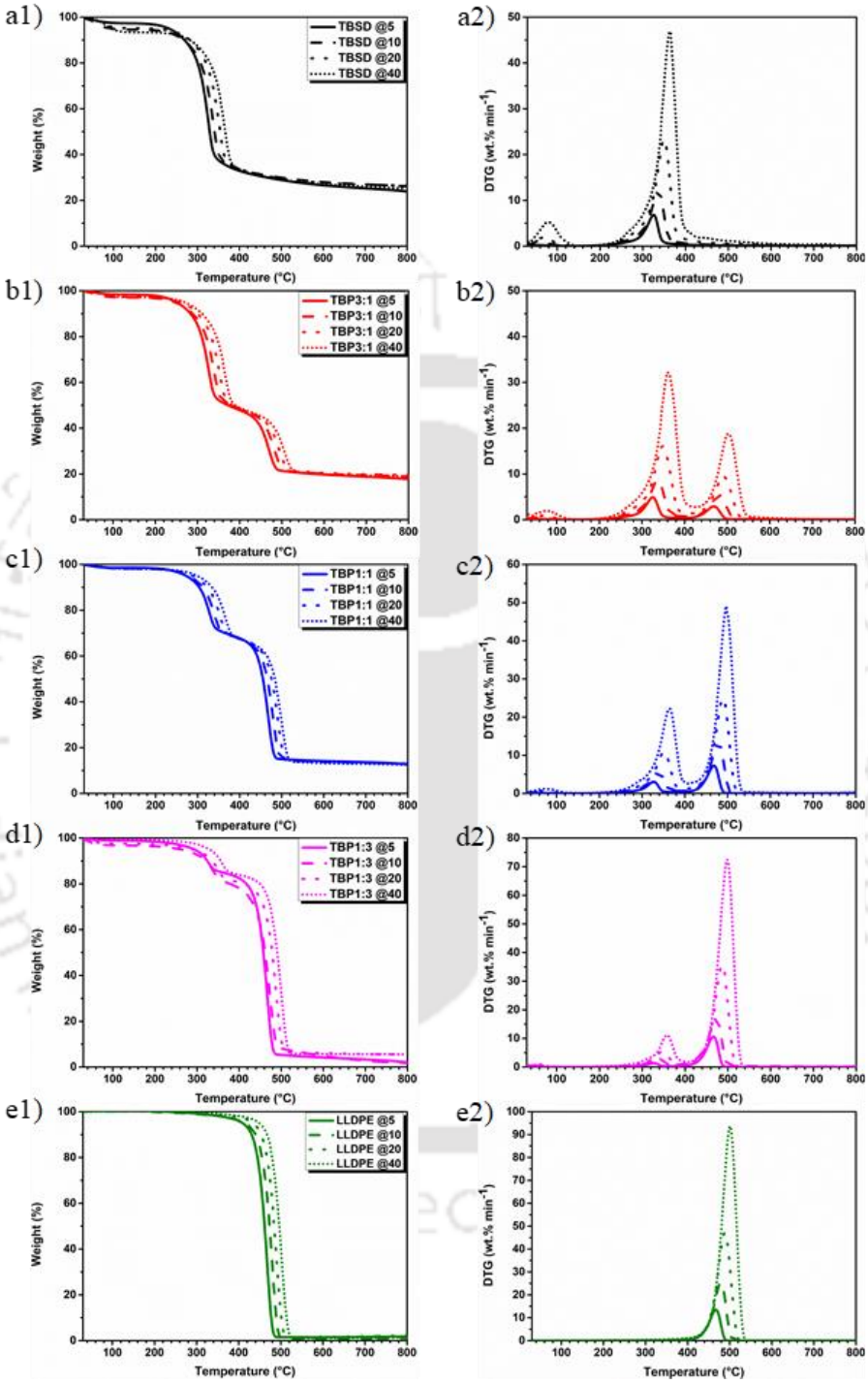

Figure A2.8. TG analysis of a) TBSD, b) TBP3:1, c) TBP1:1, d) TBP1:3 and e) LLDPE: Weight loss as a function of temperature (a1, b1, c1, d1 and e1) and DTG (a2, b2, c2, d2 and e2).

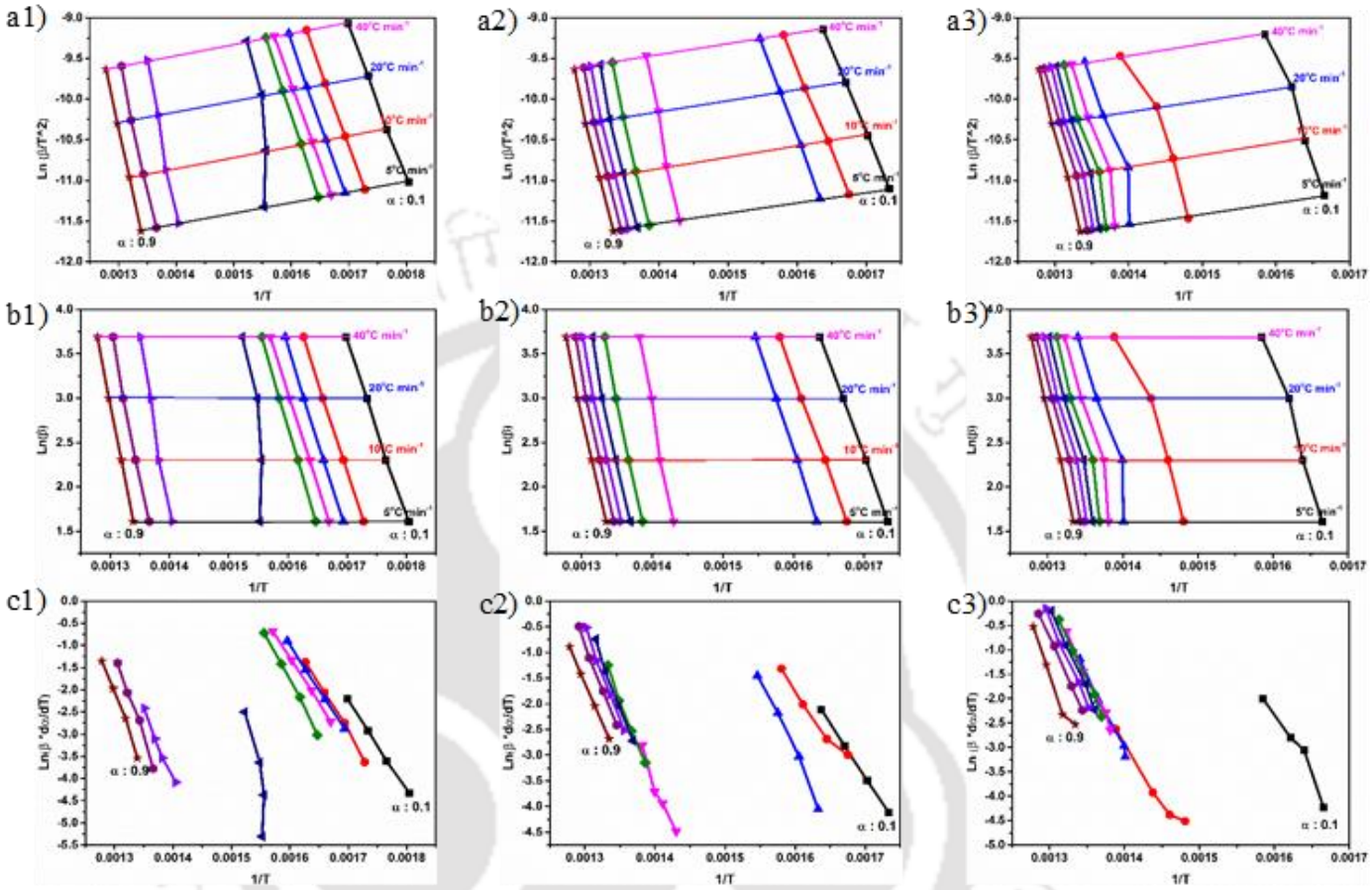

Figure A2.9. Determination of activation energy using three different isoconversional models: KAS (a), OFW (b) and FM (c) of various TBSD+LLDPE blends (TBP3:1: a1 to c1; TBP1:1: a2 to c2; and TBP1:3: a3 to c3).

Annexure A3

Table A3.1: Degradation parameters and stages of catalytic pyrolysis of TBSD and LLDPE and catalytic co-pyrolysis of blends TBP3:1, TBP1:1, and TBP1:3, in presence of HZSM-5, at a heating rate of 5°C min^{-1}.

Stages	Parameters	TBSD	TBP3:1	TBP1:1	TBP1:3	LLDPE
Moisture removal	T_{range} (°C)	30–150	30–150	30–150	30–150	30–150
	DR_{max} (wt% min^{-1})	*0.36*	*0.37*	*0.26*	*0.28*	*0.19*
Stage_1	T_{max} (°C)	50	48	52	42	55
	W_{loss} (%)	3.71	3.37	2.67	2.67	1.28
Stage_2	T_{range} (°C)	150–370	150–345	180–345	180–395	180–380
	DR_{max} (wt% min^{-1})	*2.38*	*1.77*	*1.69*	*2.49*	*3.29*
	T_{max} (°C)	327	325	319	308	299
	W_{loss} (%)	21.37	18.87	24.04	32.23	36.82
Stage_3	T_{range} (°C)	370–490	345–460	345–440	–	–
	DR_{max} (wt% min^{-1})	–	*0.57*	–	–	–
	T_{max} (°C)	–	365	–	–	–
	W_{loss} (%)	3.37	6.73	5.87	–	–
Mean Reactivity (M_R) x 10^3 (wt.% min^{-1} $°C^{-1}$)		7.28	7.01	5.30	8.08	11.01
% Residual weight after 790°C		68.70	67.25	65.85	63.36	60.51

Table A3.2: Degradation parameters and stages of catalytic pyrolysis of TBSD and LLDPE and catalytic co-pyrolysis of blends TBP3:1, TBP1:1, and TBP1:3, in presence of HZSM-5, at a heating rate of 20°C min^{-1}.

Stages	Parameters	TBSD	TBP3:1	TBP1:1	TBP1:3	LLDPE
Moisture removal	T_{range} (°C)	30–150	30–150	30–150	30–150	30–150
	DR_{max} (wt% min^{-1})	*1.32*	*1.11*	*1.03*	*1.16*	*0.55*
Stage_1	T_{max} (°C)	72	74	72	58	76
	W_{loss} (%)	2.23	3.27	3.19	4.12	1.62
Stage_2	T_{range} (°C)	150–390	150–380	180–375	180–470	180–435
	DR_{max} (wt% min^{-1})	*7.96*	*6.33*	*6.24*	*8.45*	*11.68*
	T_{max} (°C)	351	349	345	333	326

	W_{loss} (%)	20.96	20.05	22.82	31.88	37.05
Stage_3	T_{range} (°C)	390–660	380–680	375–590	–	–
	DR_{max} (wt% min^{-1})	–	*2.17*	–	–	–
	T_{max} (°C)	–	397	–	–	–
	W_{loss} (%)	4.88	8.36	6.91	–	–
Mean Reactivity (M_R) x 10^3 (wt.% min^{-1} $°C^{-1}$)		22.68	23.60	18.09	25.38	35.83
% Residual weight after 790°C		69.57	67.98	66.03	63.88	61.38

Table A3.3: Degradation parameters and stages of catalytic pyrolysis of TBSD and LLDPE and catalytic co-pyrolysis of blends TBP3:1, TBP1:1, and TBP1:3, in presence of HZSM-5, at a heating rate of 40°C min^{-1}.

Stages	**Parameters**	**TBSD**	**TBP3:1**	**TBP1:1**	**TBP1:3**	**LLDPE**
Moisture removal	T_{range} (°C)	30–150	30–150	30–150	30–150	30–150
	DR_{max} (wt% min^{-1})	*2.39*	*2.04*	*2.38*	*1.87*	*1.15*
Stage_1	T_{max} (°C)	85	84	83	87	85
	W_{loss} (%)	3.71	3.02	3.2	2.67	1.80
Stage_2	T_{range} (°C)	150–400	150–390	180–390	180–550	180–450
	DR_{max} (wt% min^{-1})	*15.37*	*12.38*	*12.01*	*15.51*	*21.62*
	T_{max} (°C)	365	362	360	353	340
	W_{loss} (%)	21.19	20.67	23.17	33.68	37.52
Stage_3	T_{range} (°C)	400–730	390–730	390–710	–	–
	DR_{max} (wt% min^{-1})	–	*4.31*	–	–	–
	T_{max} (°C)	–	411	–	–	–
	W_{loss} (%)	11.52	8.20	8.01	–	–
Mean Reactivity (M_R) x 10^3 (wt.% min^{-1} $°C^{-1}$)		42.11	44.69	33.36	43.94	63.59
% Residual weight after 790°C		69.74	68.12	65.44	61.90	60.86

Table A3.4: The activation energy (E_α) from model-free methods (KAS, OFW, and FM) for catalytic pyrolysis of torrefied biomass sawdust without NaCl (***TBSD)** and corresponding R^2 value (H-ZSM-5; SAR: 80)

α	**KAS MODEL**		**OFW MODEL**		**FRIEDMAN MODEL**	
	E_α (kJ.mol^{-1})	**R^2**	**E_α (kJ.mol^{-1})**	**R^2**	**E_α (kJ.mol^{-1})**	**R^2**
0.1	239	0.9974	236	0.9976	232	0.9906
0.2	227	0.9787	225	0.9787	228	0.9819

0.3	218	0.9987	217	0.9988	220	0.9567
0.4	213	0.9998	212	0.9999	204	0.9995
0.5	204	0.9996	204	0.9996	197	0.9999
0.6	205	0.9997	205	0.9997	201	0.9999
0.7	211	0.9997	210	0.9998	213	0.9987
0.8	227	1.0000	226	1.0000	252	0.9971
Avg.	**218**	**0.9967**	**217**	**0.9968**	**218**	**0.9905**

Table A3.5: The activation energy (E_α) from model-free methods (KAS, OFW, and FM) of catalytic co-pyrolysis of blends without NaCl (***TBP 1:3)** and corresponding R^2 value (H-ZSM-5; SAR: 80

α	KAS MODEL		OFW MODEL		FRIEDMAN MODEL	
	E_α (kJ.mol^{-1})	R^2	E_α (kJ.mol^{-1})	R^2	E_α (kJ.mol^{-1})	R^2
0.1	265	0.9647	261	0.9669	253	0.9792
0.2	233	0.9946	230	0.9945	227	0.9625
0.3	225	0.9302	223	0.9350	218	0.9064
0.4	172	0.9843	171	0.9818	192	0.9712
0.5	183	0.9162	184	0.9245	179	0.9591
0.6	191	0.9611	191	0.9651	196	0.9520
0.7	209	0.9672	209	0.9704	242	0.9589
0.8	257	0.9557	254	0.9593	279	0.9365
Avg.	**217**	**0.9592**	**215**	**0.9622**	**223**	**0.9532**

Table A3.6: The apparent activation energy, and corresponding R^2 value, from isoconversional (KAS, OFW and FM) methods of catalytic pyrolysis of TBSD, in presence of HZSM-5 with SAR (80)

α	KAS MODEL		OFW MODEL		FRIEDMAN MODEL	
	E_α (kJ.mol^{-1})	R^2	E_α (kJ.mol^{-1})	R^2	E_α (kJ.mol^{-1})	R^2
0.1	199	0.9949	198	0.9953	142	0.9632
0.2	188	0.9947	188	0.9952	179	0.9967
0.3	172	0.9981	173	0.9983	162	0.9978
0.4	173	0.9982	174	0.9984	165	0.9996
0.5	165	0.9993	167	0.9993	164	0.9995
0.6	167	0.9997	169	0.9997	172	0.9997

0.7	175	0.9965	177	0.9970	221	0.9660
0.8	255	0.9905	249	0.9957	270	0.9849
Avg.	**187**	**0.9975**	**187**	**0.9970**	**184**	**0.9889**

Table A3.7: The apparent activation energy, and corresponding R^2 value, of catalytic co-pyrolysis of blends TBP3:1, over HZSM-5 with SAR (80), from isoconversional (KAS, OFW, and FM) methods.

α	KAS MODEL		OFW MODEL		FRIEDMAN MODEL	
	E_α (kJ.mol^{-1})	R^2	E_α (kJ.mol^{-1})	R^2	E_α (kJ.mol^{-1})	R^2
0.1	147	0.9981	148	0.9984	151	0.9965
0.2	154	0.9967	155	0.9978	152	0.9881
0.3	155	0.9999	156	0.9999	164	0.9997
0.4	156	0.9998	158	0.9998	172	0.9699
0.5	161	0.9986	163	0.9988	164	0.9989
0.6	159	0.9997	161	0.9995	173	0.9869
0.7	178	0.9970	180	0.9974	182	0.9974
0.8	197	0.9955	198	0.9959	211	0.9953
Avg.	**163**	**0.9983**	**165**	**0.9984**	**171**	**0.9916**

Table A3.8: The apparent activation energy, and corresponding R^2 value, of catalytic co-pyrolysis of blends TBP1:1, over HZSM-5 with SAR (80), from isoconversional (KAS, OFW, and FM) methods

α	KAS MODEL		OFW MODEL		FRIEDMAN MODEL	
	E_α (kJ.mol^{-1})	R^2	E_α (kJ.mol^{-1})	R^2	E_α (kJ.mol^{-1})	R^2
0.1	139	0.9945	140	0.9951	133	0.9935
0.2	135	0.9940	137	0.9947	137	0.9859
0.3	135	0.9968	138	0.9972	141	0.9751
0.4	134	0.9980	137	0.9982	136	0.9979
0.5	133	0.9991	136	0.9992	135	0.9993
0.6	134	0.9989	137	0.9991	131	0.9987
0.7	132	0.9978	136	0.9981	115	0.9396
0.8	139	0.9959	143	0.9962	152	0.9995
Avg.	**135**	**0.9969**	**137**	**0.9972**	**135**	**0.9862**

Table A3.9: The apparent activation energy, and corresponding R^2 value, of catalytic co-pyrolysis of blends TBP1:3, over HZSM-5 with SAR (80), from isoconversional (KAS, OFW, and FM) methods

α	KAS MODEL		OFW MODEL		FRIEDMAN MODEL	
	E_α (kJ.mol^{-1})	R^2	E_α (kJ.mol^{-1})	R^2	E_α (kJ.mol^{-1})	R^2
0.1	160	0.9991	160	0.9992	144	0.9987
0.2	141	0.9926	143	0.9936	142	0.9831
0.3	135	0.9927	137	0.9938	134	0.9767
0.4	133	0.9913	136	0.9926	126	0.9772
0.5	127	0.9815	130	0.9843	123	0.9757
0.6	125	0.9841	128	0.9865	116	0.9681
0.7	120	0.9779	125	0.9814	112	0.9504
0.8	121	0.9754	126	0.9803	109	0.9408
Avg.	**133**	**0.9868**	**136**	**0.9889**	**126**	**0.9713**

Table A3.10: The apparent activation energy, and corresponding R^2 value, of catalytic pyrolysis of LLDPE, in presence of HZSM-5 with SAR (80), from isoconversional (KAS, OFW, and FM) methods.

α	KAS MODEL		OFW MODEL		FRIEDMAN MODEL	
	E_α (kJ.mol^{-1})	R^2	E_α (kJ.mol^{-1})	R^2	E_α (kJ.mol^{-1})	R^2
0.1	154	0.9997	155	0.9998	157	0.9995
0.2	150	0.9989	151	0.9991	163	0.9729
0.3	144	0.9976	146	0.9976	145	0.9995
0.4	144	0.9985	146	0.9987	146	0.9987
0.5	147	0.9985	149	0.9987	144	0.9972
0.6	149	0.9989	151	0.9991	147	0.9953
0.7	144	0.9949	147	0.9956	142	0.9790
0.8	144	0.9929	147	0.9938	135	0.9808
Avg.	**147**	0.9975	**149**	0.9978	**148**	0.9903

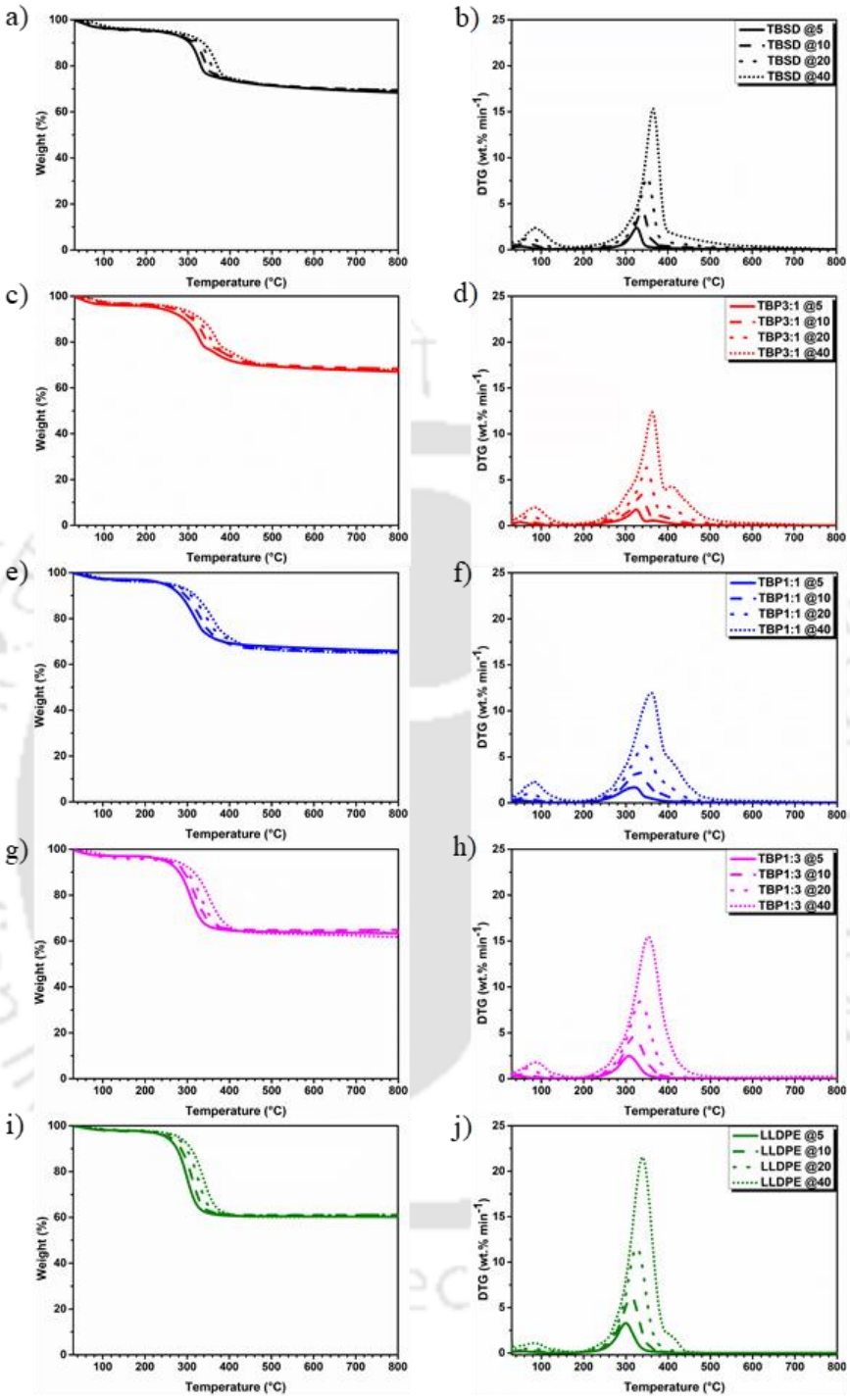

Figure A3.1. TG analysis of catalytic pyrolysis of TBSD (a, b) and LLDPE (i, j) and catalytic co-pyrolysis of blends TBP3:1 (c, d), TBP1:1 (e, f), and TBP1:3 (g, h), in presence of HZSM-5, at heating rates 5, 10, 20 and 40°C min^{-1}: Weight loss as a function of temperature (a, c, e, g and i) and DTG (b, d, f, h, and j).

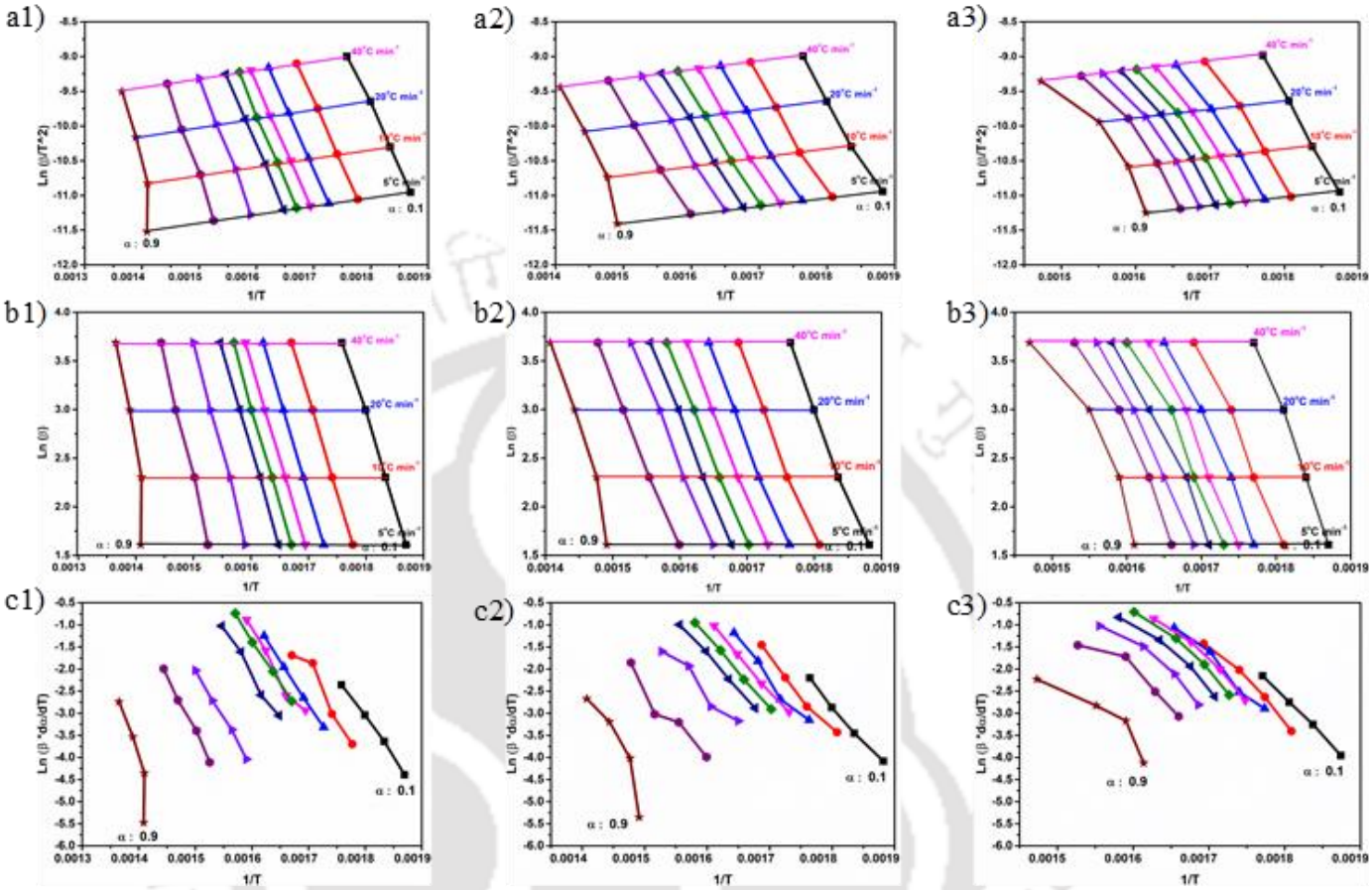

Figure A3.2. Determination of activation energy (Arrhenius plots) using three different iso-conversion models: KAS (a), OFW (b) and FM (c) of various TBSD+LLDPE blends, TBP3:1: a1 to c1; TBP1:1: a2 to c2; and TBP1:3: a3 to c3) in presence of HZSM-5

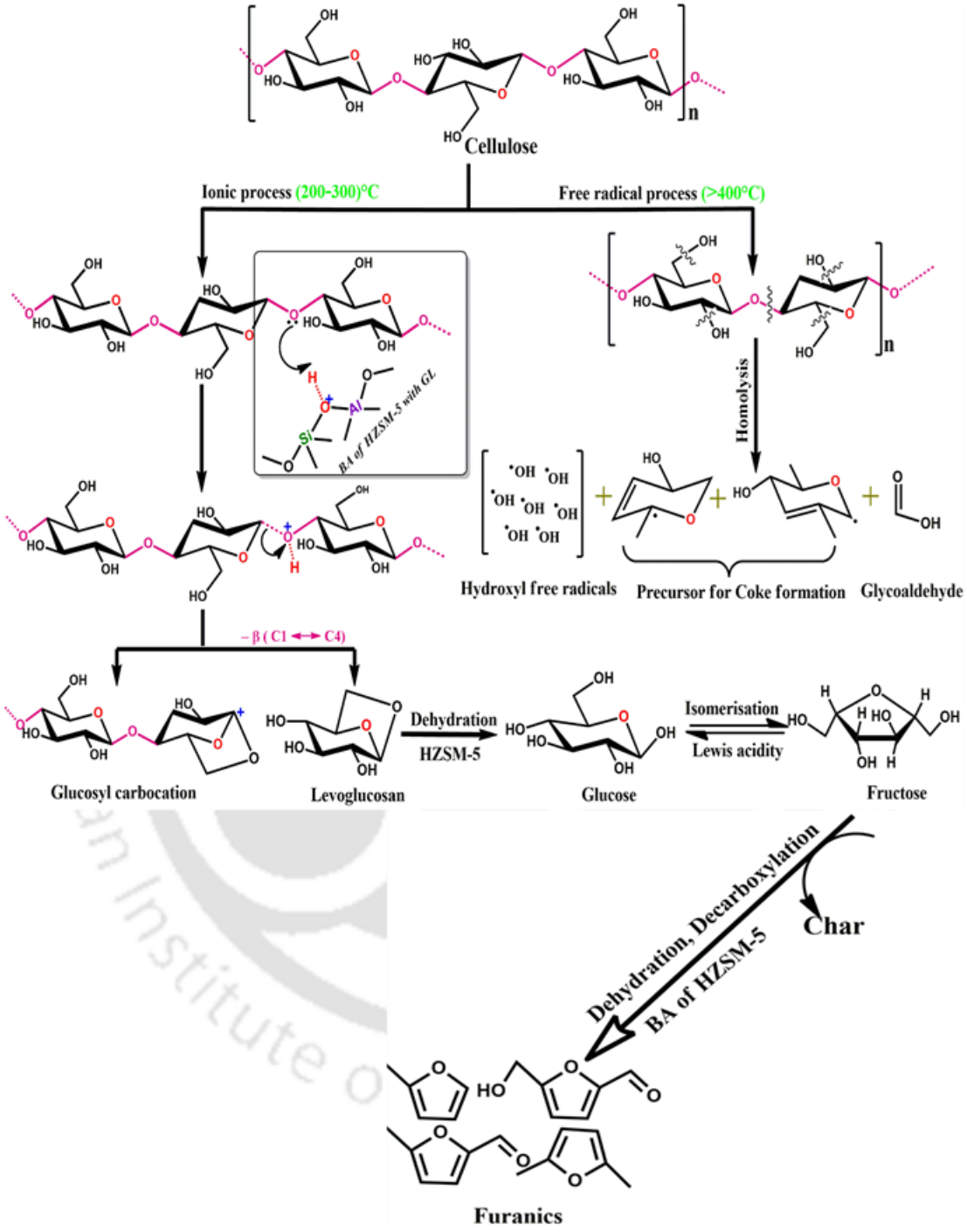

Scheme A3.1. Thermal degradation of Cellulose by two processes over zeolite catalyst Scheme [15–19] (BA: Brønsted acid site; β: Glycosidic linkage)

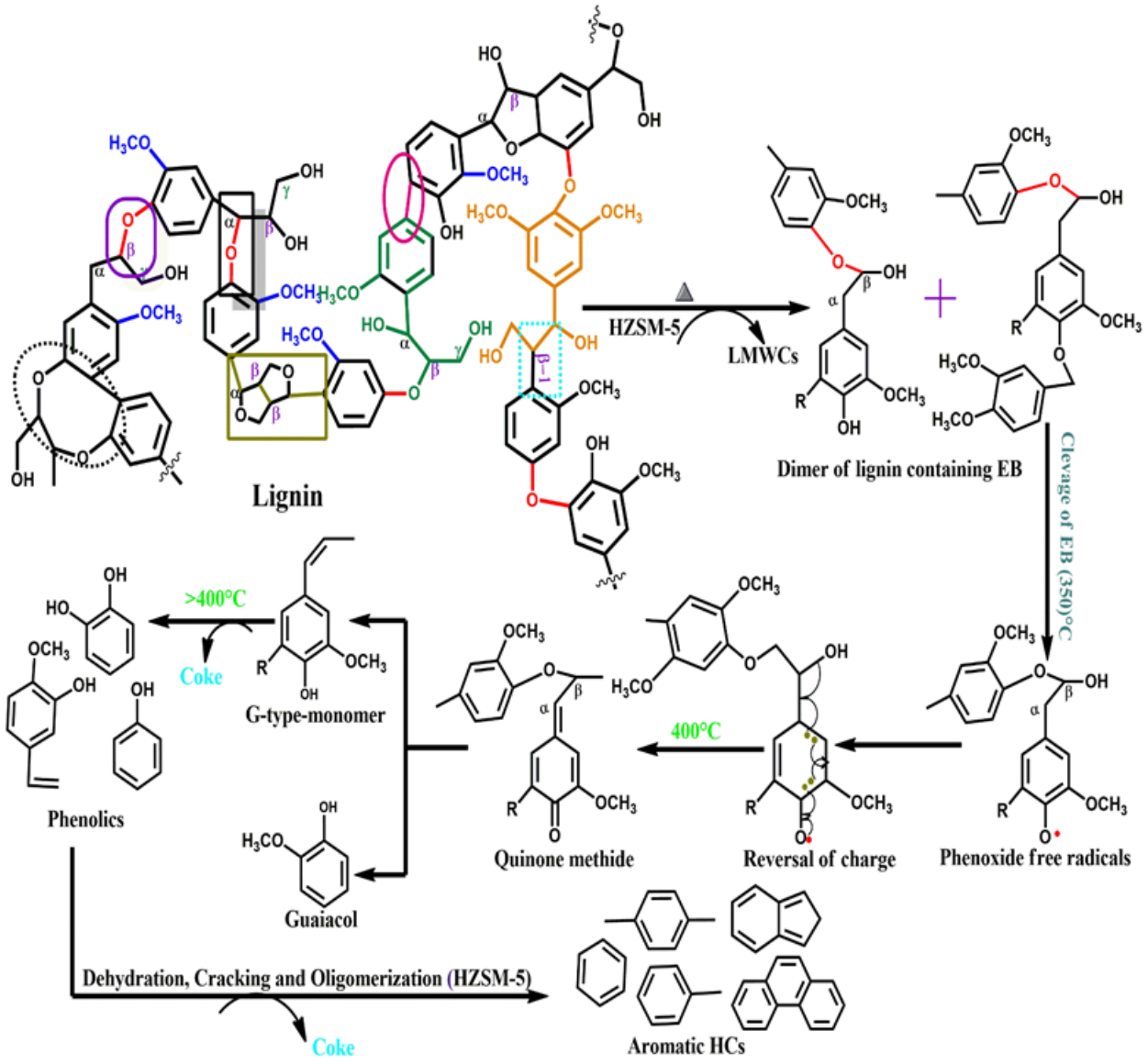

Scheme A3.2. Formation of aromatic hydrocarbons and coke from Lignin degradation pathway over zeolite catalyst [12,20,21] (BA: Brønsted acid site; EB: Etherified bond (α/β-O-4 linkage); LMWC: Low molecular weight compounds; Δ: Thermal degradation)

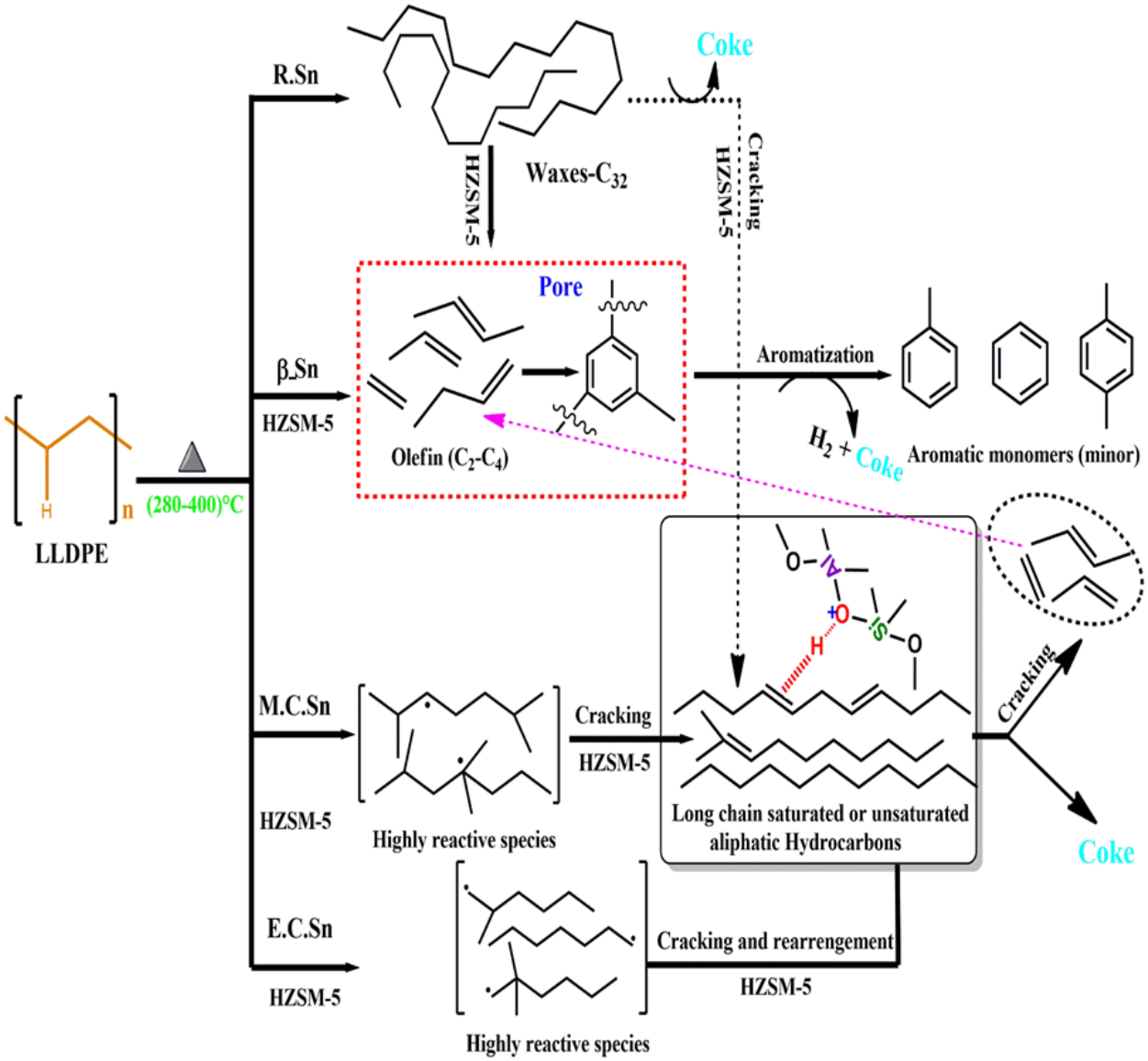

Scheme A3.3. Thermal degradation pathway of LLDPE over zeolite catalyst [22–24] (BA: Brønsted acid site; R.Sn: Random Scission; M.C.Sn: Mid Chain Scission; E.C.Sn: End Chain Scission; Δ: Thermal degradation)

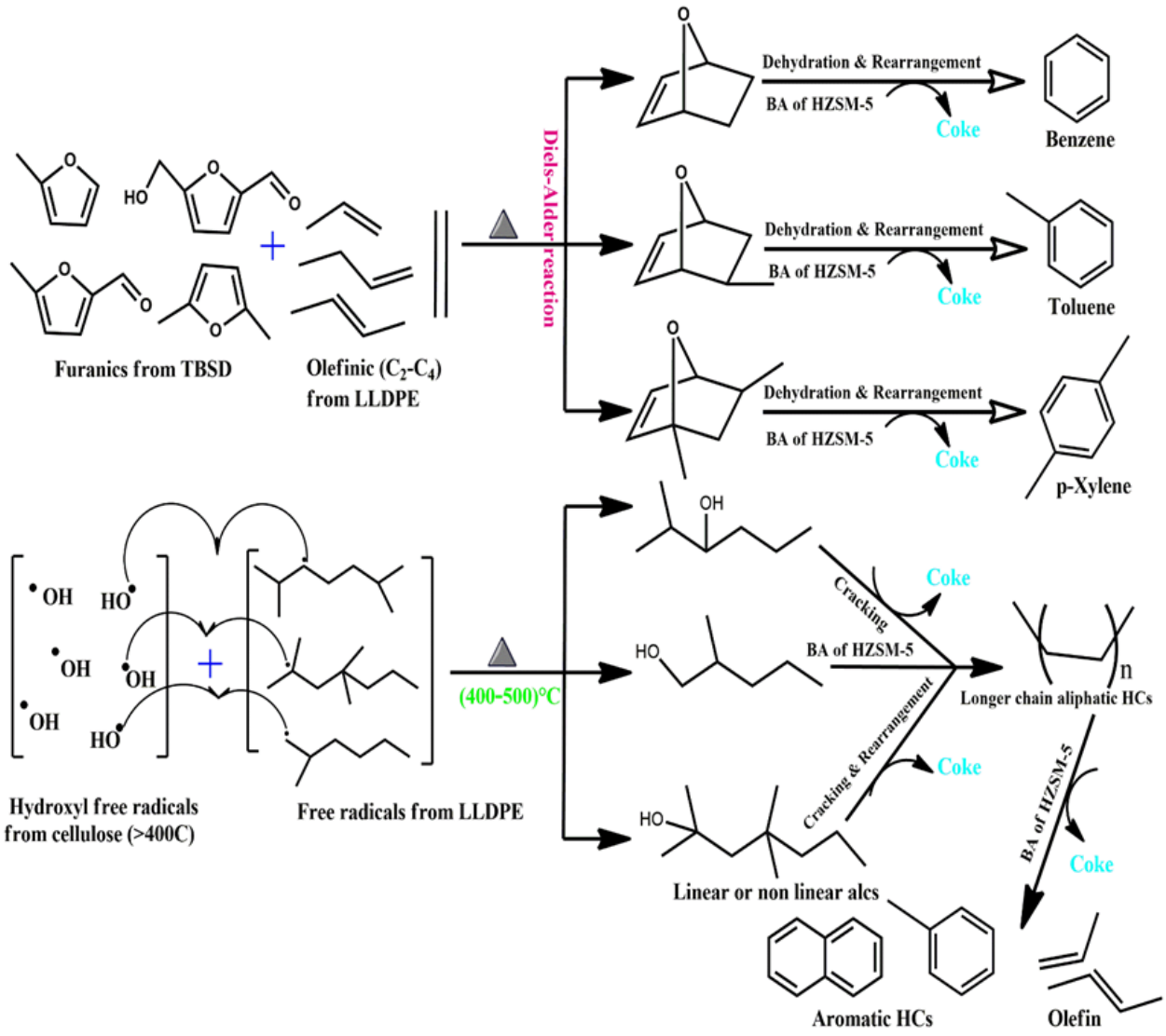

Scheme A3.4. Probable reactions between oxygenated furan derivatives obtained from TBSD with olefin (LLDPE) in copyrolysis over zeolite catalyst [19,25,26] (BA: Brønsted acid site; Δ: Thermal degradation)

Annexure A4

Table A4.1: The catalytic (co)pyrolysis reaction parameters of TBSD, LLDPE, and their blends at 5°C min^{-1} ramp rate

Stages	Parameters	TBSD	TBP3:1	TBP1:1	TBP1:3	LLDPE
Moisture removal	T_{range} (°C)	30–140	30–140	30–120	30–120	30–120
	DR_{max} (wt% min^{-1})	*0.46*	*0.26*	*0.34*	*0.31*	*0.24*
	T_{max} (°C)	50	56	47	46	52
Stage_1	W_{loss} (%)	4.3	2.15	2.85	2.49	2.15
	T_{range} (°C)	170– 390	150–275	130–300	130–300	130–320
	DR_{max} (wt% min^{-1})	*1.97*	*0.50*	*1.01*	*1.33*	*1.71*
	T_{max} (°C)	351	233	233	234	238
Stage_2	W_{loss} (%)	22.54	6.56	14.06	19.74	25.96
	T_{range} (°C)	390–625	275–390	300–385	310–380	320–550
	DR_{max} (wt% min^{-1})	*0.23*	*1.62*	*1.09*	0.75	*0.55*
	T_{max} (°C)	413	352	353	354	371
Stage_3	W_{loss} (%)	5.62	16.72	10.51	7.84	10.51
	T_{range} (°C)	–	390–550	385–485	380–450	–
	DR_{max} (wt% min^{-1})	–	0.30	*0.36*	*0.49*	–
	T_{max} (°C)	–	412	405	405	–
Stage_4	W_{loss} (%)	0	5.52	4.47	5.16	0
Mean Reactivity (M_R) x 10^2 (wt % min^{-1} $°C^{-1}$)		0.61	0.75	0.83	0.90	1.33
% *Residual weight at 790°C		65.44	65.85	64.75	62.25	60.71
Calculated residual weight[#]		5.44	4.40	3.37	2.33	0.71
*Weight of catalyst included in the residual weight. [#]after subtraction of the catalyst weight.						

Table A4.2: The catalytic (co)pyrolysis reaction parameters of TBSD, LLDPE, and their blends at 20°C min^{-1} ramp rate

Stages	Parameters	TBSD	TBP3:1	TBP1:1	TBP1:3	LLDPE
Moisture removal	T_{range} (°C)	30–140	30–140	30–140	30–140	30–140
	DR_{max} (wt% min^{-1})	*1.01*	*1.42*	*1.13*	*0.98*	*0.95*
	T_{max} (°C)	75	70	69	71	70
Stage_1	W_{loss} (%)	2.84	3.71	2.72	2.51	2.32

	T_{range} (°C)	180–425	150–305	150–330	150–335	150–340
	DR_{max} (wt% min^{-1})	*6.74*	*1.73*	*3.43*	*4.34*	*5.29*
	T_{max} (°C)	376	267	261	261	268
Stage_2	W_{loss} (%)	22.07	6.56	13.86	18.35	23.5
	T_{range} (°C)	425–730	305–420	330–410	335–405	340–560
	DR_{max} (wt% min^{-1})	*0.81*	*5.16*	*3.76*	2.57	*2.94*
	T_{max} (°C)	450	375	375	373	395
Stage_3	W_{loss} (%)	5.69	16.26	10.21	7.66	13.69
	T_{range} (°C)	–	420–700	410–670	400–600	–
	DR_{max} (wt% min^{-1})	–	1.30	*1.85*	*2.02*	–
	T_{max} (°C)	–	444	427	428	–
Stage_4	W_{loss} (%)	–	6.04	6.5	6.39	–
Mean Reactivity (M_R) x 10^2 (wt % min^{-1} °C^{-1})		1.97	2.32	2.75	2.82	4.08
% *Residual weight at 790°C		68.87	66.73	66.22	64.23	60.10
Calculated residual weight#		8.87	6.68	4.49	2.29	0.1
*Weight of catalyst included in the residual weight. #after subtraction of the catalyst weight.						

Table A4.3: The catalytic (co)pyrolysis reaction parameters of TBSD, LLDPE, and their blends at 40°C min^{-1} ramp rate

Stages	**Parameters**	**TBSD**	**TBP3:1**	**TBP1:1**	**TBP1:3**	**LLDPE**
Moisture removal	T_{range} (°C)	30–140	30–150	30–150	30–150	30–150
	DR_{max} (wt% min^{-1})	*1.71*	*2.13*	*0.75*	*1.88*	*0.78*
	T_{max} (°C)	92	87	98	87	94
Stage_1	W_{loss} (%)	2.48	3.01	0.87	2.45	0.97
	T_{range} (°C)	180–430	150–320	150–330	150–345	150–350
	DR_{max} (wt% min^{-1})	*12.89*	*3.44*	*5.88*	*7.64*	*9.72*
	T_{max} (°C)	388	285	281	281	281
Stage_2	W_{loss} (%)	21.37	6.39	11.9	17	21.21
	T_{range} (°C)	430–780	320–425	330–420	345–420	350–580
	DR_{max} (wt% min^{-1})	*1.54*	*10.52*	*7.43*	5.52	*4.94*
	T_{max} (°C)	465	390	386	385	404
Stage_3	W_{loss} (%)	6.38	15.68	11.96	8.8	12.13
	T_{range} (°C)	–	425–770	420–740	420–710	–
	DR_{max} (wt% min^{-1})	–	3.50	*4.29*	*4.64*	–
	T_{max} (°C)	–	456	438	436	–

Stage_4	W_{loss} (%)	–	7.32	7.49	7.05	–
Mean Reactivity (M_R) x 10^2 (wt % min^{-1} $°C^{-1}$)		3.65	4.67	4.99	5.22	4.68
% *Residual weight at790°C		69.39	67.60	67.42	63.87	65.36
Calculated residual weight[#]		9.39	8.38	7.38	6.37	5.36
*Weight of catalyst included in the residual weight. [#]after subtraction of the catalyst weight.						

Table A4.4: Synergism of mixed samples with four ramp rates (5–40°C min^{-1}) over MesoHY zeolite

RR	Extent of synergism											
	TBP3:1				TBP1:1				TBP1:3			
	ΔW^*	T^a	$\Delta W^\#$	T^b	ΔW^*	T^a	$\Delta W^\#$	T^b	ΔW^*	T^a	$\Delta W^\#$	T^b
5	–	–	2.42	400	1.08	247	2.51	395	0.49	238	2.48	389
10	1.65	248	1.06	410	1.37	256	2.02	400	1.89	247	1.37	399
20	1.43	273	1.26	426	1.62	288	2.85	416	0.92	273	3.31	418
40	1.36	298	0.84	434	0.27	310	2.14	421	2.0	290	–	–
RR: Ramp rate; ΔW^*: Maximum weight percentage difference (negative values); $\Delta W^\#$: Maximum weight percentage difference (positive values); T^a: Maximum temperature (°C) for ΔW^*; T^b: Maximum temperature (°C) for $\Delta W^\#$												

Table A4.5: The activation energy (E_α) from model-free methods (KAS, OFW, and FM) for **TBSD** and corresponding R^2 value (MesoHY: SAR: 80)

α	KAS MODEL		OFW MODEL		FRIEDMAN MODEL	
	E_α (kJ.mol^{-1})	R^2	E_α (kJ.mol^{-1})	R^2	E_α (kJ.mol^{-1})	R^2
0.1	176	0.9929	177	0.9935	191	0.9950
0.2	208	0.9949	207	0.9954	219	0.9969
0.3	211	0.9993	211	0.9993	211	0.9999
0.4	213	0.9996	212	0.9996	207	0.9999
0.5	202	0.9998	202	0.9998	198	0.9982
0.6	207	0.9998	207	0.9998	212	0.9962
0.7	171	0.9933	170	0.9930	250	0.9612
0.8	343	0.9523	325	0.9519	370	0.95557

Avg.	**216**	**0.9915**	**214**	**0.9915**	**232**	**0.9879**

Table A4.6: The activation energy (E_α) from model-free methods (KAS, OFW, and FM) for **TBP 3:1** and corresponding R^2 value (MesoHY: SAR: 80)

α	KAS MODEL		OFW MODEL		FRIEDMAN MODEL	
	E_α (kJ.mol^{-1})	R^2	E_α (kJ.mol^{-1})	R^2	E_α (kJ.mol^{-1})	R^2
0.1	105	0.9981	108	0.9984	108	0.9957
0.2	125	0.9886	128	0.9902	151	0.9799
0.3	176	0.9914	176	0.9923	188	0.9971
0.4	184	0.9944	184	0.9951	196	0.9953
0.5	193	0.9985	194	0.9987	190	0.9999
0.6	188	0.9984	189	0.9986	184	0.9995
0.7	183	0.9980	184	0.9983	180	0.9824
0.8	212	0.8729	213	0.8845	274	0.9411
Avg.	**171**	**0.9800**	**172**	**0.9820**	**184**	**0.9864**

Table A4.7: The activation energy (E_α) from model-free methods (KAS, OFW, and FM) for **TBP 1:1** and corresponding R^2 value (MesoHY: SAR: 80)

α	KAS MODEL		OFW MODEL		FRIEDMAN MODEL	
	E_α (kJ.mol^{-1})	R^2	E_α (kJ.mol^{-1})	R^2	E_α (kJ.mol^{-1})	R^2
0.1	97	0.9993	100	0.9994	92	0.9985
0.2	89	0.9987	93	0.9989	84	0.9953
0.3	87	0.9958	92	0.9966	84	0.9880
0.4	92	0.9869	97	0.9894	110	0.9774
0.5	139	0.9848	141	0.9868	180	0.9983
0.6	170	0.9980	172	0.9983	177	0.9993
0.7	167	0.9960	169	0.9965	152	0.9902
0.8	181	0.9649	183	0.9689	233	0.9735
Avg.	**128**	**0.9905**	**131**	**0.9918**	**139**	**0.9901**

Table A4.8: The activation energy (E_α) from model-free methods (KAS, OFW, and FM) for **TBP 1:3** and corresponding R^2 value (MesoHY: SAR: 80)

α	KAS MODEL		OFW MODEL		FRIEDMAN MODEL	
	E_α (kJ.mol^{-1})	R^2	E_α (kJ.mol^{-1})	R^2	E_α (kJ.mol^{-1})	R^2
0.1	99	0.9998	102	0.9998	95	0.9996
0.2	94	0.9984	98	0.9988	89	0.9980
0.3	89	0.9980	93	0.9984	83	0.9954
0.4	87	0.9974	92	0.9980	83	0.9928
0.5	90	0.9915	95	0.9933	103	0.9848
0.6	126	0.9746	129	0.9784	168	0.9862
0.7	160	0.9863	162	0.9881	166	0.9933
0.8	191	0.9811	192	0.9831	239	0.9843
Avg.	**117**	**0.9903**	**120**	**0.9923**	**128**	**0.9918**

Table A4.9: The activation energy (E_α) from model-free methods (KAS, OFW, and FM) for **LLDPE** and corresponding R^2 value (MesoHY: SAR: 80)

α	KAS MODEL		OFW MODEL		FRIEDMAN MODEL	
	E_α (kJ.mol^{-1})	R^2	E_α (kJ.mol^{-1})	R^2	E_α (kJ.mol^{-1})	R^2
0.1	98	0.9985	101	0.9987	98	0.9952
0.2	98	0.9937	101	0.9946	96	0.9861
0.3	96	0.9902	100	0.9917	92	0.9761
0.4	94	0.9809	98	0.9840	89	0.9543
0.5	90	0.9652	95	0.9712	89	0.9201
0.6	96	0.9548	101	0.9637	108	0.9423
0.7	122	0.9289	126	0.9408	153	0.9555
0.8	161	0.9213	163	0.9302	201	0.9580
Avg.	**107**	**0.9667**	**111**	**0.9719**	**116**	**0.9610**

Table A4.10: Various solid-state reaction mechanisms and corresponding expressions for f(α), g(α), and Z(α).

Model	Model code	differential form $f(\alpha) = \frac{1}{k}\frac{d\alpha}{dt}$	Integral form $g(\alpha) = (kt)$	$Z(\alpha) = f(\alpha) * g(\alpha)$
Nucleation model				
Power law	**P2/3**	$2/3(\alpha)^{-1/2}$	$(\alpha)^{3/2}$	$2/3(\alpha)^{-1/2} * (\alpha)^{3/2}$

Power law	**P2 (n=1/2)**	$2(\alpha)^{1/2}$	$(\alpha)^{1/2}$	$2(\alpha)^{1/2} * (\alpha)^{1/2}$
Power law	**P3 (n=1/3)**	$3(\alpha)^{2/3}$	$(\alpha)^{1/3}$	$3(\alpha)^{2/3} * (\alpha)^{1/3}$
Power law	**P4 (n=1/4)**	$4(\alpha)^{3/4}$	$(\alpha)^{1/4}$	$4(\alpha)^{3/7} * (\alpha)^{1/4}$
Avrami–Erofeyev	**A2**	$2(1-\alpha)[(-\ln(1-\alpha)]^{1/2}$	$[(-\ln(1-\alpha)]^{1/2}$	$2(1-\alpha)[(-\ln(1-\alpha)]^{1/2} * [(-\ln(1-\alpha)]^{1/2}$
Avrami–Erofeyev	**A3**	$3(1-\alpha)[(-\ln(1-\alpha)]^{2/3}$	$[(-\ln(1-\alpha)]^{1/3}$	$3(1-\alpha)[(-\ln(1-\alpha)]^{2/3} * [(-\ln(1-\alpha)]^{1/3}$
Avrami–Erofeyev	**A4**	$4(1-\alpha)[(-\ln(1-\alpha)]^{3/4}$	$[(-\ln(1-\alpha)]^{1/4}$	$4(1-\alpha)[(-\ln(1-\alpha)]^{3/4} * [(-\ln(1-\alpha)]^{1/4}$
Geometrical contraction model				
Contracting area	**R2**	$2(1-\alpha)^{1/2}$	$1-(1-\alpha)^{1/2}$	$2(1-\alpha)^{1/2} * 1-(1-\alpha)^{1/2}$
Contracting volume	**R3**	$3(1-\alpha)^{2/3}$	$1-(1-\alpha)^{1/3}$	$3(1-\alpha)^{2/3} * 1-(1-\alpha)^{1/3}$
Diffusion model				
1–D diffusion	**D1**	$\frac{1}{(2\alpha)}$	$(\alpha)^2$	$\frac{1}{(2\alpha)} * (\alpha)^2$
2–D diffusion	**D2**	$-\left[\frac{1}{\ln(1-\alpha)}\right]$	$[(1-\alpha)\ln(1-\alpha)]+\alpha$	$-\left[\frac{1}{\ln(1-\alpha)}\right] * [(1-\alpha)\ln(1-\alpha)]+\alpha$
3–D diffusion	**D3**	$\left[\frac{3(1-\alpha)^{1/2}}{2(1-(1-\alpha)^{1/3}}\right]$	$1-(^2/_3)\alpha-(1-\alpha)^{2/3}$	$\left[\frac{3(1-\alpha)^{1/2}}{2(1-(1-\alpha)^{1/3}}\right] * 1-(^2/_3)\alpha-(1-\alpha)^{2/3}$
Reaction order model				
Zero order	**F0**	1	α	$1* \alpha$
First order	**F1**	$(1-\alpha)$	$-ln(1-\alpha)$	$(1-\alpha) * -ln(1-\alpha)$
Second order	**F2**	$(1-\alpha)^2$	$\left[\frac{1}{(1-\alpha)}-1\right]$	$(1-\alpha)^2 * \left[\frac{1}{(1-\alpha)}-1\right]$
Third order	**F3**	$(1-\alpha)^3$	$\frac{1}{2}\left[\frac{1}{(1-\alpha)^2}-1\right]$	$(1-\alpha)^3 * \frac{1}{2}\left[\frac{1}{(1-\alpha)^2}-1\right]$

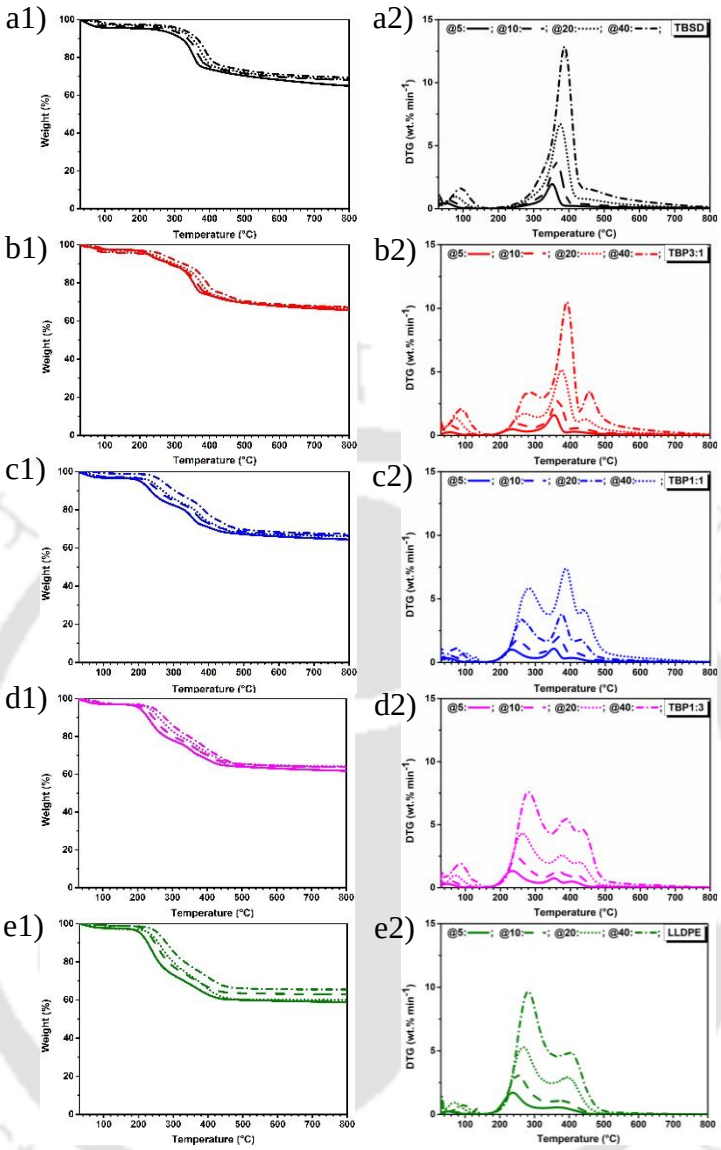

Figure A4.1. TG analysis of three different TBSD+LLDPE blends (a) TBSD (b) TBP3:1, (c) TBP1:1, (d) TBP1:3 and e) LLDPE: Weight loss as a function of temperature (a1, b1, c1, d1 and e1) and DTG (a2, b2, c2, d2 and e2) in presence of MesoHY zeolite

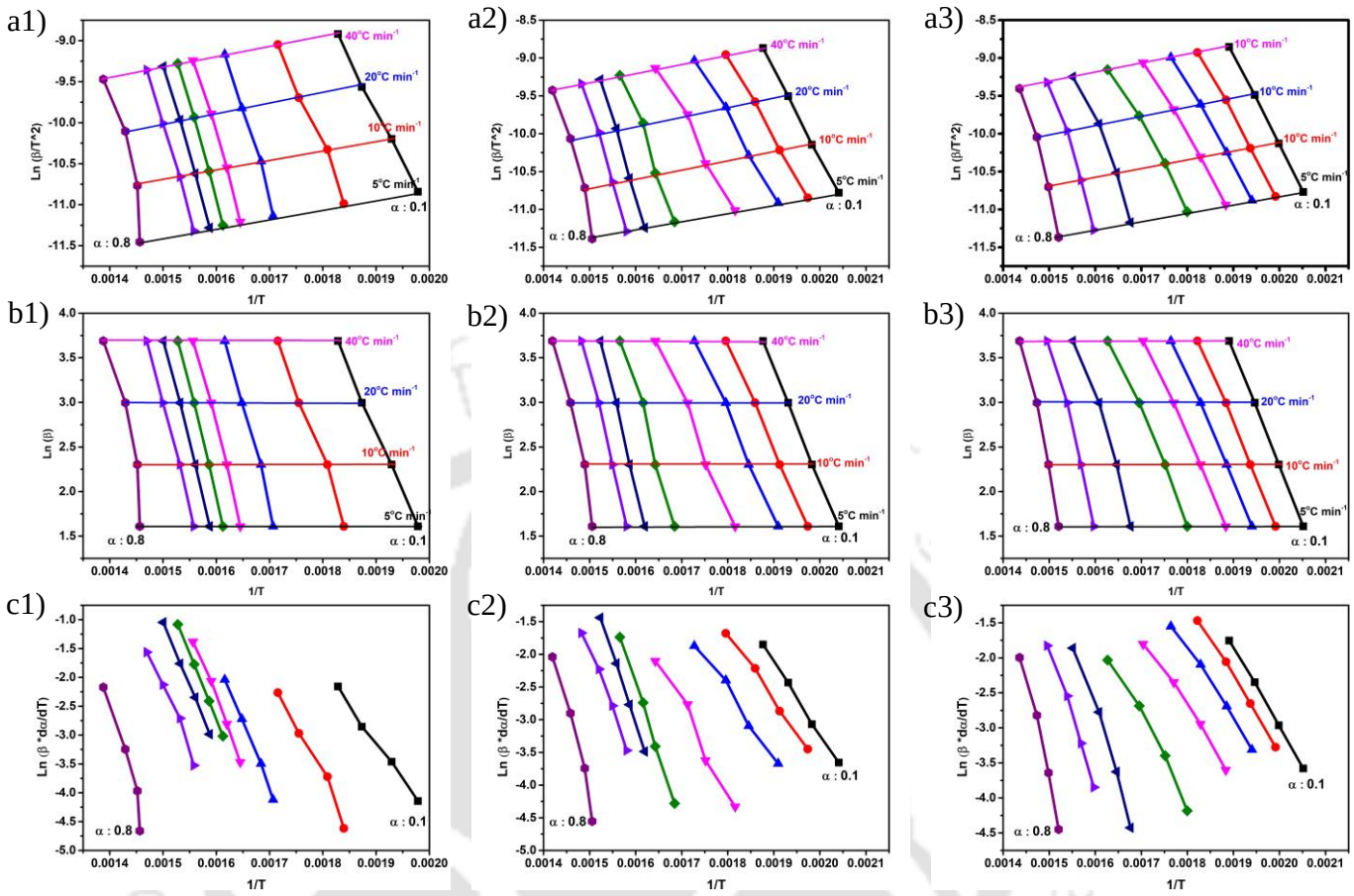

Figure A4.2. Determination of Activation energy using three different iso-conversion models: KAS (a1) OFW (b1) and FM (c1), of various TBSD + LLDPE blends, TBP3:1: a1 to c1; TBP:1: a2 to c2; and TBP1:3: a3 to c3) over MesoHY zeolite

3.5 Catalytic pyrolysis pathways for cellulose and lignin over HY catalyst

Cellulose consists of D-glucose units joined by beta glycosidic linkages [β–(C1↔C4)] and is crystalline. The CP of cellulose over zeolite gives various products such as anhydrosugars, furan derivatives, light oxygenates, olefins (C2–C6), and mono and polyaromatic hydrocarbons (MAH and PAH). [27] Formation of aromatics from CP of cellulose occurs in various reactions over a zeolite catalyst. First, the cellulose degrades into oligosaccharides and monosaccharides over the external surface of zeolite by the breaking of glycosidic linkages. Further, the C6 monomers are

converted into anhydrosugars (e.g., levoglucosan). These anhydrosugars again break down into two different oxygenates viz light oxygenates (e.g., hydroxylacetaldehyde and acetic acid) and heavy oxygenates such as furanic derivatives. The heavy oxygenates are formed by dehydration, cleavage of C2 or C4 bonds, decarboxylation, retro aldol condensation, and rearrangement (Grob type rearrangement). Moreover, these partially dehydrated oxygenates move into the pore of the zeolite where a series of reactions (i.e. dehydration, decarbonylation, decarboxylation, and oligomerisation) occur on catalytic sites (BAS and LAS) to produce aromatics by hydrocarbon pool mechanism (Scheme A4.3). The polyaromatic hydrocarbons also form due to the reactions between monoaromatics and oxygenates in the hydrocarbon pool. [28] Lignin is a complicated structure consisting of compounds such as phenyl propane, which are thermally stable. [17] The production of gaseous (CO_2, CH_4, CO, and H_2) and liquid products occurs during lignin pyrolysis.[29,30] At low temperatures (<200°C), the degradation of the phenyl propane unit is very slow. At temperatures in the range of 250°C, the side chain of a benzene ring, having different functional groups, converts to compounds such as CO_2, acetic acid, acetaldehyde. [29,30] At 350°C, the degradation of phenyl ether (β–O–4) occurs to produce phenol derivatives on the external surface of the catalyst. These derivatives then move into the catalyst pore and undergo deoxygenation and dehydration reactions at acidic sites and subsequently convert into aromatics by Diels-Alder reaction. [31,32] The depolymerization and reconstruction of lignin also occur at reaction temperatures 350°C. In the temperature range 350–450°C, decarbonylation, deolefination occur. Moreover, the reactions polycondensation and reconstruction of benzene convert it to fused structure, which acts as a precursor of coke (Scheme A4.4 and A4.5). [33]

3.6 Global degradation pathways in catalytic co-pyrolysis of torrefied biomass and plastic

In CCP, the hydrocarbons form by Diels-Alder reaction between furan derivatives and plastic-derived olefins in the hydrocarbon pool, found inside the zeolite pore. [3] The kinetic diameter of phenol (0.45–0.54 nm) and its derivatives (> 0.54 nm) [34] derived from lignin adsorb onto the surface of catalyst and form coke that reduce catalytic activity but H-transfer from plastic improves cracking activity.[3,35] Hydrogen transfer from plastic also contributes to the synergism in terms of production of aromatics (Schemes A4.3, A4.4, and A4.5) [36] and lower activation energies of the blends (Fig. 4). Overall, in CCP, the interaction is favored through a combination of Diels-Alder, hydrocarbon pool, and H-transfer reactions. [37]

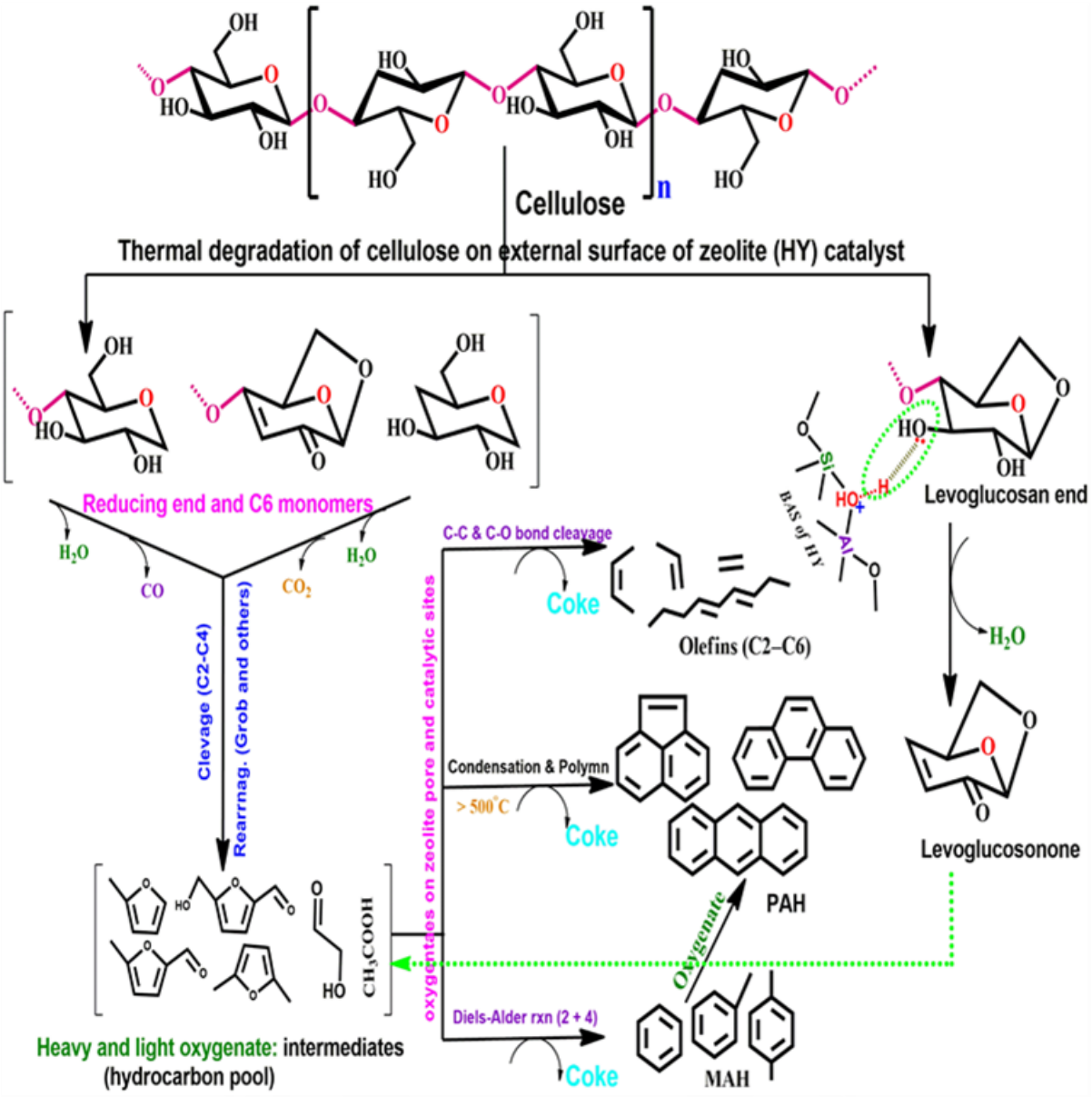

Scheme A4.3. Degradation pathways for CP of cellulose over HY zeolite. [31,38–41]

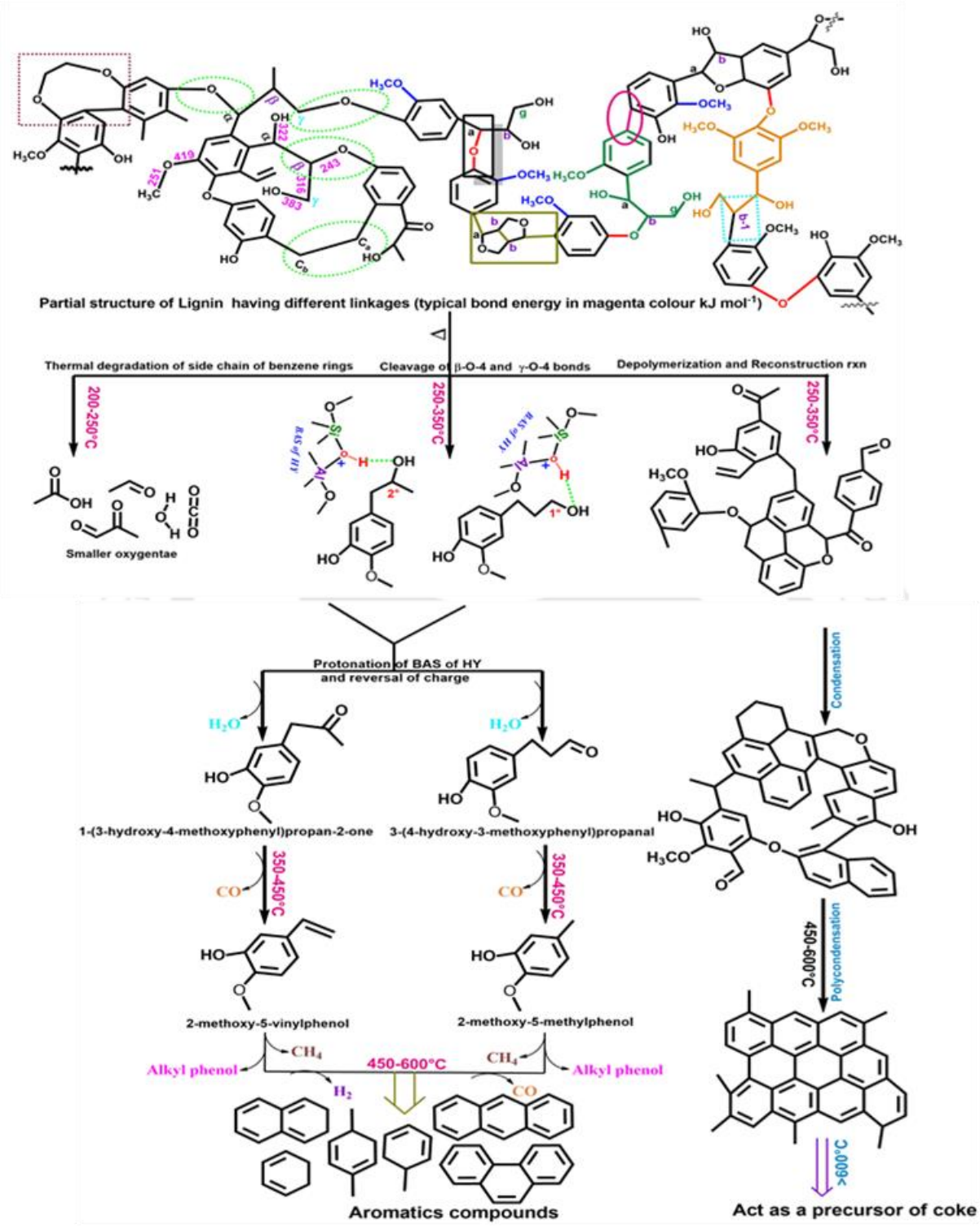

Scheme A4.4. Degradation pathways for CP of lignin over HY zeolite. [3,31,35,37,42,43]

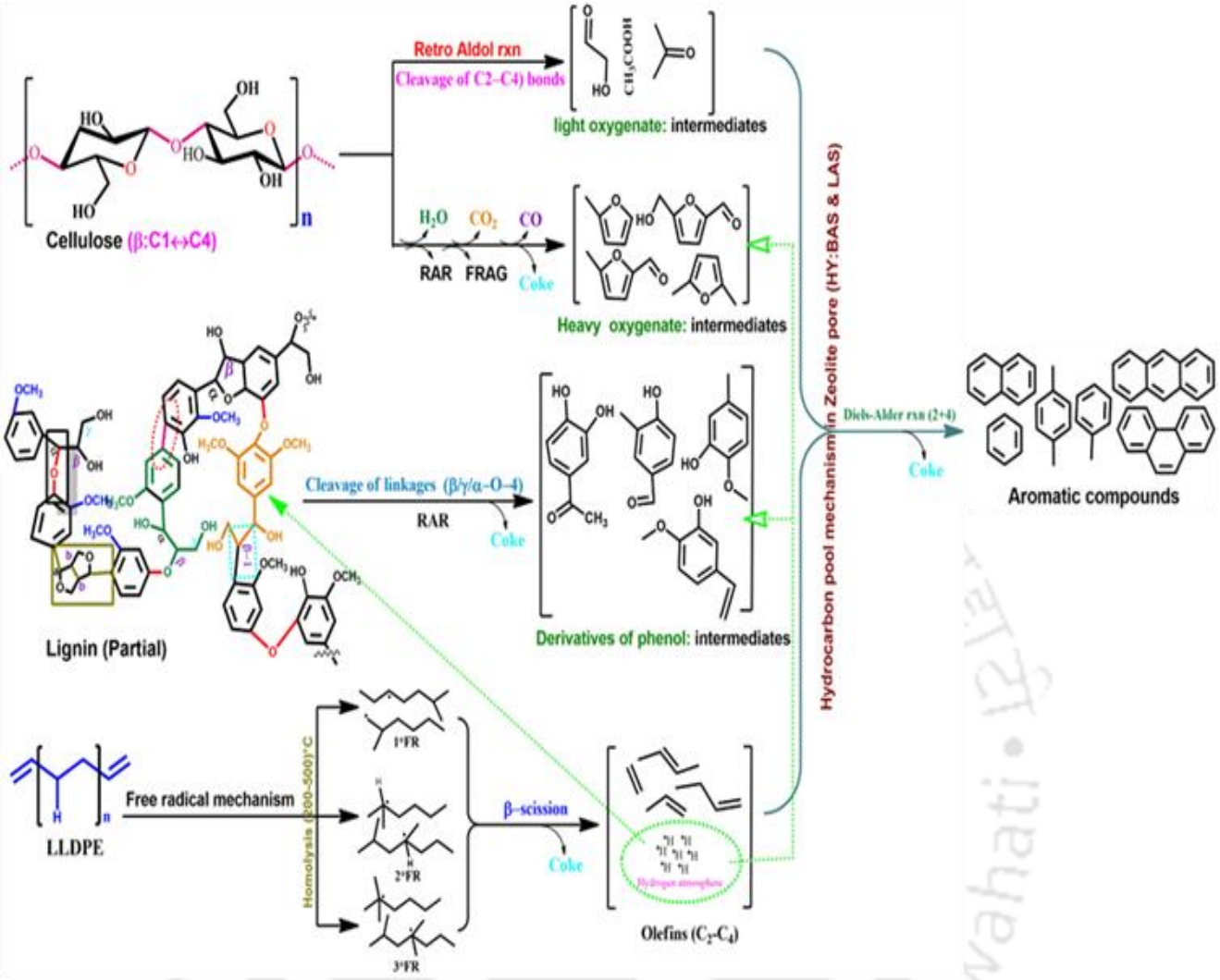

Scheme A4.5. Global degradation pathways for co-pyrolysis of TBSD and plastic by hydrocarbon pool mechanism in the pores of HY zeolites. [3,33,35,37]

References:

[1] G. Lopez, M. Artetxe, M. Amutio, J. Bilbao, M. Olazar, Thermochemical routes for the valorization of waste polyolefinic plastics to produce fuels and chemicals. A review, Renew. Sustain. Energy Rev. 73 (2017) 346–368. https://doi.org/10.1016/j.rser.2017.01.142.

[2] M. El Moustaqim, A. El Kaihal, M. El Marouani, S. Men-La-Yakhaf, M. Taibi, S. Sebbahi, S. El Hajjaji, F. Kifani-Sahban, Thermal and thermomechanical analyses of lignin, Sustain. Chem. Pharm. 9 (2018) 63–68. https://doi.org/10.1016/j.scp.2018.06.002.

[3] Z. Wang, K.G. Burra, T. Lei, A.K. Gupta, Co-pyrolysis of waste plastic and solid biomass for synergistic production of biofuels and chemicals-A review, Prog. Energy Combust.

Sci. 84 (2021) 100899. https://doi.org/10.1016/j.pecs.2020.100899.

[4] O. Dogu, M. Pelucchi, R. Van de Vijver, P.H.M. Van Steenberge, D.R. D'hooge, A. Cuoci, M. Mehl, A. Frassoldati, T. Faravelli, K.M. Van Geem, The chemistry of chemical recycling of solid plastic waste via pyrolysis and gasification: State-of-the-art, challenges, and future directions, Prog. Energy Combust. Sci. 84 (2021) 100901. https://doi.org/10.1016/j.pecs.2020.100901.

[5] Y. Fan, C. Liu, X. Kong, Y. Han, M. Lei, R. Xiao, A new perspective on polyethylene-promoted lignin pyrolysis with mass transfer and radical explanation, Green Energy Environ. (2021) 2–10. https://doi.org/10.1016/j.gee.2021.02.004.

[6] B. Engler, Benjamin; Siegmar Schoenherr; Zheke, Zhong; Gero, Suitability of Bamboo as an Energy Resource : Analysis of Bamboo Combustion Values Dependent on the Culm ' s Age, Int. J. For. Eng. 23 (2012) 114–121.

[7] L.Z. Wang S, Dai G, Yang H, Lignocellulosic biomass pyrolysis mechanism : A state-of-the-art review, Prog. Energy Combust. Sci. 62 (2017) 33–86. https://doi.org/10.1016/j.pecs.2017.05.004.

[8] F. Abnisa, W. Mohd, A. Wan, A review on co-pyrolysis of biomass : An optional technique to obtain a high-grade pyrolysis oil, Energy Convers. Manag. 87 (2014) 71–85. https://doi.org/10.1016/j.enconman.2014.07.007.

[9] J. Zhang, J. Luo, D. Tong, L. Zhu, L. Dong, C. Hu, The dependence of pyrolysis behavior on the crystal state of cellulose, Carbohydr. Polym. 79 (2010) 164–169. https://doi.org/10.1016/j.carbpol.2009.07.038.

[10] N. Giummarella, M. Lawoko, A.J. Ragauskas, A critical review on the analysis of lignin carbohydrate bonds, Green Chem. 21 (2019) 1573–1595. https://doi.org/10.1039/c8gc03606c.

[11] M. Lawoko, Lignin Polysaccharide Networks in Softwood and Chemical Pulps : Characterisation , Structure and Reactivity, 2005.

[12] H. Kawamoto, Lignin pyrolysis reactions, J. Wood Sci. 63 (2017) 117–132. https://doi.org/10.1007/s10086-016-1606-z.

[13] W.S. Carvalho, I.F. Cunha, M.S. Pereira, C.H. Ataíde, Thermal decomposition profile and product selectivity of analytical pyrolysis of sweet sorghum bagasse : Effect of addition of inorganic salts, Ind. Crops Prod. 74 (2015) 372–380.

[14] Y. Shao, X. Hu, Z. Zhang, K. Sun, G. Gao, T. Wei, conversion of furfural to levulinic acid / ester in dimethoxymethane : Understanding the mechanism for polymerization, Green Energy Environ. 4 (2019) 400–413. https://doi.org/10.1016/j.gee.2018.10.002.

[15] K.B. Ansari, J.S. Arora, J.W. Chew, P.J. Dauenhauer, S.H. Mushrif, Fast Pyrolysis of Cellulose, Hemicellulose, and Lignin: Effect of Operating Temperature on Bio-oil Yield and Composition and Insights into the Intrinsic Pyrolysis Chemistry, Ind. Eng. Chem. Res.

58 (2019) 15838–15852. https://doi.org/10.1021/acs.iecr.9b00920.

[16] D.K. Ojha, R. Vinu, Fast co-pyrolysis of cellulose and polypropylene using Py-GC/MS and Py-FT-IR, RSC Adv. 5 (2015) 66861–66870. https://doi.org/10.1039/c5ra10820a.

[17] M. Alam, D. Rammohan, A. Bhavanam, N.R. Peela, Wet torrefaction of bamboo saw dust and its co-pyrolysis with plastic, Fuel. 285 (2021). https://doi.org/10.1016/j.fuel.2020.119188.

[18] J.S. Arora, J.W. Chew, S.H. Mushrif, Influence of Alkali and Alkaline-Earth Metals on the Cleavage of Glycosidic Bond in Biomass Pyrolysis: A DFT Study Using Cellobiose as a Model Compound, J. Phys. Chem. A. 122 (2018) 7646–7658. https://doi.org/10.1021/acs.jpca.8b06083.

[19] B.S. Kim, Y.M. Kim, H.W. Lee, J. Jae, D.H. Kim, S.C. Jung, C. Watanabe, Y.K. Park, Catalytic Copyrolysis of Cellulose and Thermoplastics over HZSM-5 and HY, ACS Sustain. Chem. Eng. 4 (2016) 1354–1363. https://doi.org/10.1021/acssuschemeng.5b01381.

[20] W. Lafayette, M.M. Abu-omar, A synergistic biorefinery based on catalytic conversion of lignin prior to cellulose starting from lignocellulosic biomass, Green Chem. 17 (2015) 1492. https://doi.org/10.1039/c4gc01911c.

[21] S. Zhang, Xuesong;Lei, Hanwu; Chen, Catalytic co-pyrolysis of lignocellulosic biomass with polymers: a critical review, Green Chem. 18 (2016). https://doi.org/10.1039/c6gc00911e.

[22] S.M. Al-Salem, A. Bumajdad, A.R. Khan, B.K. Sharma, S.R. Chandrasekaran, F.A. Al-Turki, F.H. Jassem, A.T. Al-Dhafeeri, Non-isothermal degradation kinetics of virgin linear low density polyethylene (LLDPE) and biodegradable polymer blends, J. Polym. Res. 25 (2018). https://doi.org/10.1007/s10965-018-1513-7.

[23] M. Alam, A. Bhavanam, A. Jana, J. kumar S. Viroja, N.R. Peela, Co-pyrolysis of bamboo sawdust and plastic: Synergistic effects and kinetics, Renew. Energy. 149 (2020) 1133–1145. https://doi.org/10.1016/J.RENENE.2019.10.103.

[24] K. Pyra, K.A. Tarach, A. Śrębowata, I. Melián-Cabrera, K. Góra-Marek, Pd-modified beta zeolite for modulated hydro-cracking of low-density polyethylene into a paraffinic-rich hydrocarbon fuel, Appl. Catal. B Environ. 277 (2020) 119070. https://doi.org/10.1016/j.apcatb.2020.119070.

[25] H. Hassan, J.K. Lim, B.H. Hameed, Catalytic co-pyrolysis of sugarcane bagasse and waste high-density polyethylene over faujasite-type zeolite, Bioresour. Technol. 284 (2019) 406–414. https://doi.org/10.1016/j.biortech.2019.03.137.

[26] P.S. Rezaei, D. Oh, Y. Hong, Y.M. Kim, J. Jae, S.C. Jung, J.K. Jeon, Y.K. Park, In-situ catalytic co-pyrolysis of yellow poplar and high-density polyethylene over mesoporous catalysts, Energy Convers. Manag. 151 (2017) 116–122. https://doi.org/10.1016/j.enconman.2017.08.073.

[27] W. Wang, Y. Shi, Y. Cui, X. Li, Catalytic fast pyrolysis of cellulose for increasing contents of furans and aromatics in biofuel production, J. Anal. Appl. Pyrolysis. 131 (2018) 93–100. https://doi.org/10.1016/j.jaap.2018.02.004.

[28] Carlson, J. Jae, W.G. Huber, Mechanistic insights from isotopic studies of glucose conversion to aromatics over ZSM-5, ChemCatChem. 1 (2009) 107–110. https://doi.org/10.1002/cctc.200900130.

[29] D.K. Shen, S. Gu, K.H. Luo, S.R. Wang, M.X. Fang, The pyrolytic degradation of wood-derived lignin from pulping process, Bioresour. Technol. 101 (2010) 6136–6146. https://doi.org/10.1016/j.biortech.2010.02.078.

[30] T. Faravelli, A. Frassoldati, G. Migliavacca, E. Ranzi, Detailed kinetic modeling of the thermal degradation of lignins, Biomass and Bioenergy. 34 (2010) 290–301. https://doi.org/10.1016/j.biombioe.2009.10.018.

[31] C. Li, G. Ji, Y. Qu, M. Irfan, K. Zhu, X. Wang, A. Li, Influencing mechanism of zinc mineral contamination on pyrolysis kinetic and product characteristics of corn biomass, J. Environ. Manage. 281 (2021). https://doi.org/10.1016/j.jenvman.2020.111837.

[32] A. Beste, A.C. Buchanan, Role of carbon-carbon phenyl migration in the pyrolysis mechanism of β-O-4 lignin model compounds: Phenethyl phenyl ether and α-hydroxy phenethyl phenyl ether, J. Phys. Chem. A. 116 (2012) 12242–12248. https://doi.org/10.1021/jp3104694.

[33] Y. Xue, S. Zhou, X. Bai, Role of Hydrogen Transfer during Catalytic Copyrolysis of Lignin and Tetralin over HZSM-5 and HY Zeolite Catalysts, ACS Sustain. Chem. Eng. 4 (2016) 4237–4250. https://doi.org/10.1021/acssuschemeng.6b00733.

[34] E. Grabowska, Effect of micropore size distribution on phenol adsorption on steam activated carbons, Adsorption. 22 (2016) 599–607. https://doi.org/10.1007/s10450-015-9737-x.

[35] H. Yang, Z. Dong, B. Liu, Y. Chen, M. Gong, S. Li, H. Chen, A new insight of lignin pyrolysis mechanism based on functional group evolutions of solid char, Fuel. 288 (2021) 119719. https://doi.org/10.1016/j.fuel.2020.119719.

[36] X. Liu, K.R.G. Burra, Z. Wang, J. Li, D. Che, A.K. Gupta, Towards enhanced understanding of synergistic effects in co-pyrolysis of pinewood and polycarbonatee, Appl. Energy. 143 (2021) 116662. https://doi.org/10.1115/1.4049464.

[37] T. Matamba, A. Tahmasebi, S.K. Rish, J. Yu, Understanding the enhanced production of poly-aromatic hydrocarbons during the pyrolysis of lignocellulosic biomass components under pressurized entrained-flow conditions, Fuel Process. Technol. 213 (2021) 106645. https://doi.org/10.1016/j.fuproc.2020.106645.

[38] C.A. Mullen, P.C. Tarves, L.M. Raymundo, E.L. Schultz, A.A. Boateng, J.O. Trierweiler, Fluidized Bed Catalytic Pyrolysis of Eucalyptus over HZSM-5: Effect of Acid Density and Gallium Modification on Catalyst Deactivation, Energy and Fuels. 32 (2018) 1771–

1778. https://doi.org/10.1021/acs.energyfuels.7b02786.

[39] E. Leng, M. Costa, X. Gong, A. Zheng, S. Liu, M. Xu, Effects of KCl and CaCl2 on the evolution of anhydro sugars in reaction intermediates during cellulose fast pyrolysis, Fuel. 251 (2019) 307–315. https://doi.org/10.1016/j.fuel.2019.04.006.

[40] I. Itabaiana Junior, M. Avelar Do Nascimento, R.O.M.A. De Souza, A. Dufour, R. Wojcieszak, Levoglucosan: A promising platform molecule?, Green Chem. 22 (2020) 5859–5880. https://doi.org/10.1039/d0gc01490g.

[41] R. Vinu, L.J. Broadbelt, A mechanistic model of fast pyrolysis of glucose-based carbohydrates to predict bio-oil composition, Energy Environ. Sci. 5 (2012) 9808–9826. https://doi.org/10.1039/c2ee22784c.

[42] Y. Zhao, X. Yang, Z. Fu, R. Li, Y. Wu, Synergistic effect of catalytic co-pyrolysis of cellulose and polyethylene over HZSM-5, J. Therm. Anal. Calorim. 140 (2020) 363–371. https://doi.org/10.1007/s10973-019-08633-7.

[43] H.W. Ryu, H.W. Lee, J. Jae, Y.K. Park, Catalytic pyrolysis of lignin for the production of aromatic hydrocarbons: Effect of magnesium oxide catalyst, Energy. 179 (2019) 669–675. https://doi.org/10.1016/j.energy.2019.05.015.

Publications

Journal papers

- **M. Alam**, A. Bhavanam, A. Jana, J. kumar S. Viroja, N.R. Peela, Co-pyrolysis of bamboo sawdust and plastic: Synergistic effects and kinetics, Renew. Energy. 149 (2020) 1133–1145. https://doi.org/10.1016/J.RENENE.2019.10.103.
- **M. Alam**, D. Rammohan, A. Bhavanam, N.R. Peela, Wet torrefaction of bamboo saw dust and its co-pyrolysis with plastic, Fuel. 285 (2021). https://doi.org/10.1016/j.fuel.2020.119188
- **M. Alam**, D. Rammohan, N.R. Peela, Catalytic co-pyrolysis of wet-torrefied bamboo sawdust and plastic over the zeolite H-ZSM-5: Synergistic effects and kinetics, Renew. Energy. 178 (2021) 608–619. https://doi.org/10.1016/j.renene.2021.06.109
- **M. Alam,** N.R. Peela, Catalytic co-pyrolysis of wet-torrefied bamboo sawdust and plastic over the zeolite HY: Synergism and kinetics, J. Energy Inst. 100 (2021) 76–88. https://doi.org/10.1016/j.joei.2021.11.004.

Book Chapter

- **M. Alam**, S.K. Yedla, S.T. Bhutia, V.V. Goud, **N.R. Peela*** (2017) "Advancement in development of biodiesel production in last two decades: An Indian overview on raw materials, synthesis, by-products and application" in Sustainable Biofuels Development in India, A.K. Chandel, R.K. Sukumaran (eds.), Springer International Publishing, Pages 167-188. **DOI: 10.1007/978-3-319-50219-9_7**

National/International Conferences and Workshop

- **M. Alam,** "Wet Torrefaction of Bamboo Saw Dust and Its Co-Pyrolysis with Plastic" 3rd International Conference on Material science and Research (Madridge), November 28-29, 2019; Kuala Lumpur, Malaysia
- Attended an online short-term course on "Valorization of Lignocellulosic Biomass towards Sustainable Fuels, Chemicals and Materials" conducted by NIT Jalandhar - Sept. 2020
- **M. Alam,** N. R. Peela "An overview of bio-oil up-gradation by ketonization and esterification reactions" in Reflux-2016-Annual Chemical Engineering Symposium, Department of Chemical Engineering, 25-27 March, IIT Guwahati, Assam, India.